IMAGING OF BACTERIAL RESPONSES TO DNA DAMAGE CAUSED BY ANTIBACTERIAL AGENTS



Chloé Jeanne Cassaro

A thesis submitted for the degree of Doctor of Philosophy in Interdisciplinary Bioscience (BBSRC DTP) – Biochemistry

LINACRE COLLEGE

UNIVERSITY OF OXFORD

HILLARY 2024

DECLARATION

I hereby declare that this thesis is my own work and the experiments and analysis described in the following pages were performed by myself unless otherwise stated, as described below. The experiments were carried out in the Department of Biochemistry, University of Oxford. The Thesis has not been submitted for any other degree or professional qualifications.

The following experiments and analyses were not performed by myself :

- Method: R analysis scripts were written by Jai S. Bolton
- Method: Matlab software for image processing and analysis was written by Stephan Uphoff
- Method: *Escherichia coli* background strains and some of the reporter strains used were constructed by Divya Choudhary, Emma Jones, Valentine Lagage and Stephan Uphoff
- Method: T6SS pBAD plasmid collection was made by Veronika Bakulova and Rafael Custodio

ACKNOWLEDGEMENT

I am extremely grateful for the people who have made my time at the University of Oxford a memorable one. I specifically want to thank my partner Jai S. Bolton, and my dear friend Dalia S. Gala for their infallible support and help throughout the years, and the not-so-occasional comic relief and countless memories. I also want to express a special thanks to the people I worked alongside every day, Divya Choudhary, Valentine Lagage, Amy Moores, Joseph Pollaco and Fiona Sargisson. I would also like to thank my close friends, particularly Ludivine Triai, Matthew Chan, and Charlotte Caors, for being my favourite non-biologist audience and fierce allies, and Jonathan Gamwell and Gilbert Ansa for their support and much appreciated friendship.

I am also grateful to my two supervisors, Stephan Uphoff and Chris Tang for their continued support, advice, and guidance throughout my DPhil, and for giving me the freedom to explore. I would also like to thank my previous supervisors who inspired me and guided me along my scientific journey, particularly Andrew Roe, Olwyn Byron, Abdelrahim Zoued and Eric Cascales.

I gratefully acknowledge the BBSRC Interdisciplinary Biosciences Doctoral Training Program for funding my studies, and the Department of Biochemistry, Linacre College and the Doctoral Training Centre for their support.

Finally, I want to thank my family, specifically my parents Joseph Cassaro, Virginie Jaubert Cassaro, my brother Rémi Cassaro and sister-in-law Hanaé Trabuc. You gave me the strength and the confidence to go on this international journey and complete my thesis. I know your unweathering

pride, support and trust in me have led me to where I am now. Thank you for everything, and for always being there for me.

TABLE OF CONTENT

DECLARATION 3

ACKNOWLEDGEMENT 4

TABLE OF CONTENT 6

ABSTRACT 9

ABBREVIATIONS 11

CHAPTER 1 : INTRODUCTION 13

1. BACTERIA IN THE ENVIRONMENT 13
2. INHERENT TOLERANCE MECHANISMS IN BACTERIA 17
2.1. DNA REPLICATION 17
2.2. DNA DAMAGE REPAIR 18
2.3. DNA DAMAGE TOLERANCE 25
3. REGULATION OF STRESS RESPONSES 26
3.1. THE SOS RESPONSE TO DNA DAMAGE 26
3.2. OXIDATIVE STRESS RESPONSE TO REACTIVE OXYGEN SPECIES (ROS) 28
3.3. THE ACID STRESS RESPONSE TO LOW PH 31
3.4. RPOS GENERAL STRESS RESPONSE 32
4. MUTATIONS AND GENETIC ADAPTATION 33
5. SINGLE CELL IMAGING 36

CHAPTER 2 : REVIEW OF THE INTRICATE MECHANISMS OF THYMINELESS DEATH IN BACTERIA 40

1. THYMINE BIOSYNTHESIS PATHWAYS 41
2. THE INVOLVEMENT OF DNA REPLICATION IN THYMINELESS DEATH 44
3. OXIDATIVE STRESS IN THYMINELESS DEATH 47
4. DNA REPAIR PATHWAYS INVOLVEMENT IN THYMINELESS DEATH 49
5. SOS RESPONSE AND THYMINELESS DEATH 50
6. THYMINELESS DEATH AND MUTAGENESIS 52
7. THE ENVELOPE AS A SOURCE OF THYMIDINE DURING THYMINELESS DEATH 53
8. CELL MORPHOLOGY DURING TLD 54
9. EFFECT OF GROWTH MEDIA COMPOSITION ON TRIMETHOPRIM EFFICACY 56

AIMS OF THE PROJECT **62**

CHAPTER 3 : METHODS **63**

1. STRAINS **63**
2. GROWTH CURVE AND MIC DETERMINATION **66**
3. SURVIVAL ASSAYS **67**
4. MICROFLUIDICS EXPERIMENTS **67**
4.1. MICROFLUIDICS EXPERIMENTS ANALYSIS 70
5. SINGLE MOLECULE TRACKING **74**

CHAPTER 4: IMAGING CELL STATES AND GROWTH DYNAMICS IN RESPONSE TO TRIMETHOPRIM TREATMENT USING MICROFLUIDIC GROWTH CHAMBERS **76**

1. INTRODUCTION **76**
2. RESULTS **78**
2.1. TRIMETHOPRIM'S IMPACT ON BACTERIAL COMMUNITIES AT THE POPULATION LEVEL 78
2.2. TRIMETHOPRIM'S IMPACT ON CELLS' SURVIVAL AND GROWTH DYNAMICS 86
2.3. TRIMETHOPRIM'S IMPACT ON THE PHENOTYPIC DYNAMICS OF CELLS WITH DIVERSE MEDIA SUPPLEMENTATION 98
2.4. TRIMETHOPRIM'S INFLUENCE ON SIZE CHANGE DYNAMICS 104
2.5. TRIMETHOPRIM'S IMPACT ON THE PHENOTYPIC DYNAMICS OF MUTANT CELLS 110
3. DISCUSSION **116**

CHAPTER 5: CHARACTERISATION OF BACTERIAL STRESS RESPONSES TO TRIMETHOPRIM TREATMENT **124**

1. INTRODUCTION **124**
2. RESULTS **126**
2.1. TMP-INDUCED REPLICATION STRESS : EXAMINING DNA REPLICATION FOCI DYNAMICS 126
2.2. TMP'S IMPACT ON MUTAGENESIS 130
2.3. TMP CAUSES A GLOBAL INCREASE IN GENE EXPRESSION 138
2.4. TMP'S INFLUENCE ON DNA DAMAGE 143
2.5. TMP'S INFLUENCE ON OXIDATIVE STRESS 152
2.6. TMP'S INFLUENCE ON ACID STRESS 156
2.7. TMP'S PATHWAYS CROSSTALK 159
3. DISCUSSION **162**

CHAPTER 6 : CHARACTERISATION OF BACTERIAL RESPONSES TO A TYPE SIX SECRETION SYSTEM NUCLEASE EFFECTOR **174**

1. INTRODUCTION **174**
2. RESULTS **177**

2.1. T6SS Effector's Impact on Bacteria at the Population Level 177
2.2. T6SS Effector's Impact on Cell Viability, Growth and Size Dynamics 180
2.3. T6SS Effector's Impact on DNA Damage 189
2.4. Role of the SOS response in the Protection Against T6SS Effectors 194
2.5. T6SS Effector's Global Effects on Prey Cells 197
3. Discussion 199

CHAPTER 7 : CONCLUSION 204

1. Summary 204
2. Limitations 207
3. Outlook 211

REFERENCES 214

APPENDIX 214

1. Table S1 : List of strains used in the study 253
2. Table S2 : List of reagents used in this study 255
3. Table S3 : List of primers used in this study 256

ABSTRACT

Bacteria are continually challenged by a variety of stresses in their environment, requiring rapid adaptation to survive. These stresses range from competition with other microorganisms to antibiotics, the mechanisms of action of which remain incompletely understood. This thesis explores the mechanisms of action of two antibacterial agents, the antibiotic trimethoprim (TMP) and a nuclease effector secreted by the Type Six Secretion System (T6SS). Through the use of both population-level and single-cell-based assays complemented by microscopy techniques, this research investigates the intricate responses of bacteria to DNA damage.

The study emphasizes how the impact of TMP on bacterial populations can shift between bactericidal and bacteriostatic, depending on the metabolite composition of the growth medium. TMP-induced depletion of thymidine triggers significant cellular stress and a profound state of disorder marked by response heterogeneity, which correlates with lower cell survival. However, supplementing the medium with thymidine can counteract these effects. Beyond inhibiting folate synthesis, TMP disrupts critical cellular processes such as DNA replication and cell division, leading to increased mutagenesis and the induction of a range of stress responses related to DNA damage, pH changes, and superoxide accumulation. This highlights TMP's capability to simultaneously disrupt multiple bacterial functions, overwhelming the cells to the point of hindering their normal growth or survival.

By contrast, the T6SS effector directly targets DNA, causing fragmentation and appears to trigger an immediate and protective SOS response. It results in rapid and irreversible growth arrest or cell

death, which the cognate immunity can fully protect the cells from. This research challenges traditional views on antibacterial agents, suggesting a broader interpretation that includes the induction of profound cellular disorder as a key component of the bactericidal activity of complex agents like TMP. It highlights the necessity of considering both bacteriostatic and bactericidal effects in antibacterial therapies. Overall, the research provides valuable insights into the dynamics and heterogeneity of bacterial stress responses to antimicrobial agents, which impacts bacterial survival and adaptation. It also lays a foundation for further exploration into the complex interplay between the action of antibacterial agents, bacterial stress responses and bacterial survival.

ABBREVIATIONS

5AA	Arginine, threonine, leucine, proline, histidine
8oxoG	7,8-dihydro-8- oxoguanine
Ade	Adenine
AdGM	Adenine, Glycine, Methionine
AP	Apurinic/Apyrimidinic
BER	Base Excision Repair
CFP	Cyan Fluorescent Protein
cfu	Colony forming units
dNTP	Deoxyribonucleoside Triphosphate DNA precursors
DSB	Double-stranded breaks
dsDNA	Double-stranded DNA
dTDP	Deoxythymidine Diphosphate
dTMP	Deoxythymidine Monophosphate
dTTP	Deoxythymidine triphosphate
dTTP	Deoxythymidine Triphosphate
ECA	Enterobacterial Common Antigens
EPS	Exopolysaccharide
GFP	Green Fluorescent Protein
H2O2	Hydrogen Peroxide
HGT	Horizontal Gene Transfer
HJ	Holliday Junction
HR	Homologous Recombination
ICLs	Interstrand cross-links
LB	Luria Broth
LMW	Low molecular weight
M95AA	M9 minimal medium with only 5 amino acids (arginine, threonine, leucine, proline, histidine)
MIC	Minimum Inhibitory Concentration
MMR	Mismatch Repair
NER	Nucleotide Excision Repair
$O2^-$	Superoxide
$OH^\cdot$	Hydroxyl Radicals
ON	Overnight
PCR	Polymerase Chain Reaction
PI	Propidium Iodide
Pol	DNA Polymerase
RED	Rapid Exponential Death
Rhs	Rearrangement Hotspot
ROS	Reactive Oxygen Species
rpm	rotation per minute
RpoS	RNA polymerase σ–factor

SOD	Superoxide Dismustase
SSB	Single-stranded DNA-binding protein
ssDNA	Single-stranded DNA
T6SS	Type Six Secretion System
TCA	Tricarboxylic acid cycle
TEM	Transmission Electron Microscopy
THF	Tetrahydrofolate
Thy	Thymidine
TLD	Thymineless Death
TLS	Translesion Synthesis
TMP	Trimethoprim
TMR	Tetramethylrhodamine
UTI	Urinary tract infections
WT	Wild Type

CHAPTER 1 : INTRODUCTION

1. BACTERIA IN THE ENVIRONMENT

Bacteria can play dual roles as both allies and adversaries. Thriving in diverse environments, from the pressure extremes of bodies of water to the harsh temperatures of soil, and potentially damaging sun radiations, they perform crucial functions. Whether fixing nitrogen from the atmosphere, metabolizing vitamins or carbohydrates, or aiding digestion in the intricate system of the gut microbiome, bacteria are essential (Kuypers et al., 2018; Rowland et al., 2018). In the body, bacteria form the microbiome, notably in the gut made of a large number of different species which help with digestion and absorption of nutrients that we would otherwise be unable to utilise (Rowland et al., 2018). The microbiome also helps to train the human immune system (Zheng et al., 2020). However, bacteria are also known to cause various infections, ranging from mild urinary tract infections (UTI) to severe or lethal illnesses including sepsis, and as a result, research has focussed on defeating bacteria, by use of antibacterial agents targeting vital bacteria components (Table 1). Antibacterial agents have often been developed by exploiting natural products or secondary metabolites such as antibiotics produced by fungi or secreted by bacteria. They are often serving in nature to defend against competition for nutrients or to protect other organisms in a mutualistic symbiosis for instance (Hutchings et al., 2019; Seipke et al., 2012). Unfortunately for humans and researchers, bacteria have constantly been evolving a range of means to defeat these agents when under attack, and developed mechanisms such as DNA repair to survive, and resist. This has led to another threat to humans, namely antibiotic resistance. To circumvent the issue of widespread resistance, more recently research has focussed on exploiting natural bacterial

machinery for precise and targeted delivery of toxic antibacterial agents. Indeed, one such system, the type six secretion system has been engineered to specifically deliver toxic agents inside the cytoplasm of pathogenic bacteria, effectively destroying them from inside (Hersch et al., 2021).

Table 1: Examples of some antibiotics in clinical use, their class, and corresponding primary targets, from (Hutchings et al., 2019).

Antibiotic Class	Primary target	Example of antibiotic
Aminoglycosides	Protein synthesis (30S ribosomal subunit)	Kanamycin
Amphenicols	Protein synthesis (50S ribosomal subunit)	Chloramphenicol
Azoles	DNA synthesis (DNA damage)	Metronidazole
Diaminopyrimidines	Folate synthesis (dihydrofolate reductase)	Trimethoprim
Glycopeptides	Cell wall synthesis (lipid II)	Vancomycin
Lipopeptides	Cell wall synthesis (membrane disruption)	Daptomycin
Penicillins	Cell wall synthesis (penicillin-binding protein)	Amoxicillin
Polymyxins	Cell wall synthesis (membrane disruption)	Colistin
Quinolones	DNA synthesis (DNA gyrase, and topoisomerase IV)	Ciprofloxacin
Ansamycins	DNA synthesis (RNA polymerase)	Rifampicin
Sulfonamides	Folate synthesis (dihydropteroate synthetase)	Mafenide
Tetracyclines	Protein synthesis (30S ribosomal subunit)	Tetracycline

Through these different means, bacteria are frequently subjected to various stresses in their environment which can perturb their growth and cause damage to proteins, lipids, and nucleic acids. Stresses for bacteria in the environment are diverse and can include radiations, UV light, or extreme temperatures, chemical stressors such as antibiotics secreted by their own peers or oxidising agents often produced by immune cells specifically aimed at killing bacteria (Fig.1). Another important source of stress for bacteria includes competition for nutrients and niche

leading to nutrient starvation or interspecies competitive interactions, often involving secreted toxic agents (Hibbing et al., 2010). As a result of all these possible and complex interactions, a variety of internal stresses can be induced in bacteria. These include changes in pH, formation of toxic by-products such as reactive oxygen species (ROS), DNA lesions, or metabolite depletion. Importantly, DNA damage can lead to genome instability and heritable mutations, making it a highly attractive target (Shapiro, 2015). Thus, in response to these and to ensure survival and faithful replication, bacteria are armed with a wide range of tolerance mechanisms and global and specific stress responses.

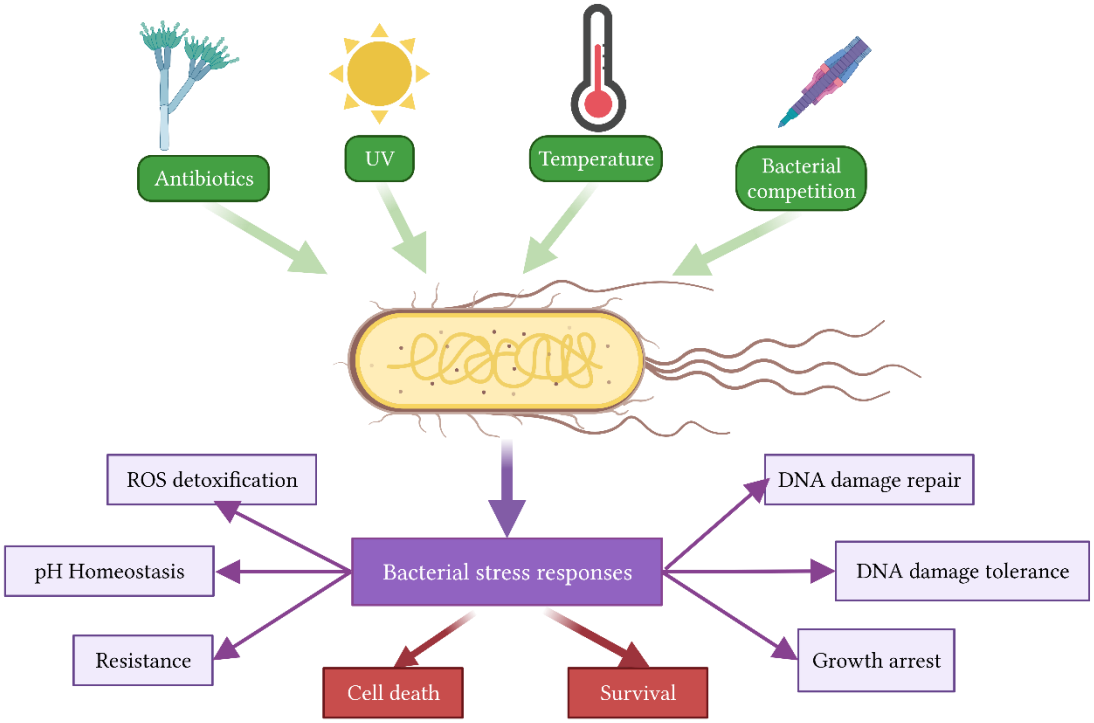


Figure 1: The many threats bacteria encounter in the environment. In the environment, bacteria are subjected to a wide variety of stressors, including antibiotics or UV light, leading to the cell's stress responses to counteract these stresses and protect the bacteria, such as ROS detoxification and DNA damage repair. The outcomes are usually survival or death of the cells.

In order to persist despite numerous attacks, bacteria have evolved a range of DNA repair pathways, often shared with humans to protect and pass on an intact genetic code whilst surviving stresses. The pathways vary in fidelity to repair or tolerate large DNA damage and allow cells to

survive in a stressful environment (Shapiro, 2015). Other responses involved in bacterial survival include global or general stress responses such as the SOS response. Bacteria also possess a panoply of specific stress responses such as the oxidative or acid stress responses, all dealing with different types of specific stresses and regulating an array of genes to protect the cells. Some of these responses, particularly the SOS response, have the potential to lead to mutations or other genetic adaptations in bacteria (Maslowska et al., 2019). This can either be beneficial causing resistance or detrimental leading to cell death which is the most desirable outcome from the attacker's point of view. Given the wide range of bacterial stress responses that exist in bacteria, only the particular responses in *Escherichia coli* investigated during this study will be discussed in detail below.

In this project, I aimed to delve into the intricacies of two antibacterial agents, each acting as a stressor. First in line is, the antibiotic trimethoprim (TMP), a broad-spectrum antibiotic. It has been used for decades to combat bacterial infections, mainly UTIs in combination with a sulphonamide (Bushby & Hitchings, 1968). Trimethoprim acts on folic acid metabolism as a competitive inhibitor of dihydrofolate reductase. It specifically inhibits the reduction of dihydrofolate to tetrahydrofolate (Burchall, 1973). Folic acid is critical in the biosynthesis of some essential metabolites and amino acids such as methionine, glycine, purines, and thymine (Bermingham & Derrick, 2002). Hence inhibition of these pathways can cause thymine starvation, disruption of DNA replication and can lead to death in a process akin to thymineless death (TLD) (Khodursky et al., 2015). The mechanisms of TMP's action are diverse and complex, encompassing ROS accumulation, acid stress, DNA replication stalling with resultant lethal DNA breaks, induction of SOS response, increased mutagenesis, or even maladaptive processing by DNA repair pathways (Giroux et al., 2017; Hong et al., 2019; Kuong & Kuzminov, 2010; Mitosch et al., 2017) (reviewed in Chapter 2).

The second system studied is the type six secretion system (T6SS). It is a contact-dependent machinery widespread in Gram-negative bacteria. It plays a crucial part in interbacterial

competition between pathogens and commensal species, as well as in host-pathogen interactions (Navarro-Garcia et al., 2019). The T6SS apparatus is composed of 13 core proteins, distributed among the membrane-spanning complex, the baseplate and the tail complex (Bingle et al., 2008). The tail complex features an outer sheath and an inner tube propelled by the contraction of the sheath to reach and puncture prey cells (Boyer et al., 2009). The T6SS can inject toxic effectors into prokaryotic and eukaryotic cells. The effectors are either fused to the tail complex components (VgrG, Hcp, PAAR) or loaded onto the machinery *via* adaptor proteins (Lien & Lai, 2017; Shneider et al., 2013). Typically, effectors are encoded as part of an effector/immunity pair, with an immunity protein protecting T6SS-expressing bacteria from self-intoxication (Benz & Meinhart, 2014). The effectors carrying a toxic activity domain can target various cellular components, with a few characterized toxins belonging to the nuclease class, specifically and directly targeting nucleic acids (DNA or RNA) and inducing cell death (Russell et al., 2014). A few stress response pathways such as the SOS response and oxidative stress have been implicated in the mechanism of action of T6SS effectors (Pissaridou et al., 2018, Dong et al., 2015).

2. INHERENT TOLERANCE MECHANISMS IN BACTERIA

2.1. DNA Replication

DNA replication is essential for the perpetuation of life; hence, it is tightly regulated in all living organisms. Bacteria are able to replicate DNA at a rate measured *in vitro* of 1000 base pairs per second for each fork, with an error rate of about 2×10^{-10} mutations per nucleotide per generation (Lee et al., 2012). Replication in most organisms including *E. coli* is performed by the replisome machinery. It starts at a single “origin” where two replication forks assemble and move along the

chromosomal DNA in opposite directions, to complete DNA replication within 40 min (O'Donnell et al., 2013). In bacteria, rounds of DNA synthesis can happen simultaneously before cell division takes place, resulting in multiple replication forks in a single cell (Cooper & Helmstetter, 1968). An origin-binding initiator protein, DnaA recognises and binds to the origin *oriC* in *E. coli*, and when complexed with ATP to form a filament, it unwinds the DNA origin region (Kaguni, 2011). The DnaB helicase, facilitated by DnaA and in complex with DnaC, is recruited to the *oriC,* forming a pre-priming complex (Chodavarapu & Kaguni, 2016). Following its dissociation from DnaC mediated by the primase DnaG and leading to its activation, DnaB unwinds the DNA and travels in a 5'-3' direction along the bound DNA strand acting as a stable anchor for the replisome (Spinks et al., 2021). As DnaB unwinds DNA, DnaG utilises the template ssDNA to synthesise RNA primers near the replication fork for extension by DNA polymerase (Frick & Richardson, 2001). Single-stranded DNA-binding protein (SSB) binds to and protects from degradation of the ssDNA produced by unwinding of DNA (Meyer et al., 1980). This prevents replication stalling due to secondary structures that could arise (Oakley, 2019). Finally, the highly processive replicative holoenzyme DNA polymerase PolIII, with a 3'-5'directed proofreading exonuclease domain DnaQ, synthesises both leading and lagging DNA strands simultaneously with a high fidelity (Johansson & Dixon, 2013). The β-binding domain of the polymerase interacts with the β_2 sliding clamp, DnaN, assembled around DNA by the clamp loader complex to lock the polymerase onto DNA and ensure high processivity (Beattie & Reyes-Lamothe, 2015). Three active polymerases are present in a single replisome, two of them always being associated with the sliding clamp when actively synthesising (Reyes-Lamothe et al., 2010).

2.2. DNA Damage Repair

In cells, unrepaired DNA damage can lead to potentially deleterious mutations or cell death – hence bacteria have evolved a range of mechanisms to respond to DNA damage in both error-prone and error-free manners and in a timely fashion. Genome maintenance being essential for the perpetuation of life, *E. coli* cells are equipped with multiple DNA repair pathways reverting damages. This includes excision pathways such as base excision repair (BER), nucleotide excision repair (NER) and mismatch repair (MMR) to repair nucleotide modifications, homologous recombination (HR) to repair DNA breaks by recombination or direct repair mechanisms (Chatterjee & Walker, 2017) (Fig.2). DNA lesions comprise base damage sites, apurinic/apyrimidinic (AP) sites, or DNA strand breaks (single and double). Unrepaired AP sites can block the progression of DNA replication forks. DNA lesions can often result from cellular metabolism by-products such as alkylating agents or ROS interacting with DNA (Dizdaroglu, 2012), occur during DNA replication due to incorrect base pairing (Schroeder et al., 2016), or result from exogenous sources such as chemicals, ROS, alkylating agents or radiations (Wozniak & Simmons, 2022). ROS and particularly hydroxyl radicals can directly oxidise the DNA backbone and cause single and double-strand breaks (Balasubramanian et al., 1998).

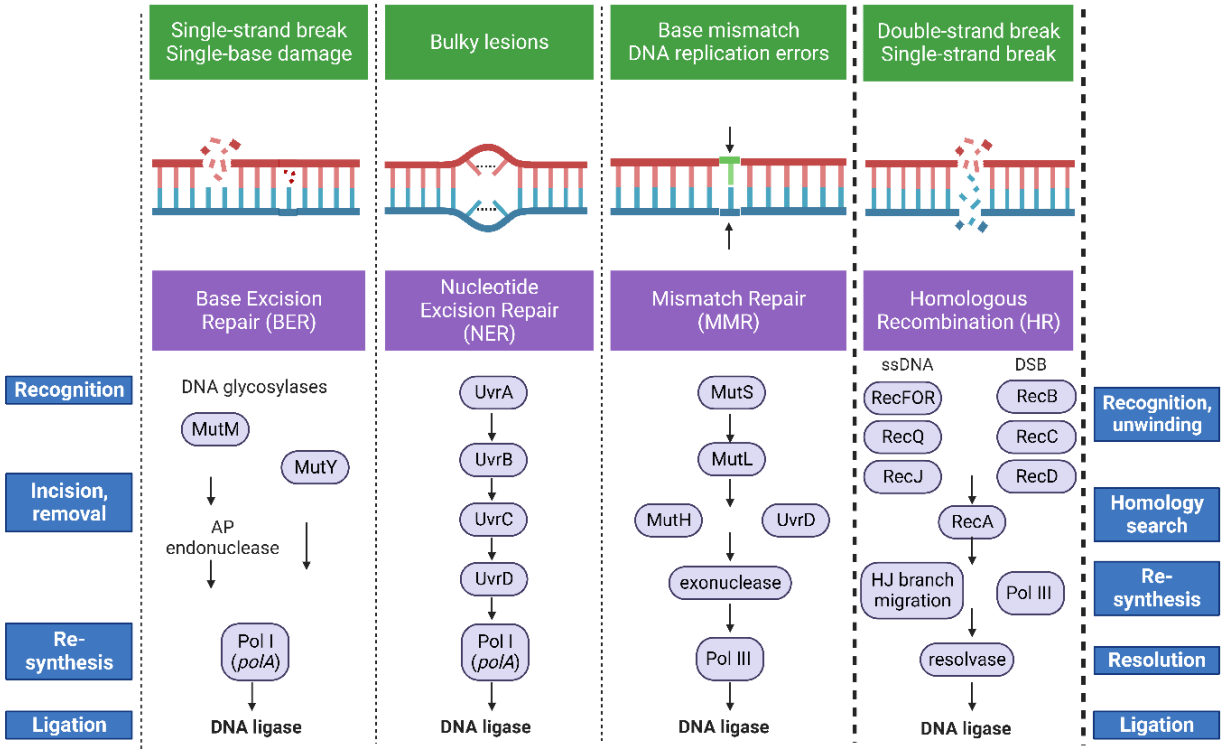


Figure 2: The arsenal of DNA damage repair pathways employed by bacteria: excision and recombination mechanisms. Depending on the DNA damage encountered, the cells are equipped with multiple pathways to recognise the lesions, excise and remove the lesion, and then resynthesise and ligate the lesion, allowing DNA replication to continue. Among these pathways, homologous recombination has two different complexes to recognise and bind lesions before recruiting a recombinase RecA. It then operates branch migration to find and use homologous DNA as a template for the synthesis of DNA, before resolution of the HJ complexes formed and DNA ligation.

2.2.1. Base Excision Repair (BER)

ROS can damage bases with the most common oxidative damage being 7,8-dihydro-8- oxoguanine (8oxoG) and can result in AP sites which are caused by hydrolysis during repair of the link between a base and its deoxyribose sugar (Dizdaroglu, 2012; Wozniak & Simmons, 2022). The BER pathway, which removes and replaces damaged DNA bases including oxidised bases, is highly conserved (Baute & Depicker, 2008). BER involves DNA glycosylases that recognise a lesion with a damaged base. These can cleave the N-glycosidic bond in DNA to release the base and create an AP site. This

involves an AP endonuclease to cleave the DNA backbone, and an exonuclease to process the backbone to generate a primer with 3' OH for DNA re-synthesis. If the glycosylases contain AP lyase activity (bifunctional glycosylase), they can bypass the need for an AP endonuclease and process the DNA backbone for the action of DNA polymerase I (Pol I encoded by polA) filling the gap and followed by DNA ligase (Baute & Depicker, 2008). In the case of 8oxoG paired with a cytosine, the DNA glycosylase MutM can recognise the base, and cleave the N-glycosidic bond, creating an AP site. (Fromme & Verdine, 2002). If 8oxoG is paired with adenine, the DNA glycosylase MutY removes wrongly paired adenine, creating an AP site for the insertion of cytosine, making it the perfect substrate for MutM (Tsai-Wu et al., 1992). Additionally, MutT hydrolyses 8oxoGTP in the nucleotide pool to produce 8oxoGMP, preventing its incorporation into DNA (Maki & Sekiguchi, 1992).

2.2.2. Nucleotide Excision Repair (NER)

For NER, the pathway is often used to repair bulky DNA lesions, such as the cyclobutene pyrimidine dimers formed by UV light. Unlike the large number of damage-specific glycosylases in the BER pathway, NER involves one set of proteins to recognise and repair a large range of lesions (Kraithong et al., 2021). In the pathway, the genes *uvrABCD* are involved. UvrA is an ATP-binding cassette ATPase acting as a damage sensor bound to DNA and ATP to search for and detect lesions in the form of the dimer $UvrA_2$. It then recruits UvrB ATPase which forms a tight pre-incision complex on DNA followed by UvrA release (DellaVecchia et al., 2004; Stracy et al., 2016). UvrC is an endonuclease that binds next to UvrB to form an incision complex and make two incisions on both the 3' and 5' ends of the lesion (Verhoeven et al., 2000). It is followed by excision of the damaged ssDNA by the UvrD helicase, leaving a 12 nucleotides ssDNA gap. The gap is then filled by DNA polymerase Pol I and ligated by DNA ligase to restore the original undamaged sequence (Kraithong

et al., 2021). Transcription-coupled repair is also part of the NER pathway, repairing lesions including R-loops which are RNA-DNA hybrids that block RNA polymerases on the transcribed strand of active genes. In that case, the RNA polymerase recognises the lesion and is displaced before the recruitment of the UvrAB complex or other NER nucleases such as XPG for R-loops (Spivak, 2016; X. Zhang et al., 2022).

2.2.3. Mismatch Repair (MMR)

The MMR pathway is involved in repairing DNA replication errors, including mis-incorporated nucleotides, and small insertions and deletions which happen at a rate of approximately 1 error for every 59 million bases replicated (Schroeder et al., 2016). The pathway requires MutS, MutL, MutH, and UvrD (Modrich, 1989). MutS has an ATPase activity and acts as a mismatch-sensing protein sliding and scanning DNA for lesions and is in the form of a homodimer when bound to mismatch (G. M. Li, 2008). MutS then recruits and activates MutL in an ATP-dependent reaction. MutL also has an ATPase activity and forms a dimer with a role in stimulating the loading of the helicase UvrD. MutL is also essential for the activation of MutH and interacts with Pol III (Guarné et al., 2004; Junop et al., 2001; F. Li et al., 2008). MutH has an endonuclease activity and recognises hemi-methylated sequences. It can incise specifically the unmethylated newly synthesised DNA strand upon recruitment (Modrich & Lahue, 1996). The UvrD helicase then binds and unwinds the DNA just past the mismatch (Dao & Modrich, 1998), generating ssDNA which is rapidly bound and protected by SSB. The ssDNA that is displaced by UvrD is degraded by an exonuclease. Then ensues DNA resynthesis by Pol III and DNA ligation (Modrich & Lahue, 1996). Interestingly, it has been shown that the β_2 sliding clamp in the replisome is involved in positioning the protein MutS on newly replicated DNA to initiate repair (Lenhart et al., 2013) and interacts with MutL to stimulate its endonuclease activity (Pillon et al., 2015), further linking MMR and DNA replication.

2.2.4. Homologous Recombination (HR)

Homologous recombination is involved in repairing DNA lesions such as collapsed replication forks, and double-strand breaks (DSB). It involves RecA, a tightly regulated recombinase which forms a nucleoprotein filament made of RecA monomers with single-strand DNA (ssDNA) at sites of DNA break. It requires ATP and Mg^{2+} as cofactors and is involved in the search for homologous double-strand DNA (dsDNA), to use as a template for repair of DNA (Del Val et al., 2019). SSB binds and stabilises ssDNA, facilitates RecA binding to ssDNA and stimulates strand exchange by binding to displaced ssDNA (Kowalczykowski & Krupp, 1987; Lavery & Kowalczykowski, 1992). RecFOR proteins are involved in loading RecA onto SSB-coated ssDNA (Morimatsu & Kowalczykowski, 2003) in the context of single-strand gap repair. In the RecFOR pathway, RecQ initiates recombination by unwinding DNA at lesion sites (Umezu et al., 1990), and RecJ is a 5'-3' exonuclease processing the unwound DNA (Lovett & Kolodner, 1989). RecBCD proteins process DSBs and load RecA directly onto ssDNA, in the context of double-strand break repair (Del Val et al., 2019). The RecBCD complex comprises two ATP-dependent helicases of opposite polarity RecB and RecD that bind to broken DNA, unwind it and translocate along the two single strands (Taylor & Smith, 2003; Wigley, 2013). It also contains the protein RecC that recognises Chi (crossover hotspot instigator) sequence to switch the complex such that it preferentially degrades the 5' end, leading to the formation of a 3' ssDNA overhang and recruitment of RecA (Cheng et al., 2020; Spies & Stephen C. Kowalczykowski, 2005). RecB also has nuclease activity that cuts ssDNA as it emerges during the unwinding process. In HR, once homology is found by the RecA nucleoprotein filament rapidly and stringently, strand invasion between the ssDNA and the homologous dsDNA proceeds, causing a D-loop or the formation of a heteroduplex complex (Camerini-Otero & Hsieh, 1995). DNA repair synthesis is initiated within the D-loop using the invading ssDNA and copying off the template invaded dsDNA.

Extension of the heteroduplex DNA results in an important intermediate, the Holliday Junction (HJ), linking recombining chromosomes (Li & Heyer, 2008). In *E. coli,* RuvA and RuvB are involved in the processing of HJ by promoting branch migration, with SSB facilitation (Michel et al., 2007; Parsons et al., 1995). Finally, the complex will undergo resolution and ligation by DNA ligase (Del Val et al., 2019). Resolution is performed by the RuvAB complex interacting with the endonuclease RuvC, which introduces symmetrical cuts in the junction, leading to the separation of the recombined DNA molecules (Bennett et al., 1993).

2.2.5. Direct DNA Repair

In contrast to the mechanisms mentioned above, bacteria also possess means to address DNA damage without excising and re-synthesing DNA, to resolve toxic lesions. Indeed, to repair certain lesions such as UV lesions or lesions from alkylating agents, cells have developed direct reversal mechanisms (Couvé et al., 2013). It has been shown that DNA alkylation damage can be toxic and causes an initial increase in mutagenesis (Uphoff, 2018), prompting the cells to repair these. In the case of UV lesions, they are repaired via photoreactivating enzymes or photolyases which are flavoproteins such as PhrB which can catalyse the reversal of pyrimidine dimers directly (Dizdaroglu, 2012). Photolyases revert DNA damages UV-light using blue wavelengths as an energy source to break the dimer bond (Kavakli et al., 2017). DNA alkylating damage can also be directly reversed by DNA-methyltransferases such as the Ada protein (Sedgwick & Lindahl, 2002), or oxidative demethylases such as the AlkB protein in *E. coli* (Trewick et al., 2002). However, it appears that the Ada protein is distributed heterogeneously within bacterial populations, with some cells having none, which delays their response to lesions and increases their mutation rate (Uphoff et al., 2016).

2.3. DNA Damage Tolerance

Whilst the cells possess a large panoply of repair systems to remove lesions or strand breaks ahead of the replisome reaching the lesions, DNA replication progression can be inhibited or stalled transiently when the replisome encounters unrepaired DNA lesions. This happens frequently each cycle even during normal growth, leading to disengagement of the replisome components and regression of the replication fork to allow for DNA repair (Bianco, 2020). It has been reported that DNA replication can reinitiate downstream of the lesion with new priming synthesis events (Yeeles & Marians, 2013). Additionally, the cells have a DNA damage tolerance pathway, translesion synthesis (TLS), using the TLS polymerases, Pol II (*polB*), Pol IV (*dinB*) and Pol V (*umuDC*). Indeed, it has been shown that the sliding clamp of the replisome can simultaneously bind Pol III and the TLS Pol IV, to enable exchange between the polymerases. This allows the cells to bypass templates with mismatched base pairs and bulky DNA lesions (Kath et al., 2014), although this DNA damage tolerance mechanism can lead to misincorporation of nucleotides (Henrikus et al., 2018). In TLS, the polymerases ensure continuity of DNA replication and allow cell survival, potentially rendering them error-prone with no proof-reading abilities (except Pol II). This leads to high chances of incorrect base insertions that could be incorporated as mutations during DNA replication (Henrikus et al., 2018). TLS is involved in the bypass of DNA damaged by UV light, oxidative damage, or alkylating agents (Maslowska et al., 2019). One example of a lesion is interstrand cross-links (ICLs), which form a bond between two DNA strands, preventing replication and transcription. ICLs are repaired by a combination of NER and HR or TLS. NER creates an incision site around the lesion from one strand and HR or TLS in the absence of a homologous template to fill in the gap. This is followed by a second round of NER excise the crosslinked fragment (Siede, 2020).

3. REGULATION OF STRESS RESPONSES

3.1. The SOS Response to DNA Damage

Since many of the DNA repair genes described above can be highly mutagenic when overexpressed (Acharya et al., 2003; Kim et al., 1997; Yang et al., 2004), bacteria have a strong incentive to exert tight control over them and only activate these in the presence of abundant damage to be repaired. An example is the SOS response which allows cell survival and continued DNA replication in the presence of DNA damage, although it can lead to elevated mutagenesis in cells (Maslowska et al., 2019). It is controlled via a variety of mechanisms, including transcriptional de-repression, post-translational activation and inhibition. It is initiated by the accumulation of ssDNA, as a result of lesions arising during DNA replication under normal growth conditions. It can also be initiated by replication fork arrest due to RNA polymerase bound to DNA and forming R loops that can turn into DSBs (Merrikh et al., 2012) or by external agents that cause direct DNA damage (Baharoglu & Mazel, 2014). The two proteins that play major roles in the SOS response are the transcriptional repressor LexA and RecA (Fig.3). Under normal growth conditions, LexA which is a dimer, represses the SOS regulon genes (40 in *E. coli,* (Courcelle *et al.*, 2001)) by binding to a specific sequence, the SOS box in their promotor region (A. P. P. Zhang et al., 2010). The formation of RecA nucleoprotein filaments on ssDNA is the trigger signal for the SOS response, as it catalyses the self-cleavage of LexA (Baharoglu & Mazel, 2014). The degradation of LexA repressor leads to the de-repression of the SOS regulon genes.

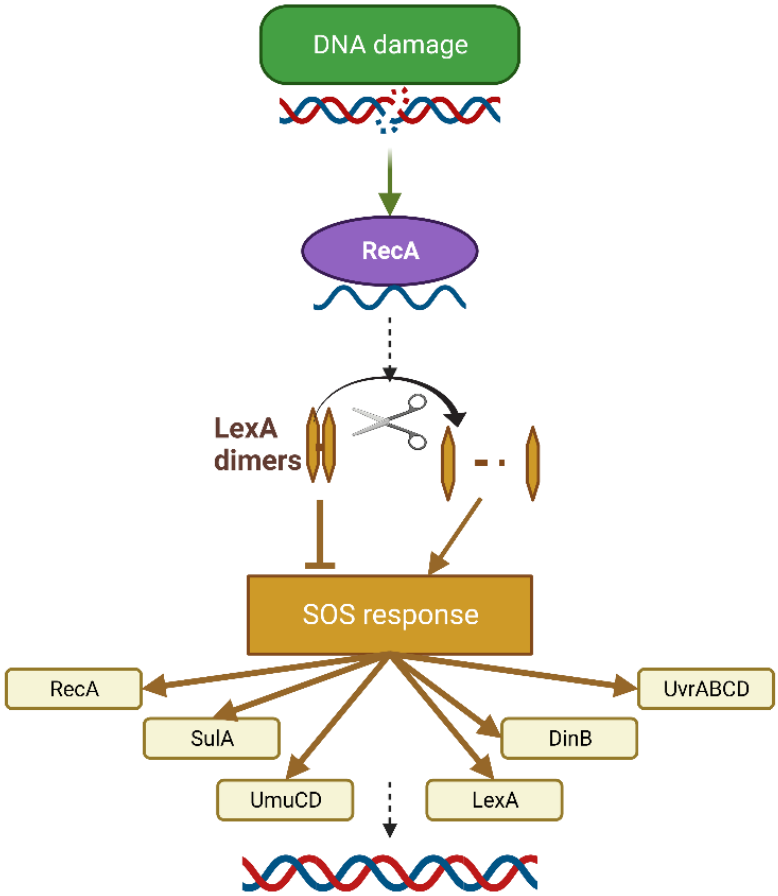


Figure 3: The SOS response is activated in bacteria in response to DNA damage. The RecA protein will recognise and bind to ssDNA, leading to its activation and catalysation of the auto-cleavage of the transcriptional repressor LexA. This leads to the induction of the SOS response genes involved in DNA repair and other functions in the cells.

The activated genes in the SOS response include *lexA* itself and are involved in diverse functions in response to DNA damage. This includes repair with genes of the NER pathway, tolerance with genes of the HR and the TLS pathways, helicases such as DinG and UvrD to remove RNA Polymerase complex and R loops in DNA (Boubakri et al., 2010; Courcelle et al., 2001). It has been shown that RecA regulates the replisomes by inhibiting the progression of Pol III and stimulating replication by TLS polymerases (Indiani et al., 2013). The protein SulA (Cole, 1983), works by interacting directly with FtsZ, a major protein involved in cell division. FtsZ self-assembles into Z rings to form the divisome in bacteria undergoing cell division (Bi & Lutkenhaus, 1991). It has been suggested that SulA inhibits FtsZ either by sequestering the protein (Mukherjee et al., 1998) or by capping and

destabilising the polymerising protein which seems more likely *in vivo* (Trusca et al., 1998; Vedyaykin et al., 2020).

The SOS response is tightly regulated so not all genes are induced at the same time but rather according to the damage detected. Indeed, DNA repair mechanisms can work together to repair certain lesions, for instance, the SOS response can be induced together with BER, NER or HR. This means that DNA repair genes are activated first, leading to DNA synthesis as a later and final step being performed by one of the TLS polymerases, which could promote mutagenesis. Several SOS proteins are involved in this precise modulation. LexA autoregulates its own gene, which allows for SOS repression when RecA filaments are disassembled and LexA is no longer cleaved (Maslowska et al., 2019). Interestingly, Pol II, which is a high-fidelity polymerase, is regulated by both the SOS response and the RpoS regulon which helps maximise cell survival, suggesting it plays a very important role in genome stability (Dapa et al., 2017). Pol IV, encoded by *dinB* in *E. coli* and also regulated by the SOS response and RpoS regulon, has been suggested to be recruited to sites of DSBs to help in the restoration of DNA replication (Mallik et al., 2015). Together with RecA, it plays a role in slowing down replication during the SOS response (Tan et al., 2015). Pol V is made of UmuC monomer and UmuD' (cleaved) homodimers activated by RecA-catalysed cleavage. It has a strong mutagenic potential necessitating tight regulation by LexA, RecA and an ATPase activity (Goodman et al., 2016). Pol V, due to its low processivity and speed also functions in delaying DNA replication until after DNA damage repair (Chaurasiya et al., 2013; Opperman et al., 1999).

3.2. Oxidative Stress Response to Reactive Oxygen Species (ROS)

The abundance of oxygen in the atmosphere has resulted in cells evolving to respond to reactive oxygen species. They typically arise endogenously as by-products of aerobic metabolism. This includes the electron transport chain and TCA cycle or an accidental collision between oxygen and flavoprotein causing their oxidation (Korshunov & Imlay, 2011). An electron reduction series then generates superoxide O_2^- , hydrogen peroxide H_2O_2, and hydroxyl radical (HO·) (Imlay, 2013b). Additionally, ROS can arise exogenously in the environment or be used as a weapon in bacterial interspecies competition. For instance, cells can use the secretion of redox-cycling molecules that can penetrate the membrane unlike O_2^- to transfer electrons to oxygen (Sen & Imlay, 2021). In contrast, uncharged H_2O_2 can penetrate the bacterial membrane and be released directly by a range of cells including immune cells such as phagocytes and lactic acid bacteria. H_2O_2 can also be formed in the environment via photochemistry and reactions between oxygen and sulphur (Imlay, 2019).

It has been shown that ROS can cause growth defects in cells and lead to amino acid auxotrophies in *E. coli* (Imlay, 2013a). Indeed, ROS can directly oxidise metal centres of key metalloenzymes, particularly dehydratases rendering them inactive and causing disruption of biosynthesis pathways (Khademian & Imlay, 2021). ROS can also react with iron in cells to form highly reactive HO· radicals via the Fenton reaction. These radicals in turn oxidise DNA leading to the formation of various DNA lesions such as 8oxoG lesions, further causing mutagenesis and DSBs (Belenky et al., 2015; Khademian & Imlay, 2021). Hence, the cells are equipped with scavenging enzymes, catalases, and peroxidases to keep the levels of ROS low. Scavenging enzymes under normal growth conditions include superoxide dismutases (SODs) to keep a steady state subnanomolar concentration at 0.1 nM of O_2^- (Imlay & Fridovich, 1991). On the other hand, catalases and peroxidases degrade H_2O_2 (Imlay, 2013a). In *E. coli*, there are two oxidative stress regulons regulating up to 50 genes (Seo et

al., 2015), the SoxRS system that protects from O_2^- and the OxyR system that detoxifies the cells of H_2O_2 (Fig.4).

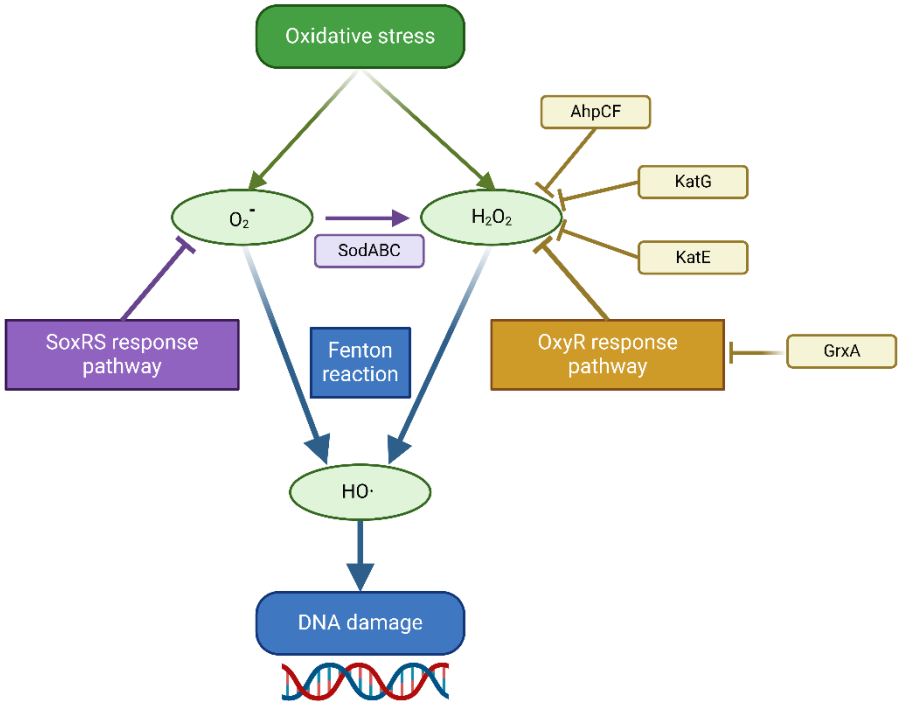


Figure 4: The mechanisms of ROS detoxification in bacteria include two pathways. The SoxRS pathway detoxifies the cells of superoxide using the dismutases SodABC to convert superoxide into hydrogen peroxide. The OxyR pathway then detoxifies the cells of hydrogen peroxide with catalases and scavengers such as KatEG and AhpC.

In *E. coli*, there are three SODs produced abundantly to prevent endogenously generated O_2^- from damaging vulnerable and vital enzymes (Imlay, 2008). Superoxide dismutases yield O_2 and H_2O_2 from O_2^- (Klug et al., 1972). They include cytoplasmic iron (FeSOD or SodB in *E. coli*) and manganese (MnSOD or SodA) cofactored enzymes and a periplasmic copper zinc cofactored enzyme (Cu–Zn SOD or SodC) (Imlay, 2013b). FeSOD and MnSOD are co-ordinately regulated by the Fur repressor to make FeSOD the default enzyme in normal growth and high iron levels. In contrast, MnSOD acts in the presence of low iron levels and superoxide-generating antibiotics and can be induced by the SoxRS pathway (Imlay, 2013a). Catalases and peroxidases scavenging H_2O_2 in *E. coli* include catalase

G (KatG), catalase E (KatE), and the two-component NADH alkyl hydroperoxide reductase (AhpCF) (Seaver & Imlay, 2001). AhpCF is the primary scavenging enzyme under normal growth conditions and transfers electrons from NADH to H_2O_2 producing water. On the other hand, KatG is a catalase expressed during the exponential phase that can be induced by the OxyR pathway whilst KatE is expressed in stationary phase and induced by the RpoS pathway.

The SoxRS system gets activated when cells are exposed to redox-cycling molecules forming O_2^-. It is regulated by the SoxR sensor protein, which becomes oxidised in the presence of O_2^-, and binds upstream of the *soxS* gene to activate transcription. SoxS is a transcriptional activator and is degraded quickly when SoxR returns to its normal state (Imlay, 2013b). SoxRS-induced proteins work to pump out ROS from the cytoplasm via drug efflux pumps such as AcrAB or TolC (X. Z. Li et al., 2015) or chemically modify them like the NADPH nitroreductase NfsA (Liochev et al., 1999), and include the superoxide dismutase SodA (Seo et al., 2015). The OxyR pathway gets activated by high intracellular levels of H_2O_2. OxyR is a transcription factor that is oxidised by H_2O_2 to produce a disulphide-bonded activator form with enhanced DNA binding ability whilst the reduced form is a repressor (Sen & Imlay, 2021). The activated genes serve to reduce H_2O_2 accumulation, repair oxidative damage, or reduce iron levels in cells. These include AhpCF and KatG, the iron-uptake repressor Fur, and GrxA a glutaredoxin that reduces the disulphide bond in OxyR to deactivate the response when H_2O_2 levels decrease (Imlay, 2013a; Sen & Imlay, 2021).

3.3. The Acid Stress Response to Low pH

In response to low pH, bacteria have evolved acid-resistance mechanisms to survive. In *E. coli*, up to five response systems have been described, AR1-AR5, protecting cells in stationary phase mainly,

with only AR2 and AR3 during exponential growth, in addition to an acid-tolerance response system (Xu et al., 2020). The AR1 system requires the sigma factor RpoS and cyclic AMP receptor protein and is repressed by glucose. The other systems are dependent on diverse exogenously supplied amino acids such as glutamate, arginine or lysine and require antiporters and decarboxylase enzymes induced at low pH (Lin et al., 1995). It has been suggested that the most effective system for protection is the glutamate decarboxylase/antiporter dependent GAD system, with the glutamate decarboxylase GadA or GadB in AR3 and the glutamate/γ-aminobutyric acid antiporter GadC (Castanie-Cornet et al., 1999). Regulation of the system is complex and involves over 20 proteins including RpoS and GAD family proteins (Xu et al., 2020). Resistance is then conferred by the consumption of an intracellular proton during amino acid decarboxylation to increase the cell pH, producing CO_2 and γ-aminobutyric acid in the process. Resistance also comes from the export of decarboxylated amino acid to further raise the intracellular pH via antiporters, in exchange for new amino acid products (Castanie-Cornet et al., 1999; Foster, 2004).

3.4. RpoS General Stress Response

On top of the aforementioned specific stresses, global gene regulation is required for cells to adapt and resist their environment. In *E. coli*, the RNA polymerase σ–factor RpoS controls up to 23% of the genome (Wong et al., 2017) and can be activated by various stresses, forming the general stress response. It is activated only during stationary phase and under growth-suppressing conditions (Weber et al., 2005). RpoS levels increase by several folds during the stationary phase although RpoS gets rapidly degraded under rapid growth conditions and are regulated by transcription, translation and protein degradation, or other factors such as small regulatory RNAs (Battesti et al., 2011; Lange & Hengge-Aronis, 1994). Since sigma factors determine promotor recognition, RpoS

then exerts control over expression levels of RpoS-dependent genes (Battesti et al., 2011). These genes have varying levels of sensitivity to RpoS, in turn controlling the responses to stress conditions (Wong et al., 2017). It thus can be involved in the acid stress response via the *gadC* RpoS-dependent gene, the stringent response whereby ppGpp stabilises RpoS or the oxidative stress response with the *katE* catalase being RpoS-dependent (Battesti et al., 2011). The stringent response is a ubiquitous stress response pathway in bacteria that is activated by nutrient starvation. When cells are starved for amino acids, it leads to ribosome stalling and accumulation of uncharged tRNA in the ribosomal A site, acting as a marker for starvation (Brown et al., 2016). The protein RelA senses stalled ribosomes and is recruited to synthesise secondary messenger molecules. This then causes an accumulation of alarmones guanosine tetraphosphate (ppGpp) and guanosine pentaphosphate (pppGpp). These are common signalling nucleotides formed from GDP and GTP respectively and synthesised by the RelA and SpoT proteins (Irving et al., 2021). These nucleotides are known to act on RNA polymerase to alter global transcription (Dalebroux & Swanson, 2012). Thus, accumulation leads to changes in cell physiology and biological processes to allow for cell survival. This includes altering DNA replication by inhibiting the primase DnaG (Maciag et al., 2010), or inhibiting *de novo* biosynthesis of purine nucleotides by targeting one of the enzymes involved PurF (Wang et al., 2019). The stringent response can cause inhibition of protein translation to reduce the cell's growth rate (Irving et al., 2021; Sanchez-Vazquez et al., 2019) while facilitating DNA lesion repair activities (Sinha et al., 2020).

4. MUTATIONS AND GENETIC ADAPTATION

Exposure to stress conditions including antibiotics can exert a selection pressure for bacteria leading to genetic adaptation which in turn results in increased resistance, as for antibiotic

resistance. Mutation rates can be increased by direct damage to DNA or induction of mutagenic processes such as low-fidelity polymerases within cells (MacLean et al., 2013). In bacterial cells, as previously mentioned, the SOS response is known to be mutagenic, even for non-damaged DNA. It causes elevated mutagenesis in cells by activating error-prone factors to allow survival despite extensive DNA damage, which could overload the DNA repair pathways and lead to mutation accumulation (Didier et al., 2011; Maslowska et al., 2019). In addition to that, it is known that oxidative stress is accompanied by an initial burst in mutagenesis which can help the cells in their genetic adaptation to stress (Lagage et al., 2023). Oxidised guanine formed in contact with ROS produced indirectly during antibiotic treatment and incorporated into DNA can cause an increase in mutation past the DNA lesions (Sobol, 2012). These lesions can also be toxic if unrepaired by BER, causing DSBs (Foti et al., 2012).

In many instances, the SOS response has been associated with the evolution of antibiotic resistance (Poole, 2012). Indeed, the SOS response can be induced by antibiotics, such as ciprofloxacin (Beaber et al., 2004; Cirz et al., 2005; Crane et al., 2021), even when used at sub-inhibitory concentrations, and can promote mutagenesis (Baharoglu & Mazel, 2011, 2014)). Thus, antibiotics can influence the development of multidrug resistance, rendering even more antibiotics ineffective for patients' treatment (Denamur et al., 2005). Multiple studies have suggested another role of the SOS response in increasing horizontal gene transfer (HGT), potentially playing a role in the dissemination of antibiotic resistance genes in bacterial populations (Beaber et al., 2004). Additionally, since SOS induction can be in response to HGT (ssDNA during conjugation and transformation) (Baharoglu et al., 2010, 2012), this can lead to genome plasticity with mutations, integration or rearrangement of adaptation factors. Indeed, it has been suggested that antibiotics can induce the expression of resistance genes to themselves via the SOS response (Da Re et al., 2009). They can also induce resistance against other antibiotic classes via rearrangement of

integrons containing resistance cassettes (Hocquet et al., 2012; Hocquet & Bertrand, 2014) and performed by SOS-regulated integrases (Cambray et al., 2011). Persistence, a reversible state of tolerance in which cells are not killed by treatment and resume growth after removal of the antibiotic stress (K. Lewis, 2010), can be induced by SOS response which in turn activates the toxin TisB, decreasing growth rate (Dörr et al., 2010).

Solutions are required to circumvent the dramatic issue of antimicrobial resistance which is a leading cause of death around the world (Murray et al., 2022). To that end, inhibitors of the SOS response are being studied (Yakimov et al., 2021). A proof of principle for quinolone resistance reversion was provided in Recacha et al., 2017. A successful example of the use of engineered bacteriophages suppressing the SOS gene network to enhance quinolone treatment and for other bactericidal antibiotics was described by Lu & Collins, 2009. Nanobodies have also been used to suppress the SOS response by targeting LexA autocleavage (Maso et al., 2022).

Whilst a lot of studies have investigated the many responses exhibited by bacteria when confronted with stressors, it remains a challenge to understand the complex mechanisms of action of antibacterial agents. Their real impact on bacteria and their metabolism sometimes leading to adaptation or resistance remains very unclear for most if not all classes of antibacterial agents currently in use for human treatments (Baquero & Levin, 2021). One common example of that is the oxidative stress response. One study has suggested ROS formation as a key element for death due to antibiotics of a large range of classes, including aminoglycosides (Kohanski et al., 2007), but this has been challenged in other conditions (Liu & Imlay, 2013). Indeed, for the antibiotic trimethoprim, many mechanisms of action have been suggested but also challenged (reviewed in Chapter 2). Currently, most of the knowledge on the mechanism of action of TMP arises from

studies using knockout and overexpression mutant population, genome-wide genetic screening for bacterial responses (Sangurdekar *et al.*, 2011), mass spectrometry for ROS measurements (Hong *et al.*, 2019), viability assays (Giroux et al., 2017; P. Rao & Kuzminov, 2019), or TMP-treated cell culture and sequencing (Baharoglu and Mazel, 2011). In the same manner, studies on the impact of toxins delivered inside prey cells via the T6SS system have revealed the involvement of many stress responses, using bacterial population assays of the DNA damage for instance (Pissaridou et al., 2018). These conventional *in vitro* biochemistry and genetic approaches, often performed at bulk population levels do not offer sufficient insight into temporal dynamics or heterogeneity. Moreover, they cannot inform on single cell level intricate mechanisms leading to different cellular states in individual bacteria, or potential survival strategies utilised by cells.

5. SINGLE CELL IMAGING

It is increasingly understood that a population-level response does not accurately represent what occurs in individual cells. Bacterial stress responses are known to be phenotypically heterogeneous in bacterial populations to improve survival of the population as a whole and diversify behaviours. Heterogeneity in genetically identical cells has been described for stochastic molecular events such as random molecular partitioning or search time, gene expression levels and noise or timings of induction (Fritz et al., 2019; Raser & O'Shea, 2005; Vincent & Uphoff, 2020). For instance, it was shown that individual cells present a lot of heterogeneity in SOS response induction, even in the absence of stress exposure (Jones & Uphoff, 2021). It was also suggested that cell-to-cell interactions between bacteria can lead to phenotypic heterogeneity in the oxidative stress responses, via mechanisms of shielding at the individual cell level (Choudhary et al., 2023). Thus, this can result in different fates in individual bacteria within a genetically identical population,

whereby cell mortality or mutation rate heterogeneity can happen. Interestingly, the dynamics followed by these stresses in individual bacteria are often unknown and studied at the population level and in end-point experiments with little time resolution. Hence, cutting-edge methods studying cells closely and at a single cell level to probe heterogeneity are needed to further the understanding of the effect of stressors in bacteria.

Indeed, it is now possible to go beyond the resolution of genetics and bulk biochemical assays and uncover molecular heterogeneity and subpopulations (Uphoff & Sherratt, 2017). For instance, the recent development and use of techniques such as single molecule tracking to get quantitative insight into DNA repair mechanisms has greatly helped the understanding of DNA lesion repair pathways. Single-molecule methods allow us to observe the progression of repair pathways, and to study them at a single molecule level inside individual living cells (Hughes et al., 2014). This permits the resolution of molecular dynamics and variations at the cell level, which has revealed cellular heterogeneity for DNA lesion repair pathways (Vincent & Uphoff, 2021). Single-molecule methods can help detect lesions as they arise (Christian et al., 2009), but they can also be used to image the proteins binding to these lesions (Uphoff et al., 2016), which can help measure the location and abundance of damage sites (Stracy et al., 2016). Single-molecule tracking studies also allow measurement of protein intracellular diffusion and spatial distribution (Rösch et al., 2018; Stracy et al., 2021; Uphoff et al., 2013). Recently, using a single molecule imaging assay in individual cells to study the SOS transcriptional regulator LexA with a Halo Tag fusion and a TMR dye it has been shown that despite the fusion, the native LexA functions were retained (Jones & Uphoff, 2021). The study has also revealed that the regulator can be found in three states within the cells, DNA-bound stationary molecules, free LexA and degraded LexA species, giving insight into the mechanisms of LexA variability underlying SOS response cell-to-cell heterogeneity, showing how valuable these techniques are. Although direct observations of proteins can provide a huge wealth

of information, labelling strategies and fluorophores attached to proteins can perturb function or cause artefacts, which must be taken into account when interpreting results (Landgraf et al., 2012).

Another type of single-cell study, using microfluidic devices combined with time-lapse microscopy, allows for assays to be carried out over multiple generations and to follow response dynamics in single cells. These enable assays to be performed under precise and controlled conditions, using fluorescent reporters in many individual cells (Potvin-Trottier et al., 2018). Given the heterogeneity that exists within a population, the possibility of imaging at an individual cell level can be highly informative about real-time dynamics and their underlying molecular causes. Recent studies have used specifically mothermachine microfluidics devices which are designed so that cells can grow in linear trenches with one open end to allow for growth medium supply. The then mother cells in the trenches divide and grow pushing off daughter cells in the medium (Moffitt et al., 2012). Important understanding of DNA repair in bacteria has come from studies employing mother machine microfluidics devices. For example, the heterogeneity surrounding the Ada protein, involved in direct DNA repair has been greatly studied using these devices. It appears that in a population, the proteins are distributed heterogeneously with cells having sometimes no protein and being unable to respond to damage (Uphoff et al., 2016). Another example is the detection of foci formed by multiple copies of the MutL MMR protein with a fluorescent fusion binding to DNA replication errors (base mismatch, insertion/deletion), used as a proxy for mutagenesis (Elez et al., 2010; Uphoff, 2018). It has been shown to correlate well with estimates of the frequency of mutation rate in cells, although not all of the DNA mismatches are converted into mutations (1%) but repaired instead (Lagage et al., 2023; Vincent & Uphoff, 2021). A final example is the aforementioned study on the heterogeneity of the SOS response, which made use of single-molecule tracking combined with mother-machine microfluidic growth chambers, showing in microfluidics that SOS-dependent genes even in unperturbed conditions have heterogeneous

dynamics consisting of pulses in certain cells only (Jones & Uphoff, 2021). Overall, it appears that cell-to-cell heterogeneity, particularly in the context of stress responses, could lead to different levels of survival in individual cells than what is seen at the population level, an example of that being persistence (Dewachter et al., 2019).

Therefore, thanks to the new dimensions in understanding that these techniques can bring, they can be used to study complex and multi-layered mechanisms of action of a wide range of antibacterial agents damaging DNA. This can include antibiotics, here trimethoprim, or simpler and directed toxic effectors involved in bacterial competition, namely type six secretion system effectors. Hence, this study will make use of recently developed single-cell and single-molecule techniques to study the dynamics and heterogeneity of the stress responses induced in *E.coli* to further understand and compare the antibacterial agents.

CHAPTER 2 : REVIEW OF THE INTRICATE MECHANISMS OF THYMINELESS DEATH IN BACTERIA

The accurate replication of DNA is crucial for bacteria to pass on their genetic material to progeny cells during cell division. This process relies on the presence of the building blocks of DNA, the 5'-deoxyribonucleoside triphosphate DNA precursors (dNTPs) (Table 2). Thymidine is unique among the dNTPs since it is exclusively required for DNA but not RNA (Table 3). Intriguingly, starvation of thymidine, a pyrimidine essential for DNA, has been associated with a lethal effect – defined as thymineless death (TLD) – rather than growth arrest (Barner & Cohen, 1954). One explanation for this phenomenon whereby thymine appears as a very particular nucleotide in cells could be the evolution and acquisition of thymine within cells. For example, thymine could have had viral origins, evolved after the RNA precursors and have been acquired without associated mechanisms to prevent cell death in its absence (Rios & Tor, 2013), which in the context of a replicating virus would not be required. Indeed, TLD is observed in both eukaryotic and prokaryotic thymine auxotrophs, making it a target for various drugs that inhibit thymine biosynthesis, including chemotherapeutics like methotrexate and 5-fluorouracil (Alqarni & Zeidler, 2020; Longley et al., 2003) and antibiotics such as trimethoprim (Bushby & Hitchings, 1968). Despite decades of research, the exact mechanisms behind TLD remain elusive, with multiple hypotheses proposed but no definitive answers.

Table 2 : Nomenclature of bases, nucleosides and nucleotides in DNA

Base	Deoxyribonucleotide monophosphate
Adenine (A)	Deoxyadenosine monophosphate (dAMP)
Guanine (G)	Deoxyguanosine monophosphate (dGMP)
Thymine (T)	Deoxythymidine monophosphate (dTMP)
Cytosine (C)	Deoxycytidine monophosphate (dCMP)

Table 3 : Nomenclature of bases, nucleosides and nucleotides in RNA

Base	Ribonucleotide monophosphate
Adenine (A)	Adenosine monophosphate (AMP)
Guanine (G)	Guanosine monophosphate (GMP)
Uracil (U)	Uridine monophosphate (UMP)
Cytosine (C)	Cytidine monophosphate (CMP)

1. THYMINE BIOSYNTHESIS PATHWAYS

In *E. coli* cells, the final product and active form in the folic acid biosynthesis pathway named tetrahydrofolate (THF), needs to be synthesised *de novo* as bacteria do not possess an active transport system for its uptake. THF is part of the one-carbon metabolism, acting as a single-carbon donor and acceptor (Bermingham & Derrick, 2002). THF biosynthesis starts with the synthesis of para-aminobenzoic acid and 6-hydroxymethyl dihydropterin pyrophosphate to form dihydropteroate with DHP synthase (FolP). This is then converted into dihydrofolate (DHF) by dihydrofolate synthase (FolC), and finally, the dihydrofolate reductase (FolA) converts DHF into THF (Kordus & Baughn, 2019). THF can exist in different oxidation states and multiple interconvertible forms, including the 5,10-methylene THF, 5-methyl-THF or 10-formyl-THF. THF plays a pivotal role in cell metabolism. Indeed, it is an essential carbon donor for the synthesis of amino acids such as methionine and glycine, purines, and pyrimidines such as adenine and thymine (Bermingham & Derrick, 2002) (Fig.5).

Glycine is produced from serine in a reversible reaction, catalysed by serine hydroxymethyltransferase and using 5,10-methylene-THF (Ducker & Rabinowitz, 2017). Methionine is formed from homocysteine by methionine synthases which catalyse the transfer of a methyl group from 5-methyl-THF to homocysteine (Dawes & Foster, 1971). Purines are synthesised by transferring a formyl group from 10-formyl-THF converting glycinamide phosphoribonucleotide (GAR) to formylglycinamide phosphoribonucleotide (FGAR). This forms one of 11 enzymatic steps in the biosynthesis of purines which involve the enzymes in the Pur gene operon (Y. Zhang et al., 2008). The order in which depletion of folate-dependent metabolites takes place during TMP treatment has been shown to be glycine, then purines, methionine, and finally thymine (Kwon et al., 2010).

Generally, thymine can either be obtained via *de novo* synthesis or salvage pathway. Thymine biosynthesis *de novo* within the folate pathway starts with the transfer of a carbon to deoxyuridine monophosphate (dUMP) from 5,10-methylene THF. This reaction generates deoxythymidine monophosphate (dTMP), catalysed by thymidylate synthetase (ThyA) (Whittaker & Blakley, 1961). dTMP is then phosphorylated to deoxythymidine diphosphate (dTDP) by dTMP kinase and deoxythymidine triphosphate (dTTP) used in DNA by dTDP kinase (Ahmad et al., 1998). In *thyA* deficient cells, there is no thymidylate synthesis, resulting in a lack of dTMP, dTDP and dTTP. Thus, cells use a salvage pathway involving deoxyribose phosphate which is generated from dUMP in thymine-starved cells, to allow incorporation of exogenous thymine. It is then converted into thymidine in the cells for further use as dTMP (Ahmad et al., 1998). Exogenous thymine can be obtained from the growth medium or via DNA degradation during starvation releasing DNA precursors (Kuong & Kuzminov, 2012). The salvage pathway requires a transport protein called

nucleoside uptake (Nup) for extracellular thymidine and phosphorylation kinase to dTMP by thymidine (McKeown et al., 1976).

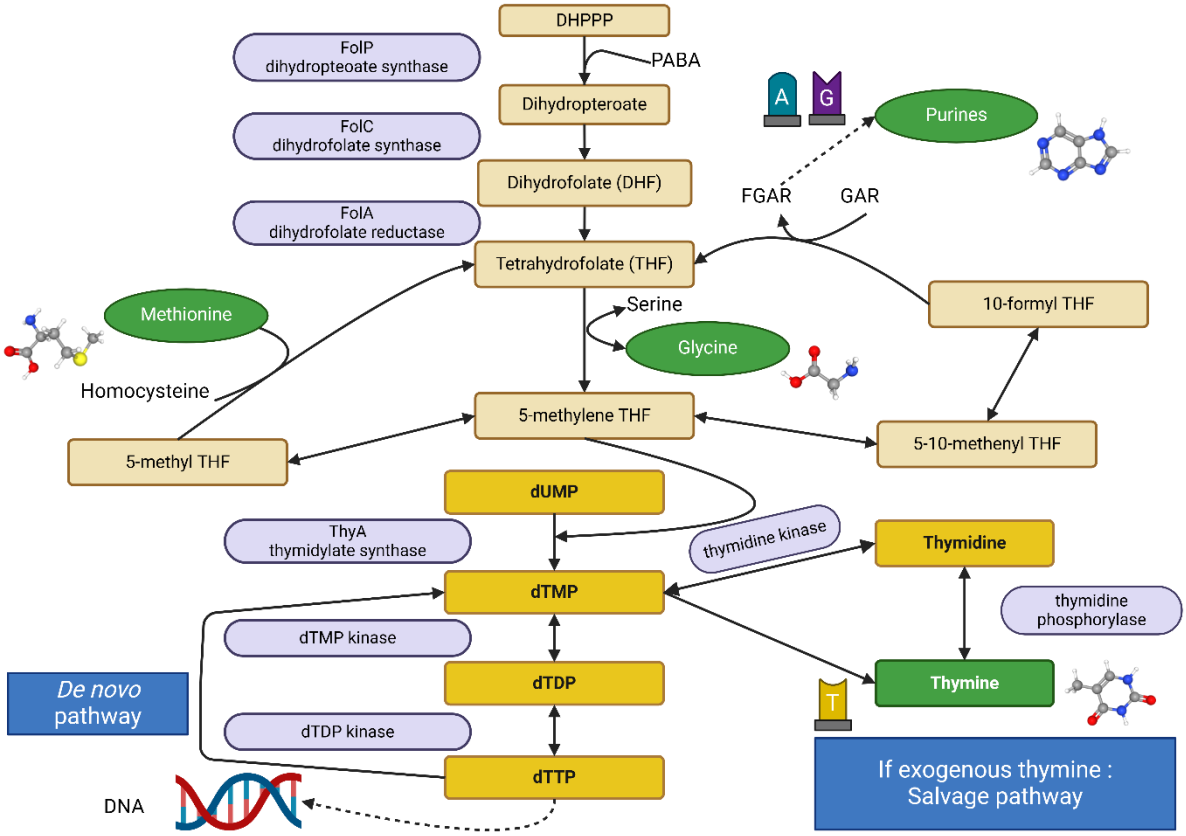


Figure 5 : Synthesis and usage of folic acid metabolites. Folic acid synthesis is complex and leads to the production of multiple metabolites including glycine, methionine, purines such as adenine, and the pyrimidine thymine. A variety of enzymes of the Fol family convert para-aminobenzoic acid (PABA) and 6-hydroxymethyl dihydropterin pyrophosphate (DHPPP) into tetrahydrofolate THF. THF is the final product and active form that can transfer 1-carbon groups at different oxidation states to form the metabolites listed above. For thymine, a de novo pathway involves kinases and thymidylate synthase to produce dTTP used in DNA. Additionally, thymidine phosphorylase can convert thymidine into thymine. For the salvage pathway using exogenous thymine or broken-down DNA, the key enzyme is thymidine kinase.

Thymine starvation can be induced by disrupting folic acid synthesis. Since folic acid is obtained from dietary sources in mammals, this makes it an attractive candidate as an antimicrobial drug target, leading to the development of a range of antifolate compounds (Estrada et al., 2016). Specifically, in bacteria, one means to disrupt it is to competitively inhibit the dihydrofolate

reductase FolA, which is the target of the antibiotic trimethoprim, a diaminopyrimidine antibiotic (Fig.6). Trimethoprim is often used in conjunction with sulfamethazole, a sulphonamide that competitively inhibits the enzyme dihydropteroate synthase, which acts synergistically with TMP (Bermingham & Derrick, 2002). The two antibiotics are commonly used in combination due to rising resistance in the targets of the individual antibiotics. In laboratory settings, the gene encoding the thymidylate synthase, thyA, is commonly deleted to study and induce TLD.

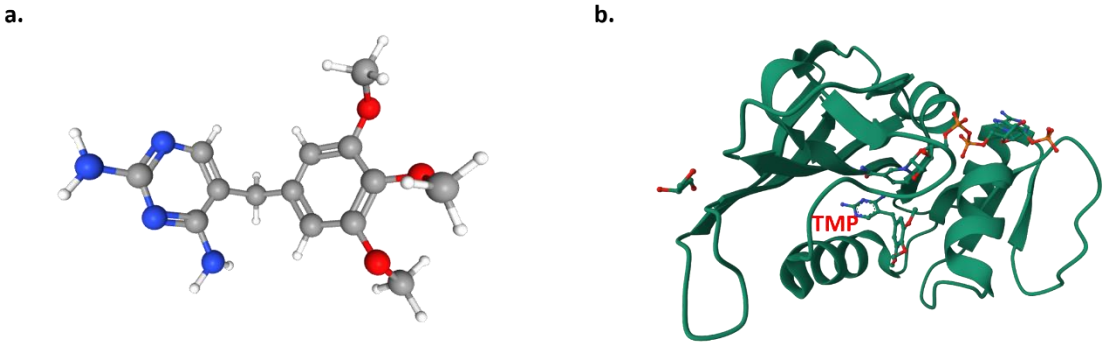


Figure 6 : Structure of the antibiotic trimethoprim. a) Trimethoprim 3D structure. PubChem Identifier: CID 5578, https://pubchem.ncbi.nlm.nih.gov/compound/5578. b) Structure of dihydrofolate reductase in complex with trimethoprim, modified from (Manna et al., 2021)

2. THE INVOLVEMENT OF DNA REPLICATION IN THYMINELESS DEATH

Thymineless death is described as comprising three phases: resistance or lag, rapid exponential death (RED) and survival phase (Fig.7). The resistance phase, serving to delay acute starvation, results from the availability of endogenous sources of thymine, leading to an accumulation of DNA but a stable titre and lasts about two generations in *E. coli*. The DNA amount returns to its original level during the RED phase, and the titre falls within a few hours. Finally, in the survival phase, the starved culture titre is completely stabilised and does not decrease any further (Kuong & Kuzminov, 2010; P. Rao & Kuzminov, 2019; T. V. P. Rao & Kuzminov, 2020).

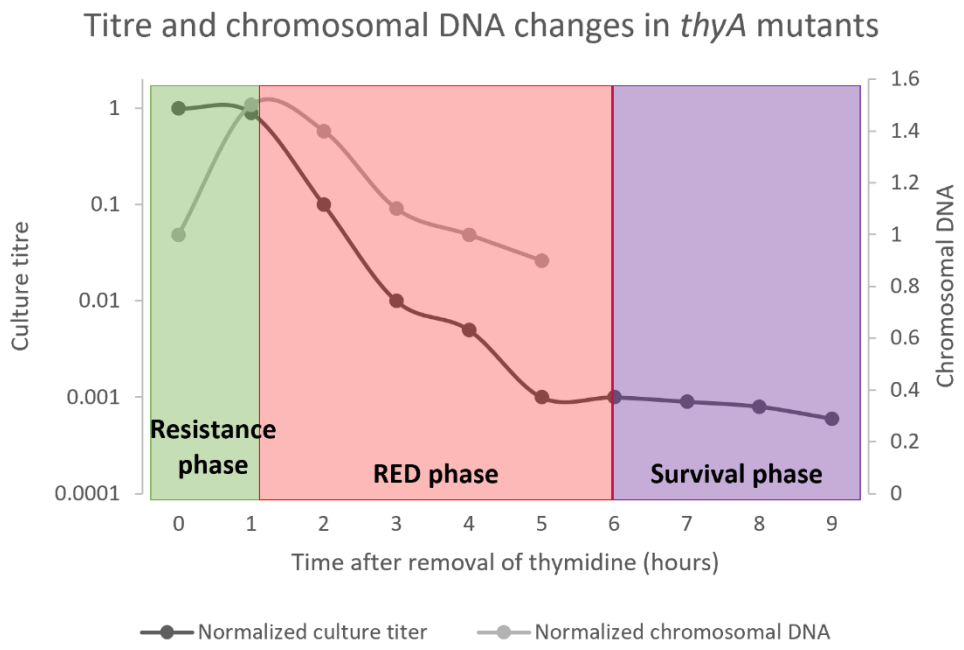


Figure 7 : Titre and chromosomal DNA changes in thyA mutants after removal of thymidine from the growth medium (Kuong & Kuzminov, 2010; P. Rao & Kuzminov, 2019; T. V. P. Rao & Kuzminov, 2020). The 3 phases of TLD are represented. Resistance phase with an increase in chromosomal DNA and a stable culture titre. Rapid exponential death (RED) phase with a decrease in chromosomal DNA and culture titre. Survival phase with a stable culture titre but unavailable data for the chromosomal DNA.

Originally, it was suggested that thymine starvation causes lethality due to unbalanced growth, whereby cell division stops but cells keep growing in length and width, and accumulating RNA, whilst DNA replication stops but processes of DNA repair continue (Cohen & Barner, 1954). This hypothesis of unbalanced growth was shown to not be the sole cause of death due to thymine starvation. Instead, it has been suggested that initiation of chromosomal DNA replication is essential for TLD. This was based on DNA labelling experiments that showed a correlation between the number of replication forks and the magnitude of TLD (Martín & Guzmán, 2011). New replication forks are formed at and around the origin of replication during TLD (Martín et al., 2014), but the newly synthesised DNA is fragmented and degraded to release thymine for further DNA replication initiations. This particularly happens during the resistance phase with a progressive decrease in *oriC* sequence and thus DNA during the RED phase, observed by Marker Frequency

Analysis (Kuong & Kuzminov, 2012). A study using fluorescent in-situ hybridization has suggested that thymine-starved cells exhibit chromosome degradation defects with a loss of the origin region, showing some small cells with segregated nucleoids whilst other cells appear elongated with a single small central nucleoid (Fonville et al., 2010).

Furthermore, a study has suggested a bimodal curve for how the amount of DNA changes over time, with an increase in DNA amount and chromosome fragmentation during the resistance phase, but a gradual decrease in DNA amount follows (P. Rao & Kuzminov, 2019). Measuring DNA synthesis rate in thymine-starved cells has indicated a decrease due to replication fork stalling. Additionally, it was suggested that stalled fork processing by recombinational repair can lead to chromosome fragmentation. Particularly, a study to identify transcriptional signatures associated with death due to thymine starvation has suggested a loss of genetic material around the origin of replication, accompanied by induction of the DNA damage response (Sangurdekar et al., 2010).

However, DNA fragmentation in thymine-starved cells is not required for cell death. It has thus been shown that TLD can still happen in cells expressing a plasmid copy of *deoA* gene (Khan & Kuzminov, 2022). The *deoA* gene encodes thymidine phosphorylase which converts thymidine into thymine instead of back to dTTP. This causes starving and halts the replication fork, further protecting DNA from disintegration and abolishing chromosome fragmentation (Khan & Kuzminov, 2022). Furthermore, TLD still occurs in non-replicating cells that are devoid of replication forks and do not exhibit DNA fragmentation (Khan & Kuzminov, 2022). Another study has shown that overinitiation of replication prior to thymine starvation does not sensitise cells to TLD. They also showed that blocking new replication initiations does not prevent TLD, but DNA in these cells is still lost, suggesting that DNA replication initiation is not needed for TLD (Khan & Kuzminova, 2019).

3. OXIDATIVE STRESS IN THYMINELESS DEATH

ROS that accumulate in cells at higher than basal level can cause toxic oxidative damage to DNA and proteins (Imlay, 2013a). This happens particularly via the Fenton reaction between H_2O_2 and iron in cells, creating toxic 8oxoG lesions, or via O_2^- oxidisation and damage of key enzymes. Hence, bacteria need to repair oxidative DNA lesions and detoxify themselves by using oxidative stress responses including the OxyR and SoxRS pathways. As for many other antibiotics, studies on the role of oxidative stress in TLD or TMP mode of action often disagree, causing a "ROS debate" (Fang, 2013).

Some studies at population level, using fluorescent dyes combined with flow cytometry or exogenous mitigating agents including catalases have suggested an accumulation of ROS during TLD, particularly after 1.5 h of starvation (Giroux et al., 2017; Hong et al., 2017; Ketcham et al., 2022). In their study, Hong et al., 2017 show the involvement of cellular respiration in ROS accumulation during TLD using a range of respiratory gene mutants. They also suggest the accumulation of ssDNA during starvation using an SSB fluorescent reporter, which is reduced in HR-deficient mutants *recQ* and *recF.* From these observations, they propose that the conversion of ssDNA lesions by ROS into DSBs underlies TLD. Indeed, ROS can cause base lesions within ssDNA, and the attempted BER of these lesions involves nucleases that cleave the DNA backbone, leading to DSB. It was also shown using catalase-overlaid LB agar plates that ROS accumulate even after TMP is removed, suggesting that cells die from post-stress ROS-mediated toxicity (Hong et al., 2019). Additionally, a transcriptional study has shown an upregulation of the oxidative stress response, particularly OxyR target genes suggesting a role of the OxyR oxidative stress response in TMP-treated bacteria (Sangurdekar et al., 2011). Another study has revealed that genes involved

in ROS production are downregulated whilst detoxification genes including the catalase *katE* are upregulated in TLD-resistant strains (Ketcham et al., 2022). However, another study has completely contradicted these findings, suggesting the absence of a role for ROS altogether (T. V. P. Rao & Kuzminov, 2022). This study used intracellular iron chelation, inactivation of H_2O_2 scavenging and treatment with sublethal H_2O_2 and found no impact on TLD kinetics. On the contrary, they observe that exogenous hydrogen peroxide treatment during TLD in cells whether catalase positive or negative, blocks TLD completely, having a bacteriostatic effect. Using hyper-TLD mutants, they show that the cells supplemented with H_2O_2 resume TLD after 2 h of arrest, suggesting that hydrogen peroxide blocks cell division in thymidine-starved cells.

The 2022 study by Rao & Kuzminov also contradicts the findings of greater sensitivity for catalase-deficient mutants in minimal medium (Giroux et al., 2017). The lack of effect of catalase absence on TLD survival was confirmed in a further study (Ketcham et al., 2022). Following on from the suggestion that ROS production can arise from DNA replication stalling (Davies et al., 2009), Giroux's team compared aerobic and anaerobic growth conditions using spot assays to assess survival of a range of mutants and Amplex red assays to measure raised ROS levels in treated cells. They also used transcription reporters at colony levels to assess increased expression of genes involved in OxyR and SoxRS oxidative stress responses in *E. coli*. Of note, they suggest that addition of exogenous catalase abolished cell sensitivity to TMP, whilst a mutated strain without catalase activity is hypersensitive to the treatment. Using strains impaired in the import of extracellular iron (*tonB* deletion), they suggest the toxicity of hydroxyl radical produced via the Fenton reaction in TMP-treated cells.

Finally, experiments using the antibiotic chloramphenicol to block protein synthesis (Okagaki et al., 1960; Pinney & Smith, 1972), or rifampicin to block RNA synthesis (Hanawalt, 1963; Martín et al., 2014) have suggested that RNA and protein synthesis are required for TLD. Specifically, this is because of the production of proteins involved in DNA replication cycles, or the impairment of transcription-dependent initiation (Martín et al., 2014; Martín & Guzmán, 2011). Another study has suggested that these antibiotics prevent TLD by reducing cellular respiration and suppressing the accumulation of ROS, which was observed using flow cytometry (Hong et al., 2017). Addition of chloramphenicol to prevent protein synthesis at the onset of starvation has been shown to eliminate TLD and chromosome fragmentation in cells (Khan & Kuzminov, 2022). However, a further study was unable to reproduce TLD blocking by rifampicin, rather showing that chronic rifampicin treatment kills thymidine-starved cells (T. V. P. Rao & Kuzminov, 2022).

4. DNA REPAIR PATHWAYS INVOLVEMENT IN THYMINELESS DEATH

It was suggested that there is an accumulation of ssDNA gaps in thymidine-starved cells (P. Rao & Kuzminov, 2019), which could in turn lead to DSBs (Kuong & Kuzminov, 2012; P. Rao & Kuzminov, 2019). Furthermore, thymine-starved cells accumulate DSBs as shown using pulsed-field gel electrophoresis and flow cytometry (Martín & Guzmán, 2011). Indeed, studies using *recQ*, *recO* and *recF* deficient mutants showed a decrease in TLD, suggesting a role of these HR genes in increasing ssDNA regions, which can then lead to toxic DSBs (Fonville et al., 2010; Hong et al., 2017; Kuong & Kuzminov, 2010). Additionally, *recBCD* mutants are hypersensitive to TLD due to their inability to repair DSBs, causing rapid chromosomal degradation and suggesting that DSBs are formed early during TLD (Kuong & Kuzminov, 2010; T. V. P. Rao & Kuzminov, 2022). Thus, RecBCD double-strand

exonuclease activity has been suggested to have a protective role in early resistance to TLD, and in helping maintenance of the nucleoid (Fonville et al., 2011).

If ROS are indeed a primary cause of TLD, then DNA repair pathways would be expected to promote survival, and loss of repair pathways would sensitise cells to treatment with TMP. However, (Giroux et al., 2017) found the opposite. Using strains harbouring a deleted BER pathway that removes 8oxoG, they conclude that the BER pathway has an important and lethal role in TMP-treated cells. Briefly, they suggest that thymine starvation causes ssDNA gaps due to the activity of BER proteins MutM removing 8oxoG lesions formed by ROS (Kasai & Nishimura, 1984) from DNA and MutY removing adenine from 8oxoG:A mismatches. If unrepaired, the ssDNA breaks can become DSBs which accumulate and lead to death as the cells become overwhelmed and cannot cope with multiple DSBs. Therefore, they suggest that base excision repair is the "ultimate contributor to death" in TLD. This model is supported by experiments showing loss of BER also increases tolerance to diverse bactericidal antibiotics that are thought to cause 8oxoG lesions (Foti et al., 2012).

5. SOS RESPONSE AND THYMINELESS DEATH

The SOS response is a global bacterial stress response which functions as the central regulator of DNA repair and mutagenesis and involves the transcription repressor LexA and the homologous recombination protein RecA (Jones & Uphoff, 2021). The response is triggered by RecA binding to ssDNA. It leads to the activation of genes involved in DNA repair and damage tolerance, including TLS polymerases also involved in mutagenesis (Goodman & Woodgate, 2013). The SOS response appears to play an important role in thymine-starved cells. Studies (Giroux et al., 2017; Sangurdekar

et al., 2011) have shown that the SOS response is induced in thymine-starved cells by assessing transcriptional gene expression profiles, using RecA reporter fusions, or mutant strains unable to induce the SOS response or deficient in some genes of the SOS regulon. Interestingly, whilst a study using a rich medium (Giroux et al., 2017) has suggested *recA* deletion mutants showed higher sensitivity to TMP, this finding was contradicted in minimal medium showing that *recA* mutants are more tolerant to thymine starvation (Fonville et al., 2010; T. V. P. Rao & Kuzminov, 2022). This indicates that DNA repair is a double-edged sword in the response to thymine starvation, potentially aiding in the repair of oxidative lesions and ssDNA gaps but also causing toxic DSBs.

Amongst the SOS response genes, *sulA*, an inhibitor of cell division, seems to play a major role in thymine-starved cells by causing an irreversible cell-cycle checkpoint because of blocked cell division, causing cell filamentation and leading to death (Fonville et al., 2010; Lewin & Amyes, 1991). It was suggested that a *sulA* deleted strain shows increased survival during thymine starvation, whilst *recA* mutants impaired for HR showed higher sensitivity to thymine starvation, suggesting that some SOS functions contribute to cell death and others to survival (Giroux et al., 2017). Indeed, a study using lab-evolved resistant strains has suggested a protective role in TLD for only a subset of SOS genes, including *sulA,* whilst TLS polymerases sensitised the cells (Ketcham et al., 2022). However, whilst the SOS response has been shown to have a causal role in TLD, it has also been suggested that TLD happens in SOS-deficient strains, albeit at a lower level (Fonville et al., 2010). Finally, it was shown (T. V. P. Rao & Kuzminov, 2020) in a *dnaA* mutant strain that is unable to replicate from the origin, that SOS-inducing DNA lesions during thymidine starvation are independent of DNA replication.

Many studies have shown that RecA is required for TLD and that its major role is through the SOS response, using various mutations or deletion of *recA* (Fonville et al., 2010), or because of SOS response-induced inhibition of division. However, studies comparing single *recA* or *recA sulA* double deletion mutants have pointed to another role of RecA. This role, independent of the SOS response, involves HR, via RecFOR or RecBCD (Fonville et al., 2010). Another study has also suggested a mechanism whereby ROS-induced DNA damage requires *recA* for HR repair (Giroux et al., 2017).

6. THYMINELESS DEATH AND MUTAGENESIS

It has been known for decades that thymine starvation is highly mutagenic (Coughlin & Adelberg, 1956), although the dynamics and magnitude of mutagenesis in relation to killing during TLD remain unknown. In a study testing for mutagenesis induced by TMP by itself or combined with sulfamethoxazole, it was also suggested that the antibiotic has high mutation rates, abolished in cells carrying an inactive *recA* (Do Thi et al., 2011). Giroux *et al.* (2017) have also observed that TLD mechanism includes increased mutagenesis, which could in turn lead to antibacterial resistance. The mutagenic effects of TMP have been attributed to multiple causes, largely linked to the toxic effects discussed above.

Indeed, hydroxyl radicals produced via the Fenton reaction, have been implicated as contributing to TMP-induced mutagenesis and oxidative DNA damage including 8oxoG lesions (Giroux et al., 2017). The imbalance in the nucleotide pool caused by thymine starvation itself is known to be mutagenic, as was shown in mutated strains with increased dCTP and reduced dGTP displaying

higher DNA replication error rates (Schaaper & Mathews, 2013). Additionally, the SOS response, largely involved in TLD as described above, is known to be mutagenic (Maslowska et al., 2019), likely by inducing TLS polymerases with low fidelity to repair DNA. However, different teams (Giroux et al., 2017; P. Rao & Kuzminov, 2019) using deletion of TLS polymerases concluded to an error-free mechanism and attributed mutations to the replicative DNA polymerase instead. Similarly, deletion of MutS, part of the MMR pathway, has been shown to make no difference to the TLD kinetics, indicating the absence of a role for DNA replication error repair (Giroux et al., 2017; Kuong & Kuzminov, 2010). Another hypothesis suggests that in starved cells, uracil is misincorporated in place of depleted thymine during DNA replication at sites of replication fork stalling. However, uracil is then removed by uracil-DNA-glycolase generating abasic sites, or ssDNA gaps that are inefficiently repaired and can be converted to lethal DSBs (P. Rao & Kuzminov, 2019). These DSBs can then be repaired by HR, known to be mutagenic likely due to the preferential use of error-prone polymerases when cells are under stress (Rosenberg et al., 2012). This mutagenic mode seems to be activated by the RpoS general stress response (Shee et al., 2011).

7. THE ENVELOPE AS A SOURCE OF THYMIDINE DURING THYMINELESS DEATH

Interestingly, it was recently suggested (T. V. P. Rao & Kuzminov, 2020) that the resistance phase experienced by cells undergoing thymine starvation is a delay of acute starvation during which cells can obtain thymine from an endogenous source that is neither chromosomal DNA nor stable RNA (P. Rao & Kuzminov, 2019). This source is the low molecular weight (LMW) dTDP-hexose pool (Okazaki et al., 1959), involved in exopolysaccharide (EPS) capsule synthesis, which is mediated by the rfe-rff gene cluster in *E. coli* (Meier & Mayer, 1985). The dTTP precursor of DNA synthesis is conjugated with glucose, resulting in a dTDP-glucose, which then undergoes modifications before

incorporation into oligosaccharides precursors of the EPS capsule. Incorporation happens particularly in the outer enterobacterial common antigens (ECA) and the dTDP is subsequently released into the DNA precursors pool. The study (P. Rao & Kuzminov, 2019) shows, using ^{3}H-dT incorporation into chromosomal DNA (Okazaki et al., 1959) that this unexpected pool of dTTP increases and becomes the major source for DNA replication during thymine starvation, thus delaying acute starvation. They confirm the involvement of the *rfbA* and *rffH* genes in recruiting dTTP into the LMW pool. Deleting genes of the ECA biosynthesis pathway, particularly *rffC* that is involved in ECA elongation (Meier-Dieter et al., 1992), makes the cells hypersensitive to thymidine starvation, leading to hyper-TLD. In hyper-TLD, the cells undergo catastrophic chromosome loss and rapid death involving lysis. Thus, they suggest that *rffC* helps extract dTTP from the LMW pools during thymine starvation, and its absence leads to catastrophic loss of chromosomal DNA, and cell envelope destabilisation leading to lysis. As a result, this study suggests a role of LMW thymine or even chromosomal DNA in cell envelope maintenance.

8. CELL MORPHOLOGY DURING TLD

It has been reported, using light microscopy, fluorescent microscopy of DAPI-stained cells, and transmission electron microscopy (TEM) that thymine-starved cells during the resistance phase undergo about two cell divisions (P. Rao & Kuzminov, 2019; T. V. P. Rao & Kuzminov, 2020, 2021). Imaging during the resistance phase has also allowed to observe the cell bodies becoming ~1.5 times wider and 2 to 3 times more elongated, with a central nucleoid that is diffuse in TEM and fluorescence microscopy. At this stage, some cells are trying to divide, but are blocked by the division septum pinching the diffuse nucleoid, and some cells display cell pole damage (T. V. P. Rao & Kuzminov, 2021). During the RED phase, after about 3 h, most of the cells are dead and the

remaining cells become even longer (4 to 6 times). Their nucleoid is still centrally located according to fluorescence imaging but invisible by TEM and they stop cell division, instead developing either nucleoid-sized cytoplasm voids or small ~0.2 µm cytoplasm bubbles, and no sign of cell lysis. After 5 h of starvation, TEM reveals signs of cell structure deterioration and loss of EPS capsule and envelope-associated clearings in large void-containing cells (T. V. P. Rao & Kuzminov, 2021). After 20 h, during the survival phase, most of the cells are dead and even more elongated (10 times), with little to no DNA remaining, and segmental cytoplasm loss, possibly reflecting the structural decomposition of dead cells. These studies have shown the cytoplasm becoming dynamic with voids and bubbles appearing during thymidine starvation, and cell envelope instability at later stages. Although the results did not show envelope instability during the early RED phase that could cause chromosomal damage, they reinforced the idea of a role of thymine for envelope maintenance via the dTDP-hexose pool involvement in ECA biosynthesis described above. Instead, it was proposed that cell widening could break DNA if it becomes attached to the cell envelope in the absence of dTTP (T. V. P. Rao & Kuzminov, 2020, 2021). Additionally, changes in DNA compaction in the nucleoid could lead to defects in DNA damage repair, and irreparable chromosomal damage could occur due to abnormal cell division events with centrally located and incompletely replicated nucleoids. It is also known that pieces of chromosomal DNA can randomly associate with the cell envelope, particularly the outer membrane as shown by (Nicolaidis & Holland, 1978). Thus, it is speculated that in elongating thymine-starved cells, the DNA could eventually be overextended if anchored to the envelope resulting in irreparable DSBs. Finally, although these studies did not provide evidence of oxidative damage during thymine starvation, they have suggested a role for reactive metabolic species attacking DNA and reflected by cytoplasmic bubbles.

9. EFFECT OF GROWTH MEDIA COMPOSITION ON TRIMETHOPRIM EFFICACY

The composition of the growth medium affects the outcome of TMP treatment: either bacteriostatic or bactericidal. Specifically, the presence of methionine, glycine, and a purine such as adenine, which are all depleted by TMP blocking the production of the THF precursors, renders the antibiotic bactericidal. It has been suggested that these metabolites maintain the integrity of the tetrahydrofolate pool by preventing the thymidylate synthetase reaction. Their absence, on the other hand, renders the antibiotic bacteriostatic and causes the cell to enter growth arrest (Amyes & Smith, 1974; Kwon et al., 2010; Sangurdekar et al., 2011). Additionally, it is well known that the effects of TLD or TMP can be reversed by the addition of thymine or thymidine in the medium, readily taken up by the starved cells to carry out the thymine salvage pathway (Amyes & Smith, 1974; Kwon et al., 2010; Sangurdekar et al., 2011). Interestingly, diverse transcriptional responses have been associated with the treatment in different supplementations. Specifically, the SOS response to DNA damage and the DNA recombination pathway only seemed to be induced in bactericidal conditions, during the lag stage (Sangurdekar et al., 2011).

A study (Kwon et al., 2010) using liquid chromatography-tandem mass spectrometry to obtain metabolomics data from cell populations, shows a hierarchical order in depletion of the folate-dependent metabolites, with glycine being depleted first, followed by purines such as adenine, methionine, and finally thymine. TMP treatment was studied in minimal bacteriostatic media using different supplementations and a *relA* mutant deficient in the stringent response which responds to amino acid and nutrient starvation. The stringent response can cause inhibition of protein translation to reduce the cell's growth rate (Irving et al., 2021; Sanchez-Vazquez et al., 2019) while facilitating DNA lesion repair activities (Sinha et al., 2020), to allow for cell survival. The results of

the study suggest that the cell's ability to first detect amino acid depletion via the activation of the stringent response leads to growth arrest whilst the subsequent purine depletion precedes and precludes TLD.

Trimethoprim is a weak base which can exist in different ionisation states. In a study using Fourier transform infrared spectroscopy, gas chromatography-mass spectrometry and liquid chromatography-mass spectrometry together with media of varying pH within healthy urine range, it has been suggested that pH plays a role in TMP's mode of action (AlRabiah et al., 2018). The study reveals that at a neutral pH and in bacteriostatic conditions, more of the TMP is recovered from cells than in a more acidic medium in which TMP is completely ionised. Indeed, at neutral pH, there is a decrease in precursors of the biosynthesis of purines and some amino acids and levels of adenine, methionine and thymine in the cells. However, levels of osmoprotectants such as proline or trehalose increase. Furthermore, it has been shown that sublethal TMP treatment activates an acid stress response in bacteria, by examining genome-wide transcriptional response dynamics in different media supplementation together with the use of fluorescent reporters, microfluidic growth chambers, and time-lapse microscopy (Mitosch et al., 2017, 2019). These studies show a rapid albeit heterogeneous acid stress response to TMP controlled by the *gadBC* operon and resulting from the depletion of adenine leading to a drop in intracellular pH, likely due to ATP, and a drop in growth rate. The single-cell experiments performed by Mitosch *et al.* provide insight into the link between better cell survival to acid stress, higher intracellular pH and a higher *gadBC* expression. It also suggests that TMP cross-protects cells from subsequent exposure to acid (Mitosch et al., 2017). The studies point out that under TMP treatment, the acid stress and SOS responses are induced independently from each other within individual cells, with no temporal order or correlation in the induction time of the two stress responses (Mitosch et al., 2019). Finally, a study has shown using various systems biology approaches, such as modulating pH, that

intracellular acidification plays a role in death events related to TLD (Ketcham et al., 2022). In this study, they used flow cytometry to probe acidification. They observed increased expression of acid stress response genes such as gadE and identified loss-of-function mutations related to pH homeostasis as beneficial in TLD. They also measured ROS accumulation by flow cytometry normalised by cell length, and suggest it happens later than acidification and could be caused by the acid stress, itself potentially linked to DNA damage.

Overall, the mode of action of TMP and the mechanisms underlying TLD are complex and not yet fully explained (Fig.8). Models so far have included roles for DNA replication initiation, maladaptive DNA repair processes, the SOS response and HR, ROS accumulation and oxidative damage, pH homeostasis, and cell envelope instability (Table 4). Although multiple hypotheses and angles have been put forward, sometimes disproved, the challenge to understand the mechanism and dynamics leading to death in thymine-starved cells remains intact and puzzling for researchers. A better understanding of the molecular processes could contribute to advances in combatting antibiotic resistance or developing new and effective antibacterial agents.

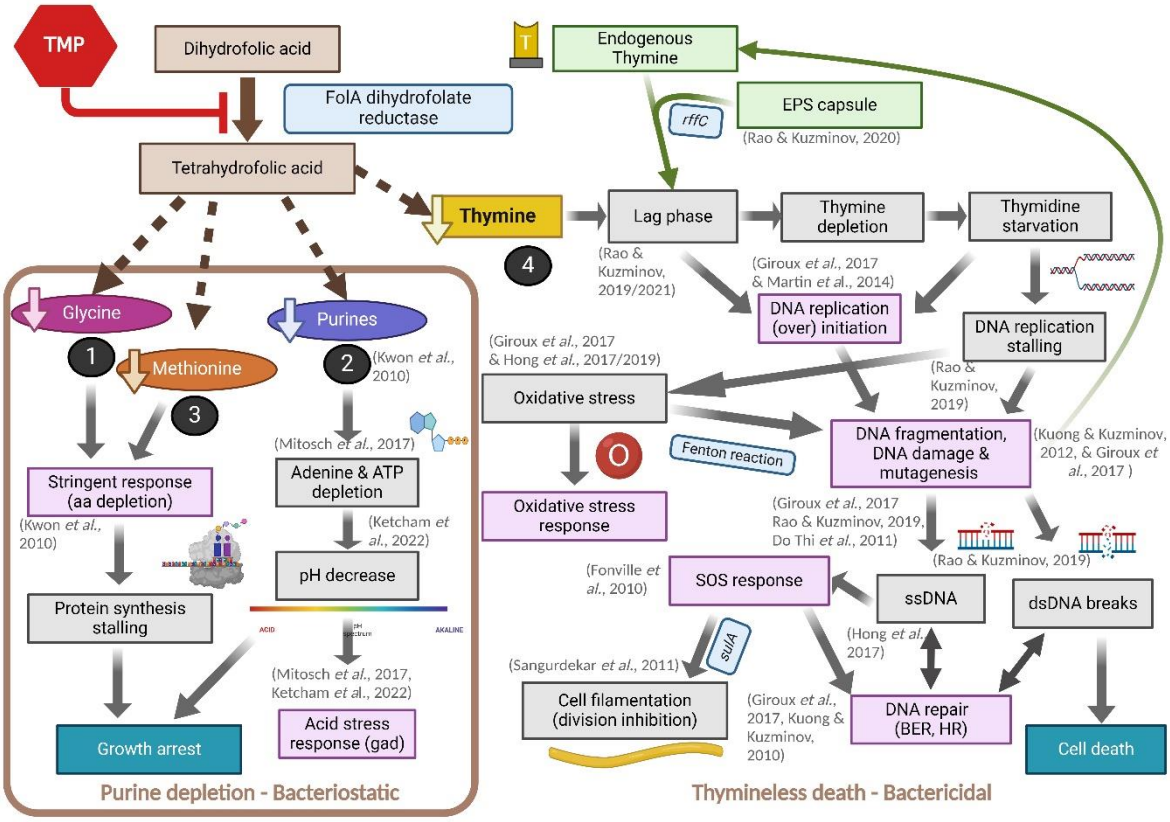


Figure 8: Current understanding of TLD-associated processes. Briefly, TMP is known to cause multiple depletions. The depletion order in the absence of metabolite supplementation in the medium is glycine, purines, methionine then thymine. The action of trimethoprim – bacteriostatic or bactericidal – depends on the medium supplementation. In a non-supplemented medium, the cells will enter growth arrest due to the stringent response, acid stress response and ATP depletion leading to protein synthesis stalling. In a medium supplemented with glycine, purine and methionine, the cells ultimately die following a lag phase during which they recruit endogenous thymine from the capsule. A combination of DNA replication stalling and over-initiation has been shown, together with oxidative stress and SOS responses, DNA fragmentation and further damage leading to mutagenesis and DNA repair pathways, in turn accumulating lethal DSBs in cells.

Table 4: Summary of genes involved in TLD and the effect of a corresponding loss-of-function

Gene name	Protein Function	Effect of gene deletion	References
ahpC	Alkyl hydroperoxide reductase	Hypersensitive to TLD	Giroux *et al.*, 2017
atpF	Proton transport	Increased tolerance to TLD	Ketcham *et al.*, 2022
deoA	Thymidine phosphorylase	Abolish chromosome	Khan & Kuzminov, 2022

		fragmentation but no change for TLD	
deoA	Thymidine phosphorylase	Increased tolerance to TLD	Sangurdekar *et al.*, 2011
dinB	TLS polymerase	No change	Giroux *et al.*, 2017, Rao & Kuzminov, 2019
dinB/polB/umuCD	TLS polymerases	Hypersensitive to TLD	Giroux *et al.*, 2017
dnaA	DNA replication initiator protein	Increased tolerance to TLD	Giroux *et al.*, 2017
dnaA	DNA replication initiator protein	No change	Khan & Kuzminov, 2019
gadE	Acid stress response	Minor increase in sensitivity to TLD	Mitosch *et al.*, 2017
katG/katE	Hydrogen peroxide catalases	No change	T. V. P. Rao & Kuzminov, 2022
katG/katE	Hydrogen peroxide catalases	Hypersensitive to TLD	Giroux *et al.*, 2017, Hong *et al.*, 2017
katG/katE, ahpC	Hydrogen peroxide scavenging	No change	T. V. P. Rao & Kuzminov, 2022
lexA	SOS response	Hypersensitive to TLD	Giroux *et al.*, 2017
lexA	SOS response	Increased tolerance to TLD	Fonville *et al.*, 2010
mutMY	BER pathway	Increased tolerance to TLD	Giroux *et al.*, 2017
mutS	MMR pathway	No change	Giroux *et al.*, 2017
polB	TLS polymerase	No change	Giroux *et al.*, 2017
recA	SOS response / HR	Hypersensitive to TLD	Giroux *et al.*, 2017
recA	SOS response / HR	Increased tolerance	Fonville *et al.*, 2010; T. V. P. Rao & Kuzminov, 2022
recBCD	HR	Hypersensitive to TLD	Kuong & Kuzminov, 2010; T. V. P. Rao & Kuzminov, 2022, Khan & Kuzminov, 2019, Khan & Kuzminov, 2022, Ketcham *et al.*, 2022
recFOR	HR	Increased tolerance to TLD	Sangurdekar *et al.*, 2010
recJQ	HR	Increased tolerance to TLD	Sangurdekar *et al.*, 2010

recQ, recO, recF	HR	Increased tolerance to TLD	Fonville *et al.*, 2010, 2011; Hong *et al.*, 2017, Kuong & Kuzminov, 2010)
relA	Stringent response	Hypersensitive to TLD	Kwon *et al.*, 2010
rffC	dTDP-fucosamine acetyltransferase	Hypersensitive to TLD	Rao & Kuzminov, 2020, Ketcham *et al.*, 2022
seqA	Control DNA overinitiation	No change	Khan & Kuzminov, 2019
sulA	Inhibitor of cell division	Increased tolerance to TLD	Giroux *et al.*, 2017, Fonville *et al.*, 2010
tonB	Transport of extracellular iron	Increased tolerance to TLD	Giroux *et al.*, 2017)
ubiG, cydAB	Respiratory genes	Increased tolerance to TLD	Hong *et al.*, 2017
umuC	TLS polymerase	Hypersensitive to TLD	Ketcham *et al.*, 2022
umuCD	TLS polymerase	No change	Giroux *et al.*, 2017, Rao & Kuzminov, 2019
uvrA	NER	No change	Giroux *et al.*, 2017
uvrA	NER	Increased tolerance to TLD	Sangurdekar *et al.*, 2011
uvrB	NER	Hypersensitive to TLD	Ketcham *et al.*, 2022

AIMS OF THE PROJECT

In this study, the overall aim is to image the real-time bacterial responses to DNA damage caused by antibacterial agents, to understand and compare their mechanism of action and attempt to identify a unifying mode of killing. For that, I investigated the widely used antibiotic TMP, with a complex mechanism still incompletely understood, and a nuclease effector delivered by the T6SS, as a simpler and targeted DNA perturbation. My methodology involves single-cell level imaging combined with microfluidic growth chambers and single molecule tracking techniques, complemented by traditional bulk population growth assays. The specific objectives are outlined as follows:

- Conduct a parallel study to understand the influence of different medium supplementation on TMP mechanism of action
- Investigate the cellular state outcomes and associated phenotypes resulting from TMP treatment
- Decipher the stress responses triggered by TMP, delving into their dynamics, temporal patterns and underlying cell-to-cell heterogeneity
- Understand the relationship between disorder, cellular response heterogeneity and survival during TMP treatment
- Investigate the potentially lethal effect of a T6SS DNA-damaging effector on the model bacterium *E. coli*
- Evaluate the importance and role of the DNA damage response expressed in prey cells for the T6SS nuclease effector

CHAPTER 3 : METHODS

1. STRAINS

All of the strains used were constructed from *Escherichia coli* K12 (AB1157) by P1 phage transduction, and chromosomal insertions using Tn7 transposition or plasmid transformation (Table S1). The antibiotics used were as follows: Kanamycin 25 µg/ml, Ampicillin 50 µg/ml, Chloramphenicol 20 µg/ml, Tetracycline 10 µg/ml.

For transductions of genes, I obtained them from the Keio collection strains from the Coli Genetics Stock Center (CGSC) (Baba et al., 2006), or from existing lab strains. P1 lysates were prepared with the inserts containing the gene of interest with an mYPet fluorescence tag, or a deleted version of the gene, and the kanamycin resistance cassette flanked by frt sites. The strains containing the insert were cultured in LB overnight (ON) and diluted $^{1}/_{50}$ the next morning for growth until an OD_{600} of 0.3 at 37°C with 4000 rpm shaking. The cells were incubated with 100 mM $Cacl_2$ for 10 min at room temperature before 30 µl of P1 wild-type lysate were added, and the cells and lysate were incubated for 4 hours. Chloroform was added before allowing for phase separation and pelleting the cells at 4°C. Chloroform was added to the supernatant containing the lysate for conservation. The target strain was grown in LB overnight, then diluted $^{1}/_{50}$ the next morning for growth until an OD_{600} of 0.8 at 37°C with shaking. The next morning, the cells were pelleted, re-suspended in water, 100 mM $MgSO_4$ and 5 mM $CaCl_2$ and incubated at room temperature for 10 min. The P1 lysate of interest was then added to the cells, at different volumes (0, 10, 50 µl), including a P1 lysate control without cells. The transductions were incubated for 20 min in a 37°C water bath. 1 M of sodium citrate and LB medium were added, and 0.8% glucose when necessary to repress the expression of

the pBAD33 plasmid, before the cells were incubated for 1 h at 37°C. The cells were pelleted and plated on LB and kanamycin. 4 colonies were streaked twice onto LB and kanamycin to purify from phage. Finally, the constructed strains were checked by fluorescence microscopy since the constructs used have been checked previously, or by PCR.

For Tn7 transposition, the plasmid containing the transgene of interest, in this case, 1 µg of pLPT32A (ampicillin resistance cassette, pSC101 temperature-sensitive origin - for attachment at the attTN7 site) containing CFP was transformed by standard heat-shock in a 42°C water bath. The transformed cells were rendered competent with multiple washes in ice-cold 100 mM $CaCl_2$. Recovery was done at 30°C on LB plates with ampicillin and kanamycin. 4 colonies were streaked on LB plates with ampicillin and kanamycin at 30°C. Then one colony was grown in LB with antibiotics at 30°C with shaking to a high density. Streaking from the liquid culture was done on LB plates with kanamycin only for incubation at 42°C to remove the plasmid with ampicillin resistance. Finally, the clones could be checked by fluorescence and streaked again for control with and without ampicillin.

For plasmid transformation by heat shock, the cells were cultured in LB overnight and diluted $^1/_{50}$ the next morning for growth until an OD_{600} of 0.3 at 37°C with shaking. The cells were then washed twice and rested for 30 min and 15 min respectively in ice-cold $CaCl_2$ before being incubated with the plasmid of interest on ice for 10 min. Heat shock was done in a water bath at 42°C for 1 min, before returning the cells on ice for 10 min. The cells were then recovered in LB for 1 h at 37°C without shaking, before being concentrated and plated on LB agar with the selection antibiotic. The plasmids were either obtained from GeneArt using custom designs (pTrc, and pBAD33), from a library of pSC101 plasmids that expressed GFPmut2 under the control of promotors of interest

(Zaslaver et al., 2006), or from other labs like the pBAD33 plasmids for T6SS studies (Custodio et al., 2021).

For the plasmids that were constructed in the lab, Gibson assembly was used, with custom-designed primers (Table S3). Briefly, the fragments of interest were amplified by standard PCR with complementary overhangs, extracted from agarose gel, and digested with DPN1 overnight. The HI-FI assembly kit was then used to ligate the fragment, and the resulting plasmid was then transformed by heat shock in DH5α competent cells.

All the strains were streaked from glycerol stock on LB with appropriate antibiotics and incubated overnight at 37°C with shaking. For growth curves, MIC determination assays and microfluidics experiments, one colony was grown in LB and antibiotics where appropriate during the day for ~6 h, and diluted $^{1}/_{50}$ in M9 minimal medium and antibiotics ON. In the case of microfluidics only, the cells were diluted $^{1}/_{50}$ in medium the next morning and grown for ~3 h to exponential phase for use. For single-molecule tracking, the cells were diluted $^{1}/_{800}$ for ON culture, and $^{1}/_{50}$ the next morning and grown for 3 h to exponential phase for use.

4 different media were used commonly in this work (Table 5), as indicated in the figure captions. For the trimethoprim experiments, M95AA and M95AA + AdGM were used. For the Type six secretion system experiments, M9 glycerol was used. For most other purposes, M9 glucose was the minimal medium used.

Table 5: Media used in the study

Medium	M9 Glucose	M9 Glycerol	M95AA	M95AA + AdGM
Composition	M9 salts (15 g/L KH2PO4, 64 g/L Na2HPO4, 2.5 g/L NaCl, and 5.0 g/L NH4Cl) 50X MEM amino acids 2 mM MgSO4 0.1 mM CaCl2 0.5 mg/mL thiamine 0.1 mg/mL L-proline 0.2% glucose	M9 salts (15 g/L KH2PO4, 64 g/L Na2HPO4, 2.5 g/L NaCl, and 5.0 g/L NH4Cl) 50X MEM amino acids 2 mM MgSO4 0.1 mM CaCl2 0.5 mg/mL thiamine 0.1 mg/mL L-proline 0.2% glycerol	M9 salts (15 g/L KH2PO4, 64 g/L Na2HPO4, 2.5 g/L NaCl, and 5.0 g/L NH4Cl) 1 mM MgSO4 0.1 mM CaCl2 0.5 mg/mL Thiamine 0.1 mg/mL 5AA (arginine, threonine, leucine, proline, histidine) 0.2% glucose	M9 salts (15 g/L KH2PO4, 64 g/L Na2HPO4, 2.5 g/L NaCl, and 5.0 g/L NH4Cl) 1 mM MgSO4 0.1 mM CaCl2 0.5 mg/mL Thiamine 0.1 mg/mL 5AA 0.2% glucose 0.3 mM Adenine 0.3 mM Glycine 0.3 mM L-Methionine

2. GROWTH CURVE AND MIC DETERMINATION

Cells were grown ON in M9 glucose and adjusted to a concentration of $5x10^5$ cfu/ml in M95AA or M95AA + AdGM in a 96-well plate at 37°C with 400 rpm shaking frequency. The antibiotic tested, TMP was then added to the cultures at different concentrations: 0, 0.25, 0.5, 1.0, 2.0 µg/ml. In addition, some wells with 0.3 mM of thymidine supplemented to the medium were tested with various TMP concentrations (0, 0.25, 1.0 µg/ml). OD_{600} readings were taken every 5 min for 24 h in an Omega Plate Reader.

Analysis was done by subtracting the average blank wells OD_{600} from the mean of 3 replicates OD_{600} measures. Growth curves show the average and standard deviations of at least 3 repeats. The final OD_{600} was measured after 24 h for each condition.

To study the effect of trimethoprim at population level, I determined the Minimum inhibitory concentration (MIC) of TMP in M9 glucose minimal medium using growth curves. For that, I assessed the lowest concentration of treatment necessary to inhibit cell growth.

3. SURVIVAL ASSAYS

Cells were grown ON in LB with respective antibiotics. The cells were then diluted $^1/_{50}$ with a range of concentrations of TMP: 0, 0.25, 1.0 µg/ml, or of arabinose for induction of pBAD plasmids : 0, 0.8, 0.05, 0.002%. 0.3 mM thymidine was also supplemented to some cultures with TMP treatment (0, 0.25, 1.0 µg/ml). The cells were grown for 3 h (T6SS) or 6 h (TMP) at 37°C with 400 rpm shaking frequency before serial dilutions from 10^0 to 10^{-8}. 7 µl of each dilution was plated on square LB agar plates with respective antibiotics and incubated at 37°C overnight. The next day, I counted the number of colonies grown at the lowest dilution factor, to calculate survival rate for each condition.

4. MICROFLUIDICS EXPERIMENTS

The microfluidic experiments were performed as described in (Uphoff, 2018) (Fig.9). This method allowed for real-time imaging of a large number of dividing cells with a controlled and continuous flow of medium. I used mothermachine microfluidics devices made of polydimethylsiloxane, using

moulds containing growth channels, 100 µm in cross-section and 25 µm high. Each one of these channels had hundreds of parallel cell channels, 1.2 µm wide by 1.2 µm high and 15 µm long with 10 µm spacing between them. The microscope coverslips were prepared using air plasma, and the whole device was bonded together at 95°C for at least 30 min. ON cultures were diluted $^{1}/_{50}$ in growth medium with 0.85 mg/ml Pluronic F127 (to prevent cell aggregation) and grown for ~3 h up to an OD_{600} ~0.5. Cells were then concentrated by centrifugation and inserted into the device. The growth medium with/out supplementation, and 0.85 mg/ml Pluronic F127, was flowed into the devices using a syringe and a motorized pump. After loading, a flow of medium from the first syringe at 2.5 ml/h was applied for ~15 min, then switched to 0.5 ml/h. Before starting the recording, cells were allowed to equilibrate in the chip for ~1h. A second syringe containing the growth medium and 0.25 µg/ml TMP or 0.002% arabinose (for T6SS experiments) was attached to the same growth channel using a junction which allowed the switch between the syringes after ~3 h. To ensure medium change when switching to the second syringe, the flow was set at 2.5 ml/h for ~15 min and then back to 0.5-1 ml/h. Experiments ran for up to ~20 h.

Automated imaging was performed on a Nikon Ti Eclipse inverted fluorescence microscope, equipped with a perfect focus system, 100x NA1.4 PlanApo oil immersion objective, Andor sCMOS camera, a 37°C temperature chamber (Okolabs) and motorized scanning stage. Fluorescence images were automatically collected using an LED excitation source (Lumencor SpectraX) at 3 min intervals for 46 or 20 fields of view per experiment. Exposure times were 300 ms for mYPet marker fused to proteins of interest (DnaN, MutL), 100 ms for the constitutively-expressed P_{RNAI}-mKate2 cell marker, 75 ms for msCFP3 gene expression reporters (*PahpC, PgrxA, PrecA*, *PsodA* – transcriptional reporters of promotor activity) or when CFP was used as cell marker, and 100 ms for GFPmut2 gene expression reporters (*PgadB* – transcriptional reporters of promotor activity).

For the propidium iodide experiments, a 1 mg/mL solution of propidium iodide was prepared from the stock and diluted in phosphate-buffered saline buffer solution at a 1/1000 dilution. The stain was then added into the mothermachine device, around 20 hours after the start of treatment, and captured under the microscope in the channel used for mKate2.

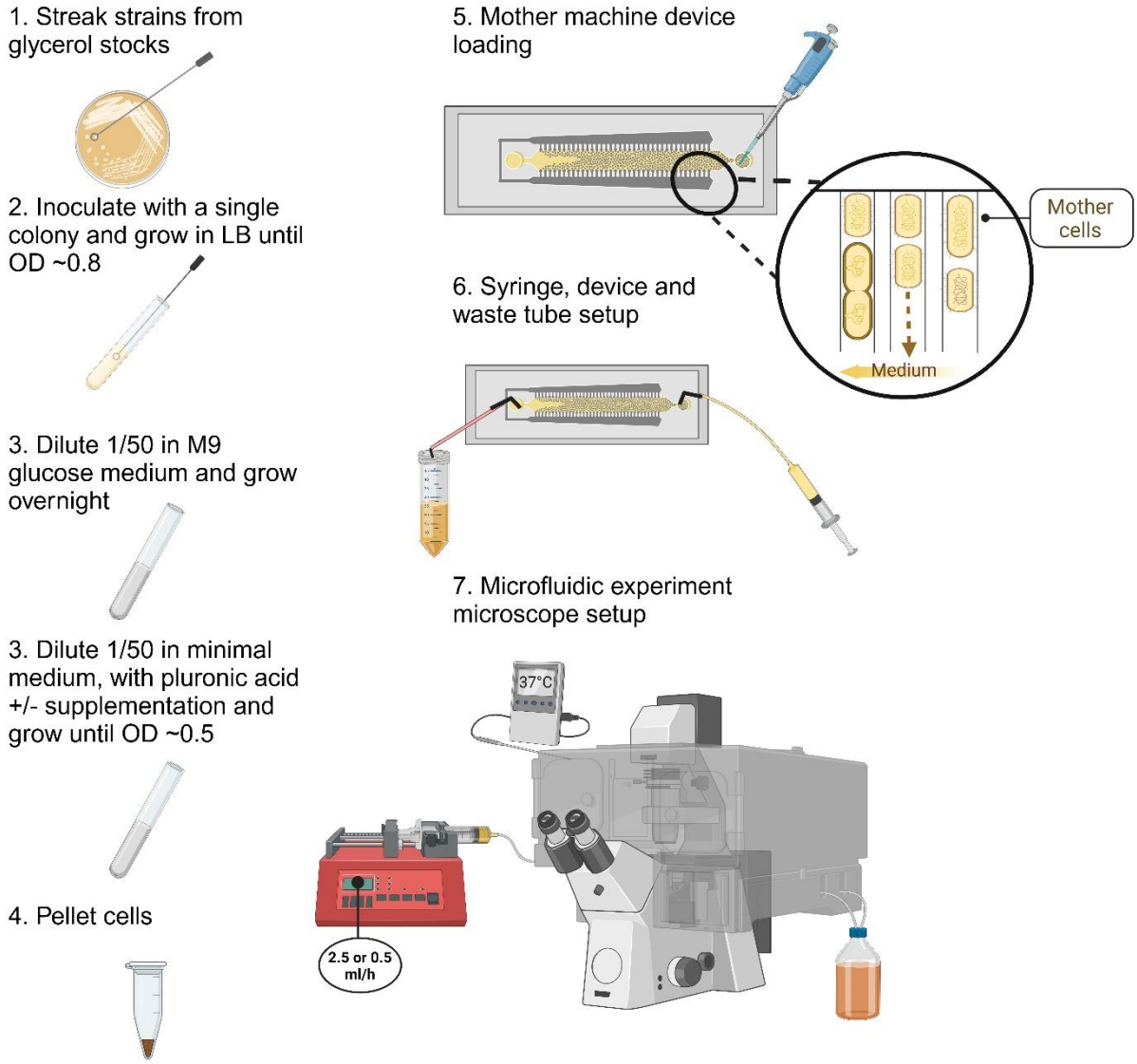


Figure 9 : Protocol for microfluidic experiment protocol. Step-by-step protocol from sample preparation to microscope set-up.

4.1. Microfluidics Experiments Analysis

For microfluidics data analysis, MATLAB and R were used. The analysis and calculations of cell characteristics were performed in MATLAB as described by Uphoff, 2018, identifying individual cells for further analysis, and using the centroid for tracking. The outlines of the mother cells located at the end of each growth channel were segmented using the cytoplasmic signal of mKate2 or msCFP3. The fluorescence intensities for all channels were calculated from the pixel intensities inside the cells from which background intensities were subtracted. The foci of protein fusions with mYPet were detected by a spot-finding algorithm, for which the threshold was adjusted for each experiment to optimise detection. For msCFP3, the reporter intensities were calculated as an average within segmented cells. Cell length was automatically extracted as a property of the segmented cells. A typical microfluidic experiment produced between 500 and 1500 single-cell traces.

Further analyses were carried using custom written scripts in R. I assigned an ID for each cell, using its field of view and position as coordinates. For each cell, I could track them and record when they disappeared from the field of view, determining whether the cells where absent or present in growth channels. This was used to calculate the number of remaining cells over time and assign a lysing status to cells that were absent at specific timepoints. I used control untreated experiments to determine the thresholds for cell length corresponding to potential filamentation, which was calculated from the mean and standard deviation for these experiments. Based off these thresholds, I assigned a cell length status, normal or filamenting, to each cell over time. This was used to classify cells in a filamenting or recovered state. I also assigned cells a growth status, by assessing fluctuations in cell length, which was done by computing standard deviation of cell length in a moving 30 min window. Actively growing cells were characterised as having a standard

deviation of cell length above a set threshold, used to classify cells in growth arrest and recovered states. I then used all these parameters (Table 6) to determine the endpoint cell state, assessed within a 100 min observation window immediately before the endpoint. The endpoints chosen corresponded to 200, 500, or 600/800 min after the start of the treatment, and the cell states were: Healthy, Lysed/Absent, Filamenting, Growth Arrest, and Recovered (Table 7). When using the bootstrapping method, the parameters were 80% of the cells, with 1000 repeats of random sampling to obtain a 95% confidence interval.

Table 6 : Cell state classification procedure. Parameters and corresponding criteria used to define the cell states.

Temporality	Parameters	Criteria
Timepoint (100 min prior)	Remaining	Present/ Absent from growth channel
Timepoint (100 min prior)	Actively Growing	Moving window for standard deviation of cell length (above threshold)
Timepoint (100 min prior)	Filamentation	Cell length (above threshold)
Lifetime	Asymmetric Division	Recovery from cell length (filamentation→normal) or growth arrest (non-growing→growing)

Table 7 : Cell state classification using the parameters defined for each cell. The resulting cell states were: Healthy, Lysed/Absent, Filamenting, Growth Arrest and Recovered. Not all parameters apply to all cell states (N/A).

	Cell State				
Parameters	**Healthy**	**Lysed / Absent**	**Filamenting**	**Growth Arrest**	**Recovered**
Remaining	Present	Absent	Present	Present	Present
Actively Growing	Yes	N/A	Yes	No	Yes
Filamentation	No	N/A	Yes	N/A	No
Asymmetric division	N/A	N/A	N/A	N/A	Yes

The cell length and fluorescence intensities were calculated by pooling all cell values per timepoint as follows :

$$Cell\ Length\ (Timepoint\ t) = \frac{\sum_{cell} Cell\ Length\ (cell)}{Nb\ of\ alive\ cells\ (t)}$$

$$Fluorescence\ Intensity\ (Timepoint\ t) = \frac{\sum_{cell} Fluoresence\ Intensity\ (cell)}{Nb\ of\ alive\ cells\ (t)}$$

For the mismatch rate, after correction for misdetection, the number of foci at each timepoint were summed up together. A misdetection was considered as a missing event in a stretch of continuous localizations and was corrected to avoid counting repeat appearances of the same mismatch event. In individual cells, I counted only the new foci when they first appeared and took into account the time between two timepoints (frametime) for the rate calculation. The mismatch rate was then calculated at the population level. To smooth out the curves obtained, I used a moving average for the mismatch rate at the population level in a window $\langle t - 5\ timepoints | t | t + 5\ timepoints \rangle$.

$$Mismatch\ Rate\ (cell)_{\ (Timepoint\ t)} = \frac{New\ foci\ (t)\ (cell)}{Frametime}$$

$$Mismatch\ Rate\ (Timepoint\ t) = \frac{\sum_{cell} Mismatch\ Rate\ (cell)_{(Timepoint\ t)}}{Nb\ of\ alive\ cells\ (t)}$$

For the DNA replication foci frequency, I calculated the number of foci per timepoint and normalised by the area.

$$DNA\ Replication\ Frequency\ (Timepoint\ t) = \frac{\sum_{cell} \frac{Nb\ of\ foci\ (cell)}{Area\ (cell)}}{Nb\ of\ alive\ cells\ (t)}$$

The expression rate of reporters was calculated as the average intensity per cell per area per time. To smooth out the curves obtained, I usually used a moving average in a window $\langle t - 3\ timepoints | t | t + 3\ timepoints \rangle$ or $\langle t - 5\ timepoints | t | t + 5\ timepoints \rangle$.

$$Expression\ Rate\ (cell)_{\ (Timepoint\ t)}$$

$$= \frac{\frac{Cell\ Fluorescence\ Intensity\ (t+1) - Cell\ Fluoresence\ Intensity(\ t)}{Frametime}}{Area\ (t+1)\ (cell)}$$

$$Expression\ Rate\ (Timepoint\ t) = \frac{\sum_{cell} Expression\ Rate\ (cell)_{(Timepoint\ t)}}{Nb\ of\ alive\ cells\ (t)}$$

For the CFP expression rate at a fixed timepoint, I excluded negative fluorescence intensity values caused by bleached outlier cells from the rate calculations. I then performed bootstrapping for which the parameters were 80% of the cells, with 1000 repeats of random sampling to obtain a 95% confidence interval.

$$Expression\ Rate\ (Timepoint = t) = \frac{\sum_{cell} Expression\ rate\ (t)}{Nb\ of\ alive\ cells\ (t)}$$

For the probability distribution at timepoint t, I used the values obtained for a characteristic (X), and determined the number or count of occurrence for each possible value of X.

$$Probability\ distribution\ of\ X\ (i)_{(Timepoint\ t)} = \frac{Counts\ of\ occurence\ of\ X\ (i)_{(t)}}{Total\ number\ of\ counts\ of\ all\ X_{(t)}}$$

For the study of temporal correlation between different reporters in a dual-reporter strain, I fitted a linear regression model to my data in R. For that, the formula used was :

$$y = \beta_0 + \beta_1 x + \varepsilon$$

5. SINGLE MOLECULE TRACKING

Single-molecule tracking experiments allowed for the recording of molecules' movement within a cell in real time. Cells with a LexA transcriptional repressor fused to a Halo Tag were grown in the relevant medium from ON culture and labelled with tetramethylrhodamine (TMR) fluorophore. The cells were then prepared with multiple rounds of wash, as described in (Banaz et al., 2019). The cells were treated for 2 h in medium with 0.25 µg/ml TMP, and 0.3 mM thymidine when necessary, always running controls without TMP in parallel. The cells were spotted on 1% agarose pads and imaged by total internal reflection fluorescence microscopy shortly after being prepared, and for no more than 3 h after preparation. Using a custom-written automating software, 5 frames per samples were imaged each after a 60 s wait time to allow the cells to bleach and reveal single foci before starting imaging, and 3 technical repeats were performed per experiment. The microscope used was a custom-built instrument equipped with a multi-laser engine (405 nm, 488 nm, 561 nm, 640 nm), a piezo sample stage and an EMCCD camera (Andor). Movies were recorded at 7 ms exposure for 10000 frames to record the intracellular movement of molecules in real time. The laser intensity was of 50% and the angle of the laser was modified to ensure maximum illumination of the samples.

The data were analysed as described previously (Banaz et al., 2019; Jones & Uphoff, 2021) using MATLAB. Cells were segmented from transmitted light snapshots using a segmenting algorithm. Fluorescent molecules were localised using an automated spot-finding algorithm and tracked over

successive frames in the movie. The diffusion coefficient was computed from each tracked molecule to analyse the mobility of molecules within cells with/without TMP treatment and thymidine supplementation. Additionally, I performed control experiments using cells expressing the molecules of interest in a single diffusive state. This was done for a control sample with paraformaldehyde-fixed cells, non-cleavable LexA K156A mutant, and cells expressing unconjugated Halo Tag, respectively corresponding to DNA-binding, transiently DNA-interacting, or fast and freely diffusing states (Jones & Uphoff, 2021). These were used to quantify the relative abundance of the three subpopulations in the cells expressing wild-type LexA-Halo. Thus, the diffusion coefficients computed for each molecule allowed the identification of molecular subpopulations with different mobility within cells.

CHAPTER 4: IMAGING CELL STATES AND GROWTH DYNAMICS IN RESPONSE TO TRIMETHOPRIM TREATMENT USING MICROFLUIDIC GROWTH CHAMBERS

1. INTRODUCTION

Trimethoprim (TMP) is a widely used antibiotic for the treatment of UTI, predominantly caused by *Escherichia coli* (Medina & Castillo-Pino, 2019). It is known as a competitive inhibitor of the FolA tetrahydrofolate reductase (Burchall, 1973). This results in cells being depleted for a range of metabolites which are produced from the folic acid biosynthesis pathway. This includes the purine base adenine, and amino acids glycine and methionine, and the pyrimidine thymidine, which is solely used in DNA synthesis (Kwon et al., 2010). Many hypotheses have been put forward to explain the mechanism of action of TMP, such as effects of thymidine depletion on cell morphology (T. V. P. Rao & Kuzminov, 2021), genome replication and integrity (Martín et al., 2014; Martín & Guzmán, 2011), or cellular division (Fonville et al., 2010).

Interestingly, in laboratory culture, the composition of the growth medium to which TMP is added can influence the outcome of the treatment. Specifically, a medium that does not contain any of the metabolites (thymidine, adenine, glycine, methionine) depleted by TMP will make the treatment bacteriostatic for the cells. On the other hand, supplementing the medium with thymidine alone is sufficient to negate the effects of the treatment, while addition of adenine, glycine and methionine makes TMP bactericidal. It has been shown using population-based assays

that cells treated with TMP experience an initial lag phase during which the cells appear almost resistant before losing viability, (Sangurdekar et al., 2011). In fact, in the context of TLD, this lag phase lasts two cell generations, during which the cell titre does not change, and DNA mass per cell accumulates, using up all available thymidine. This is then followed by the RED phase during which DNA accumulation ceases, and the cells start dying acutely. The last phase is survival whereby the cell titre is stabilised (Kuong & Kuzminov, 2010; P. Rao & Kuzminov, 2019; T. V. P. Rao & Kuzminov, 2020).

Despite decades of studies and abundant literature on the mode of action of TMP, no universal model has emerged that could explain all the observed phenomena seen in TMP-treated bacterial cultures. Importantly, it is still unknown which, if any, specific process is responsible for cell death, and which mechanism(s) prolong cell survival. In fact, TMP may perturb many processes in the cell to the extent that no single mechanism is necessary or sufficient for cell death (Kaplan et al., 2021). Most studies to date have examined the effects of TMP using population-based assays, which do not provide information on the responses and phenotypes of individual cells, thereby masking potentially important heterogeneity in cell behaviour. These assays also do not inform on the relation between the growth behaviour, morphology, and cell state, which can only be linked by monitoring single cells over time. Microscopy combined with microfluidic growth chambers is ideal to achieve this, as it allows observing living cells over prolonged periods with minimal perturbation while maintaining constant and defined growth conditions. Thus, the objective of this work was to develop a microscopy-based assay to study cell states and growth dynamics of *E. coli* in response to TMP treatment using microfluidic growth chambers. The model organism here was chosen for its physiological relevance, as it is one of the main causative agents of UTI, routinely treated with TMP (Flores-Mireles et al., 2015). I specifically focused on TMP-treated cells in minimal media with different supplementations to make TMP either bacteriostatic or bactericidal. To monitor the real-time dynamics of growth at the single-cell level, I used mothermachine microfluidic experiments

whereby daughter cells divide from a single mother cell within narrow individual growth channels. The experiments were carried out over up to 24 hours with a controlled and continuous flow of medium through the device. This allows for real-time imaging to study the changes in survival dynamics, growth, and cell length during continuous TMP treatment. Additionally, continuous medium flow removes the possibility that any secreted molecules or debris of dead cells interfere with the given treatment, thus removing a technical complication present in bulk culture assays. Together, the results from this study suggest clear differences between bacteriostatic and bactericidal conditions for TMP and a role for cell-to-cell heterogeneity in lower cell survival.

2. RESULTS

2.1. Trimethoprim's Impact on Bacterial Communities at the Population Level

I initiated the investigation of TMP's mechanism of action by characterising the population-level effects of TMP in my specific experimental conditions. The strain of bacteria studied, *Escherichia coli* AB1157 carries several auxotrophic mutations, which affect synthesis of the amino acids arginine, threonine, leucine, proline, and histidine (DeWitt & Adelberg, 1962). The strain has an amber mutation in RpoS, which regulates the stationary phase general stress response (DeWitt & Adelberg, 1962; Visick & Clarke, 1997). The media used are minimal, derived from M9, featuring essential metabolites including the five amino acids arginine, threonine, leucine, proline, and histidine (5AA), exclusively meeting the auxotrophic needs of the cells. I utilised both M95AA (bacteriostatic), and M95AA + AdGM (bactericidal), which is supplemented with adenine, and the amino acids glycine and methionine, known to rely on the folic acid synthesis pathway and are

therefore depleted by TMP. I used growth curves and spot survival assays to study the effect of TMP treatment at the population level.

My exploration began with a range of concentrations, 0, 0.25 μg/ml, 0.5 μg/ml, 1 μg/ml and 2 μg/ml of TMP in M95AA + AdGM. Through 24 h growth curve assays in liquid cultures for AB1157 wild-type cells, I determined the MIC of TMP in minimal media to be around 1 μg/ml (Fig.10), which is in line with reported values (Giroux et al., 2017; Mitosch et al., 2017). Untreated cells grew to an OD_{600} ~0.6 after 24 h, whilst a 0.25 μg/ml TMP treatment slightly delayed the onset of the exponential phase for the cells. Above this concentration, TMP had a dramatic inhibiting effect on cell growth compared to untreated cells, signifying a population-level effect from 1 μg/ml. Next, acknowledging thymidine's potential to counteract TMP treatment, I tested the effect of adding 0.3 mM thymidine to cells treated with 1 μg/ml TMP during 24 h growth curve experiments. As expected, I observed that the addition of thymidine completely rescued cell growth and restored the OD_{600} of TMP-treated cells to the level of untreated cells throughout the whole growth curve.

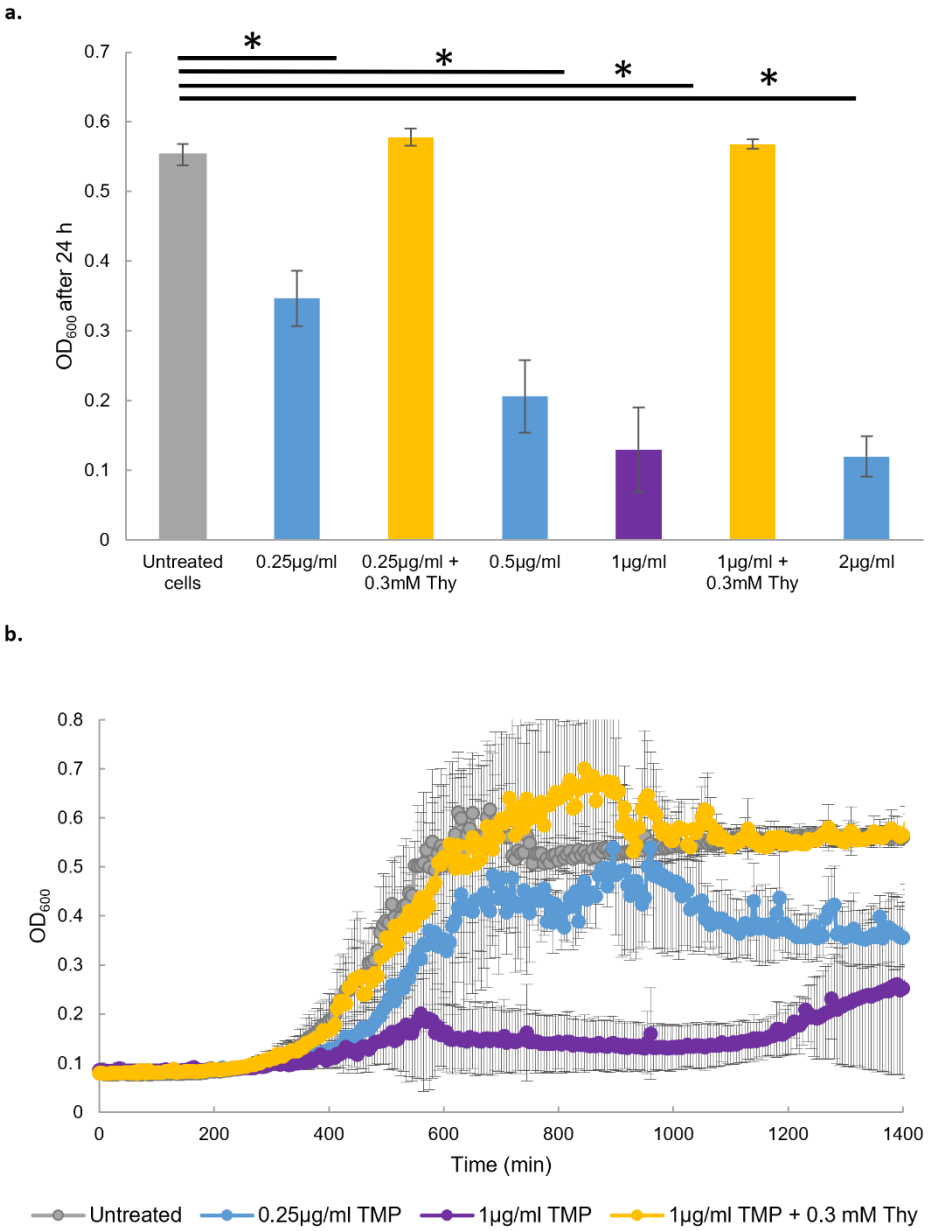


Figure 10 : 24 h growth curve assay for TMP in M95AA + AdGM minimal medium. I carried out 96-well plate-based assays, measuring OD_{600} at regular intervals for 24 h. The cells were treated with 0, 0.25 µg/ml, 0.5 µg/ml, 1 µg/ml and 2 µg/ml of TMP and when relevant, 0.3 mM of thymidine. a) Mean OD_{600} after 24 h from three experimental repeats ± standard deviation. Significance based on two-sample T-test with stars indicating p-value < 0.05. b) Average OD_{600} growth curve from three experimental repeats ± standard deviation.

Next, I compared these results to the effect in M95AA medium, which is supposed to render TMP bacteriostatic. I observed very similar trends, with a maximum OD_{600} of 0.5 for untreated cells which is slightly below the density in M95AA + AdGM, as expected due to the lack of the additional

metabolites (Fig.10). The MIC of ~1 μg/ml for TMP was similar between the two media. This suggested that the two media in bulk population assays potentiated TMP to inhibit growth. This is expected since differences between bacteriostatic and bactericidal treatments would only become obvious upon removal of the antibiotic, where cell growth should only resume if the treatment did not kill the bacteria, i.e. under bacteriostatic conditions. Thymidine addition in M95AA media also restored survival of treated cells to the level of untreated cells for a sub-inhibitory concentration of TMP (0.25 ug/ml), but the survival was only partially restored for a 1 μg/ml concentration of TMP. This was evident in the growth curve (Fig. 11), with a significant delay for 1 ug/ml TMP + 0.3 mM thymidine compared to untreated cells, although the OD after 24 h was not significantly different. This suggests that whilst thymidine addition is sufficient to rescue THF deficiency when adenine, methionine and glycine are present in the bactericidal medium, it is insufficient when these metabolites are absent in the bacteriostatic medium.

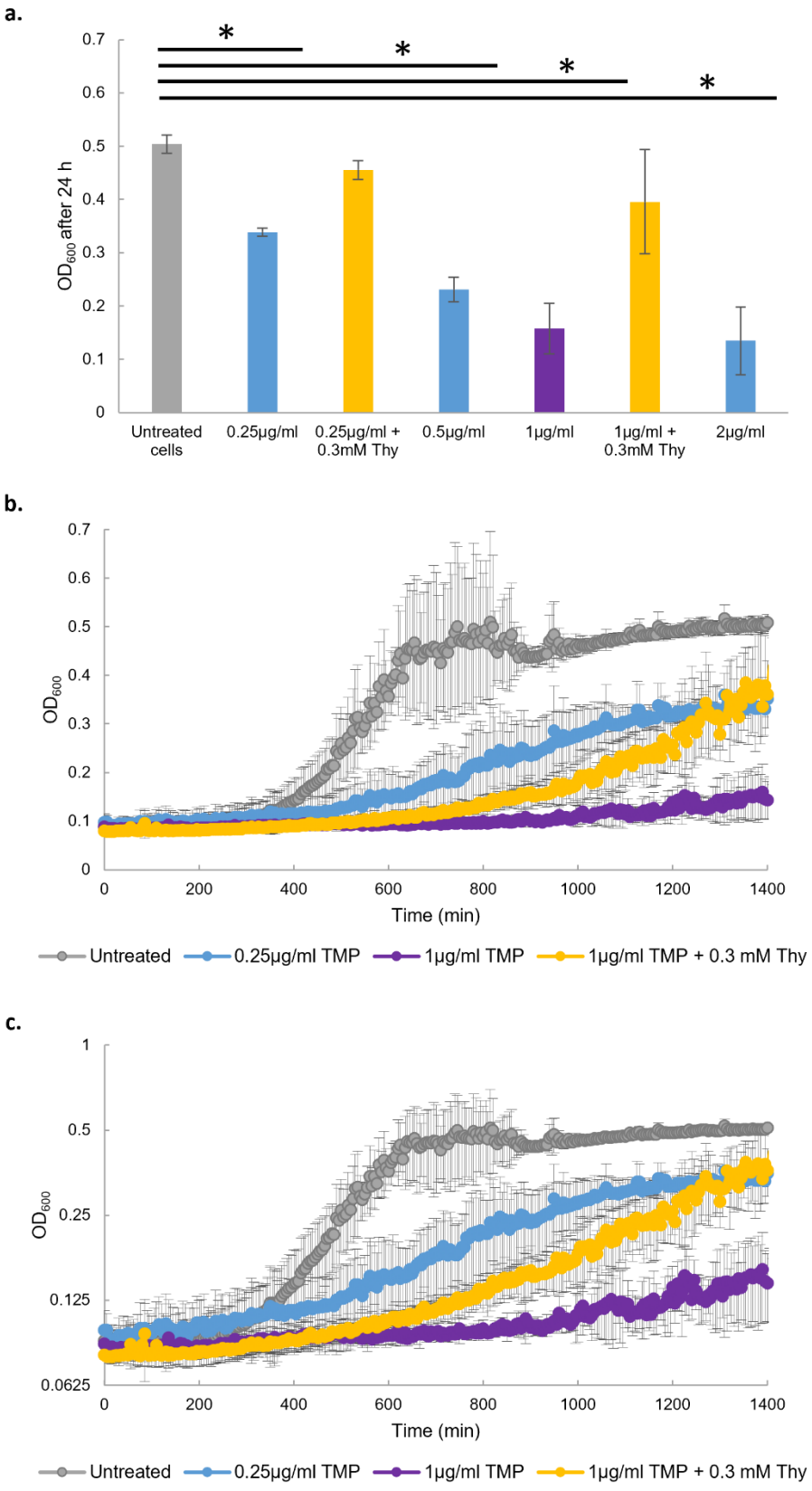


Figure 11 : 24 h growth curve assay for TMP in M95AA minimal medium. I carried out 96-well plate-based assays, measuring OD_{600} at regular intervals for 24 h. The cells were treated with 0, 0.25 µg/ml, 0.5 µg/ml, 1

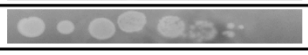
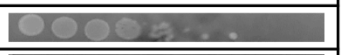
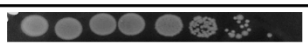
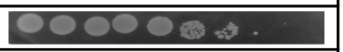
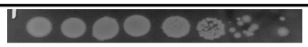
µg/ml and 2 µg/ml of TMP and when relevant, 0.3 mM of thymidine. a) Mean OD_{600} after 24 h from three experimental repeats ± standard deviation. Significance based on two-sample T-test with stars indicating p-value < 0.05. b) and c) Average OD_{600} growth curve from three experimental repeats ± standard deviation.

To further evaluate the effects of TMP and distinguish between bactericidal and bacteriostatic outcomes of treatment, I assessed its killing effects on cells by using spot survival assays. For that, the cells were treated in liquid cultures of M95AA + AdGM or M95AA for 6 h before plating them, without treatment (Fig.12). I observed a reduction in surviving cells in M95AA + AdGM which increased with rising concentrations of TMP relative to untreated cells. Addition of thymidine restored survival to a slightly lower level than for untreated cells. In M95AA, I observed similar reduction of survival with increasing concentrations of TMP, and thymidine rescue of treated cells, with an even lower survival compared to untreated cells. We did observe as would be expected from the bacteriostatic quality of treatment, that in M95AA compared to M95AA + AdGM the survival of treated cells was slightly higher, particularly at 0.25 µg/ml.

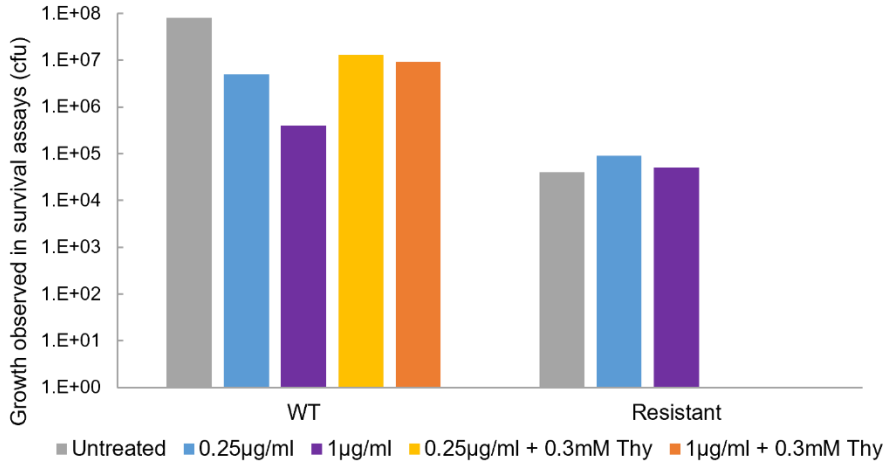
I pursued my investigation by comparing the population-level effects of TMP on wild-type (WT) and TMP-resistant strains harbouring an extra copy of the target gene *folA*, using spot survival assay (Fig.12). This was done to ensure the effects observed in the context of treatment were solely due to TMP and could be rescued with an extra copy of the target to maintain production of folic acid metabolites in treated cells. To that effect, I engineered cells by introducing an IPTG inducible pTrcHis plasmid carrying a *trc* promoter, a *lac* repressor, and a copy of the *folA* gene. The plasmid was used without induction, as preliminary analysis suggested that plasmid leaky expression was sufficient to protect the cells. The *folA* gene encodes the dihydrofolate reductase competitively inhibited by TMP. To ensure resistance, I introduced an L28R point mutation in the gene, a modification documented in the literature for its highly advantageous role in conferring resistance. This mutation happens close to the substrate-binding site of DHFR (Toprak et al., 2012), and leads

to prolonged binding times in the enzyme-substrate complex, which decreases catalytic activity but maintains formation rate in the presence of TMP (Abdizadeh et al., 2017). Accordingly, I observed no change in survival in resistant cells with increasing concentrations of TMP compared to untreated cells in both media studied. The resistant cells also presented with reduced growth compared to WT cells, even when untreated, which could suggest a fitness cost of the resistant plasmid for the cells.

a.

TMP conditions	M95AA + AdGM 10^{0} 10^{-1} 10^{-2} 10^{-3} 10^{-4} 10^{-5} 10^{-6} 10^{-7}	M95AA 10^{0} 10^{-1} 10^{-2} 10^{-3} 10^{-4} 10^{-5} 10^{-6} 10^{-7}
Untreated cells		
0.25 µg/ml		
1 µg/ml		
0.25 µg/ml + 0.3 mM Thy		
1 µg/ml + 0.3 mM Thy		

b.



c.

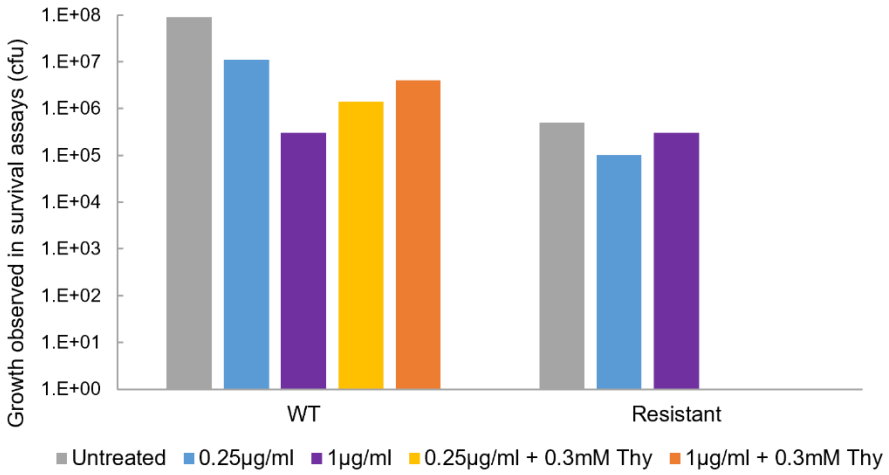


Figure 12 : Spot survival assays for TMP using serial dilutions of cells after 6 h of treatment with 0, 0.25 µg/ml, and 1 µg/ml TMP, and when relevant, 0.3 mM thymidine in b) M95AA + AdGM and c) M95AA minimal media. The proportion of surviving cells was determined relative to the colony counts without treatment. In each media, I compared WT (left) and resistant (right) strains carrying a folA L28R plasmid. The figure is from a single repeat for each condition, with representative images for the wild-type strain at different conditions in a).

2.2. Trimethoprim's Impact on Cells' Survival and Growth Dynamics

Following bulk population assay, I employed a microfluidic assay in both media M95AA + AdGM (bactericidal) and M95AA (bacteriostatic). This was done to investigate the effect of TMP on the model bacterium and explore heterogeneity and chronology of the effect of the antibiotic. This innovative method combined with fluorescence microscopy allows for single-cell-level investigation (Potvin-Trottier et al., 2018). The microfluidic growth chambers apparatus ensures a constant flow of medium to keep the cells in continuous growth conditions (Fig.13). One so-called 'mother cell' is trapped at the closed end of each growth channel while the progeny is pushed out of the channel and into the waste stream. In this way, the population of mother cells can be monitored over many division cycles under constant conditions. Since the cells can be equipped with fluorescent mKate2 segmentation marker constitutively expressed, each experiment can generate a comprehensive dataset for single cells. This includes information on cell size, growth, division events, and fluorescence intensities associated with the reporter proteins expressed by the cells.

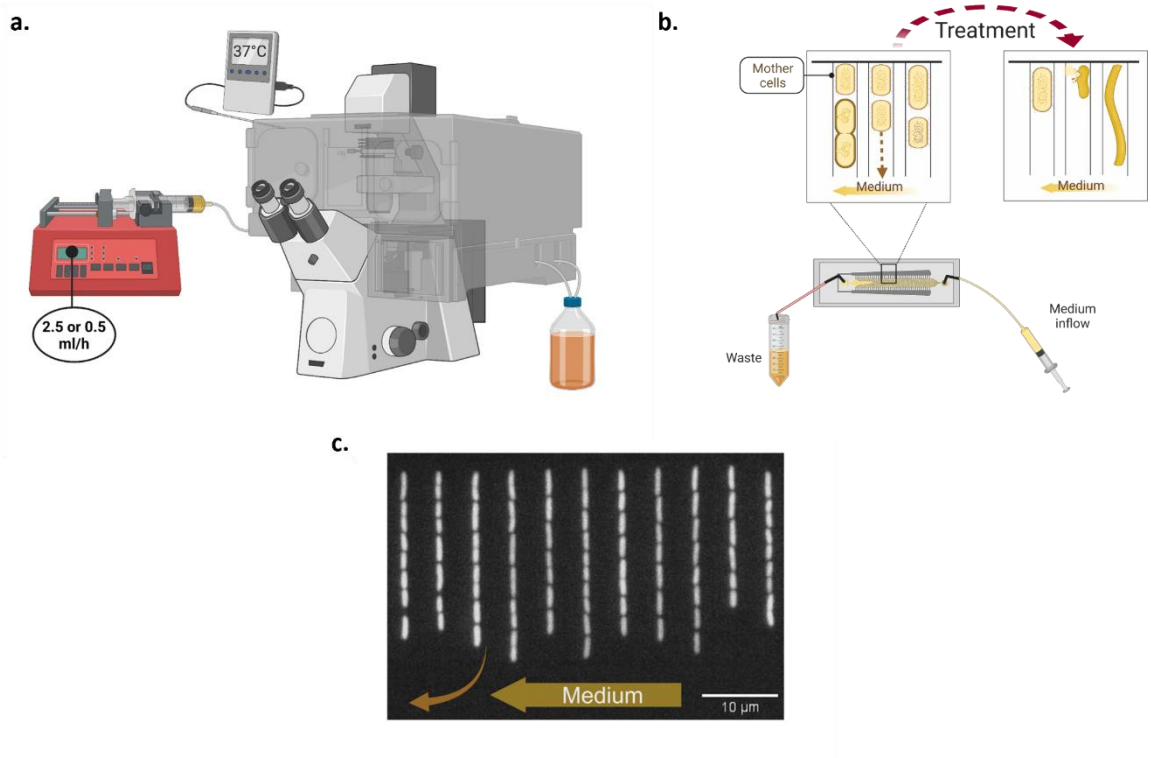


Figure 13 : Illustration of mothermachine microfluidics experiments. a) Schematic representation of the microscope set up with a 37°C incubation chamber, a fluorescence microscope equipped with LED illumination and a syringe pump which flows medium continuously into the microfluidic device positioned on the microscope stage. The flow-through medium is collected in the waste bottle. b) Schematic representation of the microfluidics device containing E. coli cells in narrow growth channels, with mother cells positioned at the closed ends of each channel at the top. Changes in cell growth, morphology, and lysis can be monitored using time-lapse microscopy after the start of TMP treatment. c) Representative image of a mothermachine microfluidics device with cells under a microscope before treatment, showing the mKate2 segmentation marker.

From the microfluidics experiments carried out, I processed the data with a custom-written script in Matlab. The cells were segmented using a constitutive mKate2 reporter, which allowed to calculate cell length, width or area and average fluorescent pixel intensities within the cells for fluorescent reporters by subtracting the background from outside of the cells (Lagage et al., 2023). Then, using a custom-written analysis script in R, I assigned an ID to each of the mother cells imaged during the experiments. Thus, my analyses enabled tracking of the cells' ID throughout the experiment. This allowed the systematic identification of cells with sustained absence from the population at specific timepoints. The resulting time-lapse microscopy data allowed me to assess

cell viability and growth using two metrics. The first metric is based simply on the presence/absence of cells in the growth channels. Cells can disappear from the channels due to lysis or filamentation, which causes a cell to grow so long that it reaches the media flow channel and is pulled out of the growth channel. I plotted the percentage of "Remaining Cells" over time normalised by the initial number of cells at the start of the experiment, before treatment. The second metric was designed to assess cell growth dynamics. To this end, I quantified fluctuations in cell size by computing the standard deviation of cell length in a 30 min moving time window for each cell (Fig.14). This was used as a proxy to characterise "Actively Growing Cells" if the standard deviation of cell length was above a set threshold.

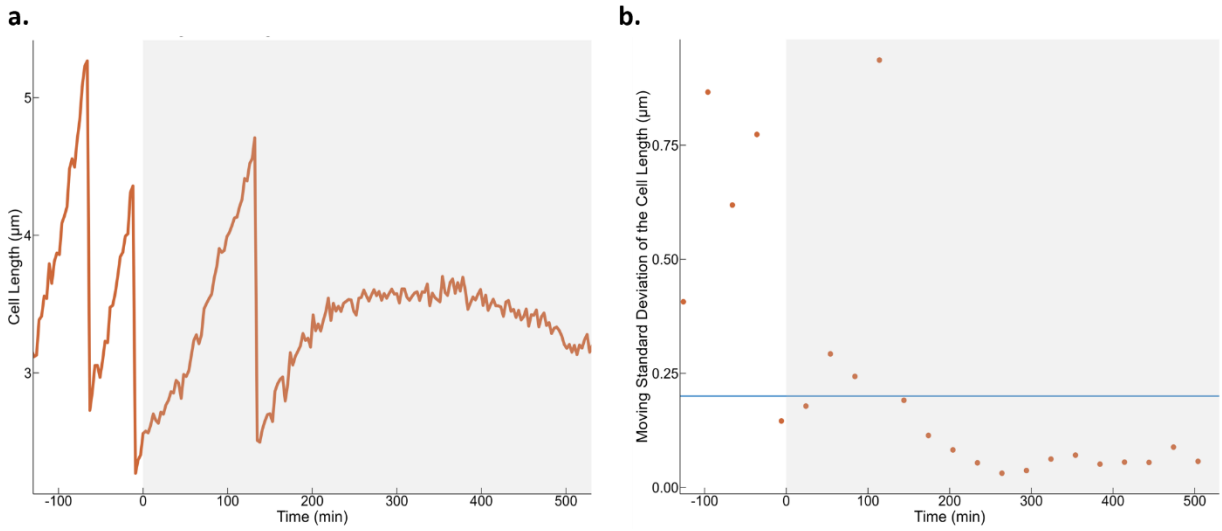


Figure 14 : Single cell trace in M95AA + AdGM for a representative cell defined in growth arrest by the 800 min endpoint and treated with 0.25 µg/ml TMP. a) Cell length trace over time with TMP treatment starting at timepoint 0. The peaks in the trace represent a cell division cycle whereby the cell approximately doubles in length before dividing into two daughter cells (only the mother cell is followed here). TMP treatment causes the cell to stop growing after ~200 min of treatment. b) Moving standard deviation of cell length computed from the trace shown in panel a. This was used in the automated data analysis to determine whether an individual cell is growing or not. When the standard deviation is above a set threshold of 0.2 represented by the blue line, the cell is considered to be actively growing.

I opted for a TMP concentration equivalent to ¼ of the MIC, i.e. 0.25 µg/ml. This intermediate concentration was chosen such that a mixture of live and dead cells would be present, providing

insight into the mechanism of action of TMP. Moreover, the exploration of sub-inhibitory concentrations of antibiotics is of great interest. It has been described that sub-inhibitory concentrations of antibiotics induce stress responses and mutagenesis which can lead to antibiotic resistance, even at concentrations 10-fold below the MIC (Gullberg et al., 2011; Kohanski et al., 2010). Firstly, I assessed how continuous 0.25 µg/ml TMP treatment affected cell survival and growth in the microfluidic devices using the two metrics described above. The remaining cell count in M95AA + AdGM medium showed little difference between treated and untreated cells until 250 min of treatment. From this point, the number of cells decreased more steeply with treatment down to around 75% remaining cells by 800 min compared to 95% without treatment (Fig.15). This trend was conserved in M95AA medium, with a higher percentage of over 90% remaining cells after 800 min. This indicates that the single-cell analysis can indeed resolve subtle differences between the bactericidal and bacteriostatic conditions.

The cell growth dynamics in M95AA + AdGM showed an initial lag phase for 100 min after the start of continuous TMP treatment during which the percentage of growing cells was unaffected (Fig.15). Following that, I observed a sharp drop in actively growing cells until about 500 min, when it reached around 25% of growing cells. The level of growing cells decreased below 25% by 800 min. This pattern matches the previously described phases of TMP action, namely an initial lag phase followed by a RED phase and a survival phase (Kuong & Kuzminov, 2010). Cell growth dynamics were strikingly different in the bacteriostatic M95AA medium, with an immediate drop in actively growing cells in the first 100 min of TMP treatment. Interestingly, cell growth recovered transiently before decreasing with similar dynamics to M95AA + AdGM medium. This recovery could be due to cells undergoing a slightly delayed final division before arresting growth (Fig.14), transiently reducing the percentage of non-growing cells. For untreated cells in both M95AA + AdGM or M95AA, the percentage of remaining and actively growing cells did not change much throughout the experiments, representing a natural process of ageing rather than a consequence of the

treatment (Fig.15). Taken together, these results show that a large number of cells enter growth arrest in bactericidal and bacteriostatic media with sublethal TMP treatment, but with differences in the dynamics between the media. The results also suggest that cell disappearance due to lysis and/or filamentation is more common in the bactericidal medium.

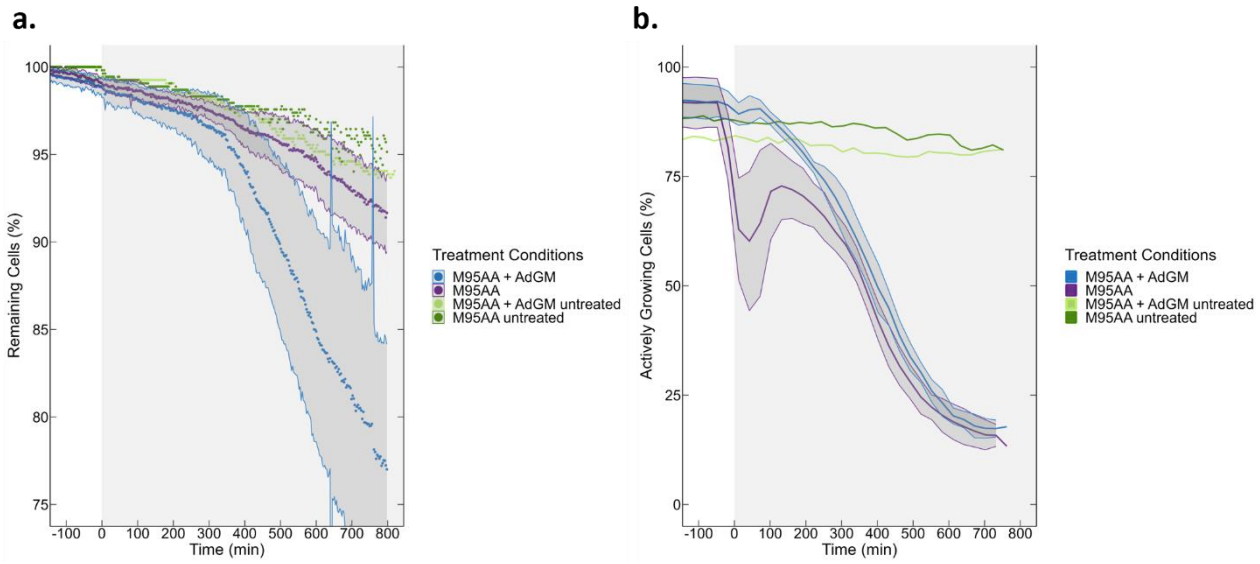


Figure 15 : Remaining and actively growing cells with continuous 0.25 µg/ml TMP treatment from timepoint 0 during microfluidic experiments or without treatment in M95AA + AdGM or M95AA media. a) Percentage of remaining cells per time throughout the experiment. b) Percentage of actively growing cells per time throughout the experiment. The curves represent mean values obtained from 1000-1500 cells per experiment for untreated cells, and an average of four separate experiments for treated cells, including standard deviation (shaded area).

Next, using the custom-written analysis script in R, I utilised the cell growth metrics defined above, as well as the cell length, to define the state of each cell at different timepoints during the microfluidics experiments (200 min, 500 min, 800 min). This enabled the division of the cell population into five subpopulations, namely “healthy”, “lysed”, “filamenting”, “growth arrest”, and “recovered” as defined in Fig.16. According to this definition, “recovered” cells exhibit filamentation or growth arrest but resumed normal growth before the relevant timepoint, whereas “healthy” cells exhibit no abnormal growth behaviour before the relevant timepoint. Given that I

observed in the survival and growth of the cells an initial lag phase lasting about 100 min, I determined that the initial effect of TMP post lag phase could already be visible by 200 min. By 500 min, a plateau was reached with only 25% of cells still actively growing, concluding the exponential phase (Fig.15). At 800 min, the proportion of remaining cells had stabilised, capturing the final effect of TMP in the survival phase. Hence, these timepoints appeared to be the most interesting for the study and are in line with the phases of thymidine starvation previously described (Kuong & Kuzminov, 2010; Pritha Rao & Kuzminov, 2020; P. Rao & Kuzminov, 2019).

		Cell Fate				
Temporality	**Attributes**	**Healthy**	**Lysed/Absent**	**Filamenting**	**Growth Arrest**	**Recovered**
Timepoint	**Remaining** Present / Absent in channels	Present	Absent	Present	Present	Present
Timepoint	**Actively Growing** Moving window for standard deviation of cell length > threshold (Both → 0.2)	Yes	N/A	Yes	No	Yes
Timepoint	**Filamentation** Cell length > threshold (M95AA + AdGM → 6.27 um M95AA → 6.1um)	No	N/A	Yes	N/A	No
Lifetime	**Asymmetric division** Recovery from growth arrest or filamentation	N/A	N/A	N/A	N/A	Yes

Figure 16 : Cell state assignment criteria. The cell states are at the top of the table, and the attributes are defined based on temporality (measured at a timepoint or during the lifetime of the cells). The attributes include being remaining, actively growing, filamentation or asymmetric division. Not all criteria are applicable for all cell states (N/A).

Interestingly, substantial variations were noted in the cell states at different timepoints when employing the two media for treated cells, although in both cases, very few cells appeared healthy after 200 min of treatment (Fig.17). In M95AA + AdGM, the cell states were quite varied at 200 min with a majority of filamenting cells, and evolved by 500 min, to a large proportion of cells still filamenting but a majority of growth arrest cells. By 800 min, an overwhelming majority of around 60% of the cells were in growth arrest and the lysed/absent cells peaked at around 20%, suggesting

a lethal effect of TMP. It must be noted that for lysed cells, the breakdown indicated that $^{2}/_{3}$ of the cells disappeared from the experiment in abnormal size, suggesting some of these may not have lysed, but escaped from the growth channels instead, whereas the remaining $^{1}/_{3}$ of cells likely lysed.

On the other hand, for M95AA at 200 min, I observed a majority of recovered cells (Fig.17). By 500 min, more than half of the cells were growth arrested and this increased by 800 min, with almost 80% of growth arrest cells, and only above 5% of lysed cells, suggesting a static effect for TMP. I observed very similar profiles at all timepoints in untreated cells in both media, with a large majority of healthy cells (Fig.18). Thus, the profiles highlighted notable differences between M95AA + AdGM and M95AA for treated cells. M95AA + AdGM exhibited a higher proportion of lysed cells with an uneven distribution of filamenting and growth arrest cells suggesting unhealthy cells. On the other hand, M95AA predominantly featured growth-arrested cells, along with a lower proportion of lysed cells. These differences were not as visible in the population-based assays and gave a first insight into the different actions of the treatment in the two media used. However, continuous treatment led in both cases to a large proportion of growth arrest cells which did not allow to discriminate the two media properly. Hence, I decided to remove the treatment shortly after the end of the lag phase and observe if any differences arose.

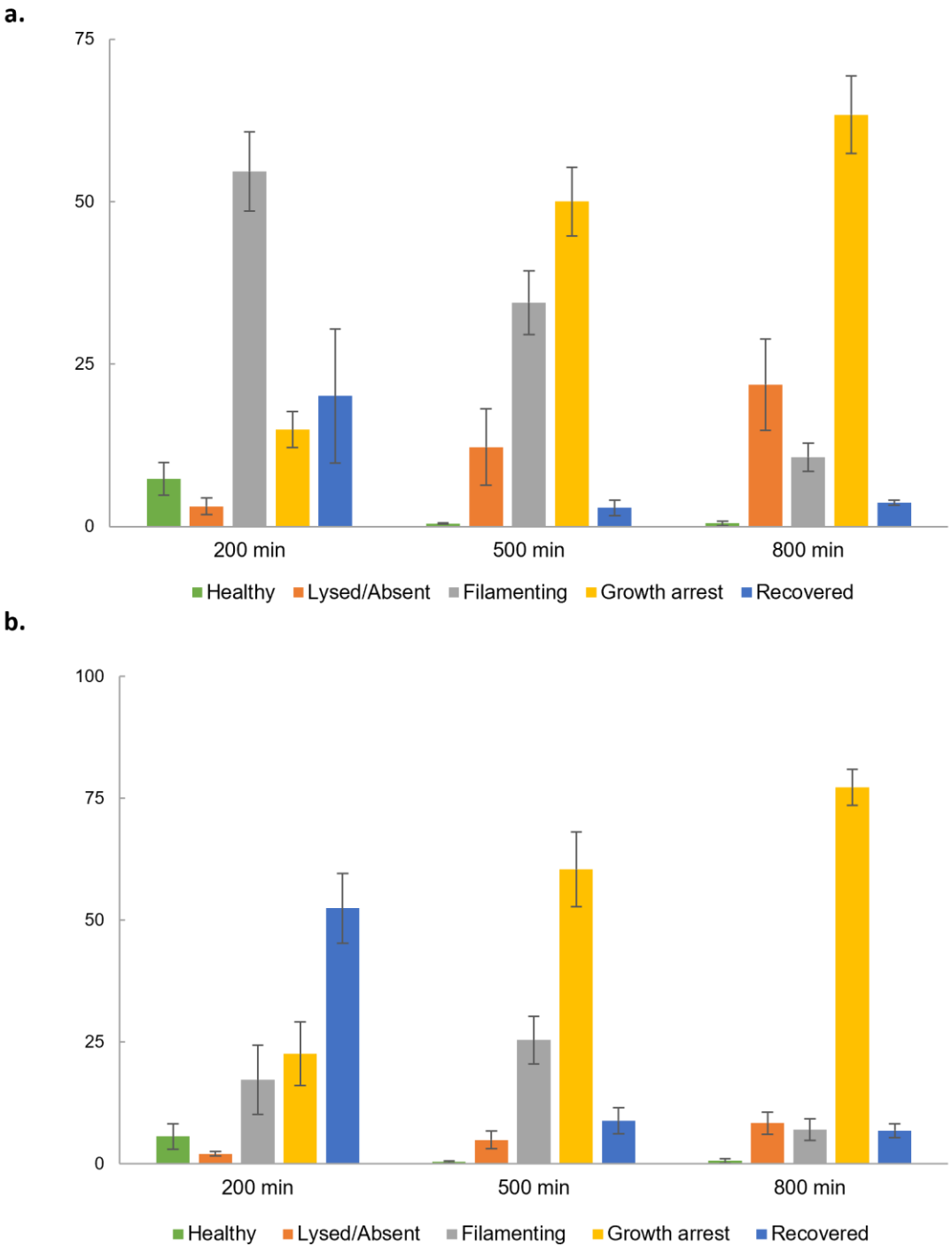


Figure 17 : Cell states distribution for 0.25 µg/ml TMP-treated cells at different timepoints in a) M95AA + AdGM and b) M95AA media. The different colours represent the cell states. The values for each cell state were obtained from four experiments, with standard deviation.

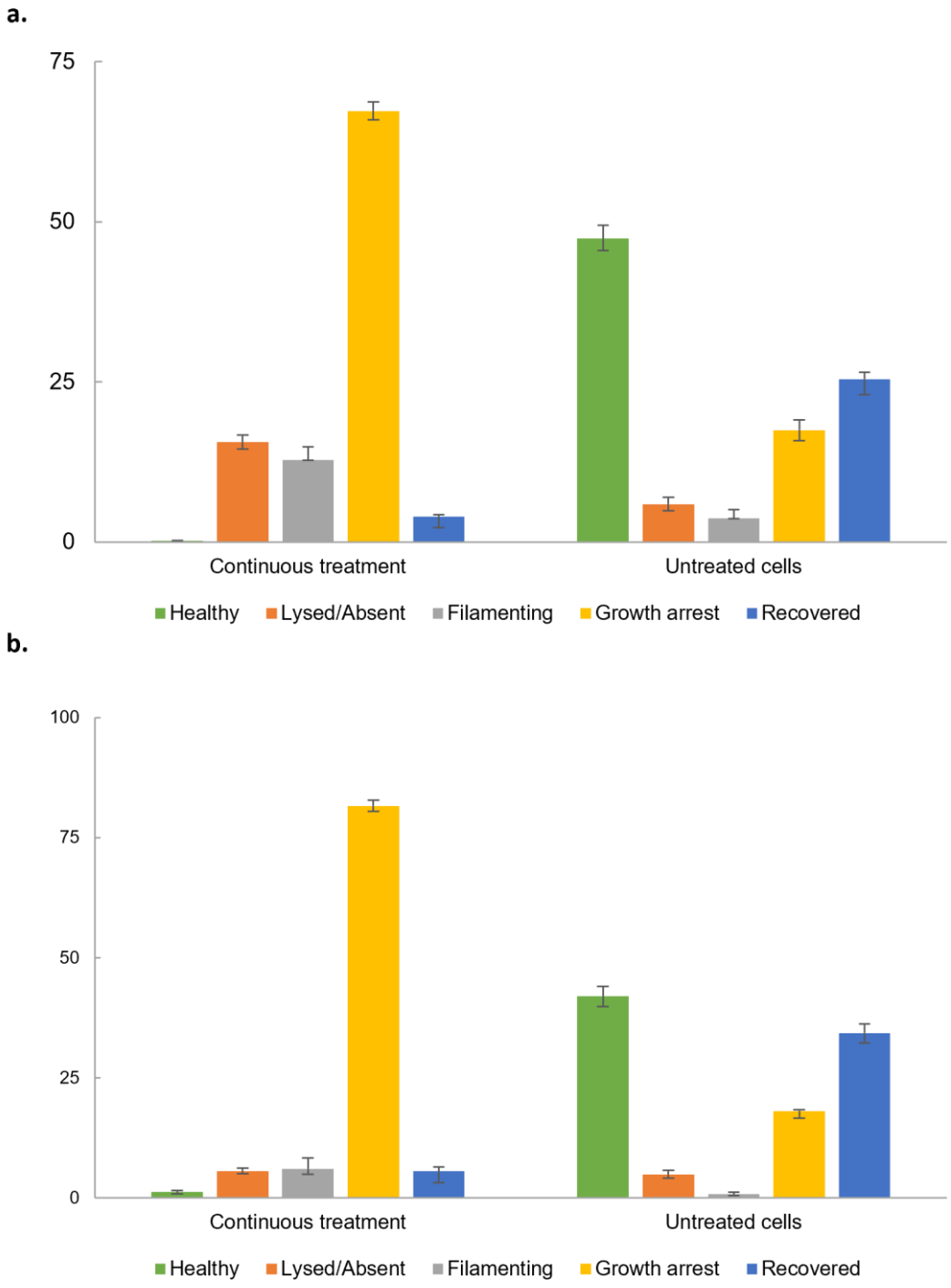


Figure 18 : Cell states distribution for 0.25 µg/ml TMP-treated and untreated cells at 800min in a) M95AA + AdGM and b) M95AA media. The different colours represent the cell states. The values are from a single repeat and include a 95% confidence interval obtained from bootstrapping (1000 repeats).

Next, I tested whether a shorter course of treatment could amplify or reduce some of the effects observed in both media. When TMP treatment was halted after 150 min by changing the medium

back to one without TMP, I observed a sharp decrease in the percentage of remaining cells in M95AA + AdGM medium. Surprisingly, this decrease was larger than for continuous treatment (Fig.19), indicating that the attempt to resume growth caused additional cell killing. However, although the percentage of actively growing cells also showed a steep decrease when treatment was stopped, it stabilised afterwards (Fig.19), showing that the surviving cells could carry on growing. Interestingly, in M95AA medium, there was no steep loss of viability when treatment was halted after 150 min, and the percentage of actively growing cells recovered almost back to pre-treatment levels. This clear difference between the two media matches the expectation that cell death is more pronounced in the bactericidal medium whereas cell growth resumes in the bacteriostatic medium after treatment is stopped.

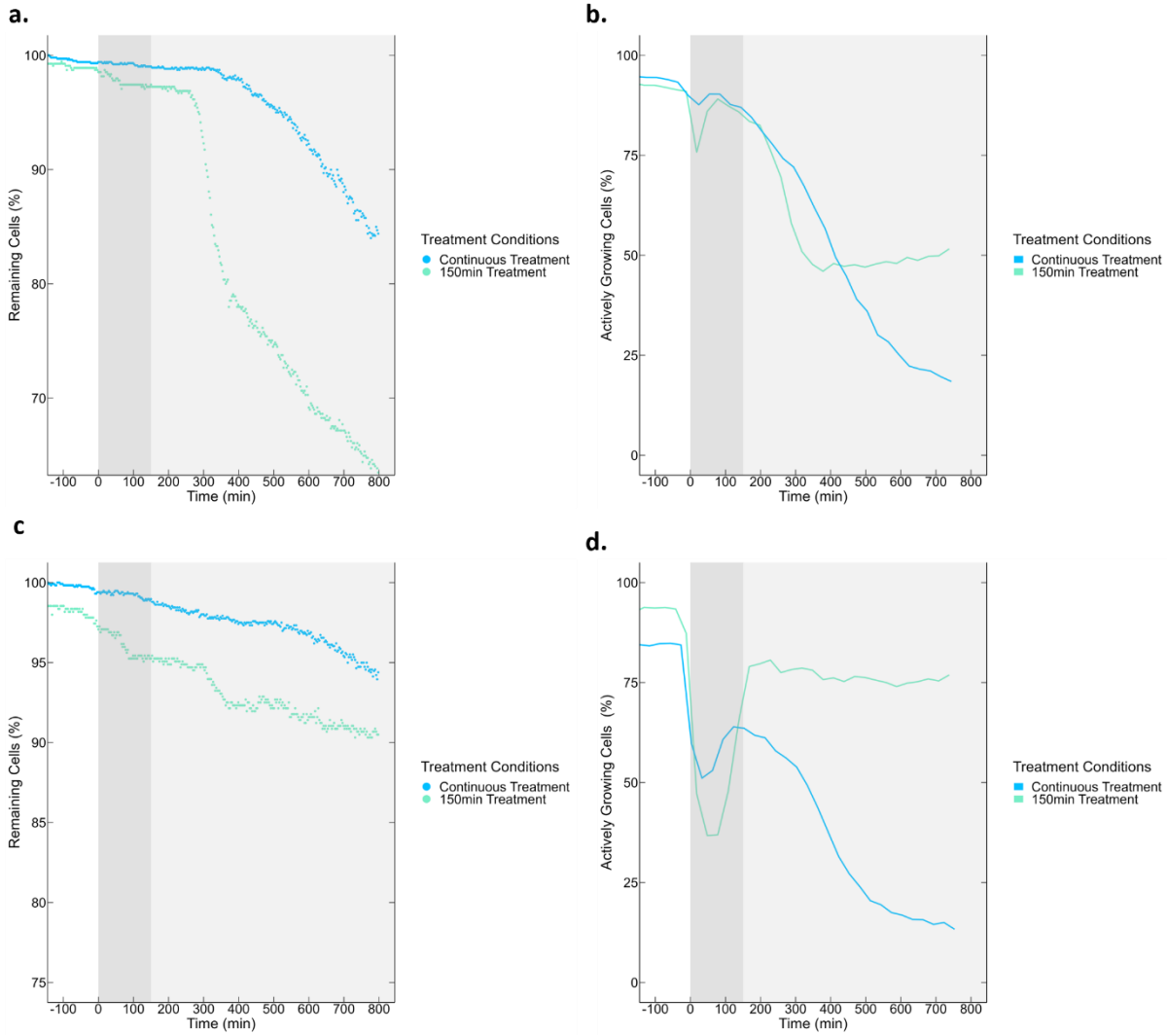


Figure 19 : Remaining and actively growing cells with continuous or 150 min course (dark grey) of 0.25 µg/ml TMP treatment from timepoint 0 during microfluidic experiments in M95AA + AdGM, and M95AA media. a) and c) Percentage of remaining cells per time throughout the experiment. b) and d) Percentage of actively growing cells per time throughout the experiment. The curves represent mean values obtained from 500-1000 cells per experiment.

The distribution of cell states provided additional insight into the differences between bactericidal and bacteriostatic media when TMP treatment was halted after 150 min (Fig.20). In M95AA + AdGM, the sharp decrease in the number of remaining cells after treatment removal could be attributed to increased cell lysis. For M95AA media, cell lysis was uncommon after treatment removal and the majority of cells recovered growth instead.

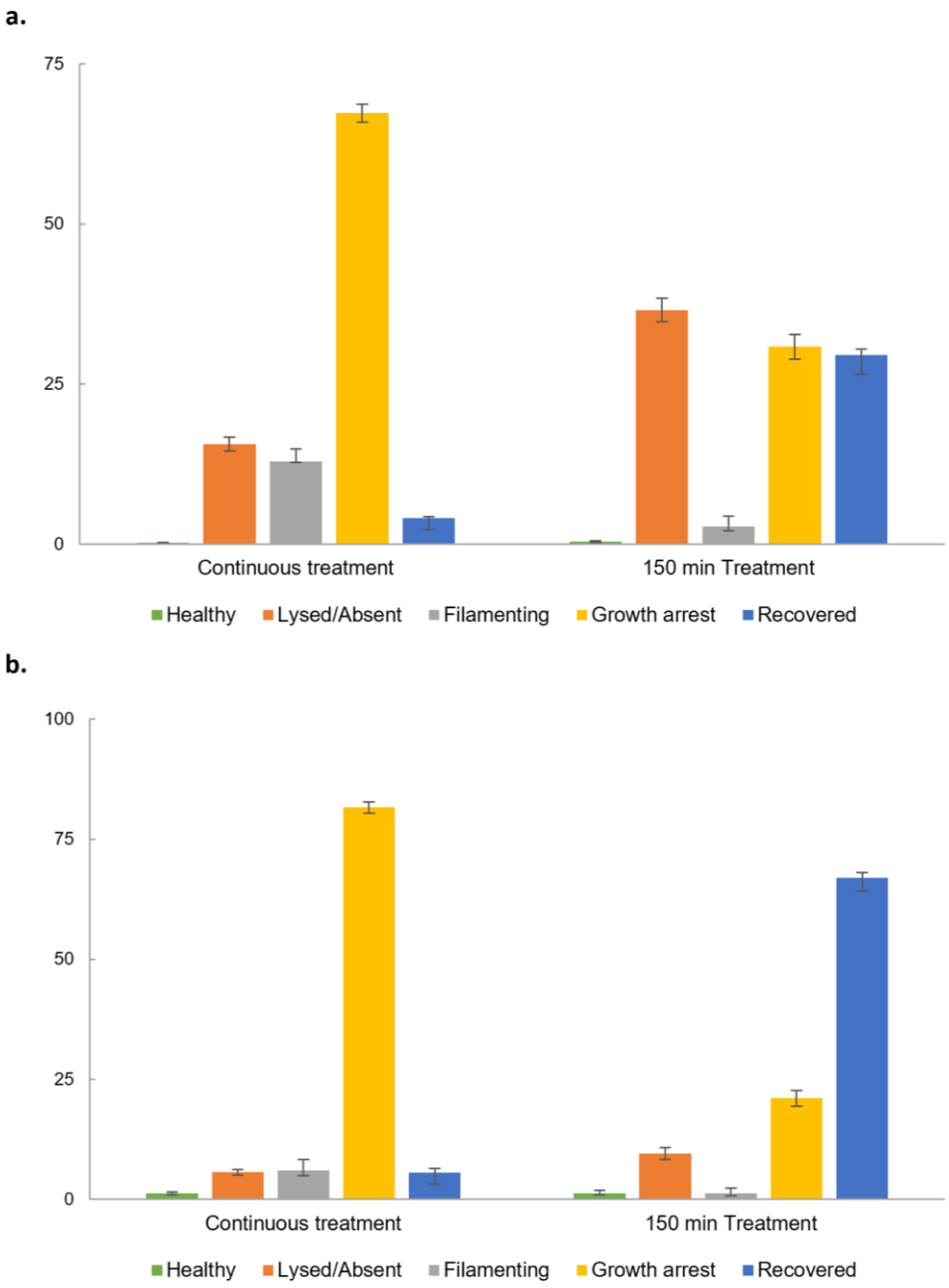


Figure 20 : Cell states distribution after 800 min for WT cells with continuous or 150 min course of treatment with 0.25 µg/ml TMP in a) M95AA + AdGM and b) in M95AA. The different colours represent the possible states. The values for each cell state are determined for 500-100 cells per experiment and include a 95% confidence interval obtained from bootstrapping (1000 repeats).

2.3. Trimethoprim's Impact on the Phenotypic Dynamics of Cells with Diverse Media Supplementation

Since I confirmed that the composition of the growth medium has an important role in the effects of TMP treatment, I performed additional experiments with different supplementations, including thymidine or adenine for the bacteriostatic medium only (Sangurdekar et al., 2011). Thus, I tried different set up with thymidine, continuously supplementing the medium with it, or removing it at different timepoints in M95AA + AdGM, to understand the role of exogenous thymidine cellular uptake (Fig.21). The different timings for thymidine supplementation could provide an insight into whether thymidine is utilized and needed continuously in the presence of TMP or if a reserve assembled before the start of treatment or for a short time during treatment would be sufficient to sustain the cells during continuous treatment.

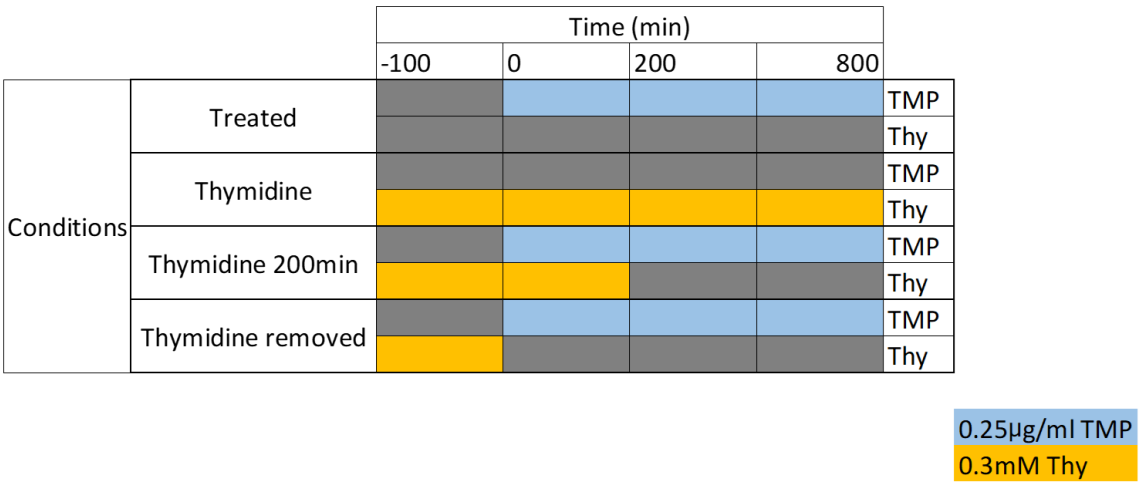


Figure 21 : Schematics of the supplementation with thymidine in M95AA + AdGM. The blue represents 0.25 µg/ml TMP, whilst yellow is thymidine 0.3 mM. The 4 possible conditions are listed on the left, and for each, a line represents the temporality of TMP treatment, and the other line represents the temporality of thymidine supplementation.

Firstly, when thymidine was added to M95AA + AdGM, I observed a small but sustained decrease in the proportion of remaining cells, and little change in the percentage of growing cells throughout the experiment (Fig.22). For the different cell states, I observed very similar profiles to untreated cells by 800 min with a large majority of healthy cells. All of the parameters were similar to untreated cells and suggested again a natural process of ageing during the experiments. To further understand the role of thymidine, I examined the effect of thymidine supplementation being removed after ~200 min of continuous treatment in M95AA + AdGM (Fig.22). I observed that the lag phase was extended in that case to 200 min after removal of thymidine for actively growing cells, and there was a small decrease in the proportion of alive cells compared to treated cells. I also observed very few healthy cells and at 800 min, the profile resembled closely the one observed in treated cells, with a majority of cells in growth arrest. This suggests that the cells can import a large enough amount of thymidine to counteract the effect of TMP for twice the time the existing supplies would normally last, reducing the death toll. However, the cells were still subject to irreversible damage causing arrest. When thymidine was supplemented in the medium but removed at the start of continuous treatment, the lag phase for actively growing cells was shortened, down to around 50 min. It also led to a different state profile than treated cells by 800 min with a larger majority of almost 80% of cells in growth arrest, suggesting that the thymidine salvage pathway activated by exogenous thymidine could be precipitating growth arrest.

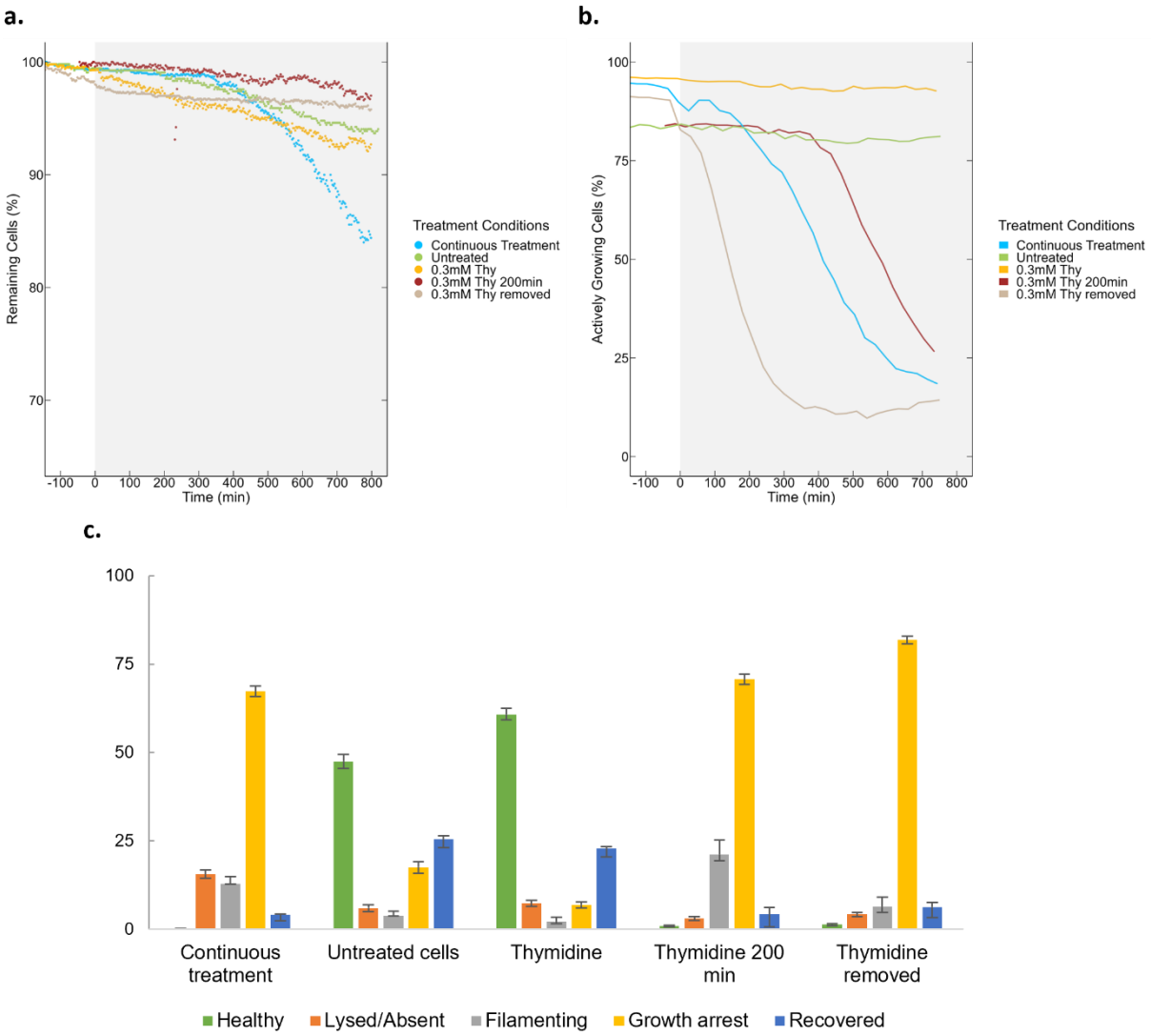


Figure 22 : Remaining and actively growing cells in cells with continuous 0.25 µg/ml TMP treatment from timepoint 0 during microfluidic experiments, with different medium supplementation or without treatment in M95AA + AdGM. a) Percentage of remaining cells per time throughout the experiment. b) Percentage of actively growing cells per time throughout the experiment. c) Distribution of cell states at 800 min. The curves represent mean values obtained from 500-1000 cells per experiment and include a 95% confidence interval obtained from bootstrapping (1000 repeats).

I then investigated the engineered cells carrying a resistant plasmid copy of *folA* in M95AA + AdGM, to verify if these were indeed resistant to TMP (Fig.23). The cells appeared quite unhealthy overall in the microfluidic growth chambers set up, as can be seen by the low level of growing cells right from the start of the experiment in both media. This was observed in the absence of TMP too. In M95AA + AdGM, I observed a small decrease in remaining and actively growing cells for both

treated and untreated cells, suggesting that this effect is unrelated to TMP. I only observed very few cells as healthy, or filamenting suggesting a high fitness cost for the plasmid. However, I also observed a lower percentage of lysed/absent cells than for WT cells, confirming resistance provided by the extra copy of FolA.

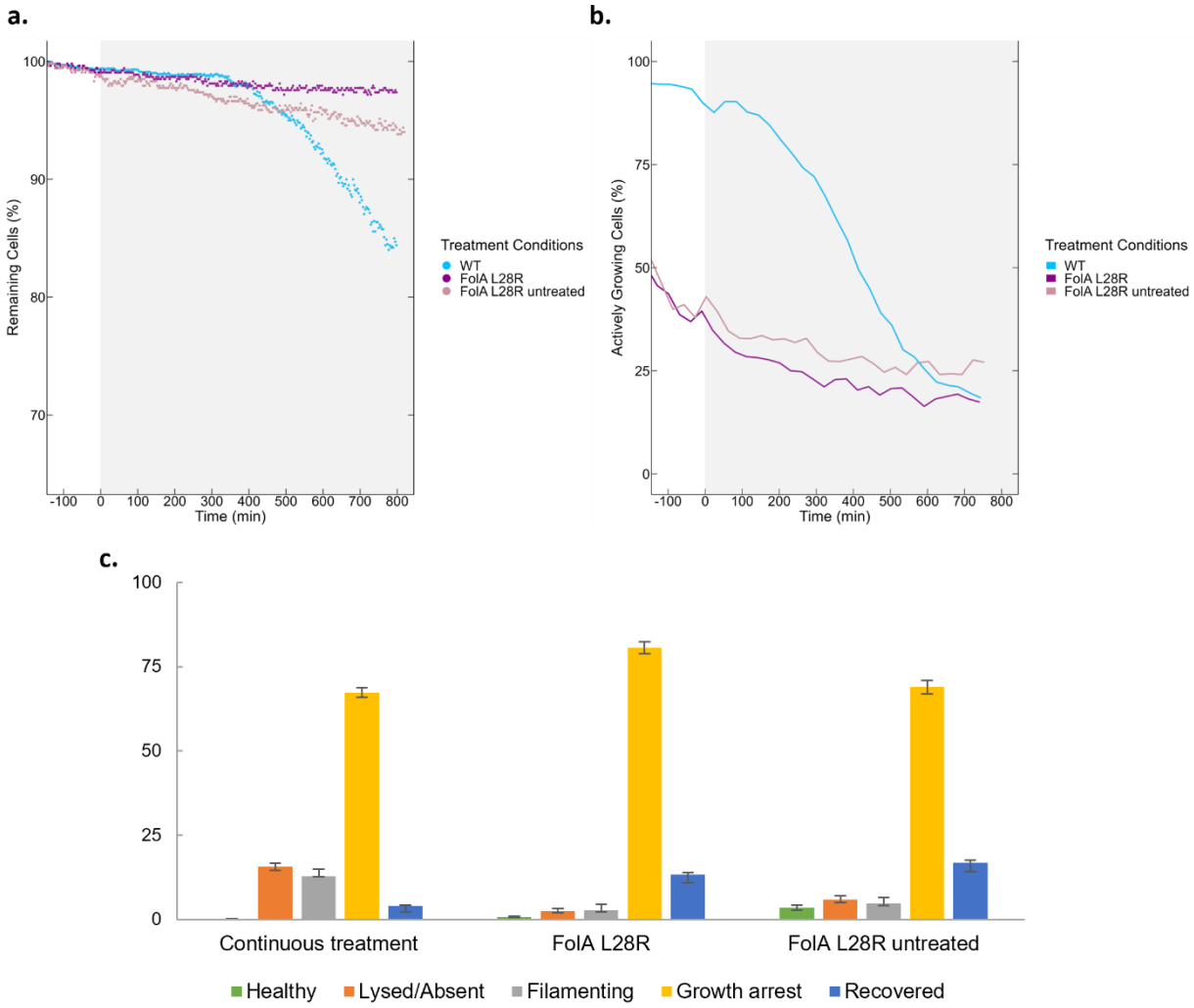


Figure 23 : Remaining and actively growing cells with continuous 0.25 µg/ml TMP treatment from timepoint 0 in wild-type or resistant cells during microfluidic experiments in M95AA + AdGM. a) Percentage of remaining cells per time throughout the experiment. b) Percentage of actively growing cells per time throughout the experiment. c) Distribution of cell states at 800 min. The curves represent mean values obtained from 500-1000 cells per experiment and include a 95% confidence interval obtained from bootstrapping (1000 repeats).

I carried out similar experiments in M95AA, with thymidine and adenine supplementation, to understand if any supplementation could rescue the cells in a bacteriostatic medium. Firstly, I

observed that thymidine supplementation had similar effects for remaining and alive cells than untreated conditions (Fig.24). However, it appeared that there was a majority of recovered cells instead of healthy. Taken together, these results suggest an effect of TMP despite the presence of thymidine in M95AA medium. Then, with the addition of adenine to M95AA, I did not detect any changes in the percentage of alive cells compared to untreated or treated cells. Instead, I noticed the suppression of the lag phase for actively growing cells, with an immediate and sharp decrease. The cell state profile for adenine supplementation resembles that of treated cells, suggesting an important role for adenine in the TMP treatment.

For strains carrying a resistant plasmid copy of *folA*, the cells in M95AA were unhealthy and in growth arrest from the start of the experiment as observed in M95AA + AdGM (Fig.24). In M95AA, whilst the proportion of growing cells decreased slightly for resistant cells, the proportion of remaining cells decreased at a higher rate than in treated WT cells, down to a lower level even, suggesting that some effects of treatment cannot be rescued by FolA. I also observed that the proportion of lysed cells was higher than for susceptible cells. This suggests that the presence of the plasmid in M95AA is very costly for the cells and unlike in bactericidal medium, the resistance provided by *folA* L28R is not sufficient to counteract the effect of TMP.

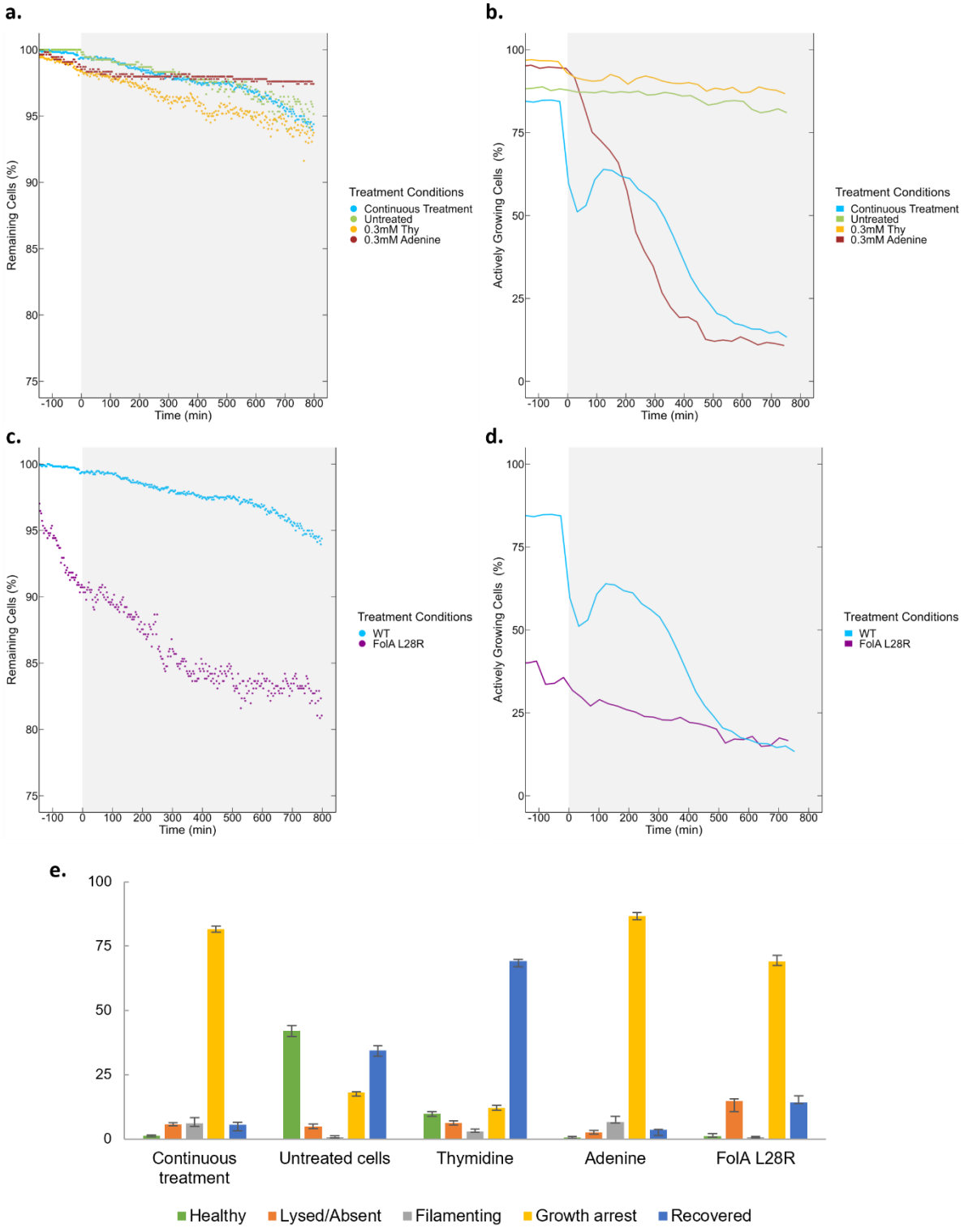


Figure 24 : Remaining and actively growing cells in WT and resistant cells with continuous 0.25 µg/ml TMP treatment from timepoint 0 during microfluidic experiments, with different medium supplementation or without treatment in M95AA. a) Percentage of remaining cells per time throughout the experiment. b) Percentage of actively growing cells per time throughout the experiment. c) Distribution of cell states at 800 min. The curves represent mean values obtained from 500-1000 cells per experiment and include a 95% confidence interval obtained from bootstrapping (1000 repeats).

2.4. Trimethoprim's Influence on Size Change Dynamics

Based on the experiments described previously, I decided to focus the analysis of the microfluidics experiment data in the first 500 min of continuous sub-MIC treatment. This was done to capture when the cells transitioned into a state of growth arrest, but before acute cell death reduced the number of cells I could investigate, keeping the cells in the exponential death phase (Fig.25). Additionally, some preliminary experiments have suggested that the reliability of the setup and particularly the flow could sometimes be reduced after 500 min. Using this predefined 500 min window of observation, I proceeded with my investigations, delving into the dynamics of cell sizes in response to TMP in M95AA + AdGM and M95AA. Since cell size changes, particularly cell length is a parameter used to define the cell states observed, this could also be used to validate the identity of the subpopulations defined. At the whole population level, I established a threshold equal to the mean cell length of untreated cells plus 4 (M95AA + AdGM) or 6 (M95AA) standard deviation to assign a normal or filamenting status to each cell.

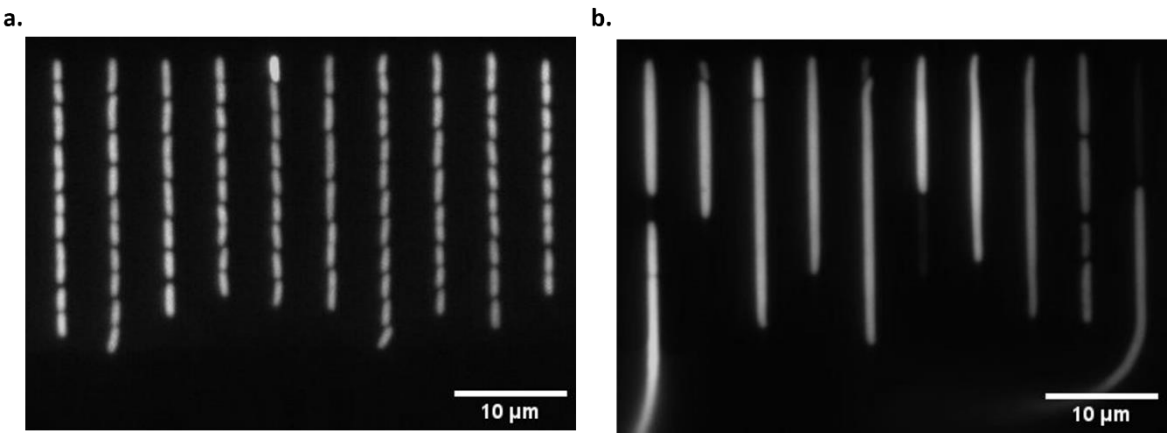


Figure 25 : Snapshots of cells with a mKate2 segmentation marker in the mothermachine growth chambers. a) Before treatment. b) After the start of treatment.

In M95AA + AdGM, I noticed for cell width and length, a clear increase for both parameters (Fig.26). The cell width increased after 100 min, plateauing around 300 min. The cell length follows a similar temporal pattern, from 3.5 µm before treatment and until 100 min, and up to a plateau with a 4-fold increase after 400 min. This was in accordance with the literature. Indeed, microscopic observation of thymidine-starved cells has shown elongated cells following the start of thymidine depletion, from 1 h, with changes of up to 3-fold, or 6-fold by 3 h (T. V. P. Rao & Kuzminov, 2020, 2021), indicating a blockage in cell division. Going forward, due to very similar trends observed for both cell length and width, I decided to explore in more detail only the cell length as a size criterion. Hence, I explored the particularity of each cell state in more detail (Fig.26c). Since no healthy cells crossed the filamenting threshold throughout the experiment, this validated the analytical classification of cell states. I noted changes in cell length for all other cell states, always after 100 min of treatment and particularly in filamenting cells increasing by up to 5-fold within 500 min. Lysed cells could also increase by almost 6-fold, which again could either indicate lysis in a filamenting state, or possible escape of the cells from the growth channels due to long lengths. When looking at the distribution at -100 min and 500 min for cell length in the bactericidal medium, I observed a clear shift in profile from normal lengths below the threshold before treatment, to large heterogeneity and on average longer lengths after the start of treatment.

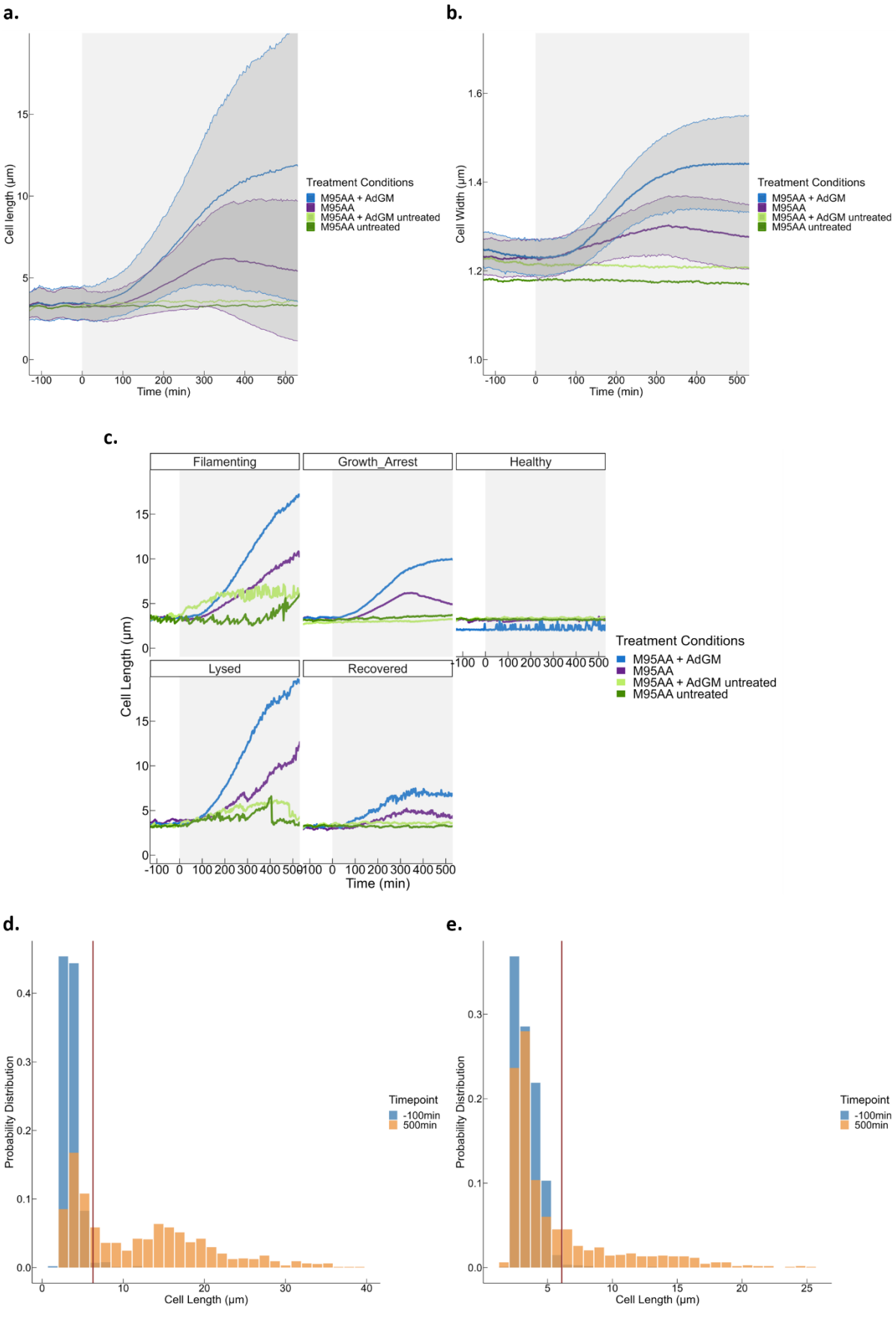

a.
Cell length (µm)
Time (min)
Treatment Conditions
M95AA + AdGM
M95AA
M95AA + AdGM untreated
M95AA untreated
b.
Cell Width (µm)
Time (min)
Treatment Conditions
M95AA + AdGM
M95AA
M95AA + AdGM untreated
M95AA untreated
c.
Filamenting
Growth_Arrest
Healthy
Lysed
Recovered
Cell Length (µm)
Time (min)
Treatment Conditions
M95AA + AdGM
M95AA
M95AA + AdGM untreated
M95AA untreated
d.
Probability Distribution
Cell Length (µm)
Timepoint
-100min
500min
e.
Probability Distribution
Cell Length (µm)
Timepoint
-100min
500min

Figure 26 : Cell size dynamics with continuous 0.25 µg/ml TMP treatment from timepoint 0 during microfluidic experiments or without treatment in M95AA + AdGM or M95AA media. a) Cell length in µm per time at the population level in both media. b) Cell width in µm per time at the population level in both media. c) Cell length in µm per time at the cell state level determined at 800 min. d) Distribution of cell length observed at 100 min before and 500 min after treatment in M95AA + AdGM and f) in M95AA. The curves represent mean values obtained from 1000-1500 cells per experiment and include a standard deviation for treated cells. For the cell length distribution, the data is from a representative experiment.

In M95AA, I noted distinct profiles. Cell width exhibited only a small increase after about 100 min (Fig.26). Regarding cell length, as expected, no healthy cells had lengths corresponding to filamentation, validating further the cell state classification analysis. Conversely, I did observe filamenting cells in both lysed and filamenting subpopulations, after 100 min of continuous treatment. However, the length only increased by 2-fold, not indicative of strong filamentation, unlike the 4-fold increase in the bactericidal medium. I observed a lower level of cell heterogeneity in the distribution of cell length with very low frequency observed for longer lengths after treatment and a similar peak in distribution between -100 and 500 min. Overall, in M95AA, some cells appeared to grow longer but to smaller lengths on average than in M95AA + AdGM which could reflect differences in responses expressed in the different media. For instance, the literature suggests in the context of thymineless death that one such response would be the SOS response, which can prevent cell division and thus lead to cell filamentation, via activation of the inhibitor of division SulA (Fonville et al., 2010).

I also carried out some control experiments in both media to observe the cell length for untreated cells and observed no changes in cell sizes indicative of filamentation at the population level for untreated cells (Fig.26). I noted a few cells filamenting throughout the experiment, but it has been suggested that even in the absence of stressor, spontaneous degradation of LexA, the transcriptional repressor of the SOS response, can happen (Jones & Uphoff, 2021), potentially leading to filamentation. Going back to treated cells, I observed the effects on cell length for TMP

removal from the medium after 150 min and noted that the initial increase in cell size was still present in both media after the initial lag phase. This was followed by a decrease, leading to an average size below the filamenting threshold by 400 min (Fig.27). The results suggest that continuous treatment causes an increase in cell length and that whilst the medium supplementation does not play a role in the timing, it influences the magnitude of the cell length changes. Finally, I observed that the conditions with low survival rates were associated with a high level of variation in length between cells, suggesting more heterogeneity is generally associated with more cell killing (Fig.28).

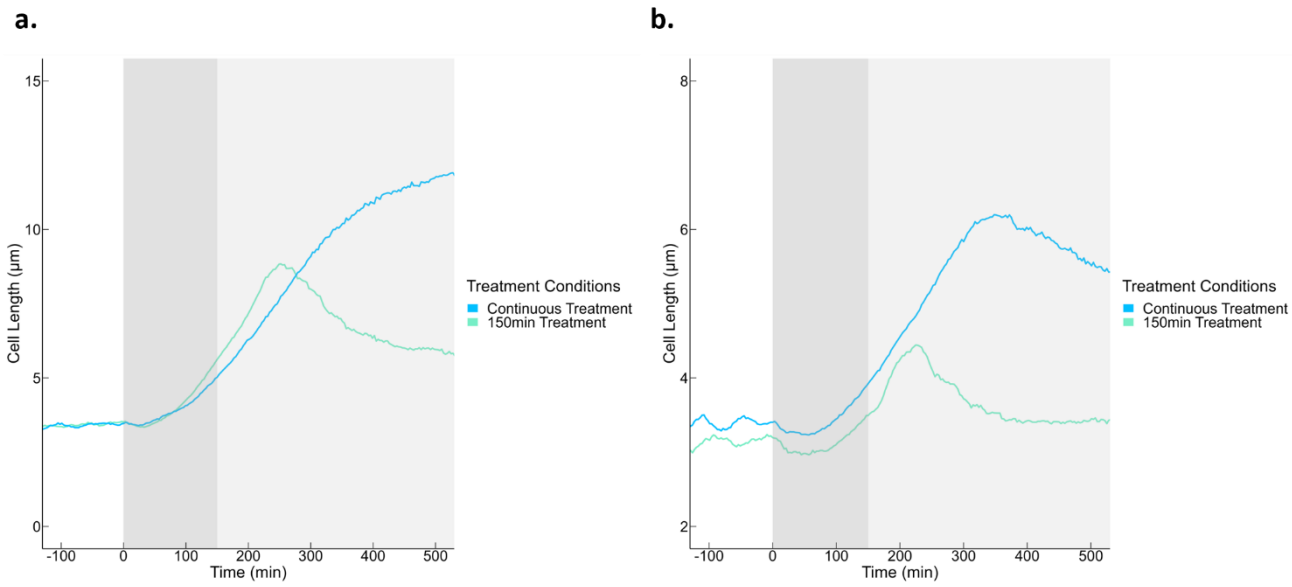


Figure 27 : Cell length dynamics with continuous or 150 min course (dark grey) of 0.25 µg/ml TMP treatment from timepoint 0 during microfluidic experiments in a) M95AA + AdGM, and b) M95AA media. The curves represent mean values obtained from 500-1000 cells per experiment.

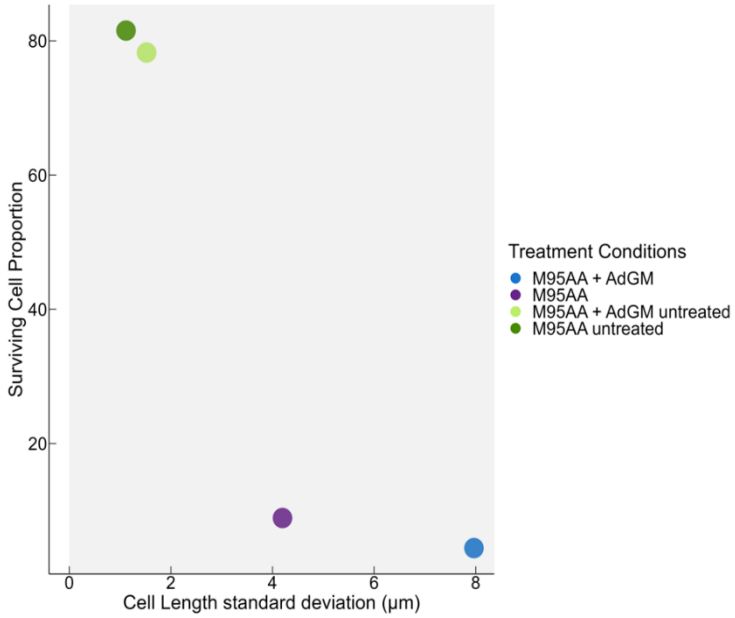


Figure 28 : Correlation between cell-to-cell heterogeneity in cell length and cell survival. The surviving cell proportion (healthy and recovered cells) is plotted against the standard deviation in cell length across all cells measured at 500 min. The points represent mean values obtained from 1000-1500 cells per experiment and cells were treated with continuous 0.25 µg/ml TMP.

Given that thymidine rescues the cells from TMP treatment, I decided to test its effects on cell length changes. Indeed, when thymidine was added in M95AA + AdGM, no changes were observed for the cell length (Fig.29), much like for untreated cells. By contrast, in M95AA, thymidine addition did not completely abolish cell length changes and I still observed a very small increase in length. M95AA supplementation with adenine did not cause any changes in the cell length profile compared to treated cells, suggesting it is not involved in filamentation processes in the cells. For resistant strains, again, there was little change in cell length in both media. Interestingly, the removal of thymidine from the medium after 200 min of treatment prolonged the lag phase before filamentation. On the other hand, removal at the start of the treatment seemed to cause cell length changes with a temporal dynamic similar to that of treated cells without supplementation. However, the cell length changes were limited to 2-fold, reached shortly after the lag phase, and suggesting rapid growth arrest instead of lysis and filamentation. Overall, it appears that thymidine and a plasmid copy of *folA* abolish filamentation, particularly in bactericidal medium for TMP-

treated cells, therefore, depletion of thymidine is a major consequence of TMP treatment, causing cell size changes.

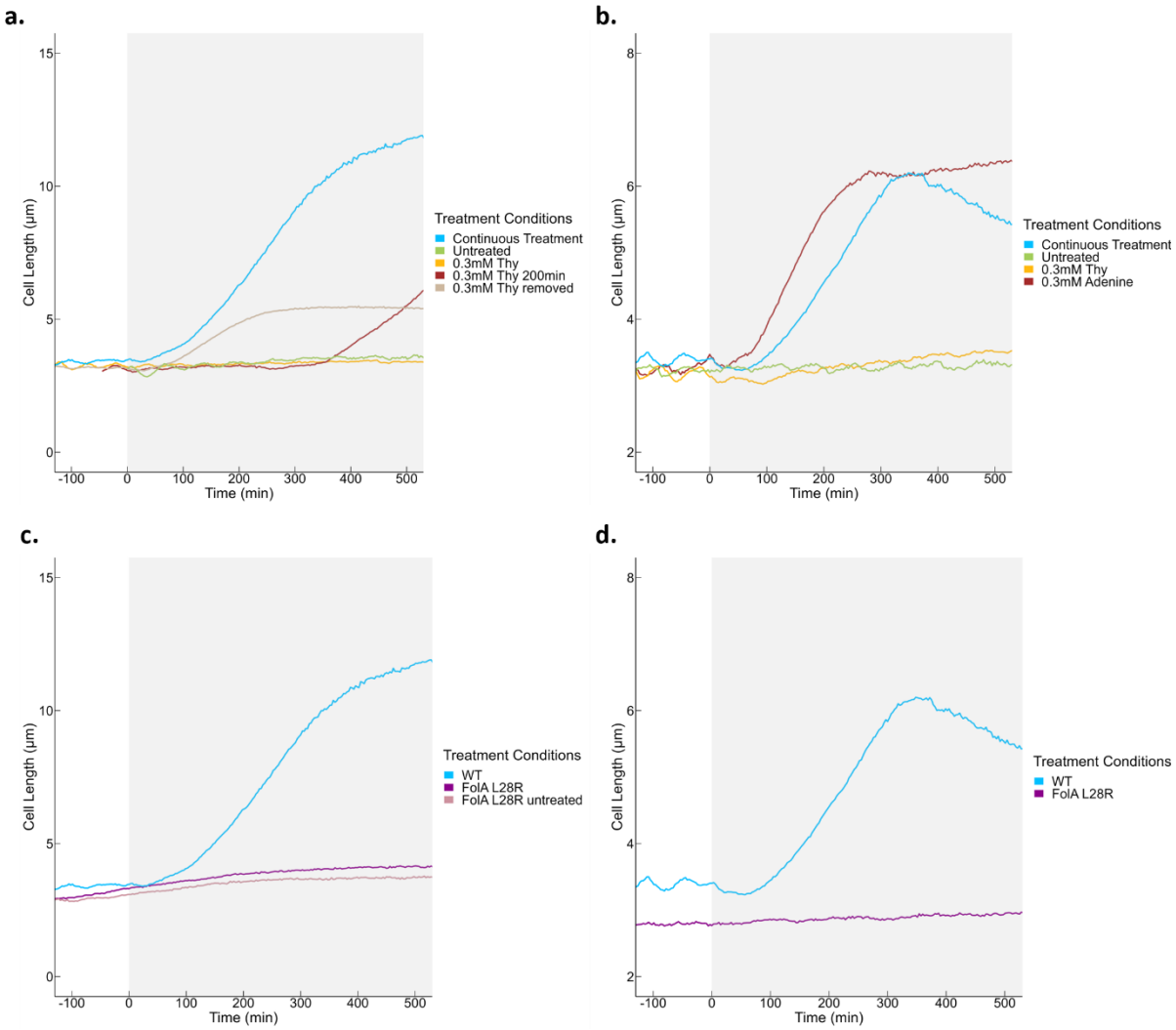


Figure 29 : Cell length in WT and resistant cells with continuous 0.25 µg/ml TMP treatment from timepoint 0 during microfluidic experiments, with different medium supplementation or without treatment. a), c) M95AA + AdGM and b), d) M95AA. The curves represent mean values obtained from 500-1000 cells per experiment.

2.5. Trimethoprim's Impact on the Phenotypic Dynamics of Mutant Cells

After gaining some insights into the metabolites involved in TMP's action and its phenotypic consequences, I turned to the role of metabolic pathways suggested to play a role for TMP. Hence, I tested the survival dynamics of a series of mutants in response to TMP treatment in both M95AA + AdGM and M95AA. Firstly, I tested the *ΔrffC* mutant, which is defective for dTDP-fucosamine acetyltransferase. It is involved in the production of dTDP required in the synthesis of the ECA and O-antigen, and thus the mutant could exhibit defects in the cell envelope (Kuhn, 1988; Meier-Dieter et al., 1990; Samuel & Reeves, 2003). This mutant has been presented as hypersensitive to TMP with a hyper-starvation phenotype whereby the cells do not undergo an initial lag phase due to envelope instability (Pritha Rao & Kuzminov, 2020). In my hands and in both media, I did not observe the dramatic changes in remaining or actively growing cells described in the literature and noted no indication of hypersensitivity (Fig.29). In fact, after the lag phase, I observed a higher proportion of alive cells in the mutant than in WT cells in the bactericidal medium.

Another example is the double mutant *ΔmutM ΔmutY* defective in 8oxoG repair. Whilst the dynamics are similar to that observed in WT cells in M95AA + AdGM, I observed the proportion of actively growing cells started to decrease after a longer lag phase of almost 200 min of continuous treatment (Fig.30). This mutant and the *ΔdinB ΔumuC* mutant, defective in TLS polymerases, presented a higher level of remaining cells at the end of the experiment. The dynamics in the other mutants tested were similar to what was observed in WT cells in M95AA + AdGM, except for a sharper drop in actively growing cells during the lag phase for the *lexA3ind*$^{-}$ mutant, suggesting that the cells entered growth arrest more rapidly. This mutant expresses an uncleavable form of LexA, preventing activation of the SOS response in the cell. In M95AA, all the mutants experienced a sharper initial decrease in actively growing cells, suggesting a precipitated growth arrest state, particularly for the *ΔdinB ΔumuC* mutant. I also observed a larger decrease in remaining cells compared to WT cells for the HR and SOS response deficient mutant *ΔrecA*.

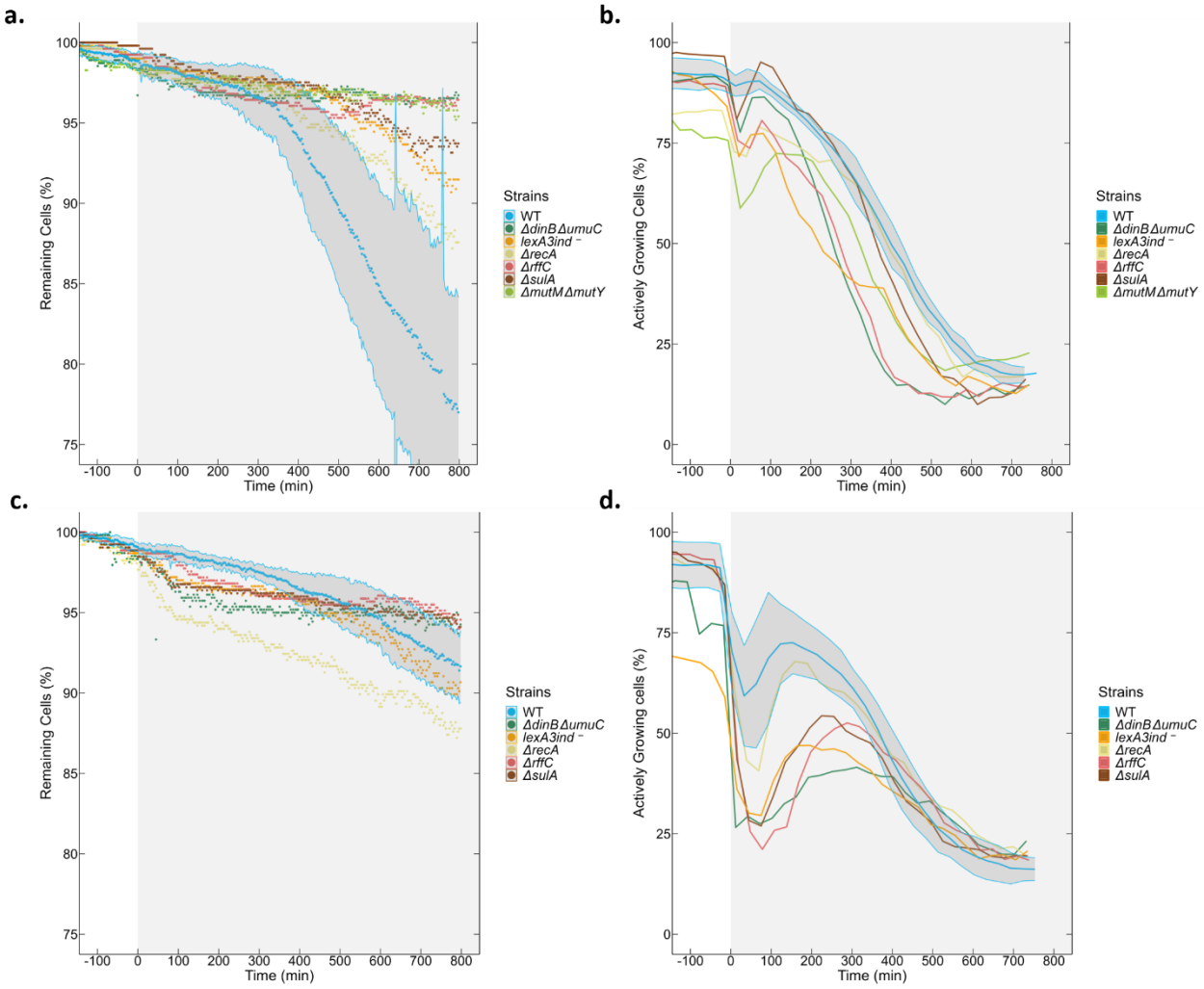


Figure 30 : Remaining and actively growing cells with continuous 0.25 µg/ml TMP treatment from timepoint 0 during microfluidic experiments in a series of WT and mutant cells in M95AA + AdGM or M95AA media. a) and c) Percentage of remaining cells per time throughout the experiment. b) and d) Percentage of actively growing cells per time throughout the experiment. The curves represent mean values obtained from 500-1000 cells per experiment. For WT cells, the curve with standard deviation (shaded area) represents an average of four separate experiments.

I investigated the cell states observed in the mutants in response to TMP treatment in both media, to determine if any pathway could cause the effects observed (Fig.31). Since I did not observe much difference in remaining or actively growing cells by 800 min, I compared the states at 200 min, when I noticed the most differences. In M95AA + AdGM I observed that most mutants had a higher proportion of healthy and recovered cells, suggesting beneficial mutations at that point. A notable exception was the profile including a large majority of growth arrest cells for the *lexA3ind-* mutant.

The *ΔdinB ΔumuC* mutant had a similar profile to the WT cells, suggesting that the mutation has little impact at 200 min. In M95AA, the profiles were quite similar to that of WT cells, with mainly recovered cells, although *ΔdinB ΔumuC* mutant had a 2-fold higher proportion of growth arrest cells. Overall, the results suggest that the deficiencies tested are not key for TMP treatment in bacteriostatic medium but may precipitate growth arrest in some cases.

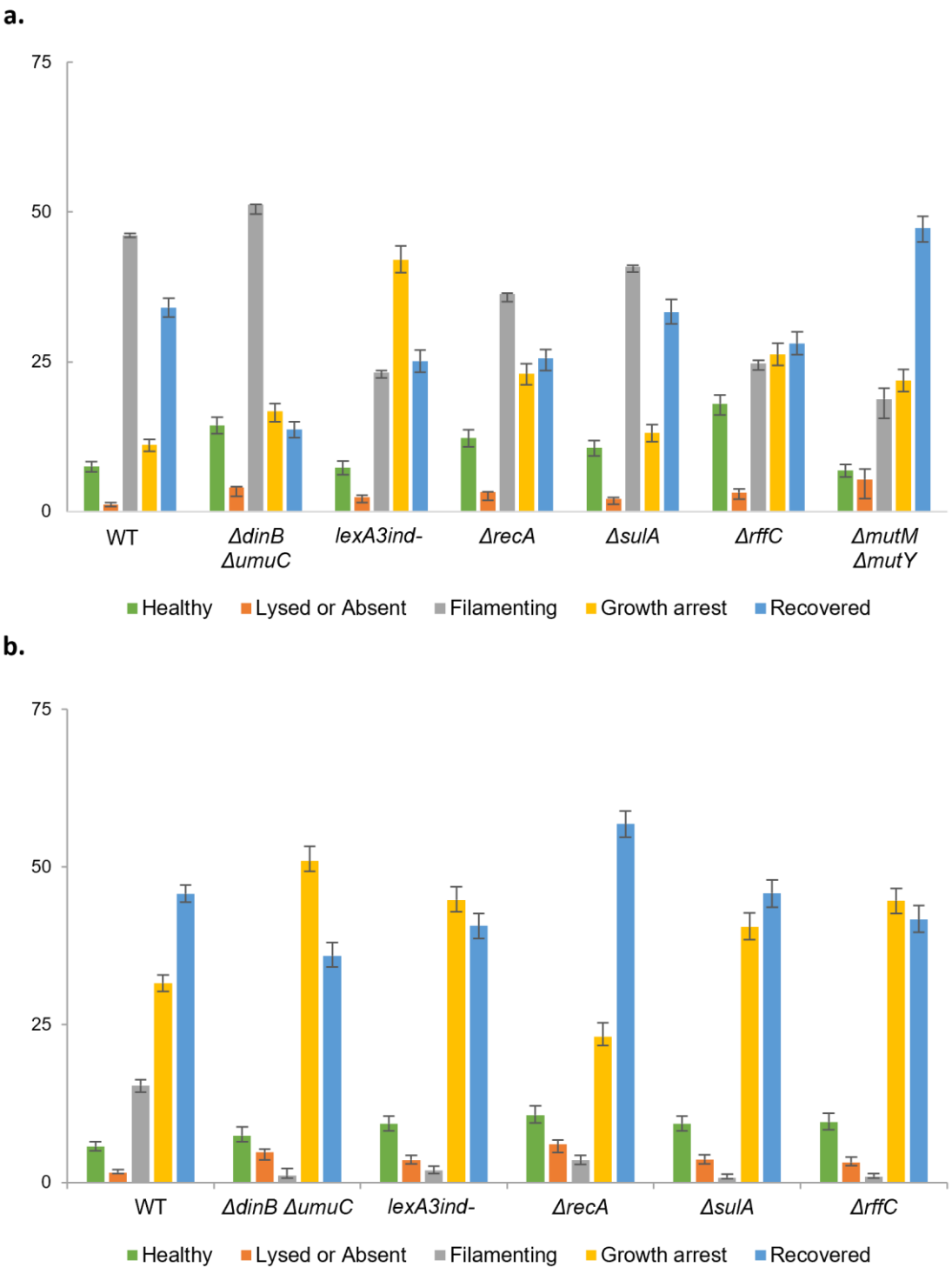


Figure 31 : Cell states distribution at 200 min for a series of WT and mutant cells with continuous 0.25 µg/ml TMP treatment during microfluidic experiments in a) M95AA + AdGM and b) M95AA. The different colours represent the possible states. The values for each cell state were obtained for a single experiment comprising 500-1000 cells and include a 95% confidence interval obtained from bootstrapping (1000 repeats). For WT cells, the bars represent an average of 4 repeats.

Next, and since a major role in cell filamentation has been suggested for SulA, the inhibitor of division induced during the SOS response, I decided to investigate the cell length in a mutant deficient for *sulA* (Fig.32). In both media, I observed that the deletion did not lead to changes in the cell length profile observed compared to WT cells. Additionally, in the *lexA3ind*$^{-}$ mutant, deficient in SOS response, I still observed an increase in the length of cells in both media. Thus, it would suggest that some of the filamentation observed could be due to SOS response but mainly filamentation is independent of the SOS response via the SulA pathway.

I also investigated the cell size dynamics in the other deletion mutants in response to TMP treatment in both media (Fig.32). In M95AA + AdGM, the BER defective mutant *ΔmutM ΔmutY*, underwent a slightly delayed cell filamentation by about 150 min from the start of continuous treatment. The dynamics observed in other mutants for cell length were similar to that of WT cells, with a 100 min lag phase, and cells reaching on average a shorter length than WT levels. In M95AA, the *ΔdinB ΔumuC* and *lexA3ind*$^{-}$ mutants did not seem to filament much, whilst the other mutants had a very similar profile to WT cells. These results suggest that most of these deletion mutations are unrelated to cell filamentation. Additionally, I observed that mutants with lower survival rates were associated with a high level of variation in cell length, suggesting a link between increased heterogeneity at the cell level, and increased disorder and killing from treatment (Fig.32).

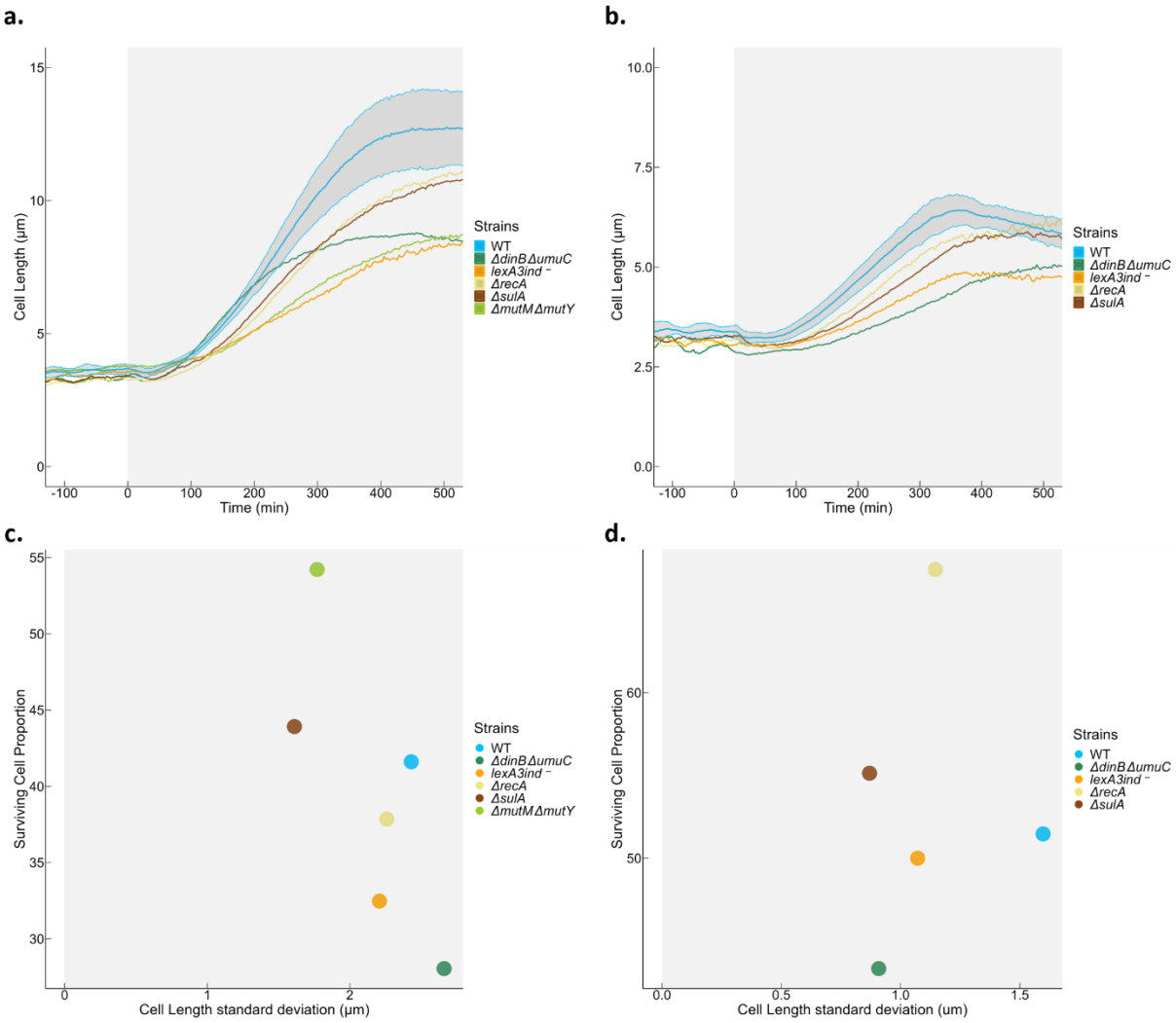


Figure 32 : Cell length dynamics with continuous 0.25 µg/ml TMP treatment from timepoint 0 during microfluidic experiments in a series of WT and mutant cells in M95AA + AdGM or M95AA media. a), b) Cell length in µm per time throughout the experiment. c), d) Correlation between cell-to-cell heterogeneity in cell length and cell survival. The surviving cell proportion (healthy and recovered cells) is plotted against the standard deviation in length across all cells measured at 200 min. The curves represent mean values obtained from 500-1000 cells per experiment. For WT cells, the curve with standard deviation (shaded area) represents an average of four separate experiments.

3. DISCUSSION

In this first chapter, I combined population-based assays and single-cell-based assays to decipher the dynamics of effects associated with TMP. I specifically investigated the cell states resulting from TMP treatment and a range of phenotypical criteria observed in treated cells. I began by analysing population-based assays that lack temporal information and subpopulation definition and concluded that optimally a ¼ MIC concentration was to be used for further experiments with TMP. I compared the bactericidal M95AA + AdGM to the bacteriostatic M95AA medium in these assays, but since the discrimination between the medium was not evident, I turned to microfluidics experiments which gathered on average 500-1000 cells per assay. I tested both WT cells and deletion mutants to decipher some of the specificity of the mechanism of action of TMP. First, I investigated the survival dynamics in cells, then thanks to my analysis, I was able to assign for each cell a state, or subpopulation, which allowed for a better level of definition in my analysis. Using these different subpopulations, I was able to examine cell size changes in treated cells and the associated cell-to-cell heterogeneity.

Firstly, in my experiments, it appeared that in M95AA + AdGM, a majority of cells were in growth arrest, but many of them also appeared lysed. It must be noted that one caveat of the analysis is that it does not account for the possibility that some cells may not be dead but rather exited the growth channel, which could be due to the cell length being longer than that of the growth chambers. Treated cells experienced a lag phase of 100 min during which no changes were observed phenotypically, except for a small drop in actively growing cells, suggesting a slowing down of the population. Interestingly, it has been suggested that TMP is dependent on the growth rate in cells (Angermayr et al., 2022). Thus, a slower growth rate reduces sensitivity, suggesting that during this lag phase, cells may be less sensitive to the treatment. However, it is also known that TMP itself can reduce the growth rate due to a bottleneck in the folic acid synthesis pathway, causing a negative feedback loop for the cell growth rate (Angermayr et al., 2022). After the initial

lag phase, the number of actively growing cells started to decrease until around 500 min, whilst the remaining cell proportion decreased only later during treatment. The cells also started to filament in all subpopulations except healthy cells, which has also been suggested in the literature (Sangurdekar et al., 2011). This suggested that many of the lysed cells may have disappeared from the experiment in a filament form, whereas growth arrest and recovered cells could likely be found in both normal and filament sizes. For the parameters studied, I observed a large cell-to-cell heterogeneity indicating a disordered metabolic state for the treated cells, which was associated with lower cell survival (Kaplan et al., 2021). When treatment was removed after 150 min, I observed very similar initial effects for the cells. However, after the removal of treatment, I noted key differences, with an increased disappearance or cell lysis during shorter treatment, and a decrease in filamentation.

In M95AA, a higher proportion of cells were in growth arrest from 500 min, with a high level of cell survival through the experiment, suggesting that very few cells die in those conditions compared to the bactericidal medium. During the lag phase, I observed an immediate and sharp decrease in growing cells, suggesting the cell's growth rate slowed down before a final division event. After the lag phase, the number of actively growing cells kept decreasing until around 500 min. Cells filamented from 100 min but reached much smaller lengths than encountered in M95AA + AdGM. When the cells were treated for 150 min, I observed recovery back to pre-treatment levels for all criteria within a very short period following removal of treatment. I particularly observed that the cells recovered from their growth arrest state, thus confirming M95AA status as a bacteriostatic medium for the antibiotic, causing the cells to enter a state of persistence they can exit. Additionally, the cell-to-cell heterogeneity seemed smaller than in M95AA + AdGM for continuously treated cells, suggesting that whilst the cells still entered a stress-induced state leading to persistence, they could exit it faster than in the bactericidal medium (Kaplan et al., 2021). This

overall suggested that in M95AA, TMP is seldom lethal, and the effects of thymidine depletion are dampened, likely representing purine depletion-induced growth arrest.

In both media, I carried out assays to assess the condition of the cells in growth arrest and determine whether they are in fact dead. The use of propidium iodide (PI) to stain dead cells did not suggest that all growth-arrested cells were metabolically dead after 20 h of continuous treatment (Fig.33). Further experiments could also be carried out to quantify the proportion and timing of cells that could exit growth arrest after treatment removal, to understand more precisely what happens to these cells. One assay would consist of extracting these cells specifically from the devices or data sets and experimenting with different treatment and recovery durations. Longer assays could also be carried out to allow time for the cells to recover after multiple hours of treatment, with the caveat that cells could start losing viability after a certain point. One hypothesis would be that the effects observed in prolonged treatment could be due to cell persistence during which the cells seem in growth arrest in both media. Indeed, TMP given in a single dose to treat UTIs has been shown to be efficient (Tolkoff-Rubin et al., 1982). I confirmed this with the short treatment experiments whereby I achieved the highest level of cell death in bactericidal medium, and lowest proportion of growth-arrested cells by the end of the experiment, suggesting again some persistence.

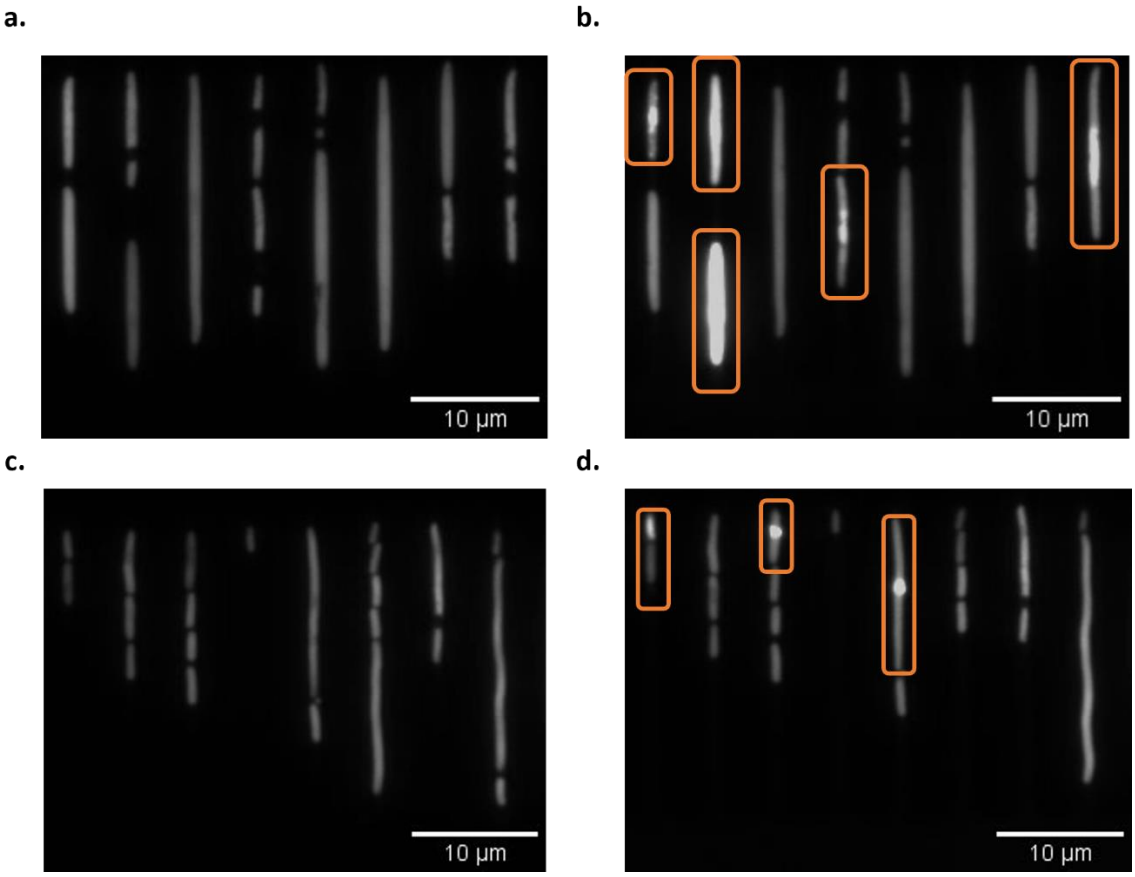


Figure 33 : Snapshots of microfluidics experiments after ~20 h of continuous 0.25 µg/ml TMP treatment in a), b) M95AA + AdGM and c), d) M95AA. a), c) RFP channel at the end of the experiment, prior to PI stain addition. b), d) RFP channel after PI stain addition, with dead mother cells circled in orange.

One interesting observation was that addition of thymidine in M95AA + AdGM was sufficient to abolish all changes observed for cell size and growth dynamics. Although just like for untreated cells, I still observed some cell death and changes in the proportions of actively growing cells, this was attributable to the natural death of cells rather than the effect of treatment. In M95AA, I observed that not all effects of TMP were abolished by thymidine, suggesting that these initial effects, particularly during the lag phase, were not directly attributable to thymidine depletion. The *folA* plasmid copy also did not rescue the cells' survival, and I observed an increase in lysed cells, suggesting that *folA* in the bacteriostatic medium was not sufficient to rescue the cells from TMP. In M95AA + AdGM, the *folA* plasmid copy was sufficient to abolish all effects and protect cells from

TMP. However, I observed poor health in those cells, suggesting a high metabolic cost of the engineered plasmid for the cells. Indeed, it has been suggested that overexpression of FolA in cells diverts energy towards folic acid synthesis which becomes deleterious (Angermayr et al., 2022). These observations confirmed the key role of thymidine depletion in the mechanism of action of TMP leading to cell death. However, my experiments have suggested that the presence of thymidine is required at the same time as TMP for it to have an impact, since removal of thymidine during treatment only delayed the effect of TMP by an extra 100 min, suggesting that the cells do not store exogenous thymidine. On the other hand, the removal of thymidine at the start of the treatment shortened the lag phase and precipitated the cells into growth arrest, suggesting potential changes in the metabolism of the cells due to thymidine supplementation and uptake independently of the treatment.

Further to that, I carefully compared a range of mutants deficient in key bacterial stress responses involved in TMP mode of action, including DNA repair, SOS response, and capsule synthesis. Survival dynamics were broadly conserved in both media with higher levels of remaining cells for most mutants. One exception was the *ΔrecA* mutant in M95AA with an immediate decrease in survival. This could be due to either a lack of HR or SOS induction, however, further experiments such as testing a double mutant *ΔrecA lexA3ind*$^{-}$ would be required to discriminate the two potential roles. The DNA repair *ΔdinB ΔumuC* and *ΔmutM ΔmutY* mutants in M95AA + AdGM both led to lower levels of lysis in treated cells. They seemed to have similar temporal dynamics, but higher levels of survival compared to the WT, indicating that these pathways when functional can be slightly detrimental for treated cells, confirming prior observations by Giroux et al., 2017. However, in M95AA, I noticed that the *ΔdinB ΔumuC* mutant had a larger and faster decrease in actively growing cells, suggesting a protective role for the TLS polymerases in the medium. In both media, I was not able to emulate the hyperstarvation state described for the *ΔrffC* mutant (Pritha

Rao & Kuzminov, 2020), although I observed a faster entry into growth arrest, suggesting that it does not play a role in the lag phase and acquisition of endogenous thymidine in my conditions. I also untangled the SOS response and particularly the SulA inhibitor of division from the cell filamentation observed in TMP-treated cells suggesting an SOS-independent mechanism causing increases in cell length and width in treated cells. One hypothesis could be nucleoid occlusion due to incomplete DNA replication, whereby the cells cannot divide due to the prevention of septum formation (L. J. Wu & Errington, 2012). It has also been suggested that in the event of the cells carrying out division despite the nucleoid occlusion, this could lead to the incorrectly replicated nucleoid being cut in two, causing further damage to the cells (T. V. P. Rao & Kuzminov, 2021).

Overall, my investigation of deficiencies in pathways that have been described as key for TMP has not pointed to a clear and singular pathway leading to cell death. Instead, it appears that all of the mechanisms and responses play an important role at different key points of the treatment albeit none of them are strictly necessary to ensure cell death or survival in my conditions. It appears that the phenotypes of the cells in the different media may be due to a more general state of disorder in the cells, described and modelled in the literature as an underlying cause of persistence in antibiotic-treated cells (Kaplan et al., 2021). Indeed, for bacteriostatic medium, the parameters observed so far are less heterogeneous and less suggestive of high levels of disorder. I thus observed that much like described in the paper mentioned, treated cells in M95AA can exit their growth arrest or persistence state quite rapidly after a short TMP treatment. In contrast, the cells in bactericidal medium present a large cell-to-cell heterogeneity with some extreme values and vastly different subpopulations, suggesting an important state of metabolic disorder in the treated cells, which appeared linked to lower survival. In that case, the cells were not able to exit their persistence state promptly when treatment was removed. To confirm this state of disorder in both

media, further understanding of the bacterial stress responses and specifically the associated cell-to-cell heterogeneity is required and will be the subject of the next chapter.

CHAPTER 5: CHARACTERISATION OF BACTERIAL STRESS RESPONSES TO TRIMETHOPRIM TREATMENT

1. INTRODUCTION

Trimethoprim is a dihydrofolate reductase competitive inhibitor, causing a depletion of metabolites associated with folic acid biosynthesis including the purine adenine, amino acids glycine and methionine, and the pyrimidine thymine. Thus, as described in Chapter 4, supplementing a minimal M95AA medium with some of these metabolites will cause differences in the mechanism of action of TMP. In the bacteriostatic M95AA, I observed the effects of a state of purine depletion leading to growth arrest, potentially associated with a persistence phenotype, with little cell-to-cell heterogeneity. Meanwhile, in the bactericidal M95AA + AdGM, the cells experienced a higher level of disorder marked by elevated cell-to-cell heterogeneity and displayed a higher level of cell death. These results led to the hypothesis that there could be a correlation between the heterogeneity of cell responses and survival, warranting further exploration (Kaplan et al., 2021). According to the existing literature on TMP, I do expect notable differences in the induction of bacterial stress responses between the bacteriostatic and bactericidal media. Most studies have demonstrated the role of certain stress responses to TMP treatment at the population level, using e.g. survival assays combined with gene deletion or overexpression (Pritha Rao & Kuzminov, 2020; T. V. P. Rao & Kuzminov, 2022), microarrays and genome-wide genetic screen of a collection of knock-out mutants for bacterial responses (Sangurdekar et al., 2011), mass spectrometry to quantify ROS (Hong et al., 2019) or using fluorescence reporters for SOS induction and RifR mutation frequency

assays (Baharoglu & Mazel, 2011). These techniques risk completely hiding cellular heterogeneity and could mask small but significant effects that can be overshadowed by the bulk population.

Many cellular processes have been suggested as being involved in the mechanism of action of TMP, leading to a range of stress phenotypes, particularly DNA replication stress, starvation, DNA damage, mutagenesis, oxidative stress, or acid stress. Current hypotheses regarding the causes of each of these stresses and their putative roles in cell killing by TMP have been described in further detail in Chapter 2 of this thesis. Briefly, since TMP causes depletion of thymidine, DNA replication stress is viewed as the central feature in the mechanism of TMP. It appears that in starved cells, new DNA replication is initiated at the start of treatment, but nascent strands are degraded to release thymine for further replication (Kuong & Kuzminov, 2012; Martín & Guzmán, 2011). Following this initial lag phase where cell viability is not yet perturbed, the DNA synthesis rate decreases and cell death ensues (P. Rao & Kuzminov, 2019), likely due to the depletion of thymidine and DNA replication stalling. Amongst the different potential responses, the SOS response induced by DNA damage seems to be common between the bacteriostatic and bactericidal media (Sangurdekar et al., 2011). TMP treatment has also been shown to be mutagenic, as seen in a study using MEGA-plates that showed a rapid evolution of *de novo* resistance mutations to TMP (Baym et al., 2016). Multiple studies have also demonstrated the formation of ROS during TMP treatment (Giroux et al., 2017; Hong et al., 2017), although this has led to debate (T. V. P. Rao & Kuzminov, 2022). Another aspect of TMP treatment is the acidification of cells, leading to an acid stress response (Mitosch et al., 2017).

Many pathways have been implicated in response to TMP treatment, however, little is known about the temporality or heterogeneity of these responses and to what extent they prolong cell survival. Therefore, I addressed these questions using time-lapse imaging with microfluidic growth

chambers and analysed the data at population, subpopulation, and single-cell levels. I explored the effect of TMP treatment on DNA replication activity and obtained the first measurements of mutation dynamics, showing how the frequency of DNA replication errors changes in real time during TMP treatment. To test the hypothesis formulated in Chapter 4 that there is a correlation between heterogeneity and death in the context of TMP, I particularly focused my attention on the relationship between cell-to-cell heterogeneity in stress responses and cell survival. I performed these measurements with *E. coli* cells expressing fluorescence gene expression reporters for the responses of interest (OxyR, SoxR, SOS, and acid stress responses) and used both M95AA + AdGM and M95AA media. To gain further insight into the central role of the SOS response, I made use of single-molecule tracking to directly observe cleavage of the LexA repressor in live cells. I also tested mutants deficient in key pathways to understand their roles during treatment. Together, the results revealed that rather than a clear singular pathway leading to cell death or promoting survival in response to TMP, there is a correlation between lower cell survival and cell-to-cell heterogeneity, or metabolic disorder marked by the induction of many stress responses during TMP treatment.

2. RESULTS

2.1. TMP-Induced Replication stress : Examining DNA Replication Foci Dynamics

Since TMP causes thymine starvation, and thymine being crucial in DNA synthesis, it is expected that TMP disrupts DNA replication (P. Rao & Kuzminov, 2019). Hence, I examined DNA replication using microfluidic experiments to follow bacteria over time. For that, I engineered cells to carry the β-clamp DnaN protein from the bacterial replisome, fused to a fluorescent protein (mYPet). This

protein forms foci, which can be quantified using automated foci-detection analysis and used as a marker for bacterial replisomes in microfluidic experiments (Moolman et al., 2014; Reyes-Lamothe et al., 2014). In my analysis, I counted the total number of foci formed in cells and normalised it by the cell area, giving the replication foci frequency, which I consider as a proxy for active DNA replication sites.

First, I performed control experiments to validate the method used (Fig.34). I examined the DNA replication foci frequency in untreated cells and cells with TMP treatment plus thymidine supplementation. I observed that the cells did not experience any changes in DNA replication foci frequency over time, remaining around 2 foci per cell over 500 minutes. These foci likely represent the 2 replication forks that travel in opposite directions during normal replication in *E. coli* (Oakley, 2019). This also suggests that thymidine addition during TMP treatment permits normal DNA replication. The foci frequency was slightly higher in M95AA + AdGM compared to M95AA indicating that the richer growth medium supports a higher replication rate.

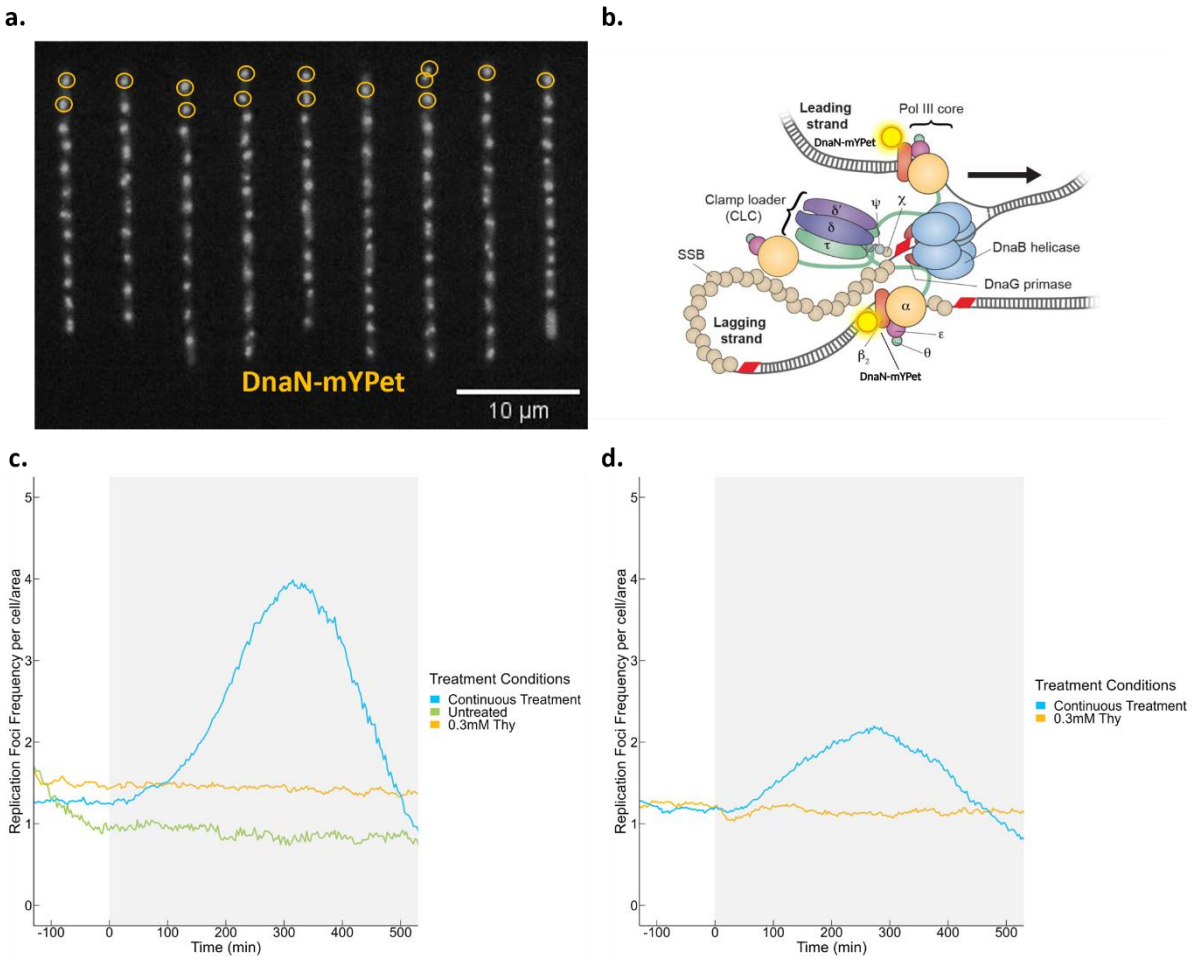


Figure 34 : DNA replication foci frequency in cells with continuous 0.25 µg/ml TMP treatment from timepoint 0 during microfluidic experiments, with different medium supplementation or without treatment in M95AA + AdGM or M95AA media. a) Snapshot from an experiment with automatically detected DnaN-mYPet foci in mother cells, highlighted in yellow. b) Illustration of the DnaN-mYPet fluorescent fusion protein (yellow circles) in the bacterial replisome, adapted from J. S. Lewis et al., 2017*. c) DNA replication foci frequency in M95AA + AdGM, d) M95AA media. The curves represent mean values obtained from 500-1000 cells per experiment.*

In both M95AA + AdGM and M95AA, I observed clear changes in the number of DNA replication sites per cell in response to continuous TMP treatment (Fig.35). In the two media, the cells seemed to experience a lag phase of around 100 min during which there was little change in the average frequency of replication sites. However, after that, I observed a large increase, which could represent repeated attempts to replicate DNA in the absence of the required nucleotides. The replication foci frequency peaked around 300 min of TMP treatment and dropped with progressing

cell death. Furthermore, cell-to-cell variation in foci frequency also increased markedly with TMP treatment (Fig.35c,35d). To probe this variation further, I split cells into different categories according to their fates after 800 min of continuous TMP treatment, as developed in Chapter 4. At the subpopulation level, the replication foci frequency changed little for healthy cells but dramatically increased in filamenting cells. Because foci frequency was normalised by cell area, these data reflect a genuine increase in the density of replication sites. The largest increase was seen in cells that ultimately lysed, suggesting that over-replication attempts may be associated with death by lysis. Interestingly, cells with growth arrest and those that recovered showed a smaller increase than filamenting and lysed cells, indicating that these cell fates avoid the stresses associated with over-replication. Cells growing in M95AA medium exhibited a smaller increase in replication foci frequency compared to M95AA + AdGM for filamenting and lysed subpopulations. However, the healthy, growth arrest and recovered subpopulations showed the same replication dynamics in both growth media. Cell-to-cell variation in replication foci frequency was generally more elevated in M95AA + AdGM compared to M95AA (Figures 35c, 35d).

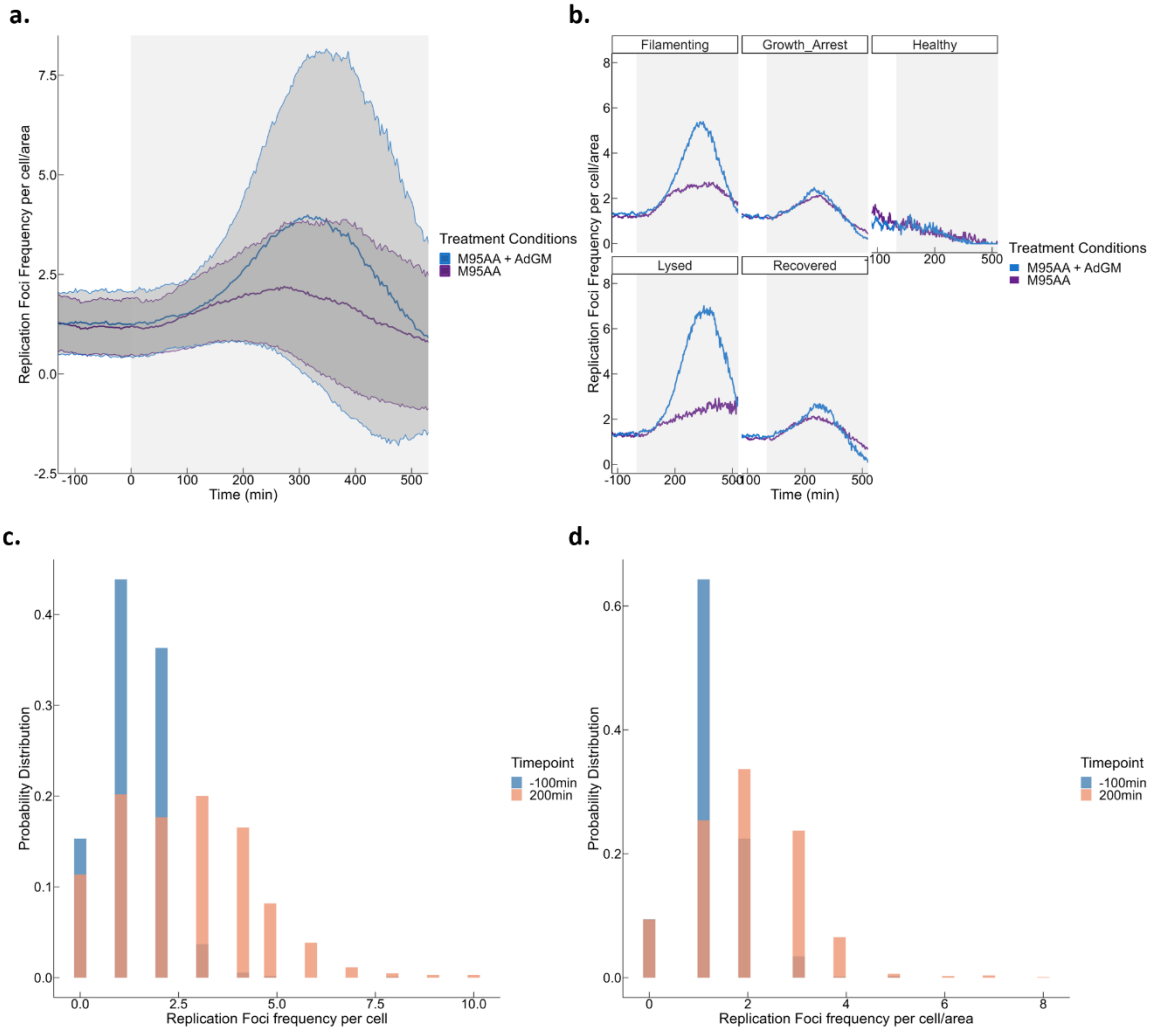


Figure 35 : DNA replication foci with continuous 0.25 µg/ml TMP treatment from timepoint 0 during microfluidic experiments in M95AA + AdGM or M95AA media. a) DnaN replication foci frequency at population level from a single repeat ± standard deviation (shaded area). b) DNA replication foci frequency at the cell subpopulation level determined at 800 min. c) Distribution of frequency observed at -100 min and 200 min in M95AA + AdGM, d) M95AA. The curves represent mean values obtained from 1000-1500 cells per experiment.

2.2. TMP's Impact on Mutagenesis

It is well known that TMP is mutagenic in bacteria (Baym et al., 2016). De *novo* evolution of resistance via chromosomal mutations in response to the antibiotic and leading to amplification or overexpression of the gene encoding dihydrofolate reductase is of great concern (Huovinen et al.,

1995). However, no studies have yet addressed the timing of mutagenesis during treatment. Conventional methods to detect mutations are based on genome sequencing or genetic reporter assays (e.g. quantifying the frequency of antibiotic-resistant colonies). These methods reveal the presence of new mutations but provide little or no information about the timing of these mutation events relative to the treatment duration or whether mutation frequencies differ between subpopulations of cells. Thus, I employed a MutL-mYPet reporter that can be imaged via time-lapse microscopy in the microfluidics experiments (Fig.36). This fluorescence reporter is a fusion between MutL protein and the fluorescent protein mYPet. MutL is recruited by MutS as part of the DNA mismatch repair pathway, forming a focus at the site of a DNA mismatch (Elez et al., 2010; Uphoff, 2018). I calculated the rate of formation of new foci per cell over time. Although not all mismatches, which correspond to nascent DNA replication errors, will be converted into mutations, this technique can give an estimate of the mismatch rate, representing the first and essential step in the formation of point mutations. The mismatch rate has been shown to correlate with the frequency of genomic mutations, thus validating MutL-mYPet as mutation reporter (Vincent & Uphoff, 2021). Firstly, I confirmed using a *ΔmutS* mutant that in the absence of MutS, MutL-mYPet does not form any more foci, indicating MMR deficiency. Since I did not detect foci formation, despite an increase in fluorescence intensity, this confirmed that the foci I observed in following experiments were genuine markers of DNA mismatches (Fig.37).

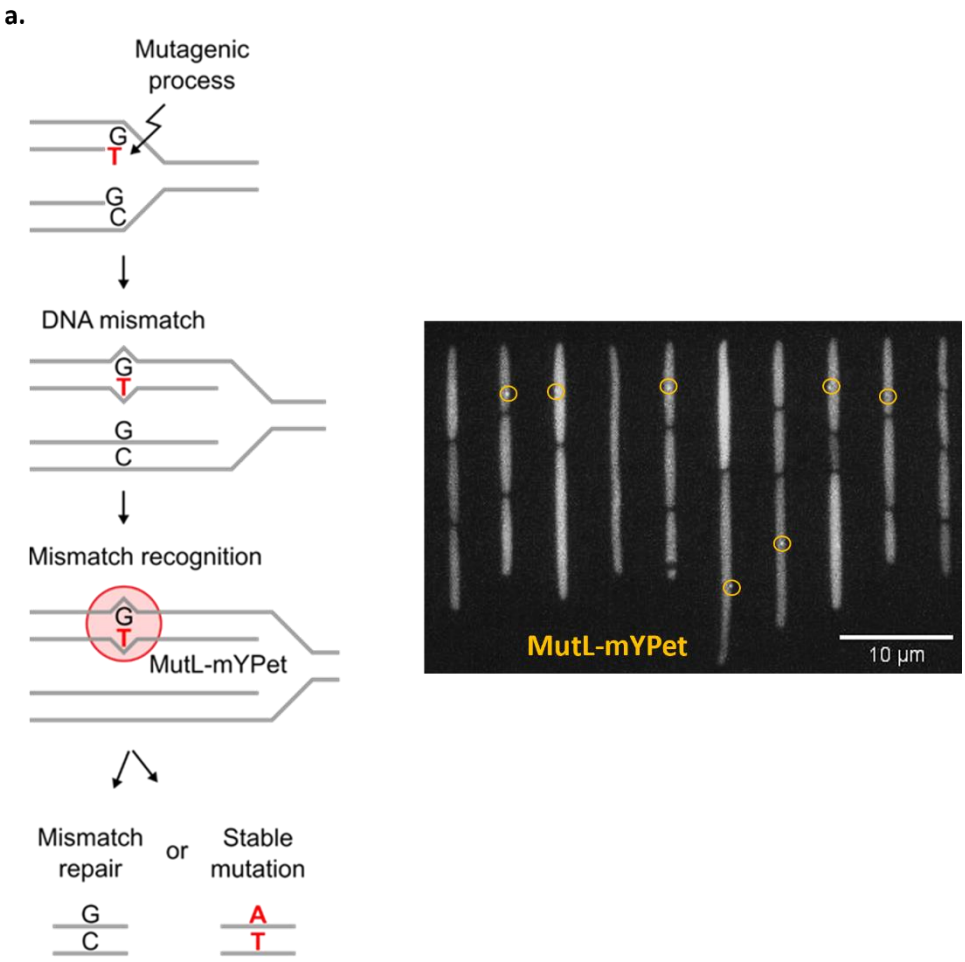


Figure 36 : Mismatch Rate during microfluidics experiments. a) Illustration of the MutL-mYPet fluorescence protein in the context of MMR, from Uphoff, 2018a. *b) Snapshot from a microfluidics experiment with some MutL-mYPet foci highlighted by yellow circles.*

I measured the mismatch rate in cells in M95AA + AdGM, along with the total cellular mYPet fluorescence intensity (Fig.37). I observed before treatment a very low frequency of foci per cell (<0.1% of cells), consistent with a low replication error rate during normal growth (Elez et al., 2010). The foci rate and mYPet fluorescence intensity increased after a lag phase of 100 min from the start of treatment. Whilst the foci rate suggested an increase in mismatches, the change in fluorescence intensity could be due to a global increase in protein levels, as described in the next section with the mKate2 marker. This increase was accompanied by elevated cell-to-cell heterogeneity in foci frequency (Fig.37d). At the subpopulation level, whilst the foci rate in healthy cells did not change

substantially, all other cell fates exhibited similar increases to that of the whole population level, with a slightly higher rate for filamenting and lysed cells. The increase and cellular heterogeneity in mismatch rate were both lower in M95AA media compared to M95AA + AdGM. When TMP was removed after 150 min of treatment, there was still a large increase in mismatch rate in M95AA + AdGM media, but not in M95AA (Fig.38). These results point to a preferential TMP treatment regimen that provides successful inhibition of bacterial growth without induction of mutagenesis which may lead to resistance evolution. My data suggest that a short treatment with TMP under bacteriostatic conditions largely avoids drug-induced mutagenesis.

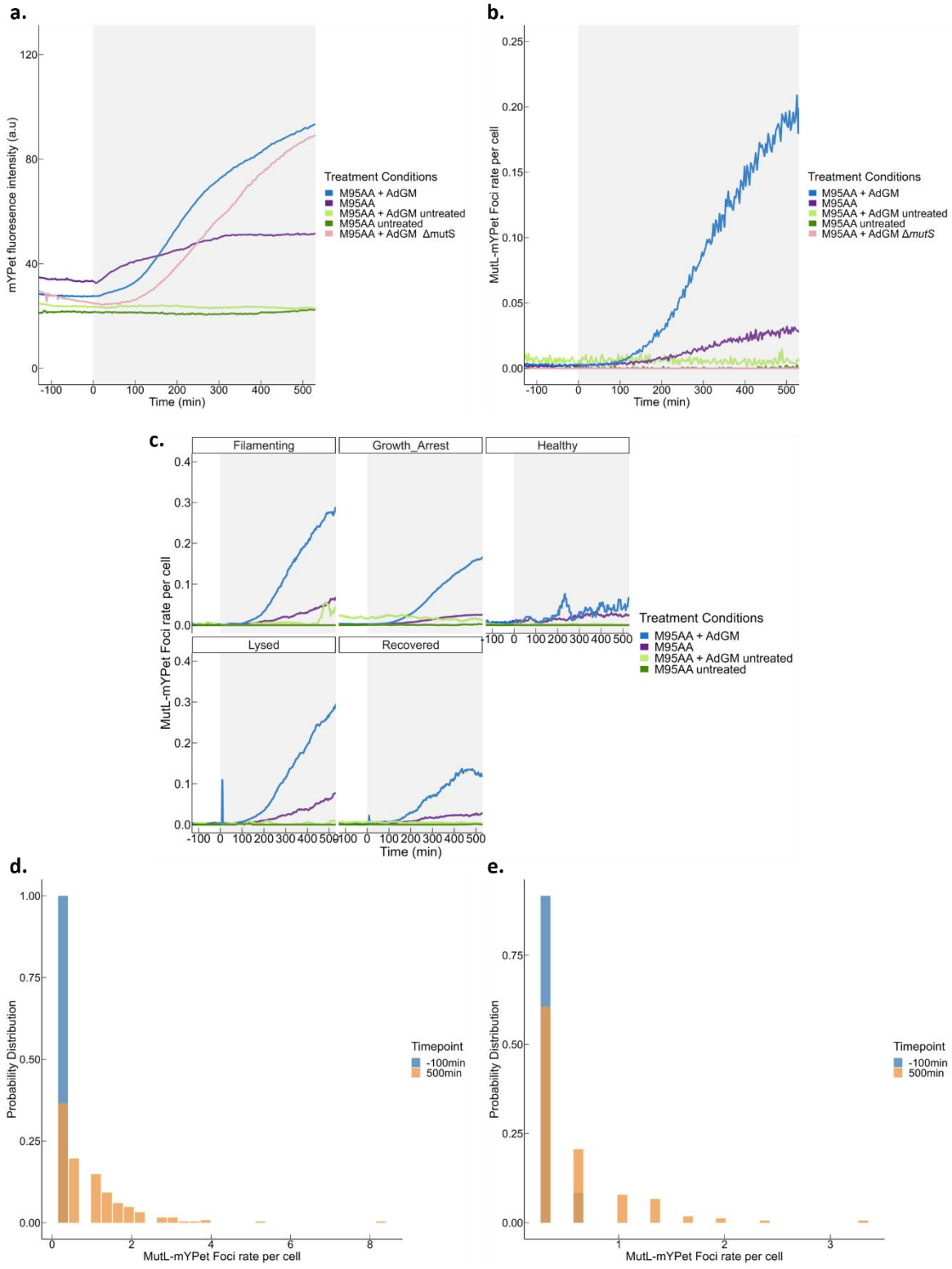


Figure 37 : Mismatch rate with continuous 0.25 µg/ml TMP treatment from timepoint 0 during microfluidic experiments or without treatment, including ΔmutS cells in M95AA + AdGM or M95AA media. a) mYPet average fluorescence intensity in cells. b) MutL-mYPet foci rate amongst cells at population level. c) MutL-mYPet foci rate at the cell subpopulation level determined at 800 min. d) Distribution of MutL-mYPet foci rate observed at -100 min before and 500 min after TMP addition in M95AA + AdGM, and e) M95AA. The curves represent mean values obtained from 1000-1500 cells per experiment.

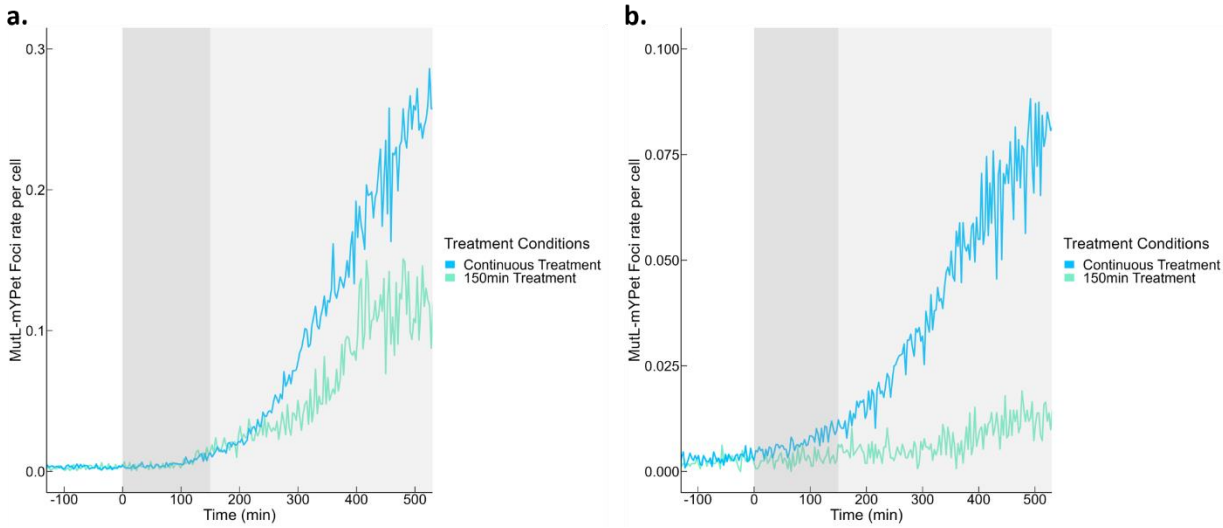


Figure 38 : Mismatch rate dynamics based on MutL-mYPet foci frequency in cells with continuous or 150 min course (dark grey) of 0.25 µg/ml TMP treatment from timepoint 0 during microfluidic experiments in a) M95AA + AdGM, and b) M95AA media. The curves represent mean values obtained from 500-1000 cells per experiment.

Since thymidine can abolish some of the effects of TMP, I also measured the mismatch rate in both media without TMP treatment, and with TMP treatment plus thymidine supplementation (Fig.38&39). In both media, I observed that the foci rate was really low and just above 0 foci per cell throughout the entire experiments for untreated and thymidine-supplemented cells, in agreement with other experiments with unperturbed growth (Elez et al., 2010; Uphoff, 2018). In resistant cells expressing a plasmid copy of *folA,* the mismatch rate gradually increased. However, this increase occurred equally with or without TMP treatment and therefore seems to suggest that the growth defects associated with FolA overexpression increase spontaneous mutagenesis. Strikingly, I observed that conditions with low survival rates are associated with a high level of variation in mutagenesis between cells (Fig.40).

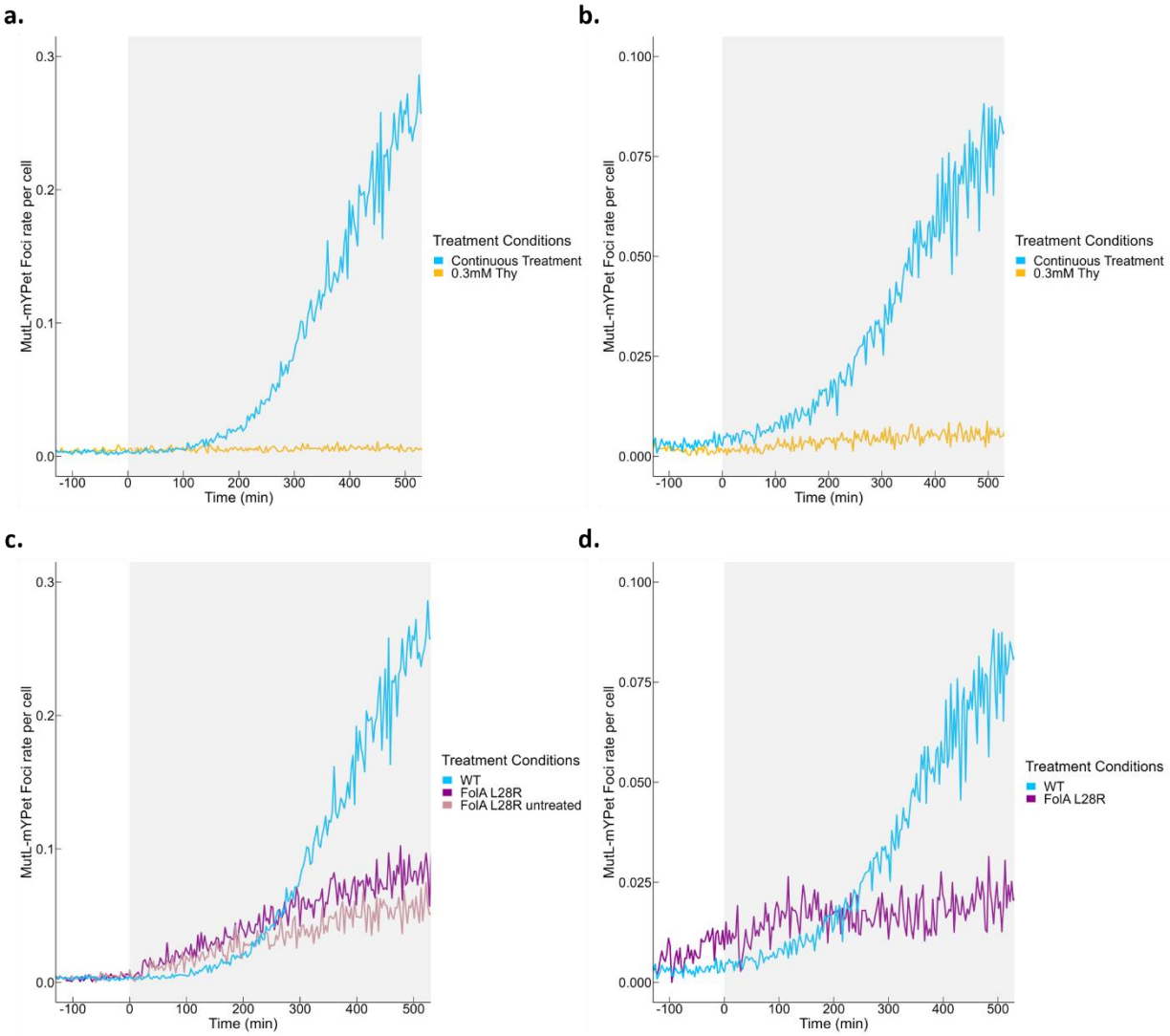


Figure 39 : Mismatch rate dynamics based on MutL-mYPet foci in WT and resistant cells with continuous 0.25 µg/ml TMP treatment from timepoint 0 during microfluidic experiments, with different medium supplementation or without treatment in a) and, c) M95AA + AdGM, and b), and d) M95AA media. The curves represent mean values obtained from 500-1000 cells per experiment.

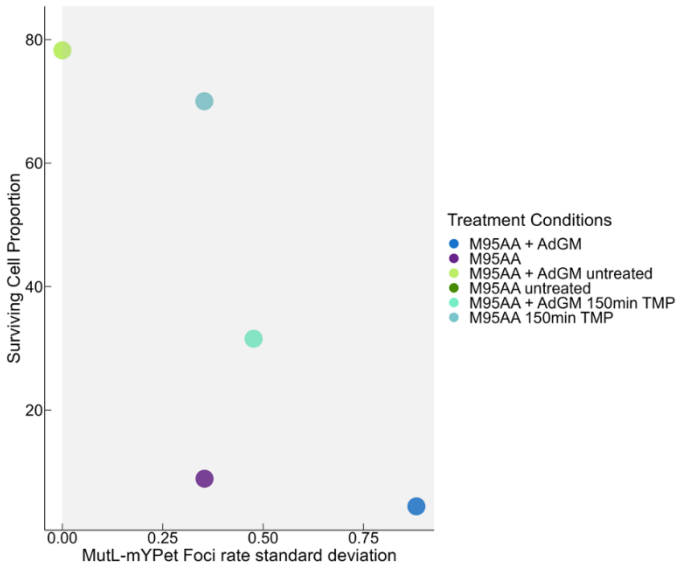


Figure 40 : Correlation between cell-to-cell heterogeneity in DNA mismatch rate and cell survival. The surviving cell proportion (healthy and recovered cells) is plotted against the standard deviation in MutL-mYPet foci rate across all cells measured at 500 min. The curves represent mean values obtained from 1000-1500 cells per experiment in untreated cells or treated cells with continuous or 150 min course of 0.25 µg/ml TMP treatment.

In both media, I also assessed the DNA mismatch rate of strains deficient in stress responses and DNA repair pathways, to determine if any pathway could be involved in the increased mutagenesis observed in treated cells (Fig.41). The SOS-deficient *lexA3ind*$^{-}$ mutant showed reduced mutagenesis, particularly in M95AA media. Conversely, *recA* deletion caused a marked increase and acceleration of TMP-induced mutagenesis in both media. Probing the role of the SOS response in mutagenesis further, I measured the mismatch rate in a double mutant deficient in TLS polymerases Pol IV and Pol V (*ΔdinB ΔumuC*). This mutant showed increased mutagenesis in both media, suggesting that TLS is not the cause of increased replication error rate, but may instead contribute to error avoidance. I also tested the double mutant deficient in BER of 8oxoG lesions, *ΔmutM ΔmutY*, in M95AA + AdGM and observed a longer lag phase of almost 300 min before the mismatch rate increased. Taken together, these results suggest that no individual pathway is solely responsible for mutagenesis during TMP treatment, but that multiple mechanisms collectively

contribute to the rate of replication errors as well as repair of mutagenic lesions. These results provide a basis for further investigations into the functions of these candidate genes.

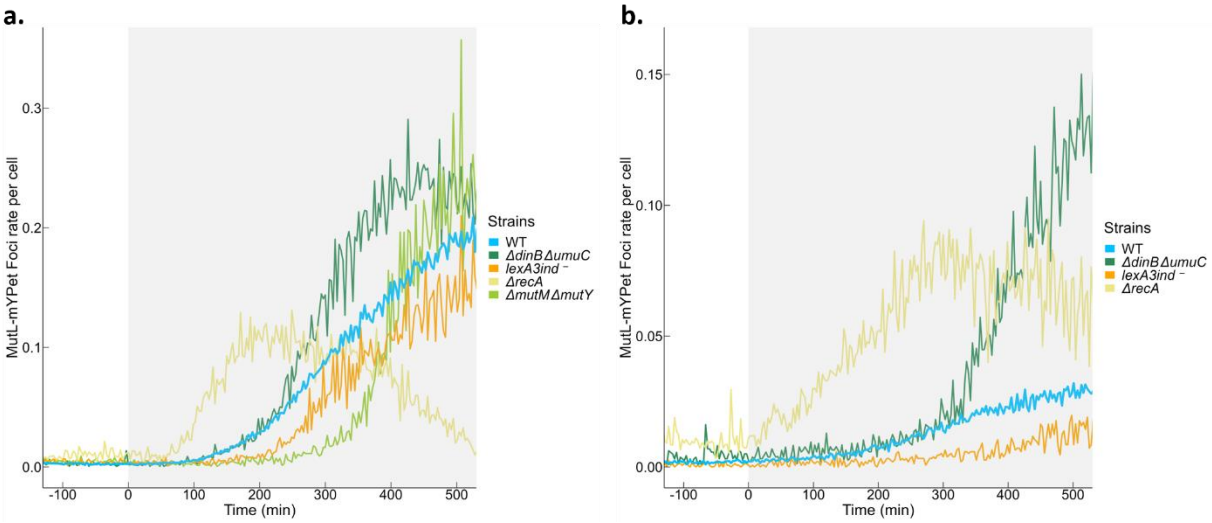


Figure 41 : Mismatch rate dynamics with continuous 0.25 µg/ml TMP treatment from timepoint 0 during microfluidic experiments in WT and mutant cells in a) M95AA + AdGM, and b) M95AA media. The curves represent mean values obtained from 500-1000 cells per experiment.

2.3. TMP Causes a Global Increase in Gene Expression

In microfluidics experiments, at each time point, I gathered a lot of data regarding the cells, using a segmentation marker, transcriptional reporter carried on plasmids, or translational fusion encoded directly in the bacterial genome. For example, I always used a cytoplasmic mKate2 fluorescence protein as a constitutively expressed segmentation marker in cells (Uphoff, 2018). This protein was expressed from a P_{RNAI} promoter, integrated at the TN7 site, and served as a reporter of a gene that is not regulated in response to stress, as it is a replication control promotor of plasmid pBR322 (Liang et al., 1999). Since I could also track the fluorescence intensity of the marker during continuous treatment, this could inform about the size and growth behaviour of the cells and protein accumulation. Indeed, for treated cells in both media, I observed a sharp increase in mKate2 fluorescence intensity on average (Fig.42). For M95AA + AdGM, this happened after a

100 min lag phase, whereas for M95AA, the increase was seen shortly after the start of the continuous treatment. The intensity reached a peak by 500 min in both cases, when a lot of the cells are in growth arrest or filamenting (Fig.42d,42e). Interestingly, in both media, the increase was seen for all cell subpopulations except healthy cells. When I normalised the change in mKate2 intensity over time by the cell area, this gave a clearer idea of the expression rate of the marker, which increased only in M95AA + AdGM (Fig.42b). In untreated cells, I did not observe any change in fluorescence intensity or expression rate. Therefore, the observed increase in fluorescence in treated cells could suggest an accumulation of protein, here a fluorescent marker, due to the slowing down of cell division, which is also known to lead to increased expression of certain genes, such as *folA* (Angermayr et al., 2022).

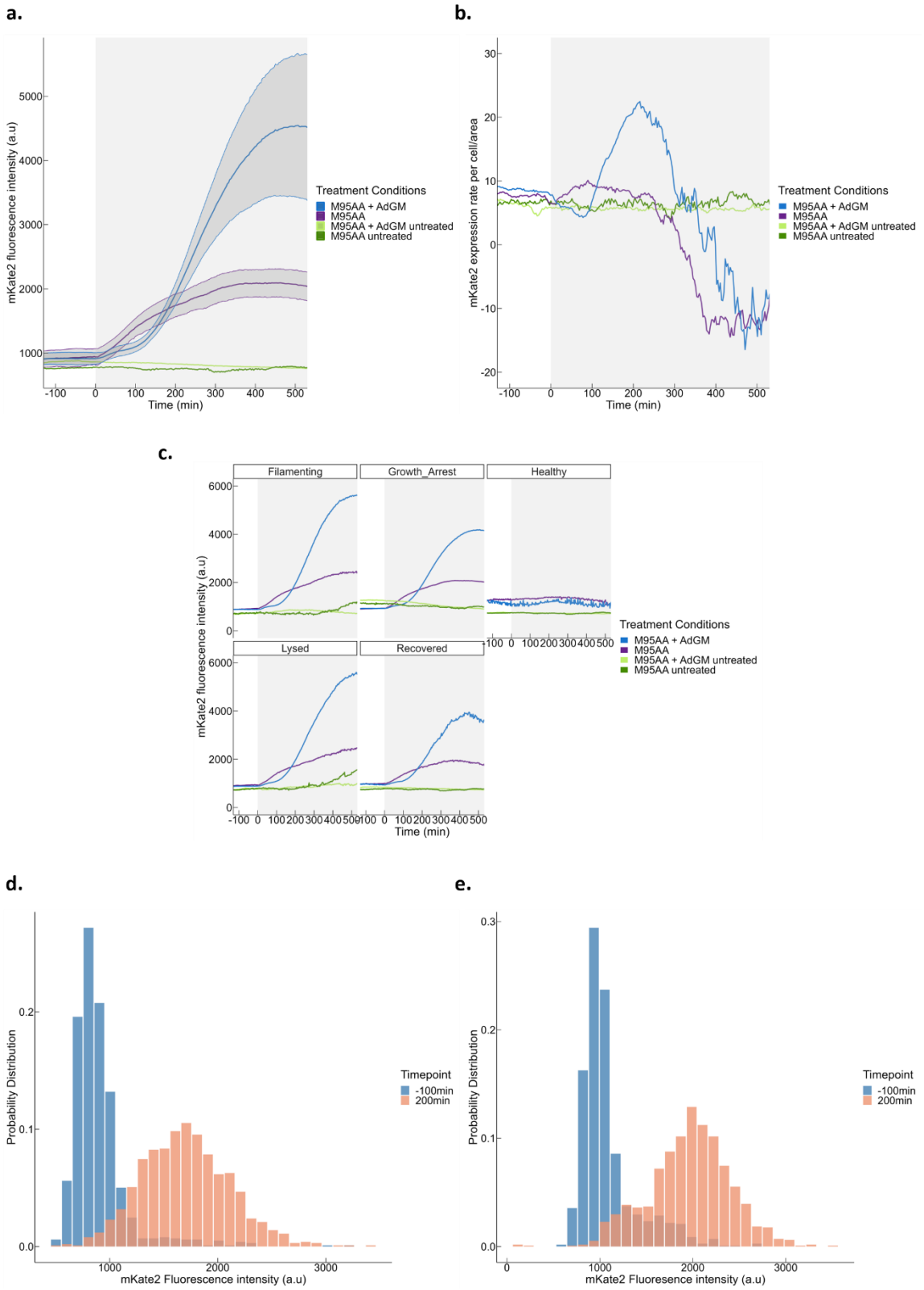


Figure 42 : P_{RNAI}-mKate2 fluorescence dynamics with continuous 0.25 µg/ml TMP treatment from timepoint 0 during microfluidic experiments or without treatment in M95AA + AdGM or M95AA media. a) Average fluorescence intensity observed in cells measured as the total fluorescence per cell at population level. c) Average fluorescence levels at the subpopulation level determined at 800 min. b) Expression rate computed as the change in fluorescence intensity over time normalised by the cell area of individual cells. d) Distribution

of intensity observed at -100 min and 200 min in M95AA + AdGM, e) M95AA. The curves represent mean values obtained from 1000-1500 cells per experiment for a single repeat for untreated cells, or four repeats ± standard deviation for treated cells (shaded area in panel a).

Since thymidine abolished most of the effects studied, I compared TMP-treated cells to cells supplemented with thymidine in both media (Fig.43). In M95AA + AdGM, thymidine abolished changes in P_{RNAI}-mKate2 fluorescence intensity. However, in M95AA, from the start of continuous treatment in the presence of thymidine, there was a small increase in average fluorescence intensity suggesting that some cells may have experienced protein accumulation. Strikingly, there was a clear relationship between survival and cell-to-cell heterogeneity in the expression of the constitutive P_{RNAI}-mKate2. This suggests an overall elevated state of disorder in gene expression, which appears to correlate with decreased survival (Fig.44). Thus, it appeared that going forward, this global increase in fluorescence intensity, likely due to protein accumulation caused by treatment, should be considered. To that end, I decided to focus mostly on expression rate which normalised changes in fluorescence intensity by the cell area for all reporters.

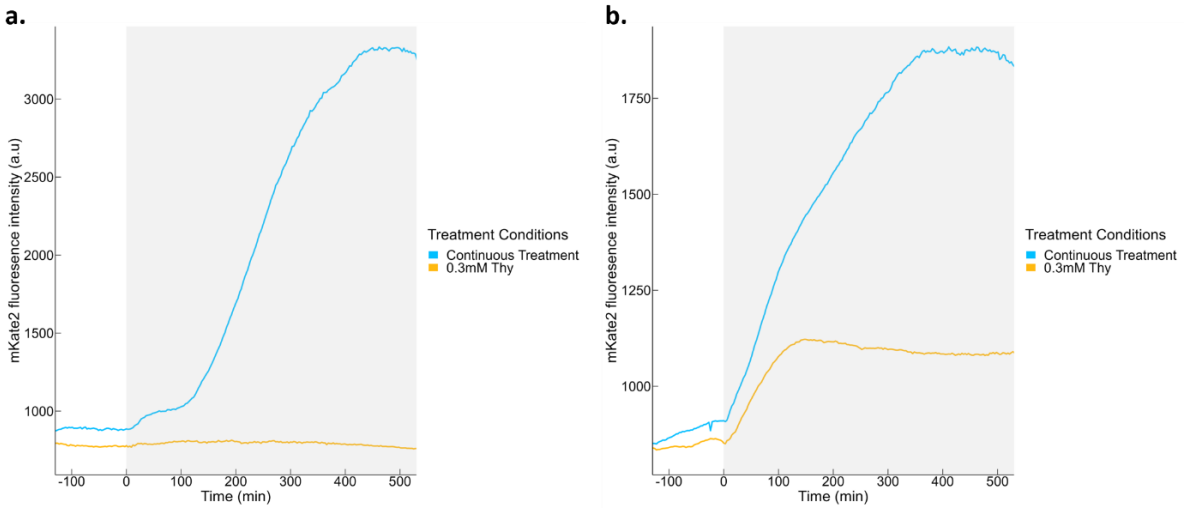


Figure 43 : P_{RNAI}-mKate2 fluorescence dynamics in cells with continuous 0.25 µg/ml TMP treatment from timepoint 0 during microfluidic experiments, with or without thymidine supplementation in a) M95AA + AdGM, and b) M95AA media. The curves represent mean values obtained from 500-1000 cells per experiment.

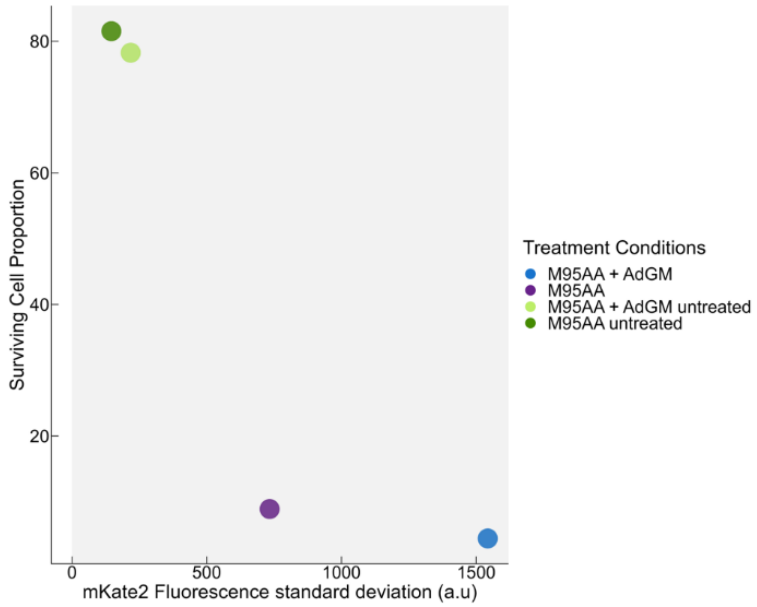


Figure 44 : Correlation between cell-to-cell heterogeneity in P_{RNAI}-mKate2 fluorescence intensity and cell survival. The surviving cell proportion (healthy and recovered cells) is plotted against the standard deviation in P_{RNAI}-mKate2 fluorescence intensity across all cells measured at 500 min. The curves represent mean values obtained from 1000-1500 cells per experiment in untreated cells or treated cells with continuous 0.25 µg/ml TMP treatment.

It is known that FolA is upregulated during TMP treatment (Angermayr et al., 2022), therefore I surveyed a strain expressing a reporter for the FolA protein, the direct target of TMP in treated cells. In M95AA + AdGM, I observed an increase in fluorescence intensity for the reporter, starting before the end of the lag phase, around 80 min. However, when I normalised the fluorescence intensity changes by the cell area, there was no increase, suggesting passive induction due to slowing down in cell growth (Fig.45). In the presence of thymidine, I did not observe any change in the FolA expression rate. At the subpopulation level, I did observe a higher increase in filamenting and lysed cells, and very little change for the other states. This could show a global induction of promotors in treated cells, particularly in filamenting cells that continue growing and attempt to produce thymidine, whereas growth arrest cells do not require further production as their metabolism could be shut off. These results suggest that the increase in FolA may be required for thymidine synthesis but is mostly due to global stress in treated cells.

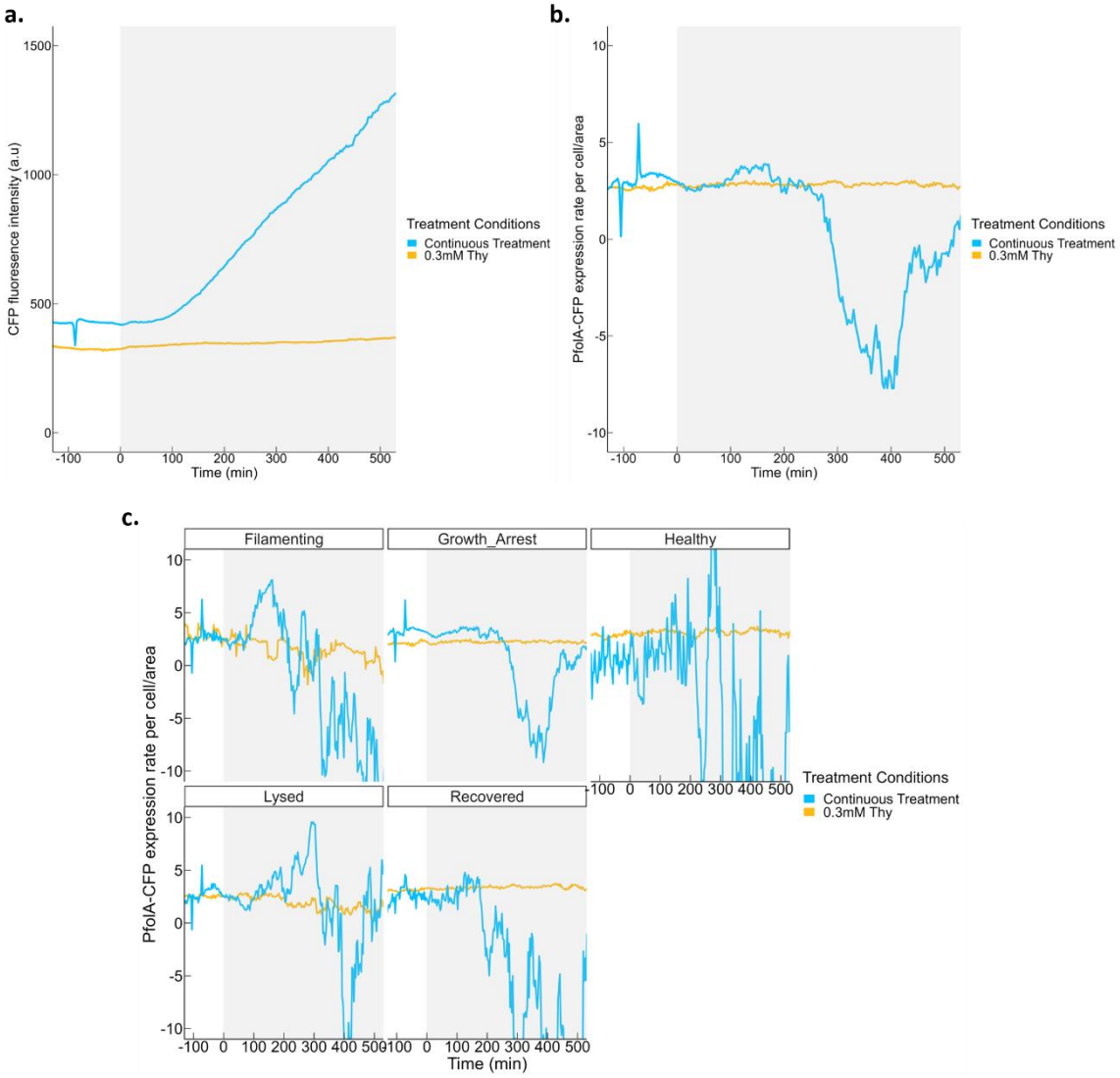


Figure 45 : PfolA-CFP fluorescence dynamics with continuous 0.25 µg/ml TMP treatment from timepoint 0 during microfluidic experiments, with or without thymidine in M95AA + AdGM. a) Average values observed at population level. b) Expression rate computed as the change in fluorescence intensity over time normalised by the cell area of individual cells. c) Expression rate for PfolA-CFP at the subpopulation level determined at 800 min. The curves represent mean values obtained from 500-1000 cells per experiment.

2.4. TMP's Influence on DNA damage

Another important stress response largely implicated during TMP treatment is the SOS response, triggered by any form of DNA damage that results in the presence of ssDNA in the cells. I conducted an in-depth analysis of the dynamics of the SOS response in both media, using microfluidics

experiments. I tested both WT and mutant cells deficient for the SOS response or DNA damage repair. For that, I used a reporter which consisted of a transcriptional fusion of the *PrecA* promotor on a low-copy number pSC101-type plasmid, with a fast-maturing fluorescent protein reporter, msCFP3. This was used as a proxy for the expression or induction of RecA, involved in and necessary for the SOS response in bacteria.

In microfluidics experiments with both bactericidal and bacteriostatic medium, I observed a large increase in fluorescence intensity of the RecA reporter from 100 min of TMP treatment (Fig.46a). When I normalised the change in CFP intensity over time by the cell area, I confirmed this observed increase in expression rate for RecA in both media, albeit at a lower level in M95AA. This increase started shortly before the end of the 100 min lag phase and increased sharply until 200 min in both media. A clear shift in the distribution of expression rates was also visible, suggesting an increase in cell-to-cell heterogeneity after treatment (Fig.46d). The increase in expression was followed by a decrease which could be due to the maximum expression of the SOS response being reached whilst the cell length kept growing, or a potential bleaching of the dying cells, leading to negative values. At the subpopulation level, the dynamics were similar for all states apart from healthy cells which showed no detectable SOS induction. This suggests that cell survival during TMP treatment is not associated with SOS induction, i.e. the response does not have a protective effect but is instead associated with stressed and dying cell subpopulations (Fig.46). In filamenting and lysed cells, I observed an almost 20-fold increase in the expression rate after 100 min in M95AA + AdGM. For untreated cells, I observed a basal SOS expression level that remained constant over time. There was no induction of the SOS response in untreated cells, except in lysed cells, which may spontaneously induce the response and filament independently of the action of any antibiotic, during unperturbed growth (Jones & Uphoff, 2021). The results suggest that in the bactericidal medium, the SOS response is sharply increased before the end of the lag phase and associated with

death rather than survival, with large variations between cells. The SOS response was also induced in the bacteriostatic medium in the presence of TMP but at a lower level than under bactericidal conditions. Interestingly, I observed a clear relationship between increasing cell-to-cell heterogeneity for the SOS response induction, and low survival in treated cells (Fig.47), suggesting that high variability in the response between cells is not beneficial.

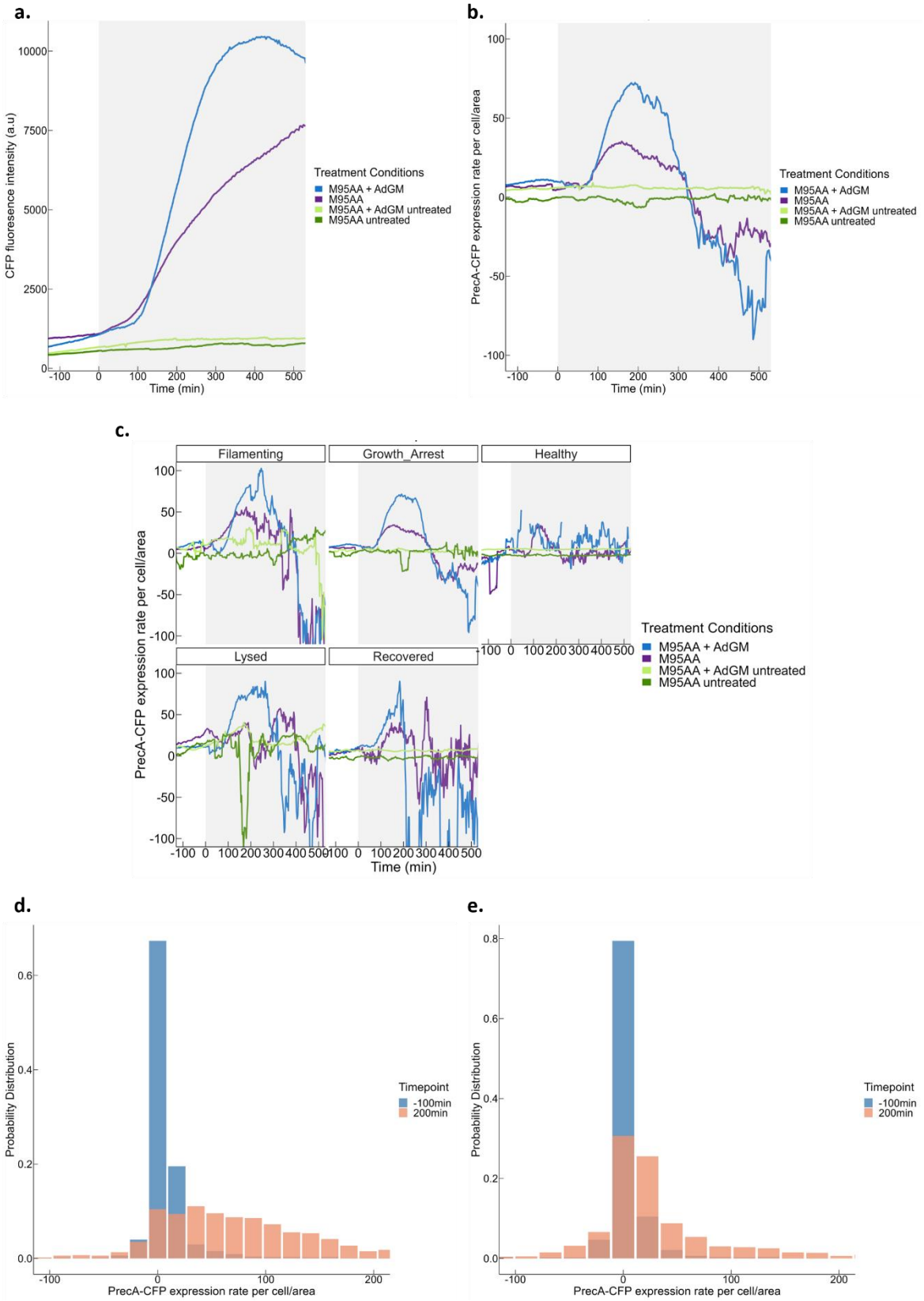


Figure 46 : SOS response (PrecA-CFP) dynamics with continuous 0.25 µg/ml TMP treatment from timepoint 0 during microfluidic experiments or without treatment in M95AA + AdGM or M95AA media. a) Average fluorescence intensity observed in cells at population level. b) Expression rate computed as the change in

fluorescence intensity over time normalised by the cell area of individual cells. c) Expression rate for PrecA-CFP at the subpopulation level determined at 800 min. d) Distribution of rate observed at -100 min and 200 min in M95AA + AdGM, e) M95AA. The curves represent mean values obtained from 1000-1500 cells per experiment.

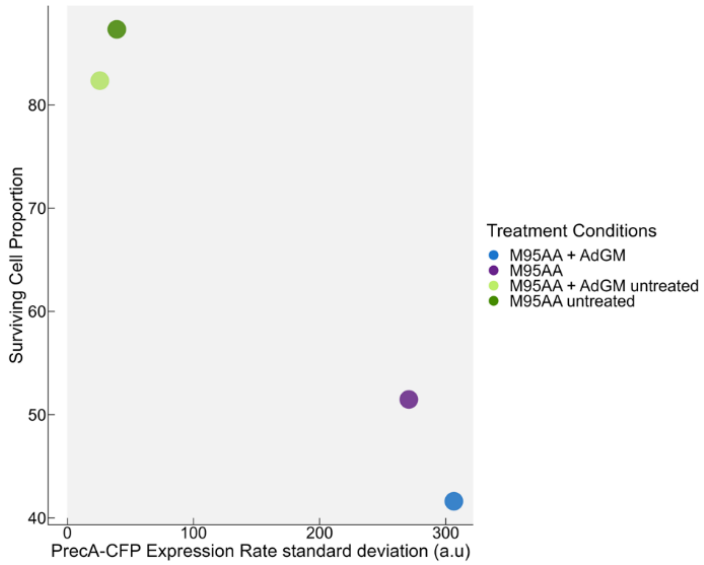


Figure 47 : Correlation between cell-to-cell heterogeneity in PrecA-CFP expression rate and cell survival. The surviving cell proportion (healthy and recovered cells) is plotted against the standard deviation in PrecA-CFP expression rate across all cells measured at 500 min. The curves represent mean values obtained from 1000-1500 cells per experiment in untreated cells or treated cells with continuous 0.25 µg/ml TMP treatment.

I also studied the SOS response in both media for cells supplemented with thymidine, to understand the importance of thymidine availability for the induction of the response (Fig.48). I did not notice any SOS response induction and thymidine completely abolished the response in treated cells. When thymidine was removed after 200 min of treatment, I observed a delayed induction of the SOS until after more than 300 min of treatment, suggesting a delay in DNA damage accumulation. When thymidine was removed at the start of the treatment, the dynamics of the SOS response were similar to treated cells, with higher values reached, indicating higher DNA damage levels. This would suggest that the SOS response induced by TMP is directly dependent on endogenous thymidine abundance within the cells, explaining the observed increase during treatment.

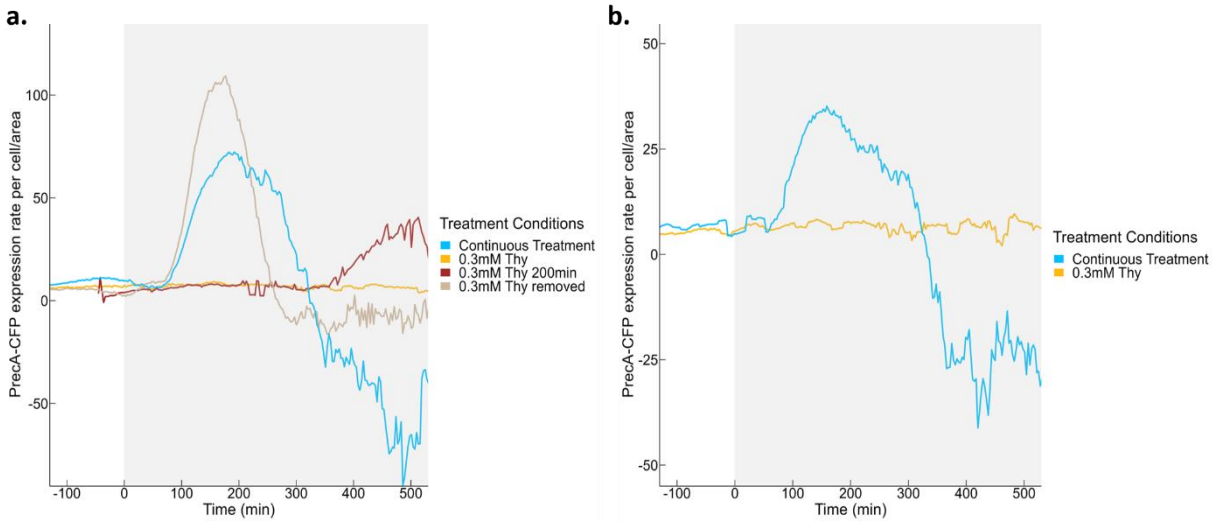


Figure 48 : SOS response (PrecA-CFP) dynamics in cells with continuous 0.25 µg/ml TMP treatment from timepoint 0 during microfluidic experiments, with different thymidine supplementations in a) M95AA + AdGM, and b) M95AA media. The curves represent mean values obtained from 500-1000 cells per experiment.

I have tested a range of mutants deficient in the SOS response or DNA repair pathways and equipped with the *PrecA* fluorescent reporter, to determine if any pathway could be responsible for the induction of the response (Fig.49). These included in both media the mutants *lexA3ind*$^-$ and *ΔdinB ΔumuC*, and *ΔmutM ΔmutY* in the bactericidal medium only. In both media, I observed that the *lexA3ind*$^-$ mutant expressing an uncleavable LexA, leading to SOS deficiency, did not show RecA induction, as expected. This confirms that expression rate changes observed in WT cells are attributable to an induction of the SOS response. The double mutant *ΔdinB ΔumuC* deficient for TLS polymerases which are controlled via the SOS response and could cause increased DNA replication stalling, seemed more strongly induced in M95AA + AdGM. This could suggest attempts to restart replication via HR in the absence of the system. Finally, I investigated in M95AA + AdGM the double mutant *ΔmutM ΔmutY*, impaired in 8oxoG repair (Fowler et al., 2003). For that mutant, I observed an induction of the SOS response at a slightly lower level than for WT cells, suggesting a potential role for the system in increasing the SOS response induction in treated cells. Indeed, it has been suggested that the processing of DNA lesions by MutM and MutY in the context of TMP

treatment could be deleterious and produce more DNA damage in treated cells (Giroux et al., 2017).

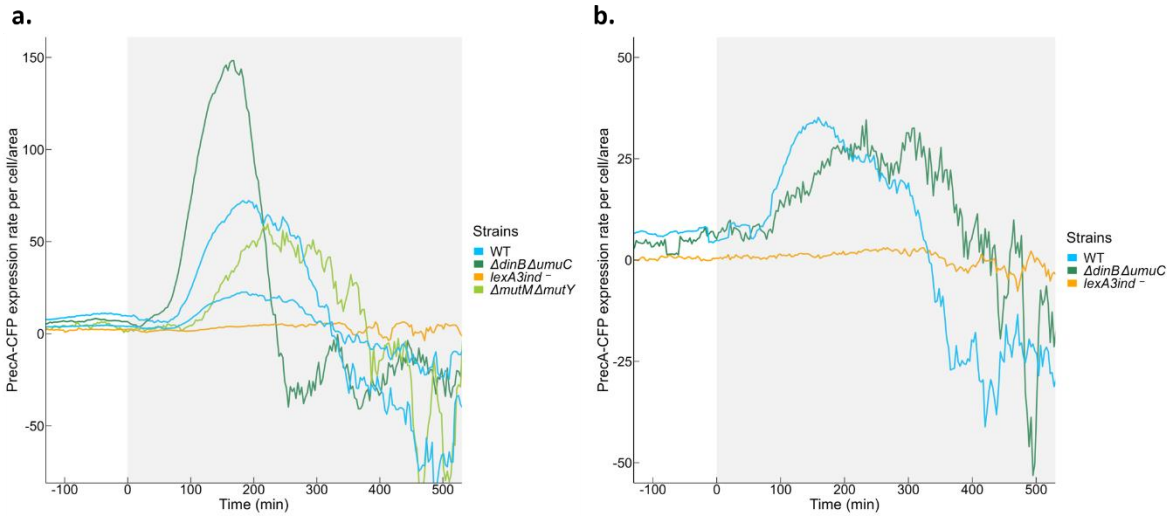


Figure 49 : SOS response (PrecA-CFP) dynamics with continuous 0.25 µg/ml TMP treatment from timepoint 0 during microfluidic experiments in WT and mutant cells in a) M95AA + AdGM, and b) M95AA media. The curves represent mean values obtained from 500-1000 cells per experiment.

Finally, I wanted to confirm that there was a genuine cleavage of LexA repressor, which is upstream of any gene expression changes due to the SOS response. This was done because the *PrecA*-CFP reporter gene expression could be affected by many other cellular processes besides the SOS response, as seen with the P_{RNAI}-mkate2 reporter. For that, I performed single molecule tracking in both media of interest, using agarose pads to immobilize the cells. The cells contained a fusion of the LexA transcriptional repressor with a Halo Tag and an attached dye that blinks on and off. This allows tracking in cells, thereby informing about the diffusion coefficients and state of molecules within the cells (Fig.50). I performed control experiments with samples of paraformaldehyde-fixed cells, non-cleavable LexA K156A mutants, and cells expressing unconjugated Halo Tag corresponding respectively to DNA-binding, transiently DNA-interacting, or fast and freely diffusing states (Jones & Uphoff, 2021). The control samples were used to derive a diffusion coefficient distribution to then fit the distribution of cells with and without TMP treatment to obtain the

fractions of LexA molecules in each of the three states. It must be noted that the diffusion coefficient reference values were measured in M9 minimal medium, not M95AA or M95AA + AdGM, but it was reasonable to assume that the values would be close to the ones in the reference medium. I carried out experiments in both media and was able to derive the proportion of cells in different states in the cells after 2 h of treatment. There are three states possible for the LexA molecules as described above. This includes immobile proteins when the molecule is bound to DNA, slowly diffusing if unbound to DNA and diffusing in the cells, or fast diffusing if the LexA molecule is cleaved which releases a freely and fast diffusing Halo Tag in the cells (Jones & Uphoff, 2021).

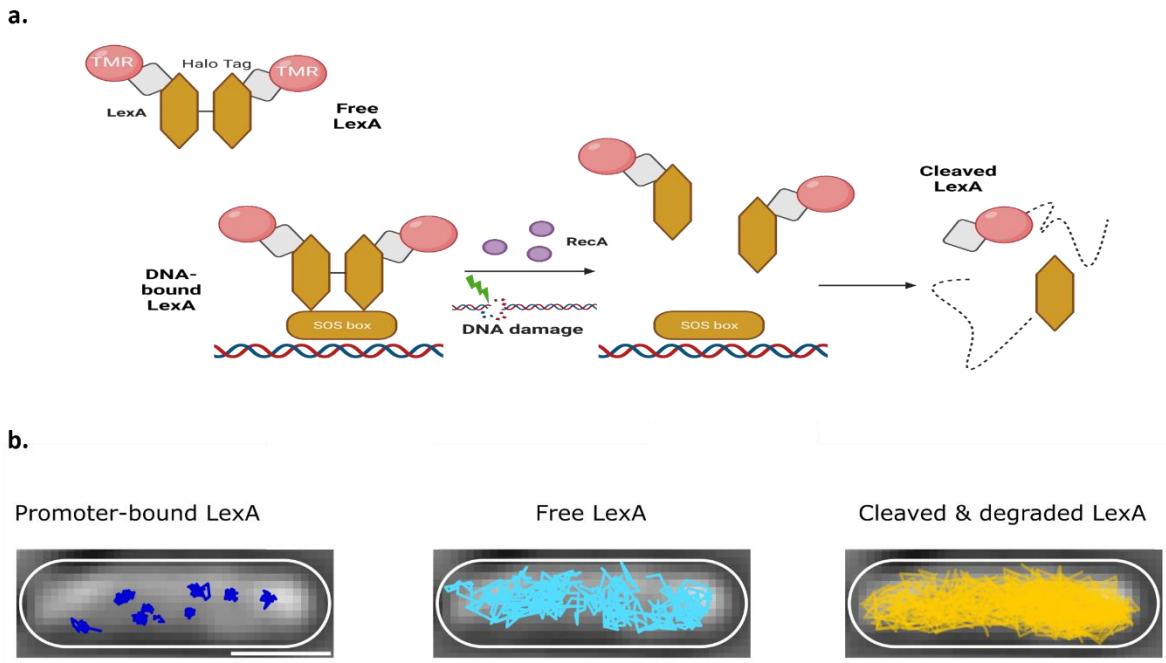


Figure 50 : Single molecule tracking experiment with LexA-Halo. a) Illustration of a LexA-Halo Tag with TMR dye, binding to the SOS box in DNA to repress the SOS response. In the presence of DNA damage, the SOS response gets activated following autocleavage of the LexA dimer, which releases the Halo Tag. b) Three potential states of the LexA-Halo Tag in a cell: promotor bound, free, or degraded, from Jones & Uphoff, 2021.

In both media, I noticed that the untreated cells had a large majority of molecules in slow diffusing or bound states, similar to cells supplemented with thymidine, whether treated or untreated, (Fig.51). When the cells were treated with TMP only, I observed a shift in the profile of LexA. There

was an increase in the proportion of molecules found in a fast-diffusing state, and a decrease in bound molecules compared to untreated cells. The fast diffusing molecules indicate a cleaved state for the LexA molecule, suggesting that the SOS response is induced under the treatment conditions tested. Conversely, the bound molecules correspond to LexA binding to the SOS box and suggest repression of the SOS response (Jones & Uphoff, 2021). These results confirm that the SOS response is induced under TMP treatment, which involves LexA cleavage.

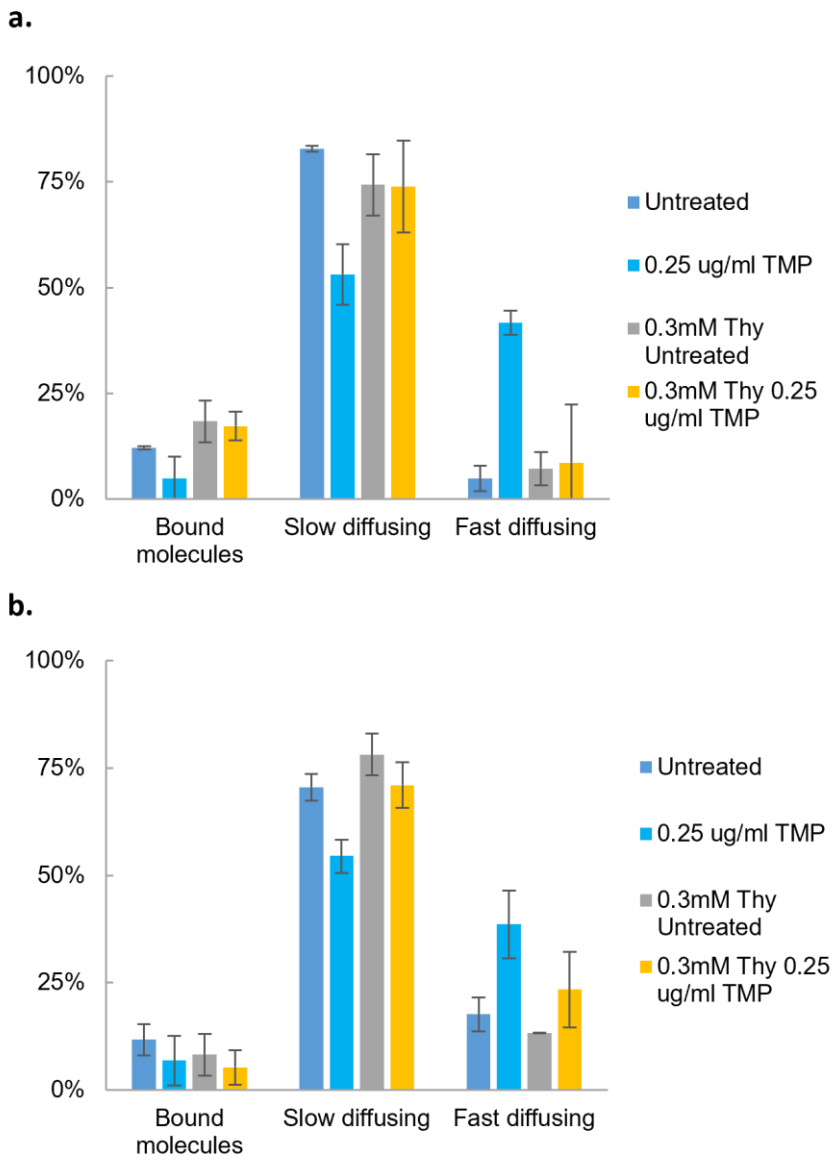


Figure 51 : LexA-Halo Tag state of occupancy in WT TMP-treated cells. The single-molecule tracking experiments were performed with 0.25 µg/ml TMP treatment, or in untreated cells and with or without

0.3mM thymidine in a) M95AA + AdGM, and b) M95AA media. The three possible states (bound, slow or fast diffusing) are shown with their relative distribution in each condition. The figure includes the average percentage observed at population level ± standard error of the mean, derived from three repeat experiments.

2.5. TMP's Influence on Oxidative Stress

ROS can damage DNA with oxidative DNA lesions, but also proteins and lipids in cells. Using microfluidics assays, I next set up to study if there were any bacterial oxidative stress responses to TMP at the single-cell level. I imaged cells carrying plasmids with the fluorescence reporter msCFP3, expressed from the promoters of a few different oxidative stress response pathways. This included the SodA (superoxide dismutase), controlled by SoxR and detoxifying the cells of $O2^-$ by converting them into H_2O_2, the primary scavenger AhpC (alkyl hydroperoxide reductase) and GrxA (glutaredoxins), which converts OxyR back to its reduced and inactive form, both controlled by OxyR to detoxify the cells of H_2O_2. I monitored the expression rate of each reporter which considers the cell area changes to normalise the fluorescence values measured and the potential protein accumulation due to cell filamentation as described previously.

In M95AA + AdGM, I observed an increase in SodA induction after a 100 min lag phase. This was followed by a decrease to negative values as dead cells lead to bleaching and suggest the presence of superoxide during treatment (Fig.52). For the H_2O_2 stress, I investigated AhpC and GrxA and observed little changes in expression rate after the lag phase. However, it is possible these could be false-positive results for gene induction, where protein accumulation occurs passively due to a slow-down in cell growth without any actual increase in the expression rate of the protein, as observed with the P_{RNAI} reporter above. Thus, these results suggest a very small amount of H_2O_2, if any, present during treatment. In the bactericidal medium, I investigated the basal level of expression of the three oxidative stress response reporters in untreated and thymidine-

supplemented cells. I observed no increase over time in the basal expression level of the AhpC and GrxA reporters as cells grew in the microfluidic growth chambers. The SodA reporter experienced some fluctuations but overall, there was no increase for untreated cells, and thymidine completely abolished the induction of the SodA reporter. This suggests that in the bactericidal medium, whilst superoxide stress increases, the hydrogen peroxide stress seems comparatively minor or absent, and in any case, both responses seem to be mildly activated.

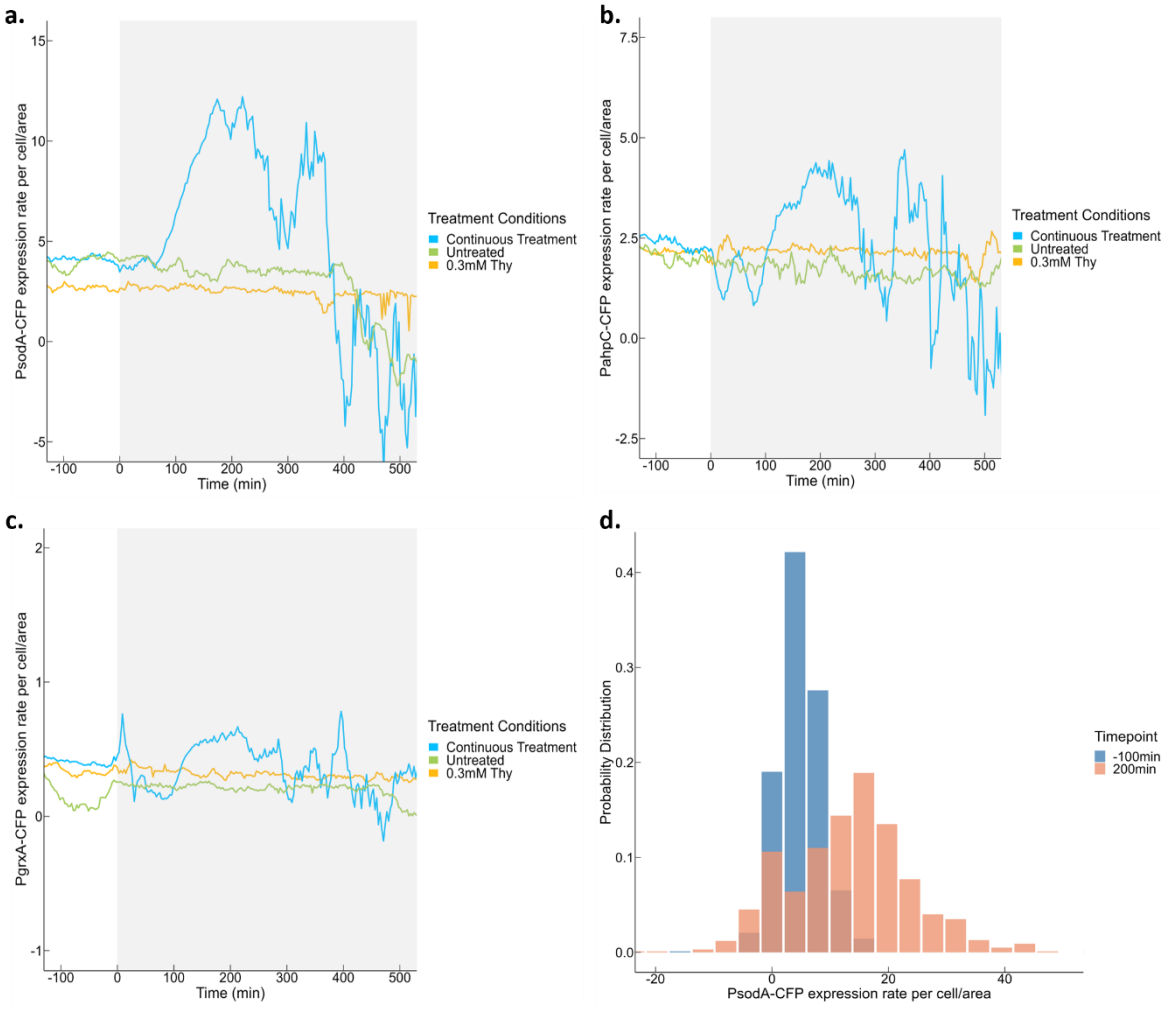


Figure 52 : Oxidative stress response dynamics in cells with continuous 0.25 µg/ml TMP treatment from timepoint 0 during microfluidic experiments, with thymidine supplementation or without treatment in M95AA + AdGM. Cell expression rate for a) PsodA-CFP, b) PahpC-CFP, c) PgrxA-CFP. d) Distribution of rate observed at -100 min and 200 min in M95AA + AdGM. The curves represent mean values obtained from 1000-1500 cells per experiment.

In M95AA, I studied the expression rate for the same reporters for superoxide and hydrogen peroxide stresses (Fig.53). The expression rate for the SodA reporter did not increase as much as in M95AA + AdGM after a 100 min lag phase, and this increase was abolished in the presence of thymidine. For H_2O_2 stress, I investigated the AhpC and GrxA reporters and did not see much change in expression rate from the basal level measured before the start of treatment. These results suggest that in the bacteriostatic medium, the superoxide and hydrogen peroxide stresses were even lower than in bactericidal medium.

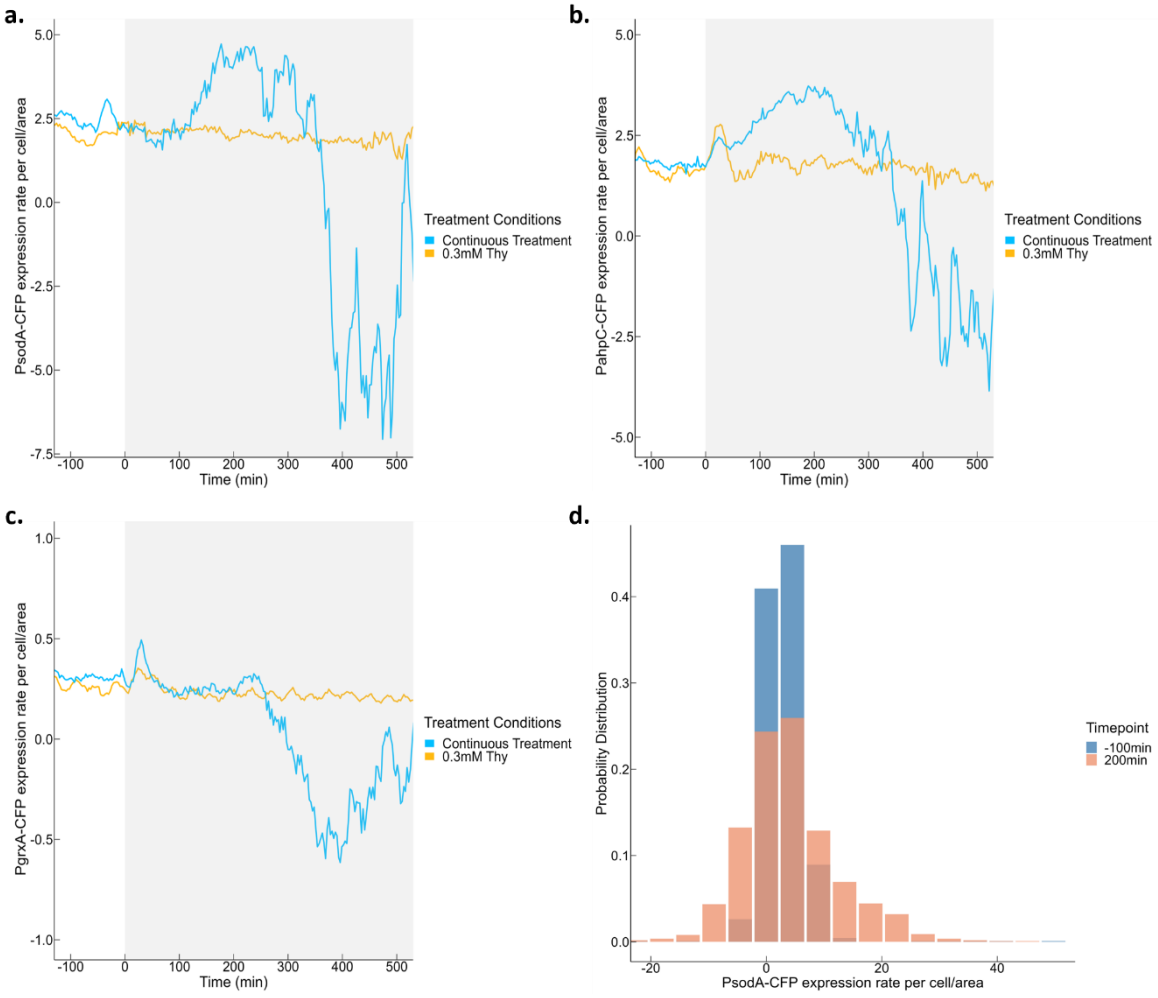


Figure 53 : Oxidative stress response dynamics in cells with continuous 0.25 µg/ml TMP treatment from timepoint 0 during microfluidic experiments, and with thymidine supplementation in M95AA. Cell expression rate for a) PsodA-CFP, b) PahpC-CFP, c) PgrxA-CFP. d) Distribution of rate observed at -100 min and 200 min in M95AA. The curves represent mean values obtained from 1000-1500 cells per experiment.

The DNA damage caused by TMP may lead to oxidative stress, and vice versa, or the two stresses could be independently caused by TMP. I thus examined in both media the SOS deficient *ΔrecA* mutant, with a SodA reporter for superoxide stress (Fig.54). In treated cells, I observed an increase after the lag phase with dynamics and expression rate very similar to the WT cells, suggesting that in both media, SoxR response pathway is independent of the SOS response. Finally, for the superoxide stress, I examined the relationship between expression rate heterogeneity and cell survival (Fig.55). I observed a strong link, suggesting that conditions leading to lower survival also show increased cell-to-cell heterogeneity in superoxide stress response.

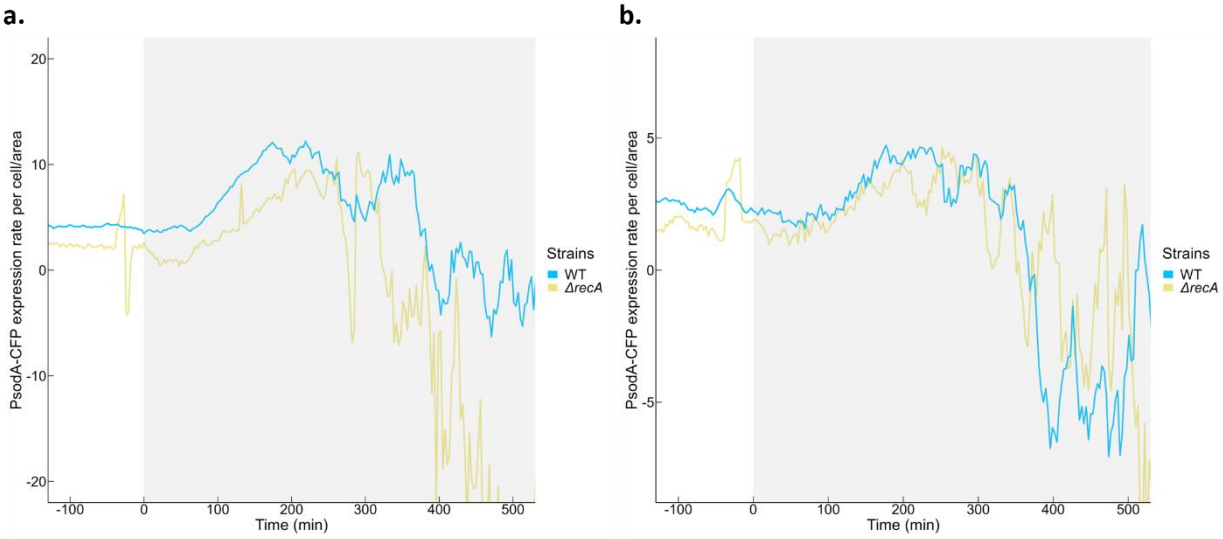


Figure 54 : Oxidative stress response (PsodA-CFP) dynamics with continuous 0.25 µg/ml TMP treatment from timepoint 0 during microfluidic experiments in WT and mutant cells in a) M95AA + AdGM, b) M95AA. The curves represent mean values obtained from 500-1000 cells per experiment.

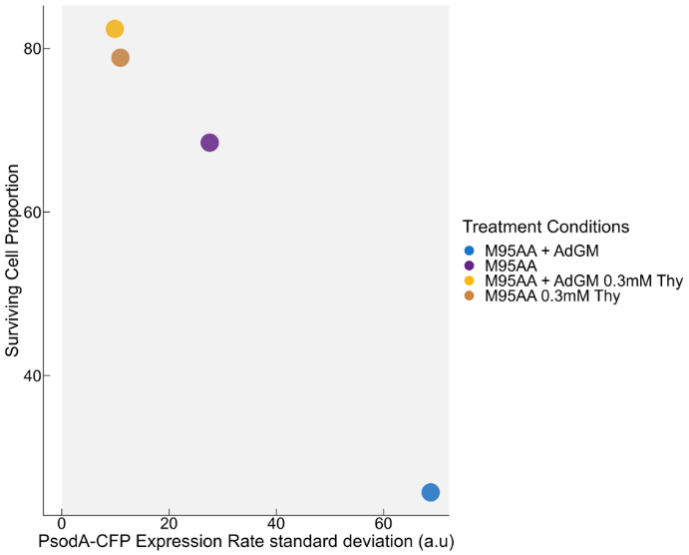


Figure 55 : Correlation between cell-to-cell heterogeneity in PsodA-CFP expression rate and cell survival. The surviving cell proportion (healthy and recovered cells) is plotted against the standard deviation in expression rate across all cells measured at 200 min. The curves represent mean values obtained from 1000-1500 cells per experiment in treated cells with continuous 0.25 µg/ml TMP treatment.

2.6. TMP's Influence on Acid Stress

Next, I investigated the acid stress response as a consequence of TMP treatment. It has been described in treated cells, resulting from the depletion of adenine which leads to a drop in intracellular pH (Mitosch et al., 2019). For that, I used microfluidics experiments with a reporter for the GadBC operon for acid stress response, specifically the promotor for the *gadB* gene, which is a glutamate decarboxylase involved in resistance to low pH (Castanie-Cornet et al., 1999). It was transcriptionally fused to a GFP fluorescent protein, due to technical difficulties to replace the GFP to msCFP3. Given the similarity in maturation time for the two proteins, I assumed that their dynamics would be similar, allowing for temporal comparison between the different reporters studied (Balleza et al., 2018).

Therefore, I tested the acid stress response in M95AA + AdGM and noticed no changes in fluorescence intensity of the reporter throughout the experiment when the cells were treated (Fig.56). I then investigated the expression rate which takes into account cell area changes. Again, I did not see any changes at the population level, suggesting no acid stress response induction in the bactericidal medium. On the other hand, in the bacteriostatic medium M95AA, I observed an increase in fluorescence intensity of the GFP reporter, with little lag phase. I confirmed these observations with the expression rate as a more accurate measure of promotor activity and observed an immediate induction of the acid stress response, followed by a decrease in expression after 100 min, likely due to growth-arrested cells. In untreated cells, I did not observe any changes from the basal level of acid stress response in either medium, although the baseline in the bacteriostatic medium seemed higher, which could not be explained by the pH of the media themselves as they were quite similar (6.76 in M95AA + AdGM and 7.03 in M95AA). In all cases, the drop observed for the GFP fluorescence before the start of the treatment could be due to the cells adapting to the microfluidic growth chamber environment. The cells could have potentially experienced acid stress in the bulk culture before the loading of the devices. Overall, this suggests that acid stress is only experienced in the bacteriostatic medium for TMP-treated cells.

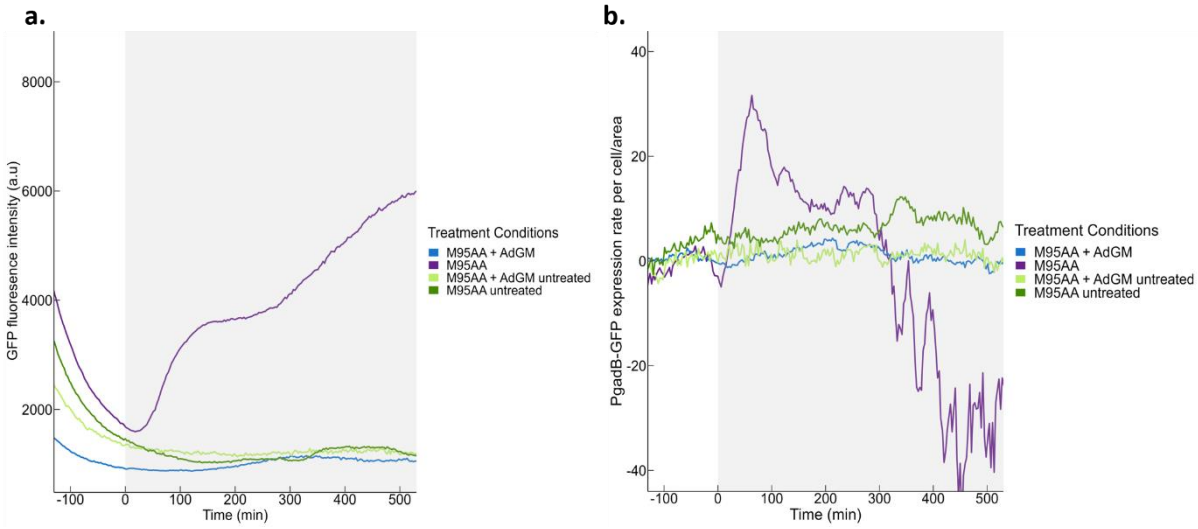


Figure 56 : Acid stress response (PgadB-GFP) dynamics with continuous 0.25 µg/ml TMP treatment from timepoint 0 during microfluidic experiments or without treatment in M95AA + AdGM or M95AA media. a)

GFP average fluorescence intensity in cells at population level. b) Expression rate computed as the change in fluorescence intensity over time normalised by the cell area of individual cells. The values represented are for 1000-1500 cells on average per experiment.

I then tested in both media the effects of medium supplementation on the acid stress response in TMP-treated cells, including thymidine and adenine, both likely depleted by treatment (Fig.57). In M95AA + AdGM, it appeared that much like treated cells as described before, there is no change in the expression rate of the acid stress response reporter throughout the experiments, suggesting that in the presence of thymidine, the response is not induced. I observed in M95AA that thymidine supplementation did not abolish the induction of the acid stress response observed in treated cells. Indeed, I observed from the start of the treatment an increase in expression, similar to treated cells. By contrast, supplementing the medium with adenine in M95AA was enough to emulate the profile seen in untreated cells, suggesting that adenine starvation leads to acid stress in TMP-treated cells.

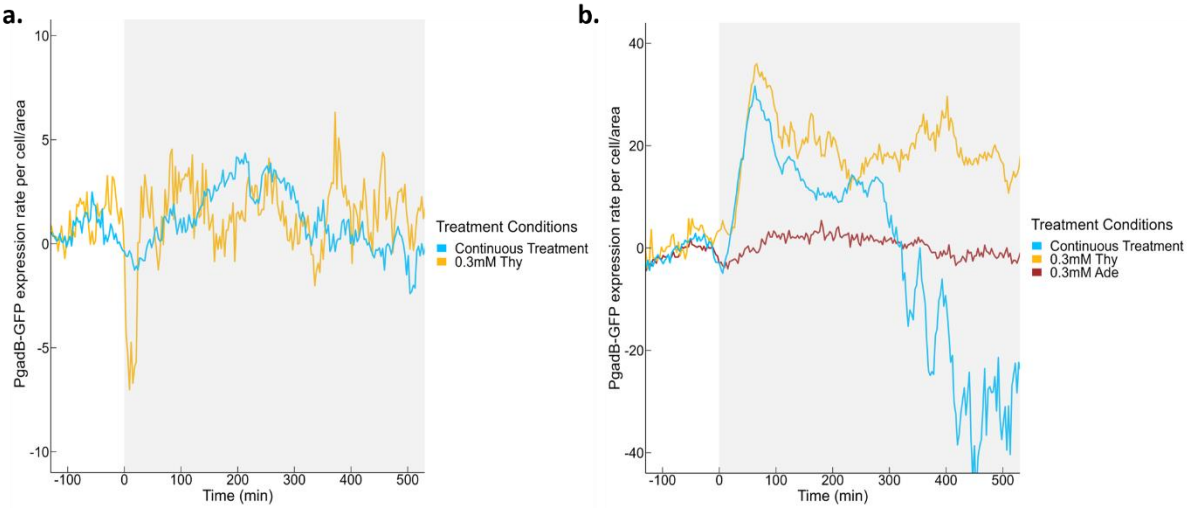


Figure 57 : Acid stress response (PgadB-GFP) dynamics in cells with continuous 0.25 µg/ml TMP treatment from timepoint 0 during microfluidic experiments, with different medium supplementation in a) M95AA + AdGM, b) M95AA media. The curves represent mean values obtained from 500-1000 cells per experiment.

2.7. TMP's Pathways Crosstalk

After studying in detail in both media at population and subpopulation levels the dynamics of the different stress responses mentioned above, I aimed to understand the temporality of these responses compared to one another, and their interplay if any. For that, I used a variety of strains carrying two stress response reporters at the same time, including RecA, SodA or MutL.

Firstly, I compared the timing of the SOS response using a RecA reporter to the SodA reporter for superoxide stress in a dual-reporter strain, allowing to measure the expression in a same cell at the same time. In M95AA + AdGM, I observed that the SOS response was induced shortly before the end of the 100 min lag phase at the population level, in a pulsatile manner, whereas the induction of SodA seemed gradual and started later than RecA (Fig.58). As a result, the highest expression levels, similar between the two reporters, were reached at different points, around 150 min for RecA, and 300 min for SodA, suggesting different dynamics. I also looked at the correlation between the two responses in single cells and noted a significant positive correlation throughout the experiment. Overall, it seemed that the responses have different timelines and dynamics in treated cells, with the SOS response seen in actively growing cells, whereas $O2^-$ accumulate in later stages when cells enter growth arrest or when dying. However, it appears that there is a constant relationship whereby cells with high induction of SOS response also have high levels of superoxide stress response.

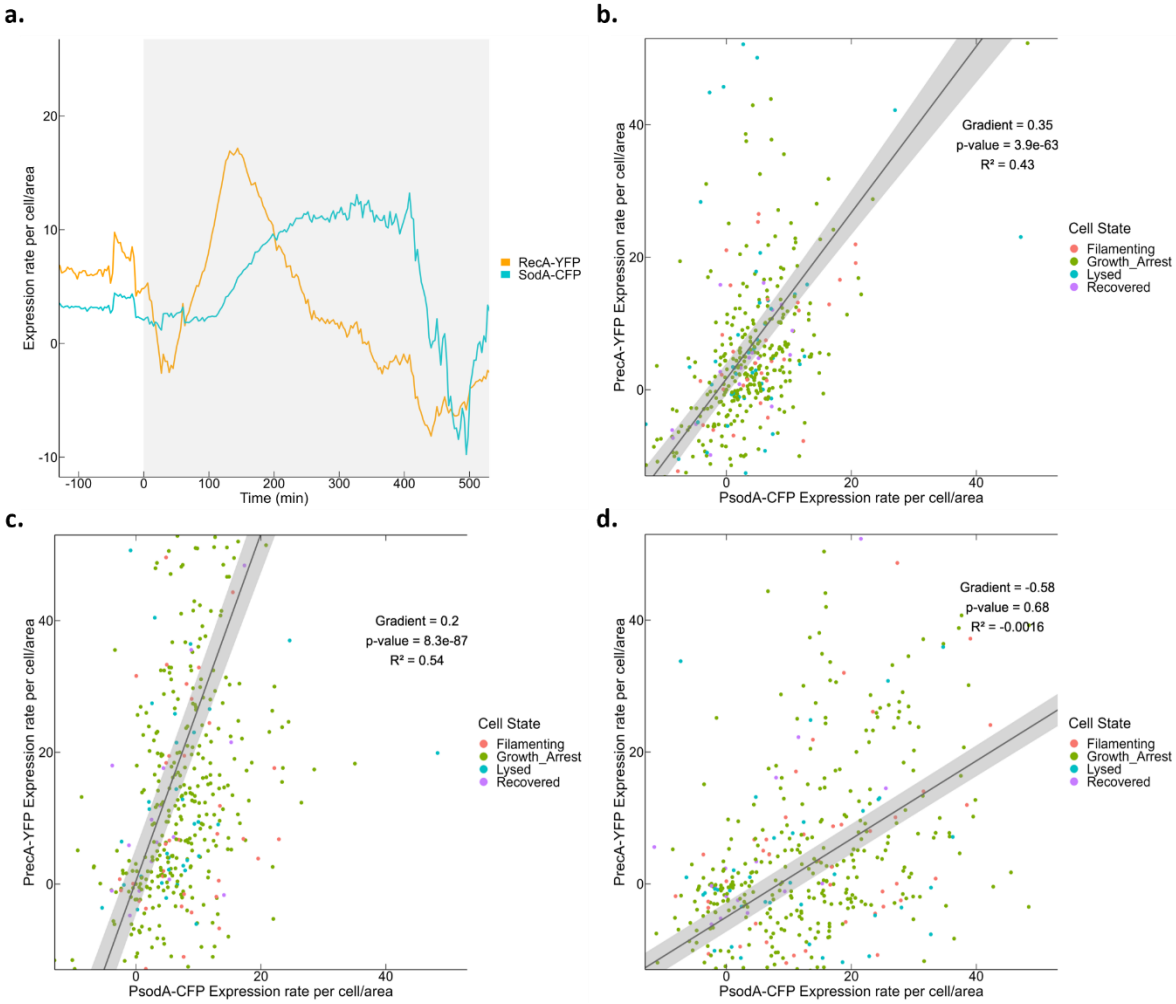


Figure 58 : PrecA-CFP and PsodA-CFP response dynamics in WT cells with continuous 0.25 µg/ml TMP treatment from timepoint 0 during microfluidic experiments. a) Expression rates for RecA and SodA in M95AA + AdGM. b) Expression rate of RecA vs SodA for individual cells at -100 min pre-treatment, c) 150 min and d) 300 min of continuous treatment, including a fitted linear regression curve showing correlation, with a p-value < 0.05. The values represented are for 1000-1500 cells on average per experiment. The figure includes the R^2 value as a measure of how well the model fits the data, and the gradient of the linear model curve.

Then for both media, I investigated the timing of cell length changes and the SOS response in the same cell to test for a temporal relationship (Fig.59). In both media, I observed that the SOS response was induced shortly before the increase in cell length at the population level. The two pathways did not show any correlation after 300 min of continuous treatment, suggesting different timelines. I also compared the timing of the mismatch rate and SOS response or superoxide stress response in the same cell in M95AA + AdGM, to understand the timeline of events in treated cells

(Fig.60). When investigating the mismatch rate and the SOS response, I observed very different timings, with a delayed mutagenesis induction compared to the SOS response. In fact, the mismatch rate started to increase when the SOS response reached its highest value, and peaked after the decrease in SOS response, suggesting that the two pathways do not act simultaneously in treated cells.

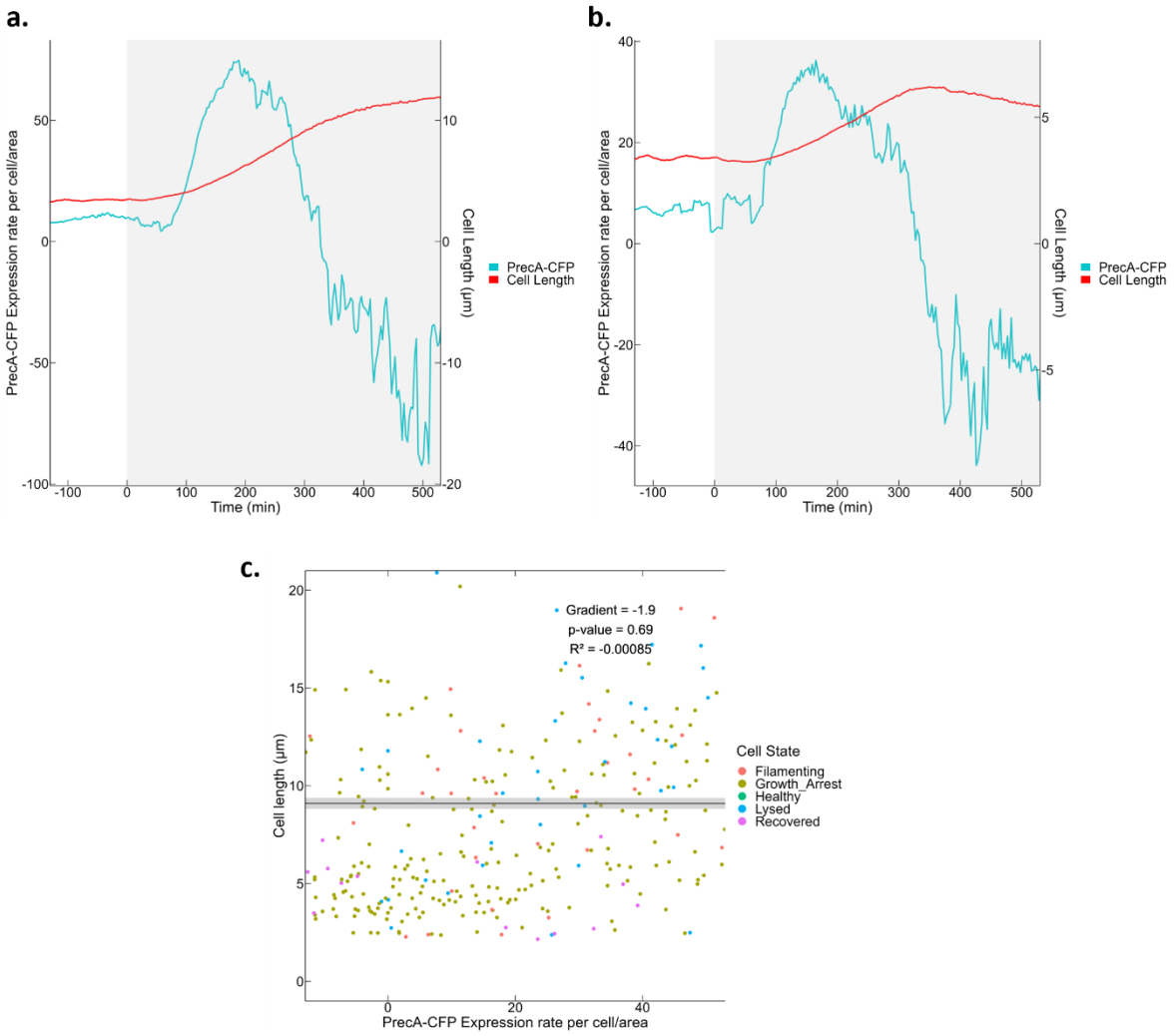


Figure 59 : Cell length and SOS response dynamics observed in WT cells with continuous 0.25 µg/ml TMP treatment from timepoint 0 during microfluidic experiments. a) Expression rate for RecA and the cell length in M95AA + AdGM and b) M95AA. c) Cell length vs RecA expression rate for individual cells at 300 min of continuous treatment in M95AA + AdGM, including a fitted linear regression curve showing no correlation, with a p-value < 0.05. The values represented are for 1000-1500 cells on average per experiment. For panel c, the figure includes the R^2 value as a measure of how well the model fits the data and the gradient of the linear model curve.

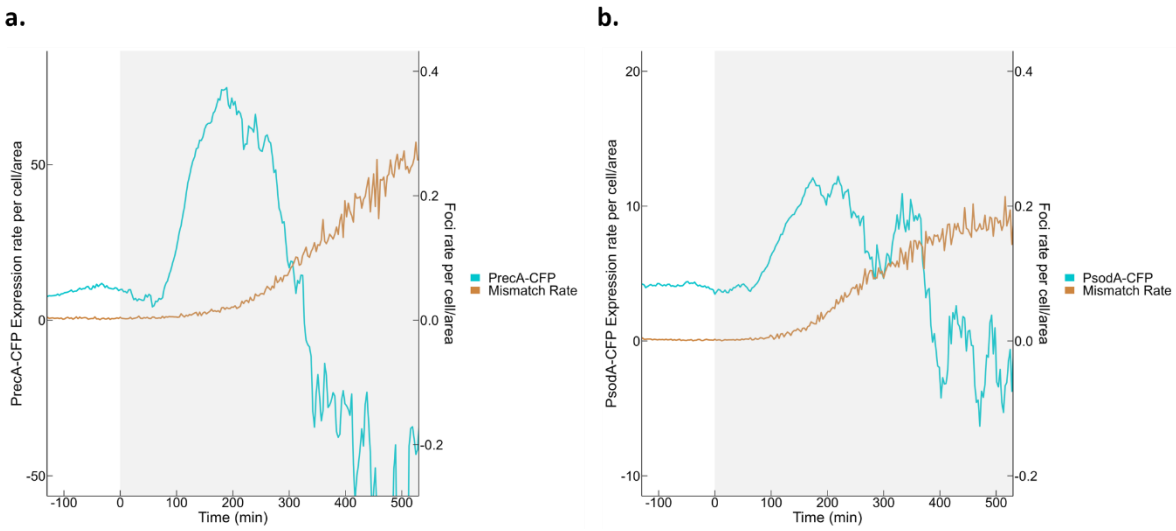


Figure 60 : Stress response dynamics in WT cells with continuous 0.25 µg/ml TMP treatment from timepoint 0 during microfluidic experiments in M95AA + AdGM. a) RecA expression rate and the mismatch rate. b) SodA expression rate and the mismatch rate. The values represented are for 1000-1500 cells on average per experiment.

3. Discussion

In this chapter, I aimed to study key response pathways to TMP treatment in bacterial cells. My study was multifaceted and included a large panel of fluorescent reporters in microfluidics experiments as well as single-molecule tracking experiments to validate my findings. Hence, I explored the impact of the treatment on the cell's genome stability, from DNA replication disruptions to DNA damage resulting in SOS response or mutagenesis. I also investigated oxidative and acid stress responses in the cells. My studies included dynamics and temporal studies for both wild-type and mutant cells in an attempt to identify necessary pathways for the survival or death of treated cells. The experiments also allowed to determine the dynamics of pathways relative to each other and explore cellular heterogeneity in the respective responses. Importantly, I observed in bactericidal and bacteriostatic media that treatment was accompanied by an accumulation of proteins and a global increase in fluorescence intensity associated with high cell-to-cell

heterogeneity and derived from the increase in the P_{RNAI} reporter fluorescence. It has been described in TMP-treated cells as potentially due to a universal upregulation caused by changes in growth rate (Angermayr et al., 2022). This marked protein accumulation could present a challenge in population-based assays using techniques such as flow cytometry as it could cause false positive responses. This has been suggested because of a lack of cell volume normalisation (T. V. P. Rao & Kuzminov, 2022), thus motivating the use in this study of techniques that provide quantitative data for the cell length and fluorescence marker simultaneously, particularly in the study of stress responses.

Firstly, I observed that the number of DNA replication sites increased after a lag phase of around 100 min, which I had defined as the time delay before cell growth and survival are affected (see Chapter 4). This suggests that the cells may be initiating multiple rounds of DNA replication unsuccessfully, likely leading to DNA replication stalling and additional stress for the cells. However, it has been suggested that DnaN does not always colocalise with the replication fork (Mäkelä *et al.*, 2021), implying that the foci observed may not always reliably represent active DNA replication sites. Both the loading and unloading of the beta-clamp require the ATP-dependent clamp loader complex and it has been shown that clamps dwell at completed Okazaki fragments behind the replication fork (Moolman et al., 2014). Further experiments would be needed to address if the increased frequency of DnaN-YPet foci during TMP treatment represents active replication forks or an accumulation of clamps behind stalled forks which cannot be unloaded due to a reduction in cellular ATP levels. It has also been suggested that DnaN could guide MutS to mismatches in nascent DNA, suggesting a role of DnaN in coupling DNA replication and mismatch repair (Lenhart et al., 2013). Further investigation of active DNA replication could be carried out, one example could be BrdU assays, but these involve providing cells with a modified version of thymine, which could erase the effects of TMP (Gratzner, 1982). Overall, the data suggest a stronger DNA replication disruption

in the bactericidal medium, leading to difficulties for the cells to survive and replicate or divide. This failure to complete DNA replication can lead to the observed cell filamentation (Chapter 4) due to nucleoid occlusion which prevents cell division septum formation when chromosome segregation is incomplete (Bernard et al., 2010).

I also investigated mutagenesis induced by TMP treatment, using a reporter for mismatch rate as a proxy. Importantly, whilst some mismatches arising during DNA replication will be converted into stable mutations and represent mutagenesis in the cells, the MMR pathway will repair most of the mismatches (Modrich, 1991). However, it is known that the mismatch rate correlates with the frequency of genomic mutations (Vincent & Uphoff, 2021). Another caveat is that not all types of mismatches are well recognized and repaired by the MMR pathway, and these would not be detected in the experiments (Uphoff, 2018). Additionally, MMR proteins can also be recruited in HR (Elez et al., 2010). In fact, it has been suggested that the MMR pathway could inhibit HR when it is done with divergent DNA sequences (Tham et al., 2013) and could risk genome stability. The caveats of the technique must be considered when assessing mutagenesis in the cells, as it may not tell the whole story. In my conditions, I was able to study the mismatch rate and determine that it increases after a 100 min lag phase in both media with a lesser increase in bacteriostatic medium. Importantly, it has been suggested that resistance mutations can arise from TMP treatment, particularly in the dihydrofolate reductase gene (Carter et al., 2023). Hence, I found that a short treatment in a bacteriostatic medium did not induce mutagenesis, providing an alternative and effective regimen which could help reduce antibiotic resistance. I also observed that thymidine supplementation completely abolishes the increase in mismatch rate, suggesting that depletion of thymidine is the cause of increased mutagenesis as opposed to depletion of the other metabolites during folate biosynthesis inhibition. By using SOS response-deficient mutants, I observed that the response plays a role initially in keeping the mismatch rate in treated cells low. Additionally, I

observed that mutagenesis is induced after the SOS response, suggesting that it may initially help the cells repair DNA, before potentially causing mutagenesis.

I also analysed in depth the role of oxidative stress response to TMP in both bactericidal and bacteriostatic media. For that, I used reporters for the SoxR pathway detoxifying O_2^- via the superoxide dismutase SodA, and the OxyR pathway detoxifying H_2O_2 via the primary scavenger AhpC and using the protein GrxA to turn off the pathway. Interestingly, my results contradict studies that suggest a large accumulation of ROS in TMP-treated cells (Giroux et al., 2017; Hong et al., 2017). These studies were performed at population level, using FACS without cell area normalisation, or using external catalase that is described as membrane impermeable and would only scavenge exogenous H_2O_2 (Sands, 1960). Instead, using microfluidics experiments in WT cells, I did not see a significant increase in oxidative stress response, particularly not in the bacteriostatic M95AA. In M95AA + AdGM, I observed an increase in SodA, and very little increase in AhpC and GrxA, indicating potentially very low levels of H_2O_2 but high degree of cell-to-cell heterogeneity strongly related to low survival in cells, disproving the hypothesis that oxidative stress is completely absent during trimethoprim treatment (T. V. P. Rao & Kuzminov, 2022). In all cases, thymidine supplementation of the media completely abolished the observed induction of superoxide stress response, suggesting that the depletion of thymidine during treatment could lead to an accumulation of superoxide. This accumulation appeared gradual and coincided with the increase in growth-arrested cells, suggesting that ROS may be indicative of worse health. I also observed that the SOS response is not required for the activation of the oxidative stress response in treated cells, suggesting that the SoxR response pathway is independent of the SOS response, and the two run on different timelines. Further work would be required to understand whether oxidative stress, which could be present at low levels during TMP treatment is a cause or rather a consequence of

death. For instance, observing oxidative lesions in DNA and their temporal dynamics via sequencing could help understand the dynamics associated with oxidative stress.

Since oxidative stress can cause both direct and indirect DNA damage, which can result in mismatches or mutagenesis, I also studied the response to DNA damage in bacteria, namely the SOS response. I confirmed in my study that the SOS response is induced by TMP treatment, as seen by LexA cleavage. In treated cells, particularly in the bactericidal medium, there was a strong induction of the response even before the end of the lag phase, particularly in lysed and filamenting cells. I also noted a high cellular heterogeneity in the response, which was linked to poor outcomes for the cells. This high variability in the SOS response to TMP treatment has been noted before, particularly for the response time of individual cells, unlike for other treatments (Mitosch et al., 2019). This was noted in the bacteriostatic medium too but at a lower level. The effects in bacteriostatic medium could be due to the depleted metabolites, particularly adenine, and their role in modulating the SOS response (Maslowska et al., 2019). I also observed that the TLS polymerases Pol IV and Pol V have a dampening role in the SOS response. On the other hand, the BER pathway more strongly induces the SOS response likely due to increased DNA damage caused by maladaptive repair during treatment (Giroux et al., 2017). Overall, I observed a strong SOS response induction in TMP-treated cells, suggesting global DNA damage and associated stress, however this response did not appear protective for the cells. Instead, it appeared that SOS-deficiency in bactericidal medium recapitulates the growth arrest dynamics observed in bacteriostatic medium. This could be beneficial for cell survival during TMP treatment, and further experiments, such as single-cell DNA and RNA sequencing could be carried out to assess whether SOS-defective mutations could be selected for in response to TMP. Multiple timepoints during treatment and mutants including SOS response deficiency could also be tested to identify genome

location of mutagenesis, temporality as compared to gene expression of stress responses, and understand the role of SOS response for mutagenesis during treatment.

I proceeded to look at the acid stress response, which is only expected to be induced in the bacteriostatic M95AA, due to it being caused by adenine depletion (Mitosch et al., 2019). Indeed, I did not observe any changes in acid stress for the bactericidal medium, but a strong induction from the start of the treatment without lag phase for the bacteriostatic medium. I observed that adenine is sufficient to abolish the acid stress response, whereas it is unrelated to thymidine depletion. This suggests that the acid stress response is associated with the bacteriostatic medium only in the absence of adenine, and acidification takes place during the lag phase. Since the bacteriostatic medium leads majorly to growth arrest or persistence of the cells, the acid stress due to adenine depletion may be an element of the pathway leading to growth arrest, allowing for less cell-to-cell heterogeneity and disorder at the cellular level.

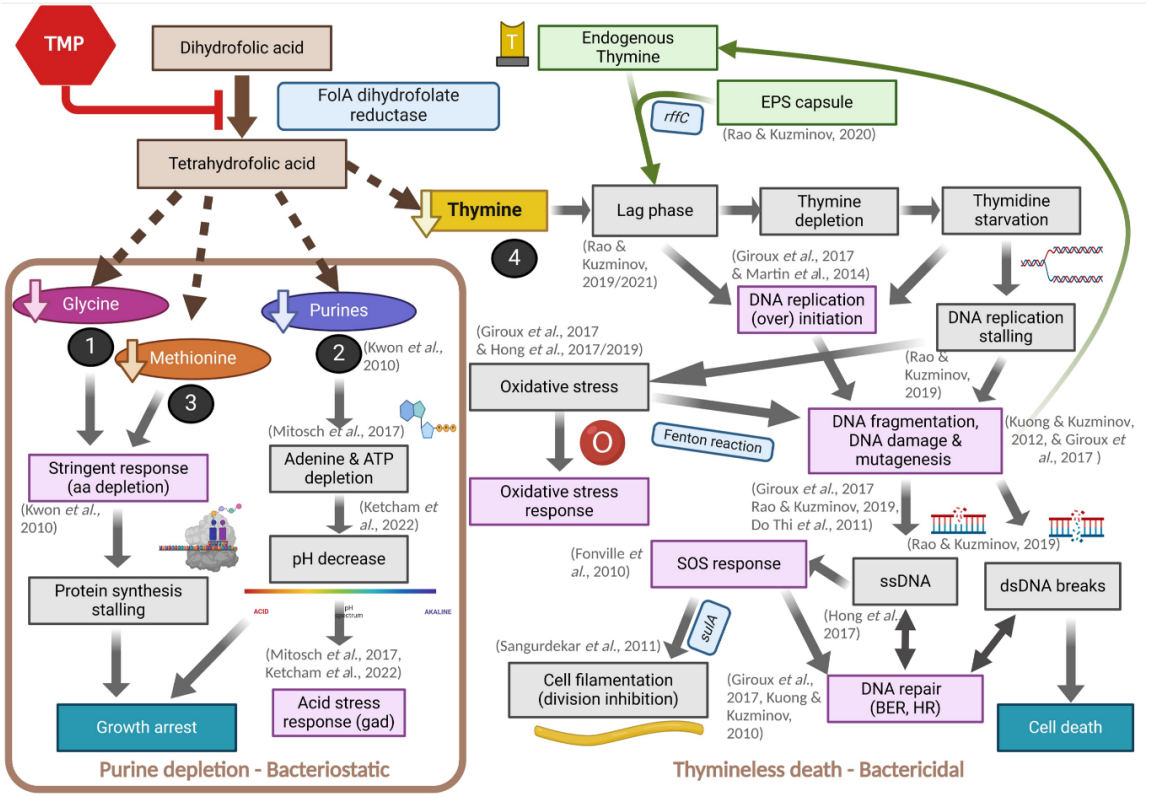
For the FolA reporter, I expected an increase in expression, according to the literature (Angermayr et al., 2022) and due to slowing down of the growth rate in treated cells, but only noted a modest increase in expression. However, this increase happened during the lag phase when the cells are slowing down, suggesting that much like the accumulation of fluorescence for the P_{RNAI} reporter, it is related to delayed growth in cells. This could also suggest that the increase does not only intervene to help production of thymidine in depleted cells but also as part of a global response in TMP-treated cells. I also investigated the relationship between stress responses and their temporality in the same cell. I observed in M95AA + AdGM that the SOS response and cell filamentation happen on different timelines and are not correlated. This confirms the behaviour of the cell length and SOS response in the *ΔsulA* mutant described in Chapter 4. Indeed, the changes

in cell length observed in treated cells are not solely attributable to the SulA inhibitor of division induced by the SOS response (Fonville et al., 2010), but likely due to an SOS-independent mechanism. I also observed that the SOS response precedes the superoxide stress response in treated cells and presents with a more pulsatile dynamic. However, the two responses exhibit a strong positive correlation, indicating that cells with higher SOS response also have higher superoxide stress response. Finally, I noted that mutagenesis was the last phenomenon observed in treated cells, induced strongly but well after the SOS response, suggesting that it could play a role in protecting the cells from mutagenic processes.

In summary, I observed very interesting differences between the two media supplementations, although not across all the responses studied (Fig.60). The bactericidal medium induced all major stress responses studied, except the acid stress response. This includes DNA replication disruption, mutagenesis, SOS and oxidative stress responses, and global stress, induced much more strongly, usually after a 100 min lag phase. All these responses could be linked to thymidine depletion and presented a high degree of cell-to-cell heterogeneity, suggesting a profound state of disorder in cells. However, I observed that in bacteriostatic medium, the most strongly induced response was acid stress, which is due to adenine depletion. I also observed a major difference at the subpopulation level in the bactericidal medium across all the stress responses studied whereby expression rates and thus induction of all responses is stronger in filamenting and lysed cells. This suggests that cell-cell heterogeneity in stress responses is associated with divergent cell fates. Specifically, elevated induction of stress responses is correlated with lower survival, as opposed to elevated responses being associated with a better ability to tolerate TMP treatment.

Overall, it does not appear that a single pathway is responsible for the different cellular states observed following treatment. In fact, no single pathway deletion fully blocks the disorder in the cells, with some decreasing survival further. The different pathways all play a role in the outcome for the cells, in a metabolic interplay creating a general state of disorder in the cells (Fig.61). This state of disorder interconnects the pathways and determines the dynamics of recovery and subsequent survival following acute treatment, as described by (Kaplan et al., 2021). This appears at much more critical level in bactericidal medium with higher cell-to-cell heterogeneity and global dysregulation, leading to worse outcomes and preventing further growth or cell survival. By contrast, cells in a bacteriostatic medium were able to return to a normal state shortly after removal of treatment. This suggests the possibility of a rapid exit from the arrested state, possibly due to a lower level of disorder and less abrupt disruptions for the cells in bacteriostatic medium. Cell-to-cell heterogeneity leading to different bacterial subpopulations in the context of treatment for a UTI treatment could cause recurrent infections in patients. To conclude, this study has suggested that much like it was described by Kaplan et al., 2021 in the context of antibiotic persistence, TMP in different media can cause both regulated and dysregulated states characterized by interconnected pathways and leading to vastly different recovery dynamics.

TMP Mechanisms of Action : Literature



TMP Mechanisms of Action : This study

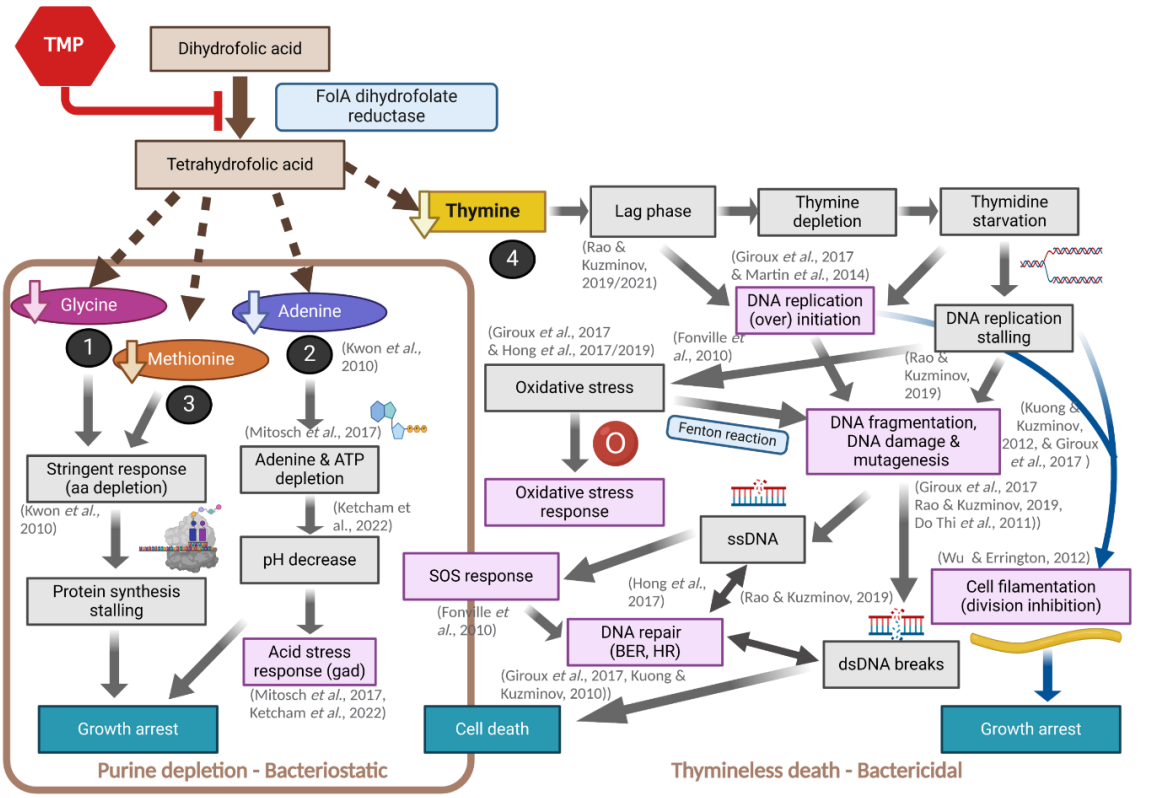


Figure 61 : Understanding of the TLD-associated processes following this study (bottom), as compared to the knowledge from the literature (top). The processes studied here using a bacteriostatic and a bactericidal medium are represented in pink. I confirmed the lag phase observed during TMP treatment but did not confirm the role of endogenous thymine from the capsule. The bacteriostatic and bactericidal processes are not as clearly separated as originally thought. Some cells in a bacteriostatic medium will induce the SOS response and DNA repair processes and die, but the acid stress response is the main pathway induced. In the bactericidal medium, some cells may enter growth arrest, and most of them will induce the SOS response, DNA repair pathways, and superoxide stress response. The filamentation process will also take place, but independently of the SOS response, together with DNA replication overinitiation.

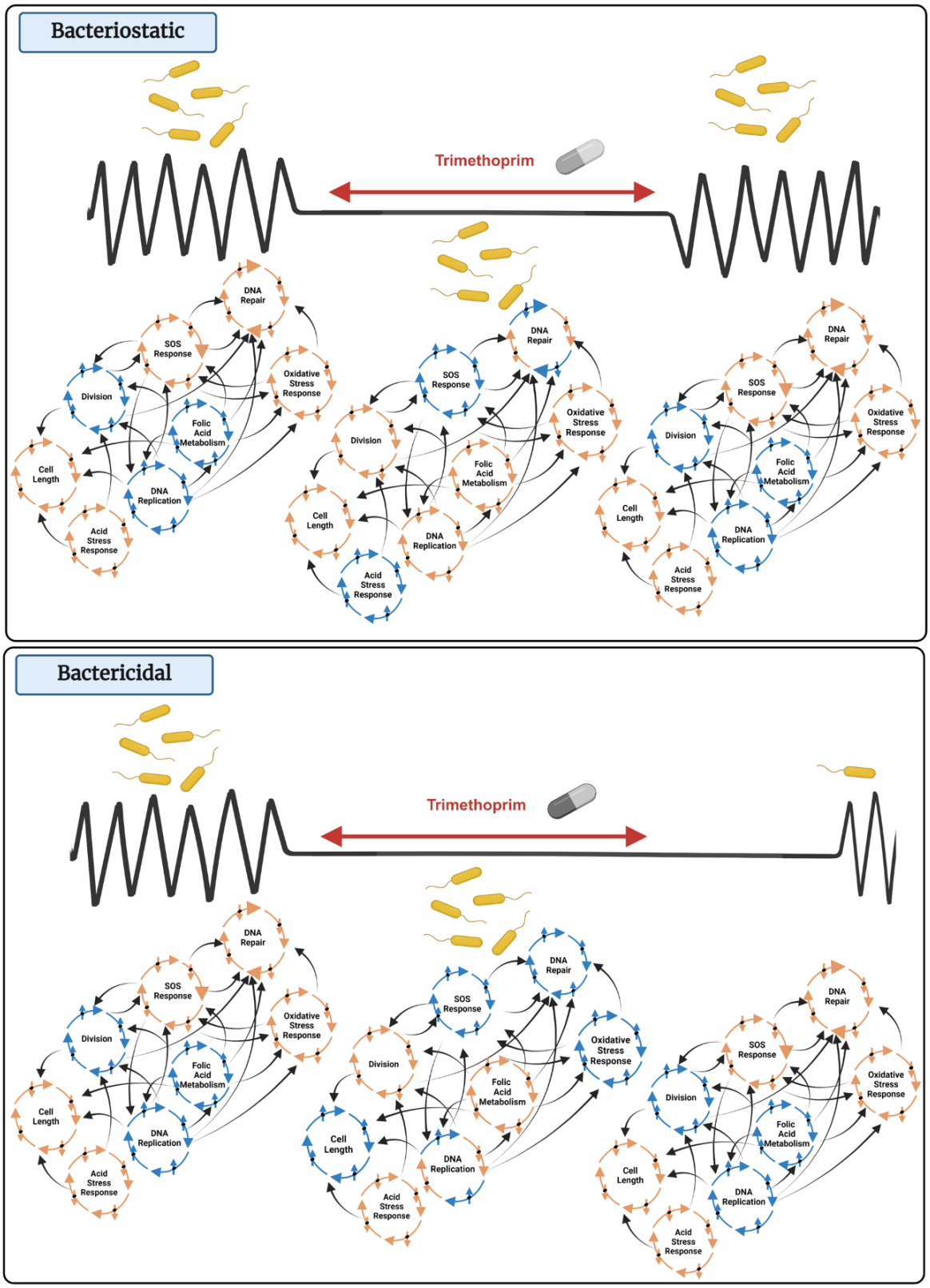


Figure 62 : Hypothetical model of the different states of disorder for the TMP-treated cells, based on the findings in this study. At first, the cells are growing normally (black sawtooth line), in a regulated and stable state including a lot of interplay in the metabolism. For bacteriostatic conditions, cells will enter a more disordered state, with some pathways being activated (blue) and others repressed (orange) during TMP

treatment (red arrow). When the treatment is removed, the cells will return to a regulated state. By contrast, in a bactericidal medium, the cells move from a regulated state to a highly disordered state, with a lot of changes in the interconnected pathways. Consequently, after removal of treatment, not many cells will be able to return to a normal regulated state. This would leave most of the remainder cells as possibly dead or in a state of persistence.

CHAPTER 6 : CHARACTERISATION OF BACTERIAL RESPONSES TO A TYPE SIX SECRETION SYSTEM NUCLEASE EFFECTOR

1. INTRODUCTION

Interactions between bacteria and their environment or neighbouring bacteria are central to niche colonisation and bacterial survival. These interactions are facilitated by the export of proteins or DNA into cells or extracellular space, via nano machineries called secretion systems (Costa et al., 2015) The type six secretion system (T6SS), is a versatile apparatus composed of 13 core proteins, including a membrane-spanning complex, a baseplate and a tail complex (Bingle et al., 2008) (Fig.63). The tail complex features an outer sheath and an inner tube propelled by the contraction of the sheath and is equipped at the tip with a spike complex functioning as a sharp puncturing device (Boyer et al., 2009). It is present in 25% of Gram-negative bacteria (Ho et al., 2014) and allows bacteria to transport effectors from the bacterial cytoplasm into the extracellular environment or into a target eukaryotic or prokaryotic cells (Costa et al., 2015). Effectors have toxic activities against a range of bacterial components such as cell wall, membrane, or nucleic acid, causing cell death or growth inhibition (Alcoforado Diniz et al., 2015) Nucleic acid-damaging effectors are called nucleases. They can target and damage DNA or RNA and are an abundant category of effectors that can cause cell death (Jana & Salomon, 2019). T6SS effector genes are usually adjacent to a gene encoding an immunity protein for self-protection. Immunity proteins bind to and inhibit the activity of their cognate effector (Benz & Meinhart, 2014).

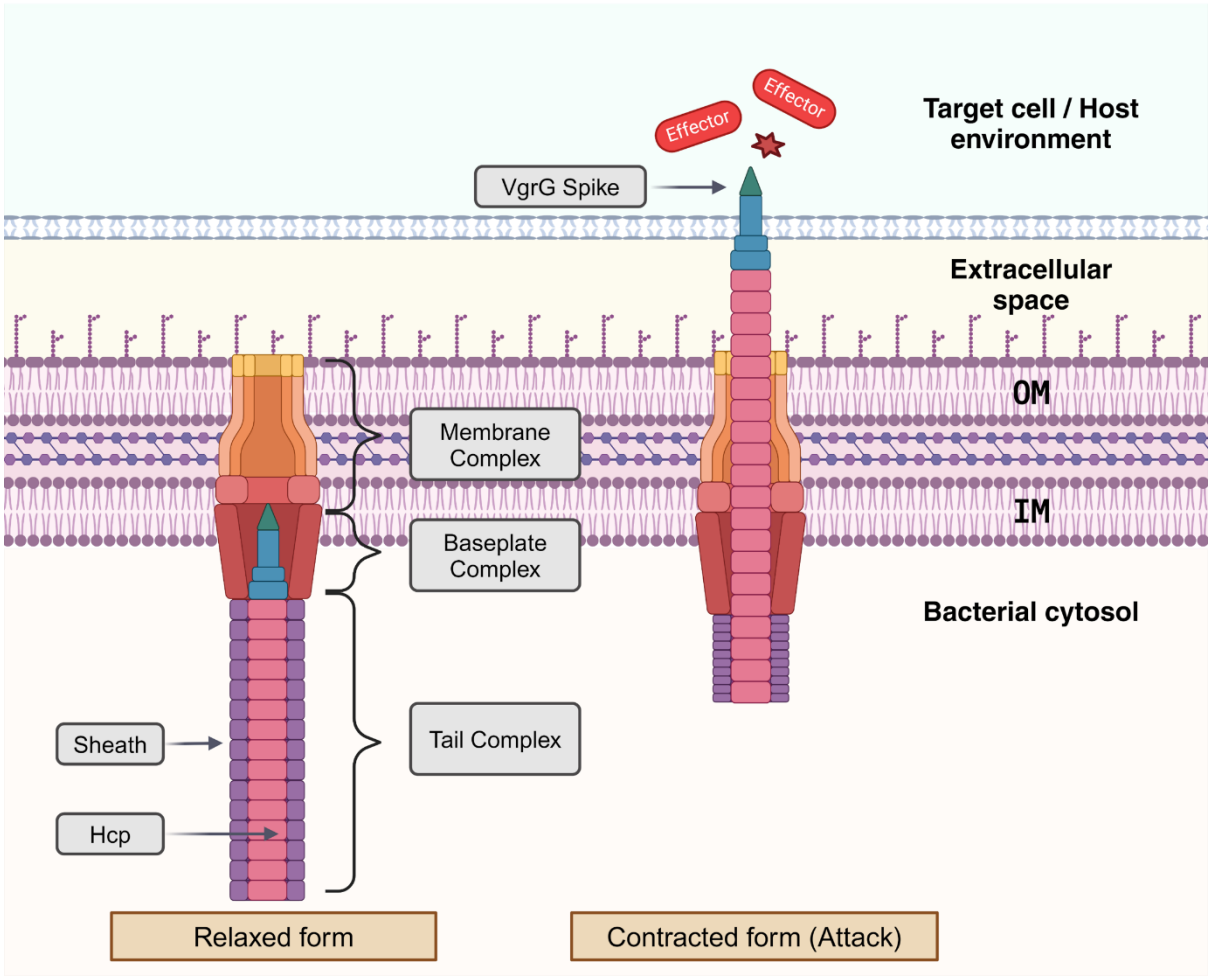


Figure 63 : Representation of the T6SS in a gram-negative bacterium. The figure represents the two possible forms of the apparatus, relaxed, or contracted during an attack. The apparatus can puncture a prey cell during an attack and release toxic effectors.

A lot of knowledge has arisen about the genetics and structural aspects of the T6SS and its associated effectors and cognate immunities. However, little emphasis has been placed on the responses of the target cells and their survival strategies in the face of T6SS attack. T6SS effectors with DNAse activity are known to cause DNA damage that leads to induction of SOS response in prey cells. This has been described for a DNAse effector with a Polymorphic Nuclease effector domain in *Vibrio*, through increase in the expression level of SOS response reporter genes (Jana et al., 2019). Another DNAse named Tse7 containing a Tox-GHH2 domain in *P. aeruginosa* has been shown to cause an increase in DNA degradation accompanied by an induction of SOS response

measured by flow cytometry, and growth arrest (Pissaridou et al., 2018). Another example is an effector in *Yersinia pseudotuberculosis* which has been shown to cause filamentation and growth arrest in prey cells by interacting directly with FtsZ, involved in cell division (Wang et al., 2022). It has also been suggested that the lethal action of T6SS system from *Vibrio*, particularly via lysozyme-like enzyme targeting cell wall, is associated with an increase in ROS, and bacterial SoxS induction, suggesting superoxide stress (Dong et al., 2015). Finally, protective mechanisms against T6SS attack have been described at the population level, such as the production of extracellular polymeric substances providing collective protection in *E. coli* (Granato et al., 2023). Individual bacterial cells can also protect themselves against T6SS attack by inducing the envelope stress response (Hersch et al., 2020).

Most studies to date on T6SS effectors have examined their effects using population-based assays and focussed almost exclusively on identification of the target of the effectors. In this study, I chose to focus on the target bacterial cell responses to T6SS effectors expressed intracellularly. I used *Escherichia coli* as a model organism, carrying a plasmid-encoded T6SS effector with or without its cognate immunity. This allowed dissociation of the potential effects related to the puncture of the cell by the T6SS from the action of the effector itself. I used microscopy combined with microfluidic growth chambers as described in Chapters 4 and 5. This allowed observation of cells over prolonged periods with minimal perturbation, while maintaining constant and defined growth conditions. It enabled investigation in real time of the growth dynamics and responses involved in the action of the T6SS effector in a model organism. Thus, the objective of this work was to explore stress responses displayed by cells in detail including the temporality and potential heterogeneity within the population. For that, I specifically focussed on a DNAse effector from the commensal bacterium *Neisseria cinerea*. The effector was the Nte3-predicted endonuclease, and I tested it either by itself or expressed along with its cognate immunity protein, Nti3 (Custodio et al., 2021). This effector was

characterised by sequencing and conserved domains were identified. Indeed, Nte3 is composed of a conserved Rhs (rearrangement hotspot) repeat-containing domain and associated with polymorphic toxin (Busby et al., 2013). It belongs to the HNH/Endo VII (His-Me finger) nuclease fold family with a conserved LHH motif, predicted to be associated with DNAses (D. Zhang et al., 2012). HNH nucleases are endonucleases with a common DNA-binding and cleavage motif, and a catalytic mechanism for hydrolyzing nucleic acids (C. C. Wu et al., 2020). On the other hand, the immunity was predicted by homology and proximity and could act by binding to or directly inactivating the toxin (Kennedy & Comstock, 2024). I aimed to gain an understanding of the intracellular killing and protective mechanisms triggered by the presence of a T6SS nuclease effector in individual prey cells and observed a very different mode of action than for the antibiotic TMP.

2. RESULTS

2.1. T6SS Effector's Impact on Bacteria at the Population Level

I started my study of the T6SS effector targeting DNA by assessing the population-level action in *Escherichia coli* AB1157 used here as a model organism. In this project, I focused my efforts on the Nte3 nuclease, expressed by a pBAD33 derivative plasmid with arabinose-inducible expression (Guzman et al., 1995). The cognate Nte3 immunity could also be expressed on a similar plasmid as part of an operon with the Nte3 effector (Fig.64). Since the expression from this plasmid is repressed by glucose and induced by arabinose, I utilised a minimal M9 medium with glycerol instead of glucose throughout my experiments. I tested a range of concentrations of arabinose as inducer (0.8%, 0.05% and 0.002%), and 0.8% glucose as a control for repression of expression.

Firstly, I used a colony counting assay to study cell survival at the population level when the T6SS effector was produced intracellularly, bypassing delivery by a predator cell into the acting prey, *E. coli*.

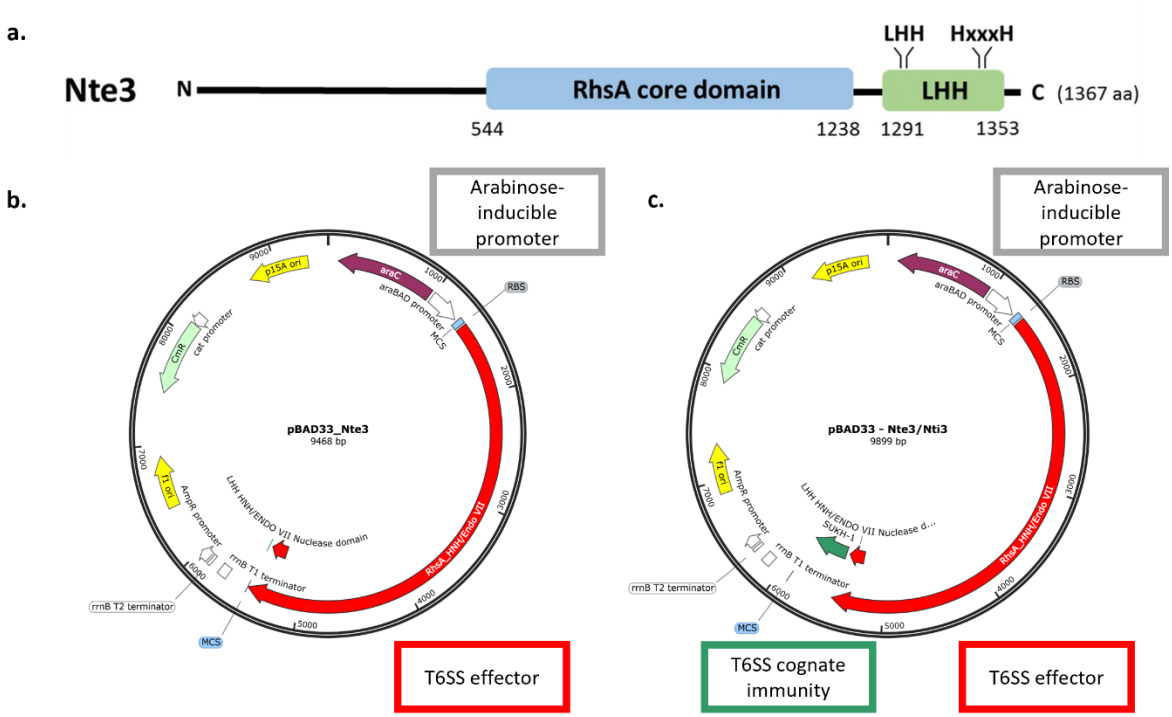


Figure 64 : Nte3 and pBAD33 plasmids used in the study. a) Domain map for the Nte3 effector, adapted from Custodio et al., 2021. *b) Plasmid map for Nte3 effector only. c) Plasmid map for the Nte3/Nti3 effector/immunity pair. The pBAD33 plasmid contained an araC inducer gene, an araBAD promotor, and an operon with either the Nte3 effector only or the Nte3/Nti3 effector/immunity pair.*

I tested both the survival of the effector alone and the effector/immunity pair by using spot survival assays. For that I induced Nte3 nuclease expression in cells in liquid cultures of M9 glycerol for 3 h before plating them without any more induction (Fig.65). At the highest arabinose concentration tested (0.8%), I observed a lot of killing by the induced effector with a relative survival approximately 2-fold lower compared to the strain expressing the effector/immunity pair or the repressed effector grown in the presence of glucose. The lowest concentration of arabinose tested (0.002%) allowed for high survival of cells with a decrease of less than 1-fold compared to glucose-repressed cells, suggesting subtle effects at the population level. The effector/immunity pair did

not display much change in survival between repressed and induced conditions indicating that the immunity protects cells from the toxin. Thus, I opted for the lowest concentration of arabinose 0.002%, for further experiments, ensuring that some cells would survive and could be followed in microfluidics studies.

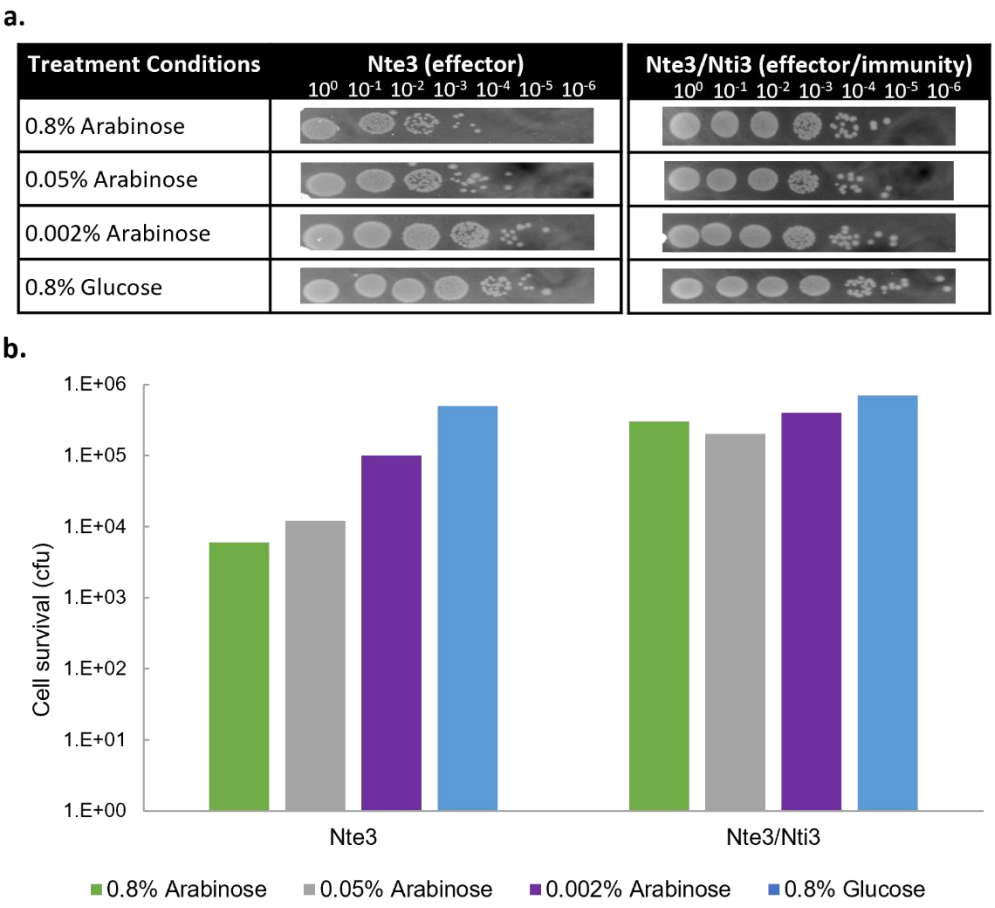


Figure 65 : Spot survival assays for T6SS effector Nte3 only (left) or with immunity (right) in M9 glycerol minimal medium. I carried out spot survival assays, using serial dilutions of cells after 3 h of induction with 0.8% glucose to repress or 0.8, 0.05 and 0.002% arabinose to induce effector expression. b) Proportion of cells at each condition, determined from the colony counts of the cells repressed with 0.8% glucose for a single repeat for each condition. Panel a) shows representative images for the wild-type strain at different conditions.

To assess the protein expression level and dynamics of the pBAD promoter under arabinose induction, I engineered a pBAD33 plasmid containing msCFP3 as a fluorescent reporter, without the effector. I used the strain in microfluidic experiments and investigated the average msCFP3

fluorescence intensity and its dynamics after arabinose induction (Fig.66). I observed a rapid induction after 0.002% arabinose was added to the medium. Fluorescence increased gradually over time but displayed a high level of cell-to-cell heterogeneity. This suggests heterogeneity of induction between the cells, with some cells that are not induced at all. Overall, considering the maturation time of the CFP protein, of up to 6.4 min (Balleza et al., 2018), it appears that the plasmid is rapidly induced after addition of arabinose, and the response gets stronger over time with continued induction. This suggests that the system should reflect bacterial responses to a T6SS effector in most cells. However, this experiment also revealed that cells experience variable timing and magnitude of expression, which would need to be considered when interpreting potentially heterogeneous responses and cellular states.

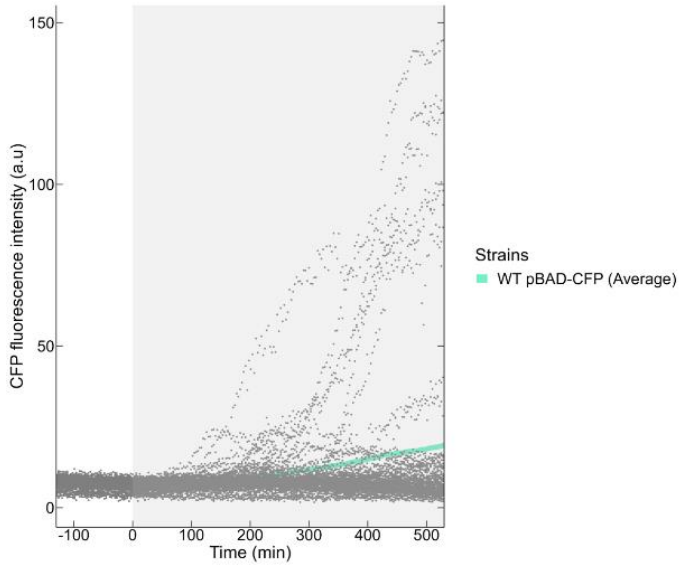


Figure 66 : pBAD-CFP fluorescence dynamics observed in cells after continuous induction with 0.002% arabinose from timepoint 0, in M9 glycerol medium. The figure includes the average fluorescence values (cyan) observed in 500-1000 cells. The grey traces correspond to representative cells from the experiment.

2.2. T6SS Effector's Impact on Cell Viability, Growth and Size Dynamics

With knowledge acquired from bulk population assays, I optimized the microfluidics experiments and used 0.002% arabinose to induce expression of Nte3. The technique and engineered *E. coli* used were as described in Chapters 4 and 5. I engineered the *E. coli* cells to carry pBAD33 encoding the T6SS nuclease effector with or without its immunity protein. This was to gain insights into the effects of the T6SS nuclease effector expressed intracellularly, providing temporal information, and exploring heterogeneity in population. I used the previously described methods of analysis to determine cell states, assigning ID to cells and tracking them over time to assess different parameters including cell viability and growth dynamics. I assessed these parameters in cells with continuous induction with 0.002% arabinose with either the Nte3 effector only or the Nte3/Nti3 effector/immunity pair; I also observed cells without induction.

Firstly, I assessed how the Nte3 effector affected cell survival and growth in the microfluidics growth chambers (Fig.67). The remaining cell count decreased by 15% over 500 min when the nuclease was by itself or with its cognate immunity, with almost no difference between the two conditions. The count of remaining cells with Nte3 effector without induction also decreased, which could be due to leaky expression of the plasmid, as it was not repressed by glucose in this case. In contrast, cells with the effector only and arabinose induction had a steep decrease in actively growing cells shortly after induction, down to less than 20% of cells by 300 min, compared to around 75% for other conditions. The decrease in actively growing cells before the start of arabinose induction observed in cells could again be due to leaky expression of the plasmid in the absence of glucose. These results suggest that the immunity protein abolishes the effects of the nuclease on bacterial growth, with little protection effect from lysis. Additionally, for cells with the effector/immunity pair, some of the lysis, at similar level to effector only, could be due to an imbalance between the proteins in the artificially induced system, whereby not enough immunity proteins are present.

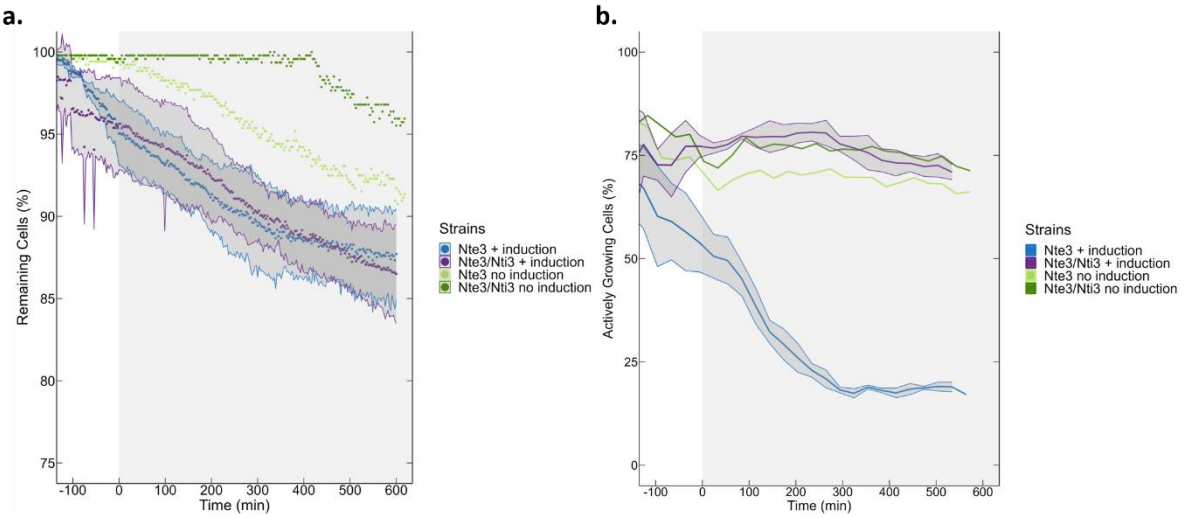


Figure 67 : Remaining and actively growing cells with continuous 0.002% arabinose induction or without induction of the Nte3 effector with/without Nti3 immunity from timepoint 0 during microfluidic experiments in M9 glycerol. a) Percentage of remaining cells per time. b) Percentage of actively growing cells per time. The curves represent mean values obtained from 500-1000 cells per experiment for cells without induction, and three experiments for cells with induction, including standard deviation (shaded area).

I then used the previously described parameters (Chapter 4), to define the states of each cell at different timepoints during microfluidics experiments (200 min, 500 min, 600 min). This allowed the categorisation of cells into five subpopulations, namely “healthy”, “lysed”, “filamenting”, “growth arrest”, and “recovered” (Fig.68). There were some striking differences between the profiles observed for cells carrying the effector only compared to the effector/immunity pair. For the effector only cells, an overwhelming majority of cells promptly entered into a growth arrest state, even from 200min. In contrast, the states were evenly distributed for the effector/immunity pair, with a large proportion of cells still healthy at the end of experiments. I also observed a high proportion of healthy cells for the cells without induction carrying either the effector only or the effector/immunity pair (Fig.69). This indicates that the immunity confers a high level of protection to the cells.

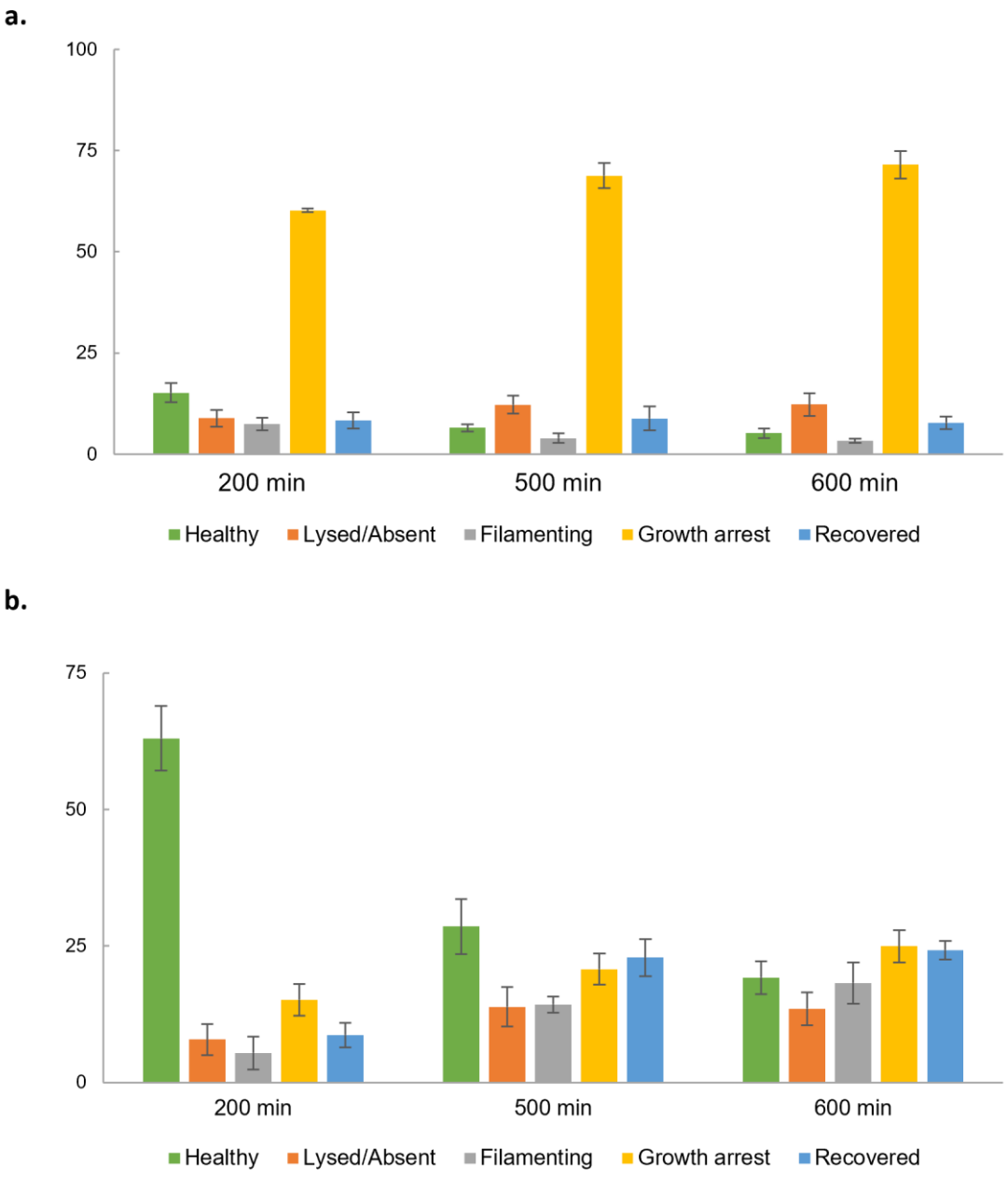


Figure 68 : Cell states distribution for 0.002% arabinose induction at different timepoints M9 glycerol for a) Nte3 effector and b) Nte3/Nti3 effector/immunity pair. The different colours represent the possible states: healthy, lysed, filamenting, growth arrest and recovered cells. The values for each cell state are an average of three experiments, with standard deviation.

The control cells carrying pBAD-CFP had similar remaining and actively growing cell dynamics to the cells carrying the effector/immunity pair. I did observe that the growing cells experienced a decrease after 300 min, which was not observed in the effector/immunity cells (Fig.69). This

difference was reflected by a smaller proportion of cells in healthy state as compared to cells without induction. However, the subpopulation profile observed for pBAD-CFP was similar to that observed for the effector/immunity pair. This could be suggestive of a fitness cost of the plasmid itself, as it does not carry an effector. Overall, these results indicate that the T6SS nuclease effector acts largely by arresting cell growth in cells from the start of induction.

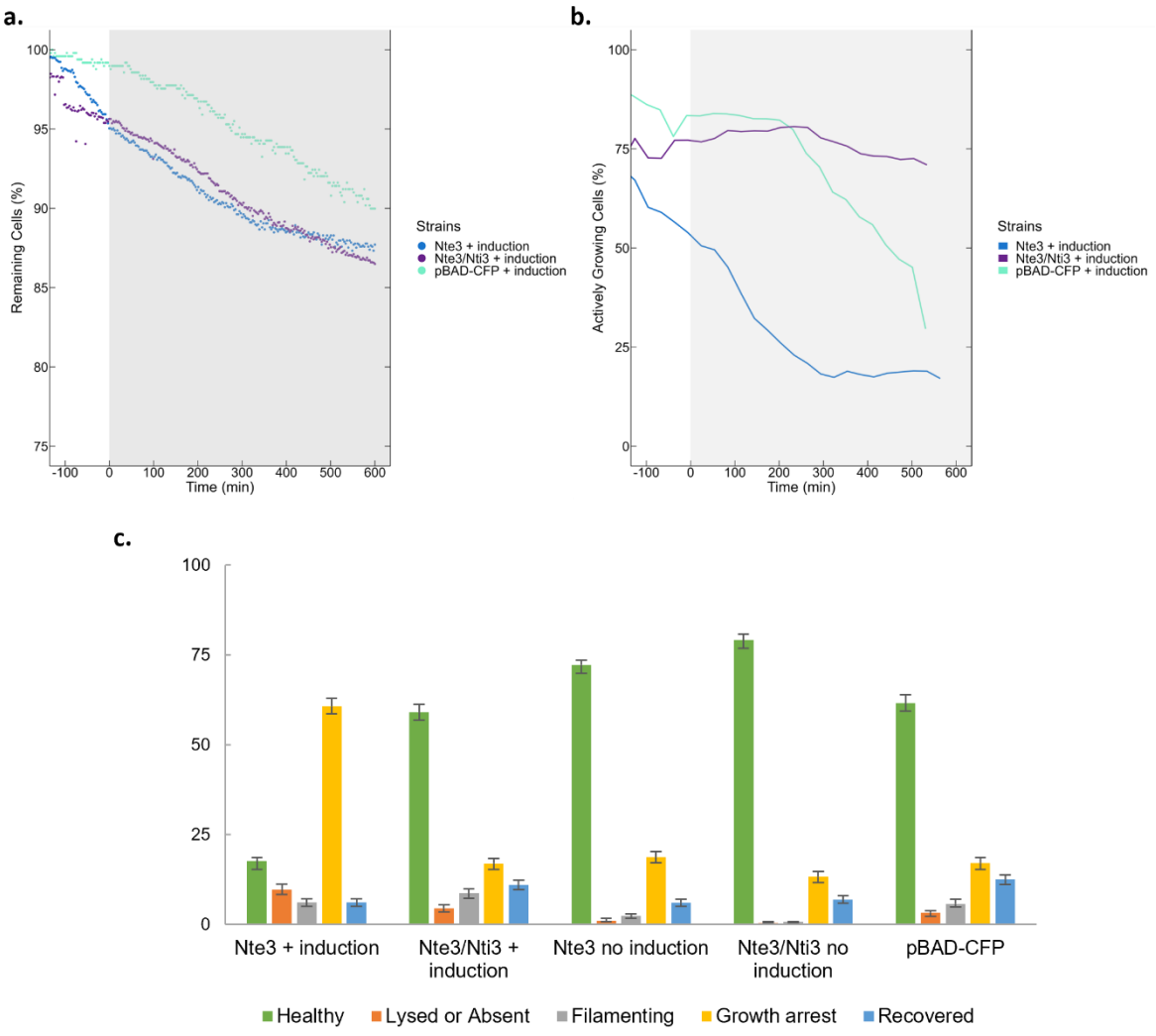


Figure 69 : Remaining and actively growing cells with continuous 0.002% arabinose induction from timepoint 0, including a control strain with pBAD-CFP plasmid in M9 glycerol. a) Percentage of remaining cells per time. b) Percentage of actively growing cells per time. c) Distribution of cell states observed at 200 min. The curves represent mean values obtained from 500-1000 cells per experiment with three repeats for induced cells and include a 95% confidence interval obtained from bootstrapping (1000 repeats).

After confirming the effects of expressing the nuclease by itself, I decided to engineer an inactivated version of Nte3 to assess cell survival in these conditions. For this, I used a plasmid carrying a point mutation in the active site of the Nte3 effector and leading to the H1306A mutation. The histidine change to alanine by site-directed mutagenesis targeted the second H in the LHH motif of the effector. It was bioinformatically and structurally predicted to be involved in activation of a water molecule needed for hydrolysis by the effector, thus affecting its activity (Veronika Bakulova, unpublished, D. Zhang et al., 2011) (Fig.70). I observed that the inactivated mutant led to increased survival of the cells, in terms of proportion of both remaining and actively growing cells over time. The observations for the inactivated mutant were very similar to cells without induction. I also noted that the large majority of cells with the inactivated effector were healthy cells, however, they represented a smaller proportion than for cells without induction. The profile was nonetheless very close to cells without induction and with far fewer growth arrest cells than the WT version of the Nte3. These results suggest that the mutation impairs but does not abolish the growth arrest caused by the effector.

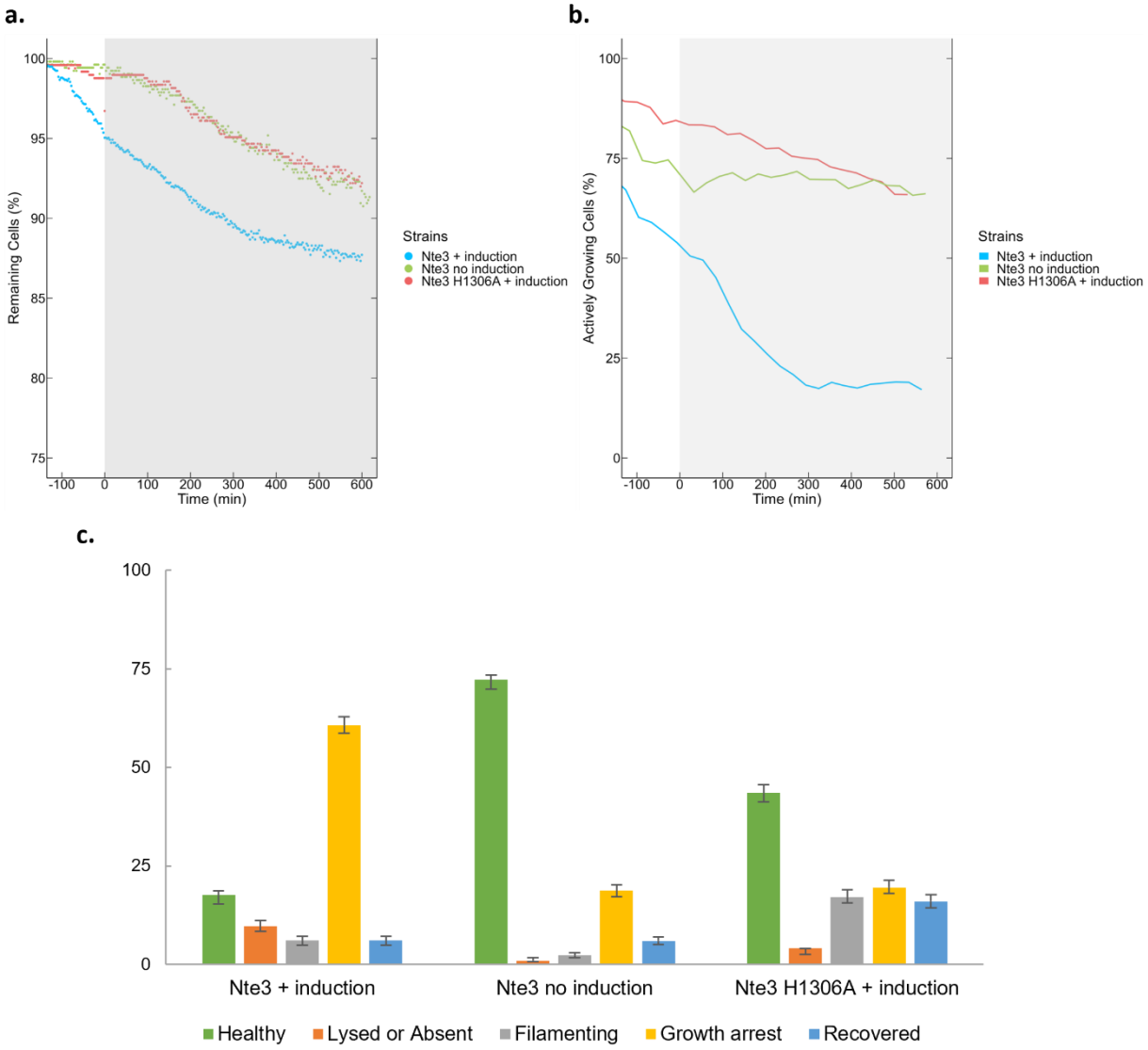


Figure 70 : Remaining and actively growing cells with continuous 0.002% arabinose induction from timepoint 0 for an inactivated version and a WT version of the Nte3 effector with or without induction in M9 glycerol. a) Percentage of remaining cells per time. b) Percentage of actively growing cells per time. c) Distribution of cell states at 200 min. The curves represent mean values obtained from 500-1000 cells per experiment, including a 95% confidence interval obtained from bootstrapping (1000 repeats).

Interestingly, the cell length did not change very much at the population level, irrespective of whether cells were expressing the effector by itself or with its cognate immunity (Fig.71). Since the cells without induction underwent similar changes to cells with effector only and effector/immunity pair, this finding is consistent with leaky expression from the plasmid even in non-inducing conditions. The cell lengths measured were very consistent with little cell-to-cell heterogeneity.

These results also indicate that less than 30% of the cells defined as lysed could have grown too long and exited the growth chambers, suggesting instead that most of the cells in the lysed or absent subpopulation lysed during the experiment.

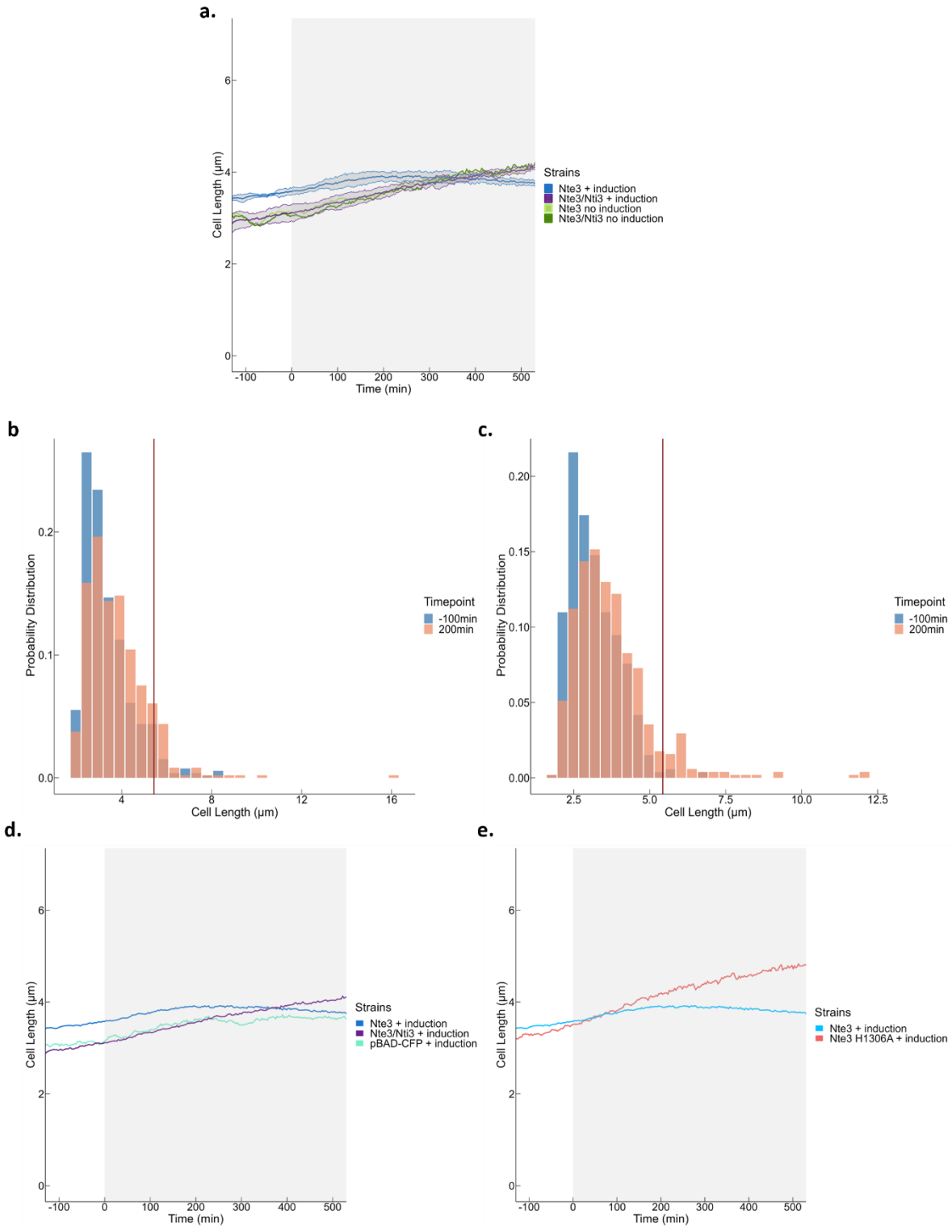


Figure 71 : Cell size dynamics with continuous 0.002% arabinose induction or without induction from timepoint 0 during microfluidic experiments in M9 glycerol. a) Cell length in µm per time at the population level. b) Distribution of cell length observed at 100 min before and 200min after induction for Nte3 effector, or c) for Nte3/Nti3 effector/immunity. d) Cell length in µm per time for induced cells. e) Cell length in µm per time for WT and inactivated Nte3 effector. The curves represent mean values obtained from 500-1000 cells per experiment, and three repeats with standard deviation (shaded area) for cells with induction. For the cell length probability distribution, the data is from a representative WT experiment.

I carried out control experiments with the strain carrying the empty pBAD-CFP and observed as expected that the cells did not filament. Compared to the cells containing the same plasmid with the effector only or effector/immunity pair, I did not observe any differences (Fig.71). Again, this confirms that the cells in the presence of the Nte3 nuclease do not experience dramatic changes in cell morphology indicative of filamentation. I also tested the inactivated version of the effector, containing the H1306A substitution, and observed some small changes in the cell length (Fig.71). These changes did not indicate more cell filamentation but rather pointed to day-to-day experimental variation. Overall, the results suggest that the cells containing a T6SS nuclease effector do not experience dramatic changes in cell length, including filamentation.

2.3. T6SS Effector's Impact on DNA Damage

Due to the known DNA-damaging effect of nuclease effectors, I next decided to investigate whether the induced DNA damage, including DSBs, could lead to mutagenesis. For that, I used the MutL-mYPet reporter in microfluidics experiments, which is known to form foci at sites of mismatch during DNA replication and can be used as a proxy for mutagenesis as described in Chapter 5 (Vincent & Uphoff, 2021). I then calculated the rate of appearance of new foci per cell over time in the presence of the effector only or with the effector/immunity pair. It must be noted that not all mismatches in cells will in turn form mutations, but the mismatch rate can be used to understand mutagenic processes.

I began by investigating cells carrying the effector only or effector/immunity pair in M9 glycerol + 0.002% arabinose. I measured the average mYPet fluorescence intensity first to gauge changes

observed, then the mismatch rate was measured at the population level. For both conditions, I did not observe many changes in mYPet fluorescence intensity or the mismatch rate. In fact, the profiles observed for cells without induction were very similar to cells with induction (Fig.72). Overall, this suggests that the action of the Nte3 effector is not accompanied by mutagenic DNA damage or changes in the mismatch rate.

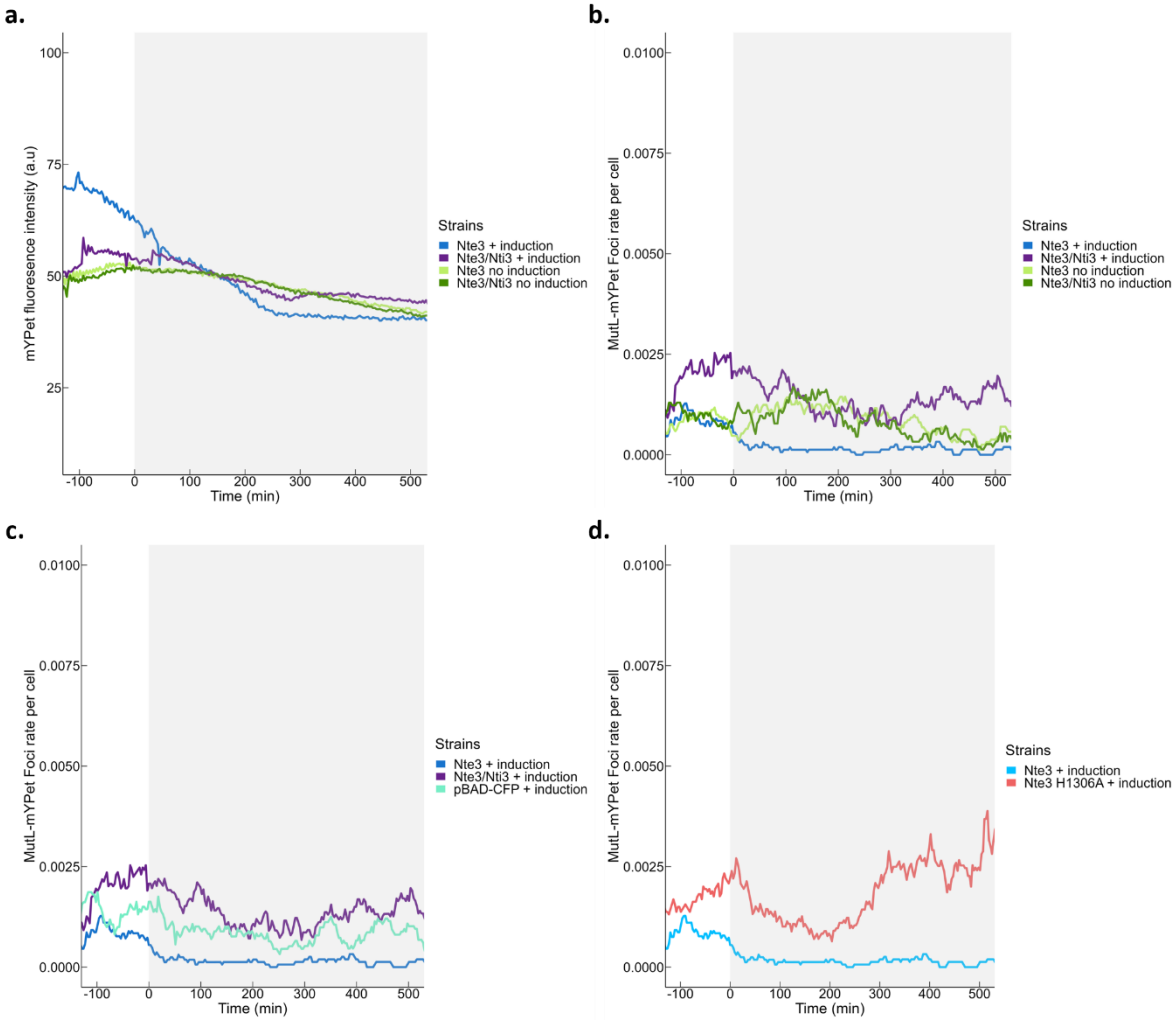


Figure 72 : Mismatch rate with continuous 0.002% arabinose induction or without induction during microfluidic experiments in M9 glycerol. a) mYPet average fluorescence intensity in cells. b) MutL-mYPet foci rate or mismatch rate in cells at the population level. c) MutL-mYPet foci rate for induced cells. d) MutL-mYPet foci rate for WT and inactivated Nte3 effector. The curves represent mean values obtained from a single repeat with 500-1000 cells per experiment.

I then assessed the mismatch rate in cells with pBAD-CFP plasmid, and did not observe any changes over time, which confirms that mutagenesis is not associated with the presence of the plasmid itself (Fig.72c). I also tested the mismatch rate for the inactive version of the effector, and although I did not observe a dramatic change in the values, it appeared that the basal level was higher than for the WT effector (Fig.72d). However, the large noise observed over time, also visible in cells without induction, suggests that these observations are not suggestive of a mutagenic property for the Nte3 effector. Taken together, these results suggest that the Nte3 nuclease effector does not lead to an increase in mismatch rate and thus mutagenicity in prey cells.

Since I did not observe mutagenic properties for the Nte3 effector, I next examined the SOS response, induced by DNA damage in bacterial cells, and known to be triggered by various T6SS effectors (Pissaridou et al., 2018). I analyzed the dynamics of the SOS response in the presence of the T6SS effector nuclease using a *PrecA*-CFP reporter in microfluidic experiments as a proxy for the induction of the SOS response, as described in Chapter 5.

In the Nte3 effector only cells, I observed a large increase in fluorescence intensity for the RecA promotor soon after induction of the effector (Fig.73). For both cells without induction and effector/immunity pair induced cells, I saw a small increase in fluorescence intensity, starting from a lower basal level. However, when normalising the fluorescence by considering the area of cells, the curve became rather flat, suggesting a mostly passive increase unrelated to SOS induction. In induced cells with the effector only, a small increase in SOS induction was observed in a small window between 100 and 300 min suggesting a potentially short-lived response. The observed decrease leading to negative values was likely due to a bleaching of dying cells. The strain carrying the effector/immunity pair did not present a clear increase in expression, suggesting that the SOS

response is not induced in the presence of the immunity protein. I also noticed some fluctuations in all strains without induction, suggestive of an artefact when assessing induction based on fluorescence intensity while cell growth rate changes. This reinforced the need to consider the expression rate rather than absolute fluorescence intensity in this study. At the subpopulation level and at a fixed timepoint of 300 min of arabinose induction, I observed dramatic fluctuations in SOS response (Fig.73c). For the effector only cells, healthy and recovered subpopulations had the highest rate of induction of SOS response, with large cell-to-cell variation seen in healthy cells, whereas for the effector/immunity pair, this was observed particularly for the lysed cells. This could suggest that healthy and recovered cells induce the SOS response more strongly during an attack, whilst cells that lysed, often independently of the T6SS action, also have high rates of expression of the SOS response. Overall, the results indicate that the SOS response is somewhat induced in response to T6SS effectors and presents some important fluctuations at the cell subpopulation level.

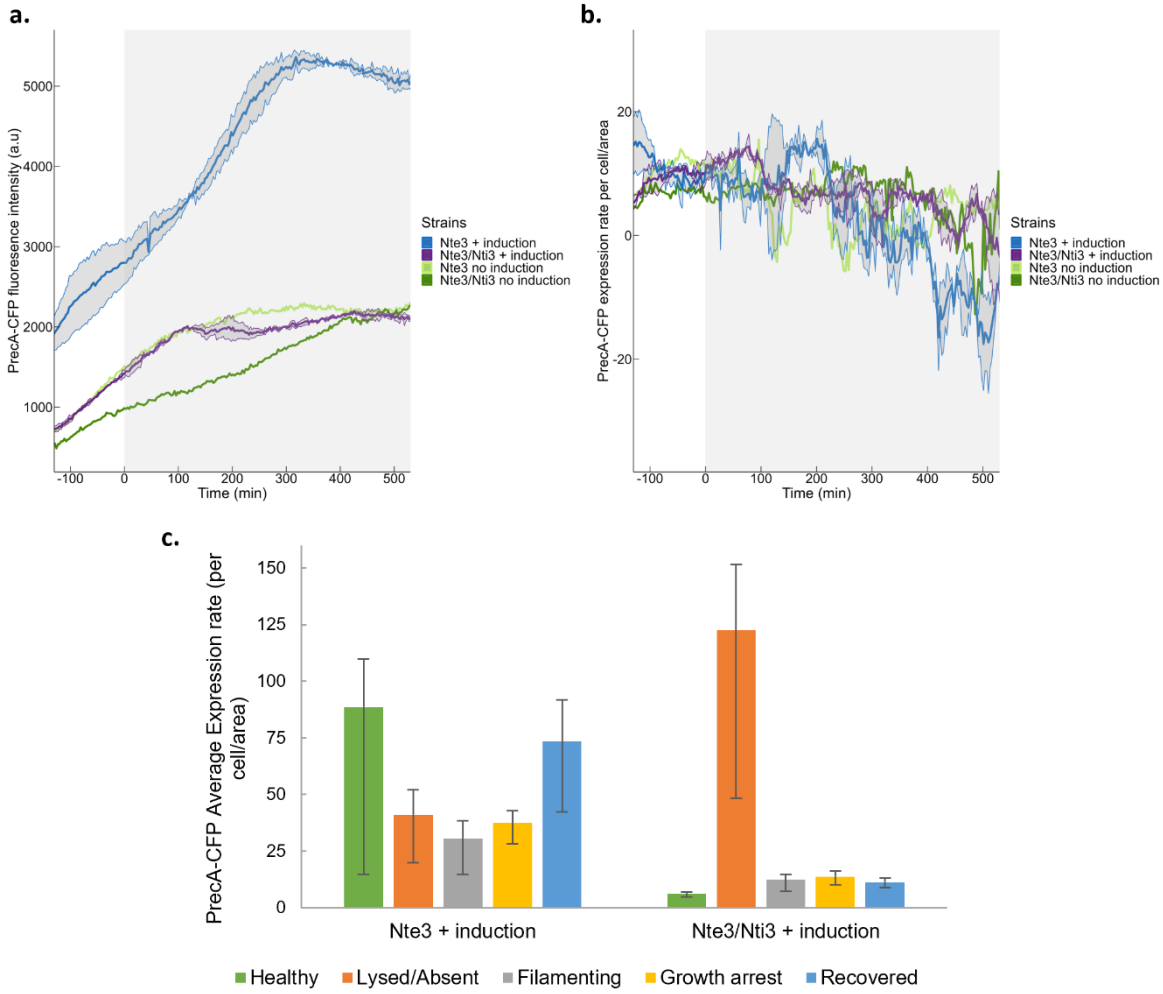


Figure 73 : SOS response (PrecA-CFP) dynamics with continuous 0.002% arabinose induction from timepoint 0 during microfluidic experiments, or without induction in M9 glycerol. a) Average fluorescence intensity levels observed in cells. b) Expression rate computed as the change in fluorescence intensity over time normalised by the cell area of individual cells. c) Average PrecA-CFP expression rate measured at 300 min for the different cell subpopulations. The curves represent mean values obtained from 500-1000 cells per experiment. For a) and b) two repeats were performed for the cells with induction. For c) a single repeat was performed, and the 95% confidence interval is derived from 1000 bootstrapping repeats.

I also tested the cells without arabinose induction, and the cell carrying the inactivated version of the Nte3 effector for SOS response induction and observed similar levels for both these cells at 300 min (Fig.74). The low level of SOS induction observed closely resembled that of cells with the induced effector/immunity pair. Overall, the results suggest that the SOS response could play a role in prey cells, but whether that role is protective or not warrants further studies. For that, I decided

to use a strain deficient for the SOS response, the *lexA3ind*$^-$ mutant, and investigate the link between healthy cells and the SOS response noticed above.

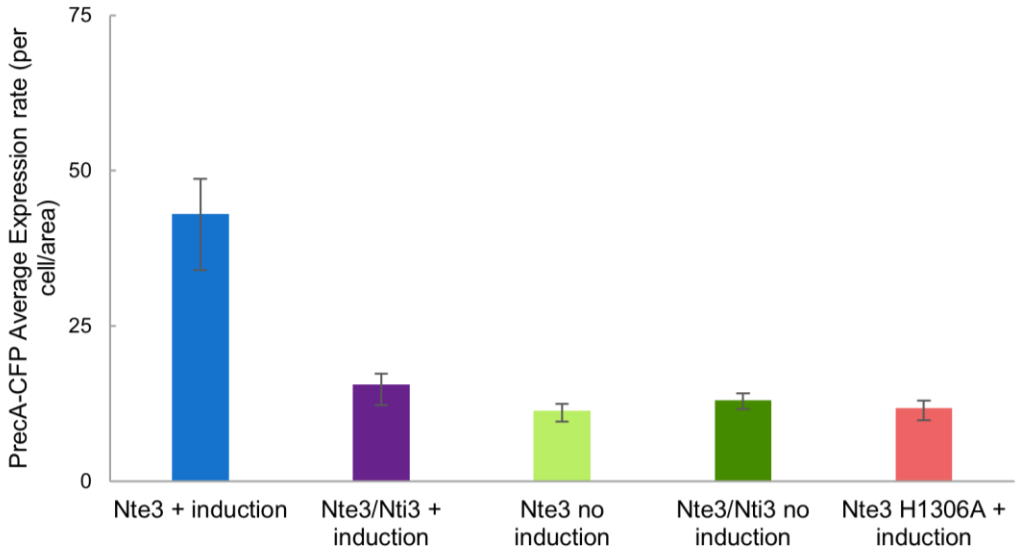


Figure 74 : PrecA-CFP expression rate with or without 0.002% continuous arabinose induction and for the inactivated version of the effector in M9 glycerol at 300 min. The figure represents the average PrecA-CFP expression rate obtained from 500-1000 cells per experiment. The 95% confidence interval is derived from 1000 bootstrapping repeats.

2.4. Role of the SOS response in the Protection Against T6SS Effectors

As mentioned previously, the data suggest that the SOS response could play a role in the reaction to T6SS effectors, particularly the Nte3 nuclease in this case. Some responses have been described as protective for the prey cells in the context of T6SS, often at a population level (Granato et al., 2023). Thus, I explored whether the SOS response could be considered protective against the T6SS Nte3 nuclease. Using microfluidic growth chambers and the reporters described earlier, I compared the WT cell data to that of the SOS-deficient *lexA3ind*$^-$ mutant. These cells, like the WT, carried the Nte3 effector only or the Nte3/Nti3 effector/immunity pair.

Firstly, I tested the induction of the SOS response in the SOS-deficient cells, with the *PrecA*-CFP reporter as a control for deactivation of the system at the 300 min timepoint (Fig.75). As expected, the SOS response in the mutant strain was not induced whether with the effector only or with the effector/immunity pair. This also suggests that any changes observed in WT cells for the expression rate of the RecA reporter would be solely due to SOS response induction.

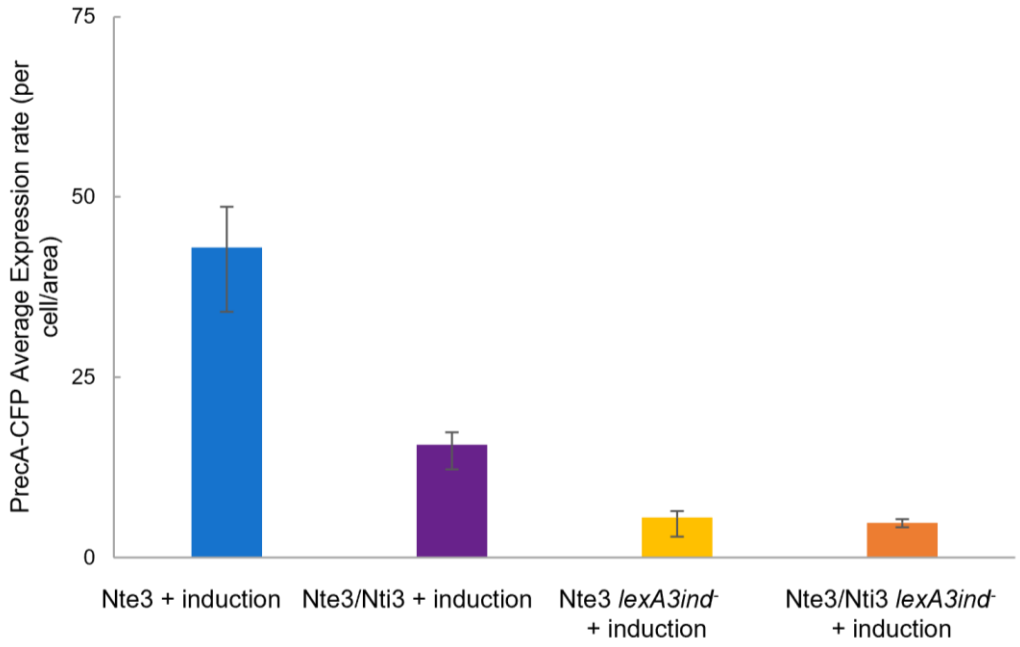


Figure 75 : PrecA-CFP expression rate in WT and lexA3ind- mutant cells with 0.002% continuous arabinose in M9 glycerol at 300 min. The figure represents the average PrecA-CFP expression obtained from 500-1000 cells per experiment. The 95% confidence interval is derived from 1000 bootstrapping repeats.

For the Nte3 effector only, I noted that the proportion of remaining cells in the *lexA3ind*$^-$ mutant strain was slightly higher than for the WT cells but followed similar temporal dynamics (Fig.76). However, the changes for actively growing cells were more dramatic in the *lexA3ind*$^-$ mutant, with an immediate and steeper decline in numbers from the start of arabinose induction. These differences were even more pronounced when comparing the cell states after 200 min of induction. Indeed, I observed few to no healthy cells in the mutant, and a very large majority of growth arrest cells for the WT. Interestingly, the profiles observed for cell survival, growth or even cell

subpopulations were very similar between the mutant and the WT in the presence of the cognate immunity, although I observed a larger decrease in the mutant for actively growing cells (Fig.77). These results indicate that a lack of SOS response results in a state of growth arrest in prey cells subjected to the Nte3 nuclease effector. This suggests that the SOS response, much like the cognate immunity, could be protective in cells likely by delaying entry into the growth-arrested state. Overall, the study of the SOS response suggests that it plays a significant role in protecting prey cells against T6SS nuclease effector.

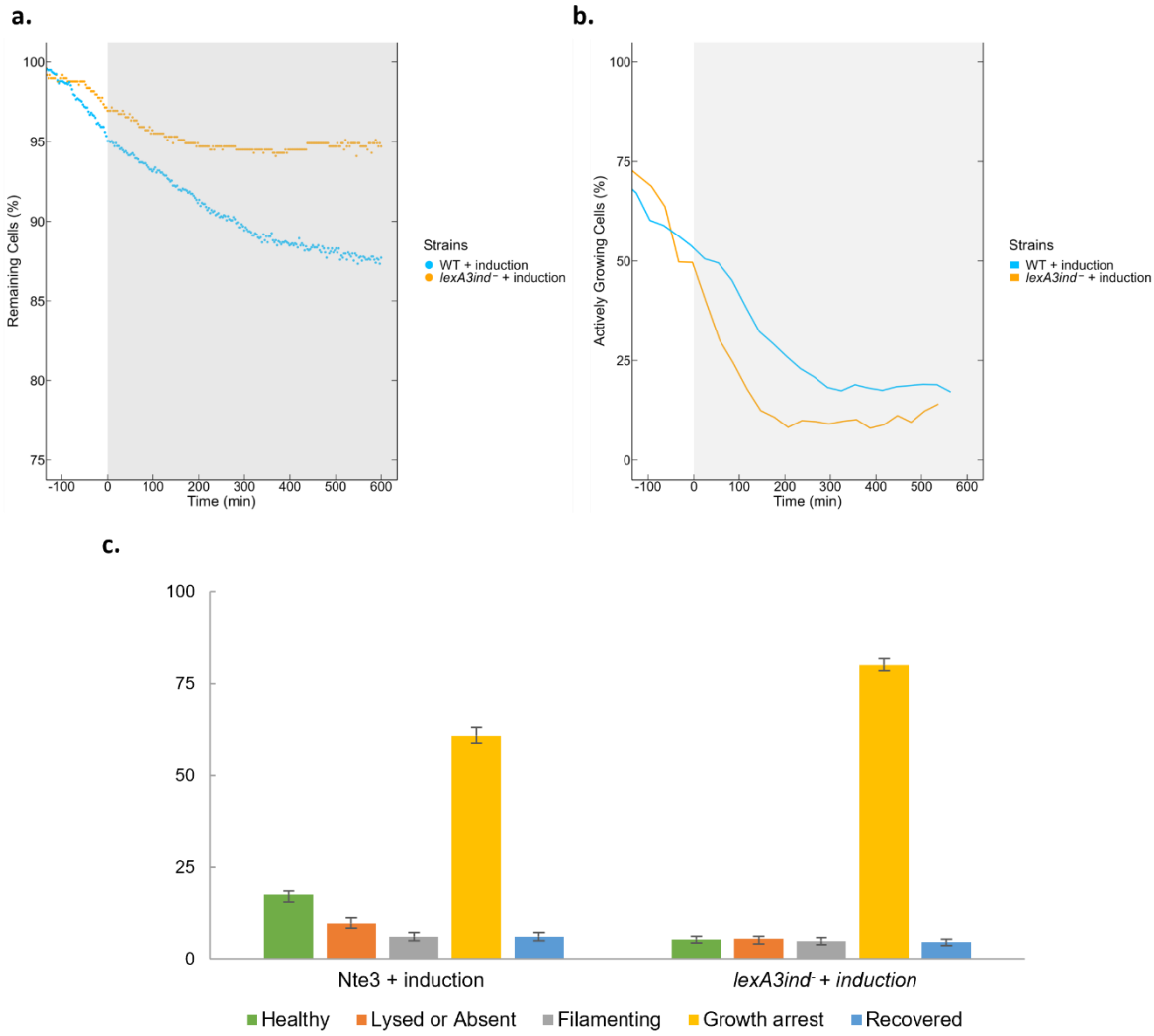


Figure 76 : Remaining and actively growing cells with 0.002% continuous arabinose induction from timepoint 0 in M9 glycerol for WT and lexA3ind- mutant cells with Nte3 effector. a) Percentage of remaining cells per time. b) Percentage of actively growing cells per time. c) Distribution of cell subpopulations at 200 min. The curves represent mean values obtained from 500-1000 cells per experiment, including a 95% confidence interval obtained from bootstrapping (1000 repeats).

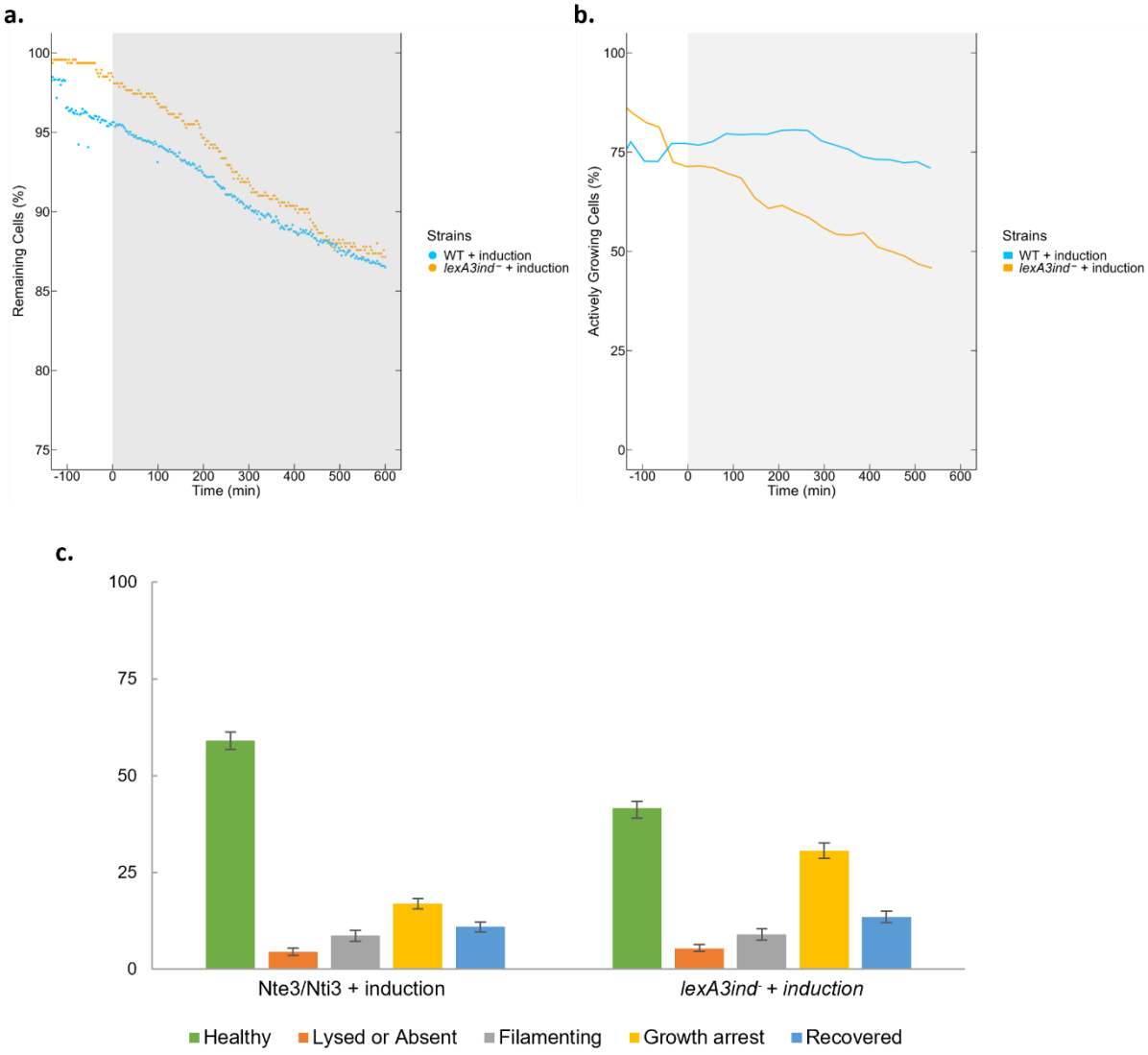


Figure 77 : Remaining and actively growing cells with 0.002% continuous arabinose induction from timepoint 0 in M9 glycerol for WT and lexA3ind- mutant cells with Nte3/Nti3 effector/immunity. a) Percentage of remaining cells per time. b) Percentage of actively growing cells per time. c) Distribution of cell subpopulations at 200 min. The curves represent mean values obtained from 500-1000 cells per experiment, including a 95% confidence interval obtained from bootstrapping (1000 repeats).

2.5. T6SS Effector's Global Effects on Prey Cells

The action of some antibacterial agents can be accompanied by changes in the global gene expression of cells, as I observed with TMP. I thus decided to investigate if it also occurs with the Nte3 effector. I used the cell segmentation marker mKate2, carried by every cell in the experiments,

and constitutively expressed from the promotor P_{RNAI} (Uphoff, 2018). As described in Chapter 5, this was used as a proxy for changes in cellular gene expression for cells containing the effector only or the effector/immunity pair (Fig.78). I measured both the average fluorescence intensity measured per cell and the expression rate or average fluorescence normalised by cell area. For cells with and without arabinose induction, I did not notice any changes in gene expression after induction of the plasmid, suggesting artefacts in the fluorescence intensity instead of true changes in expression. These results suggest that the prey cells do not experience global changes in gene expression.

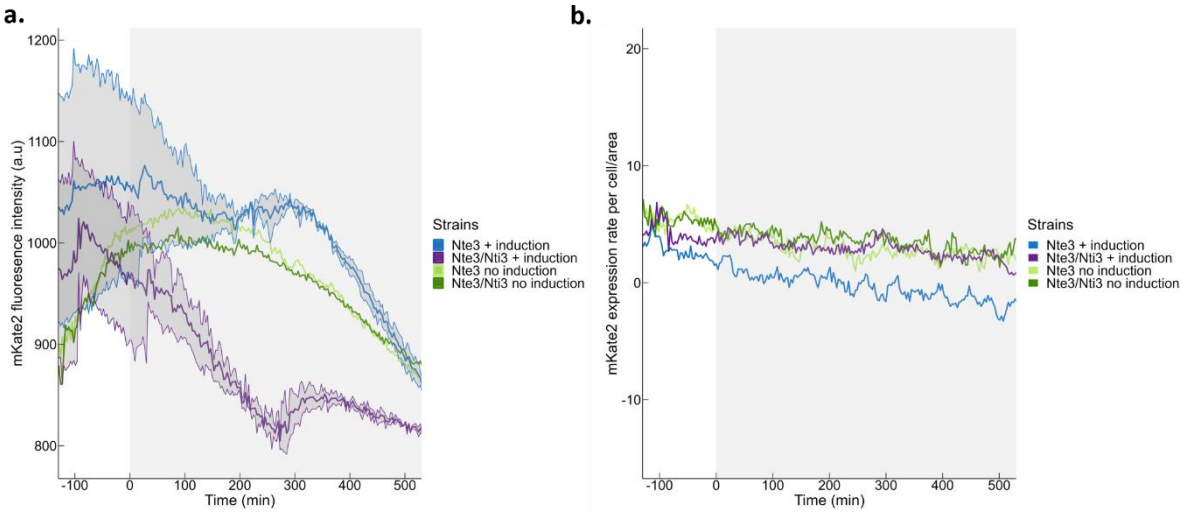


Figure 78 : P_{RNAI}-mKate2 fluorescence dynamics with 0.002% continuous arabinose induction from timepoint 0 during microfluidic experiments or without induction in M9 glycerol. a) Average fluorescence intensity observed in cells. b) Expression rate computed as the change in fluorescence intensity over time normalised by the cell area of individual cells. The curves represent mean values obtained from 500-1000 cells per experiment for cells without induction, and three repeats with standard deviation (shaded area) for cells with induction.

Next, I broadened my investigation into the effects of T6SS effectors in prey cells, by including oxidative stress response. A study has associated an increase in ROS and an induction of the SoxR pathway with the action of T6SS effector (Dong et al., 2015), thus I focussed my efforts on the superoxide pathway and utilised a *PsodA*-CFP reporter. I monitored the expression of the SodA reporter in cells with arabinose induction. This permitted insights into the dynamics of the oxidative

stress response in prey cells using microfluidic device, for strains carrying the Nte3 effector only or the Nte3/Nti3 effector/immunity pair (Fig.79). I measured the expression rate of the SodA reporter and observed, within the first 100 min of induction, an initial small peak for the effector only. For the effector/immunity pair, the oxidative stress response did not experience much change from the basal level. Overall, these results suggest that the effector could cause small level of oxidative stress in prey cells right from the start of induction.

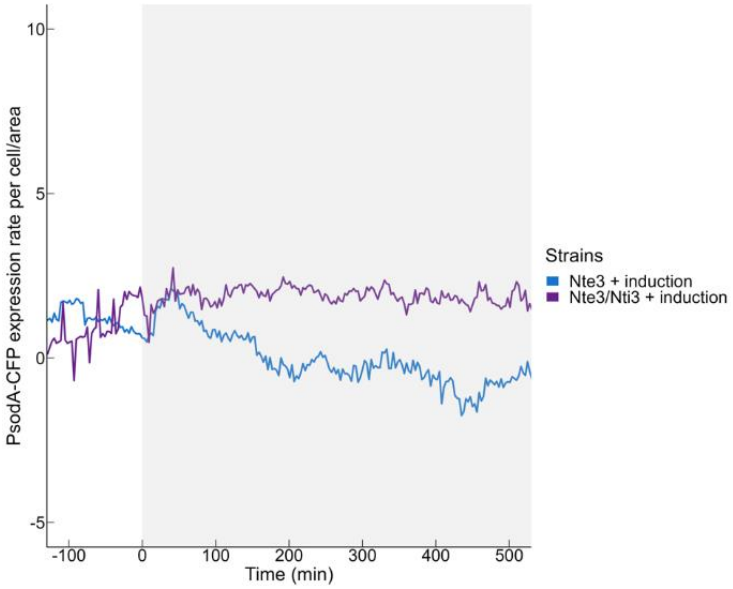


Figure 79 : Oxidative stress response (PsodA-CFP) dynamics with 0.002% continuous arabinose induction from timepoint 0 in M9 glycerol during microfluidic experiments. The figure represents the PsodA-CFP expression rate for Nte3 effector only and Nte3/Nti3 effector/immunity. The values represented are for 500-1000 cells on average per experiment.

3. DISCUSSION

In this chapter, I studied in depth the intracellular impact of a T6SS nuclease effector, Nte3, focusing on the prey cell and its responses. I combined population with single-cell-based assays to decipher the dynamics of the effects associated with the nuclease. The population-based assay gave a first insight into the lethal effects of the effector and allowed optimisation of conditions for the

microfluidics experiments, to further obtain temporal and subpopulation level definition. In a minimal medium, I compared the consequences of effector expression with that of the effector/immunity pair, gathering 500 to 1000 cells per assay, and including subpopulation-level data. I also included a SOS-deficient *lexA3ind*$^{-}$ mutant, along with an inactivated version of the Nte3 effector to ensure the effects observed were due to the activity of the effector. Thus, I investigated phenotypic criteria including survival, and cell size changes in the cells, allowing for cell state assignment. I then explored the impact of the nuclease on DNA, including mutagenesis and the SOS response to DNA damage, and oxidative stress response. I studied the responses' dynamics for both WT and mutant cells in an attempt to identify necessary pathways for the effects of the effector at a population level.

Firstly, I observed that the Nte3 nuclease effector in prey cells precipitates a growth arrest state, which is largely represented at the population level. A lethal effect can also occur in prey cells, although in certain cells, it could be a result of an imbalance in the induction of effector and effector/immunity whereby the concentration of immunity is not sufficient to counteract the effector. The major mode of action for the T6SS effector seems to be cell stasis in the absence of a cognate immunity. Accordingly, the immunity protein was enough to prevent the high level of growth arrest observed in prey cells and diminish the induction of responses to levels without induction. It must be noted that the pBAD33 plasmid used could itself confer a fitness cost, which I observed in the controls as it caused a steady decrease in healthy cells over time. However, since the decrease observed for both pBAD33-CFP and the plasmid containing the immunity were similar, this could be attributed to the plasmid only. This suggests that the immunity protein successfully protects the cells against the Nte3 effector. In the case of cells without induction, it is possible that due to the lack of glucose repression, some leaky expression of the effector or effector/immunity pair could make cells unhealthy and explain the fluctuations observed at the population level.

I assessed the cell size in the prey and did not observe any changes over time. The experiments suggest that the cells remain of very similar and standard sizes throughout the experiments with some limited exceptions of filamentation. In fact, in the context of the T6SS nuclease, it appears that many of the cells cease to grow rather than prevent division. Although I did note some cells growing longer, no dramatic filaments were observed, unlike what I noticed with the antibiotic TMP, and this only seemed to concern a minority of the population. Overall, I demonstrated that filamentation in the presence of the nuclease is not increased, which is consistent with the SOS response not being induced, and thus repressing the SulA inhibitor of division (Fonville et al., 2010). This instead suggests that the cells do not experience cellular replication after activation of the effector, showing failure to divide rather than true filamentation in T6SS prey cells.

It is known that nuclease effectors can damage DNA since they can induce the SOS response in bacteria, and because DSBs and other DNA breaks are produced in their presence (Pissaridou et al., 2018). DNA damage would necessitate repair which could lead to mutagenesis, especially in the context of SOS response via TLS polymerases which are mutagenic (Maslowska et al., 2019). However, the nuclease effector did not appear to have a mutagenic effect, reducing the chances of evolving *de novo* resistance to the effector or any other antibacterial agents, such as antibiotics (Pribis et al., 2019). It must be noted that the mutagenic potential was measured by focusing only on mismatches that arise during DNA replication. However, the analysis did not consider other DNA changes that can lead to mutations. It could also be speculated that the absence of increased DNA replication errors in prey cells is due to the state of growth arrest the cells enter, repressing growth and replication (Bergkessel et al., 2016) and thus the potential for DNA replication errors.

I studied in more depth the SOS response in prey cells in relation to the T6SS nuclease effector, as its role has been suggested in many studies as described above. In the system used, the SOS response seems induced at a lower level than described previously (Jana et al., 2019), but with heterogeneity at the cell level. This could be due to a higher concentration of effector artificially induced in prey cells than would normally be delivered by the T6SS. This was a main caveat for this study, as it could overwhelm the cells and prevent them from inducing a response. Overall, it appears that the prey cells do not induce an SOS response when the effector is induced unless they survive the T6SS effector's attack. This would suggest that upon entry into prey cells, the effector can cause DNA damage that the cells do not have time to respond to if the effector is present at high concentrations. However, if a cell is able to induce an SOS response, which is potentially more likely in the case of lower effector concentration, then it might survive or recover from the attack. Interestingly, using an SOS-deficient strain, I confirmed that the SOS response has an important protective role in T6SS prey cells, shielding them from acute growth arrest. It appears that the SOS response delays growth arrest in prey cells, which likely utilise this time to try and repair DNA damage. I also explored an indicator of global transcriptional responses to identify a trend in expression and did not notice anything suggestive of changes in the prey cells. This suggests that the cells are so rapidly killed following induction of the effector that they do not have time to react at a metabolic level.

Finally, I investigated oxidative stress responses, focussing on the superoxide pathway, and observed a very small increase in the response among prey cells. This effect is exclusively seen when the effector is induced alone and suggests that the T6SS effector overwhelms the cells too rapidly to react. It is known that ROS can directly cause oxidative DNA damage and form 8oxoG lesions. These arise due to the Fenton reaction which converts ROS into highly reactive HO· radicals (Khademian & Imlay, 2021). Thus, it could be postulated that ROS play a role in the DNA damage

causing the SOS response. However, further studies involving SOS-deficient, or superoxide detoxification-deficient strains would be required, with appropriate fluorescent reporters for each. Many other stress responses could also be studied for the impact of T6SS, including the acid stress response which has been suggested as potentially protective in prey cells, and could be the subject of further studies (Kamal et al., 2020).

In conclusion, the effects observed in prey cells in the presence of the T6SS Nte3 nuclease effector suggest that the cells enter a state of profound metabolic disorder when attacked, from which they seem unable to exit (Kaplan *et al.*, 2021). The disruption experienced, unlike what is observed for TMP, does not occur after a prolonged delay. Although I observed that the SOS response can slightly delay the growth arrest and protect cells, this does not give the cells sufficient time to survive. Instead, the cells undergo almost immediate and permanent growth arrest when the effector is induced, they stop growing in length or dividing and very often lyse or enter prolonged growth arrest. This growth inhibition effect has been described for other Rhs proteins, confirming the observations for the Nte3 nuclease (Koskiniemi et al., 2013). Most of the cells were affected almost immediately with little to no cells remaining healthy after 200 min of action, suggesting that the nuclease effector plays a significantly static role for the prey cells. This effector overwhelmed the cells rapidly, making it impossible for the cells to recover from an attack.

CHAPTER 7 : CONCLUSION

1. SUMMARY

Antibacterial agents are critical in the fight against pathogens capable of rendering us very sick. However, for many of the agents currently in use, only the proximal mode of action, or primary target, is known, whilst the ultimate killing mechanisms are often unclear (Baquero & Levin, 2021). In this study, I imaged the bacterial responses to DNA damage caused by antibacterial agents in real time to gain better understanding of their ultimate mechanisms. I also reviewed the literature on the antibiotic trimethoprim, which causes a range of stress phenotypes and has been used for decades without a clear understanding of its mechanism of action. Specifically, I studied and compared the mechanism of action of two antibacterial agents: the antibiotic TMP, and a nuclease effector delivered by the type six secretion system. The antibiotic TMP was used as a complex cell stressor, with effects on cell metabolism and DNA replication, whereas T6SS was a more defined stress, targeting and fragmenting DNA directly. In both cases, I began by testing the antibacterial agents in population-based assays to get a first insight into their effects and particularly the associated cell survival. These experiments did not provide information on cell-to-cell variability or temporal dynamics, as has been seen in the literature. Thus, I delved further with single cell-based assays to investigate the dynamics and cell-to-cell heterogeneity of the known effects of these antibacterial agents on bacterial cells, deciphering their link to growth behaviour and cell survival. This study allowed to further understand the multi-layered mechanisms of action of the agents by addressing multiple pathways in individual cells and their dynamics. For TMP, this was done

specifically in relation to the phases described for its mode of action (Kuong & Kuzminov, 2010; Pritha Rao & Kuzminov, 2020; P. Rao & Kuzminov, 2019).

In the first place, in chapter 4, because of the known impact of medium composition on the action of TMP (Amyes & Smith, 1974; Sangurdekar et al., 2011), I compared two medium supplementations under controlled conditions and in real time to evaluate the differences in bacterial survival. In both cases, I used a minimal medium and a sub-inhibitory concentration of TMP. In one medium, I provided a range of metabolites known to be depleted by TMP, which rendered the antibiotic bactericidal. The medium without metabolites rendered the antibiotic bacteriostatic, precipitating the cells in a state of growth arrest that they could exit after removal of the antibiotic. The differences between the media appeared clearly after removal of treatment, with no possibility for the cells to recover in bactericidal medium. The comparison also revealed that TMP induced growth arrest, cell lysis, and filamentation in both media, with significant heterogeneity among treated cells. A lag phase of 100 min was observed, during which cells did not exhibit clear phenotypic changes to TMP. This was followed by a decrease in actively growing cells and an increase in cell filamentation, particularly in the bactericidal medium. Another important aspect was the large heterogeneity observed in the bactericidal medium. This observation was the first indication that TMP action could be associated with the cells entering a state of profound disorder (Kaplan et al., 2021), and required further testing. Thymidine supplementation was enough to abolish most of the effects of TMP, particularly in a bactericidal medium, confirming the role of thymidine depletion in the mechanism of action of the antibiotic. Mutant analyses indicated that various stress responses can play a role at different points in the treatment timeline. However, no single pathway could explain all the effects of TMP treatment by itself, instead contributing to the overall disorder observed in treated cells.

Next, in Chapter 5, I investigated in more detail key pathways for the action of the antibiotic to determine whether any pathway could be responsible for the mechanism of action of TMP. I employed microfluidics experiments with fluorescent reporters and single-molecule tracking to gather single-cell level data. The analysis revealed an increase in DNA replication sites after the 100 min lag phase, indicating potential DNA replication disruptions or over-initiation due to thymidine depletion, particularly in the bactericidal medium. The presence of TMP led to an accumulation of proteins in the treated cells and a global increase in gene expression. Additionally, mutagenesis increased after the lag phase during continuous treatment, with thymidine depletion playing a crucial role. However, short treatment in a bacteriostatic medium did not induce mutagenesis, which could have implications in the fight against antibiotic resistance by reducing its incidence in response to TMP treatment with that regimen. I also examined oxidative stress responses, observing a gradual accumulation of ROS, particularly superoxide, associated with lower cell survival. The SOS response was induced by TMP, displaying high variability and heterogeneity between cells. Acid stress response was observed in bacteriostatic conditions only due to adenine depletion. Overall, the findings for TMP demonstrated distinct responses in bactericidal and bacteriostatic media. Bactericidal conditions induced stronger stress responses and higher cell-to-cell heterogeneity, directly related to poor outcomes for the cells. This also highlighted the multifaceted and interconnected nature of stress responses in bacterial cells under TMP treatment. These results confirmed that TMP works by causing a state of profound disorder that the cells cannot exit, rather than pointing out a single responsible pathway. This model was suggested to explain antibiotic persistence dynamics (Kaplan et al., 2021) and suggests that in response to acute stress, cells will recover with either fast or slow and heterogenous dynamics depending on the disorder triggered. From the results obtained in this study, the disorder model seems applicable to TMP, with a distinction between a more regulated state in bacteriostatic conditions and a globally disrupted state in bactericidal conditions.

Finally, in Chapter 6, the focus was on understanding the impact of a T6SS nuclease effector, particularly its effects on prey bacterial cells and their responses to identify intracellular killing and protective mechanisms. The study utilized single-cell-based assays to unravel the dynamics associated with the nuclease's action, shown to be lethal in a population-based assay. Comparisons were made in a minimal medium between the effector's impact and that of the effector/immunity pair, including the exploration of phenotypic criteria such as survival and cell size changes. The Nte3 nuclease effector was found to induce a growth arrest state in prey cells, with division being prevented. The immunity protein successfully reduced growth arrest levels, emphasizing its protective function. The nuclease did not exhibit a mutagenic potential, suggesting a reduced risk of *de novo* resistance development, which could offer a benefit for T6SS effectors being explored as potential antibiotics. The SOS response was induced in prey cells upon effector activation and had a protective role for the cells by delaying growth arrest and potentially facilitating DNA damage repair. Overall, the T6SS Nte3 effector was found to induce a rapid disorder causing growth arrest in prey cells, with disruptions occurring more rapidly than for TMP, and cells undergoing immediate and permanent arrest. The two DNA-damaging antibacterial agents appeared to share very little similarity in their mode of action, with vastly different responses and dynamics triggered in bacterial cells. Despite a common resulting state of disorder in the cells, the mechanisms leading to it in both cases were not indicative of unifying pathways leading to death.

2. LIMITATIONS

This study identified a common caveat of the conventional assays designed to quantify gene expression changes in response to antibiotics. In the case of TMP, it clearly appeared that the global

expression of genes was increased during treatment, but that this was not the consequence of a genuine regulatory mechanism but rather a passive accumulation of proteins due to a slowing of cell growth (Angermayr et al., 2022). To account for that, I computed the expression rate of the reporters in addition to their average intensity. However, this led to a decrease in the expression rate and even negative values after several hours of TMP treatment. This was likely due to dying cells, in which photobleaching of the fluorescent proteins could be misconstrued as a decrease in expression and could suggest unreliable data past a certain timepoint due to cell death.

This study, albeit quite comprehensive and including a wide range of key pathways and stress responses for both antibacterial agents, could be extended further. For instance, I carried out non-conclusive preliminary measurements of the stringent response during TMP treatment, particularly relevant in the bacteriostatic conditions as it is activated by nutrient and amino acid starvation (Irving et al., 2021). For the T6SS, the acid stress response could be studied, or further exploration of the oxidative stress response which has been implicated previously (Dong et al., 2015). A more extensive mutant analysis could also be conducted, with deficiencies in key response pathways to understand synergies or interactions leading to cell death.

Although I aimed to ensure uniformity and allow for comparable results in the experiments, I did have to use a few different fluorescent protein reporters, sometimes in the same strains, in order to compare timings within cells, or because of technical issues. Additional controls for the timings of all the proteins and reporters used could be envisaged to ensure precision, due to the potential differences in maturation time for the fluorescent proteins used (Balleza et al., 2018). Another limitation of the experimental design was that the study focussed on individual cells, isolated in growth chambers. This study did not consider the microenvironment of the cells, and how neighbouring cells' behaviour could alter that of the studied cells. It is known that neighbouring bacteria can act as a shield in the context of oxidative stress (Choudhary et al., 2023). Although the

preliminary analysis did not suggest such an effect for the antibacterial agents studied, it could be interesting to extend the study into the behaviour of cells within biofilms. Additionally, the cell state assessment carried out in the study also has a caveat, since it cannot properly relate the possibility of some cells exiting the growth channel. This could potentially affect the overall observations of lysed/absent cells and introduce uncertainties on the precise lethality of the antibacterial agents.

In this study, the analysis of mutagenic potential focused solely on mismatches that form during DNA replication, potentially overlooking other types of DNA lesions such as direct DNA damage caused by ROS which could also lead to mutations if unrepaired (Imlay, 2003). Further studies could involve reporters for other DNA repair pathways. Another avenue that could be explored would be genome-wide sequencing of the healthy cells remaining at the end of experiments, to analyse the mutations directly caused by a sub-inhibitory concentration of TMP. It could also be of interest to extend the study to investigate longer-term effects of antibacterial agents on the bacterial cells, focussing particularly on cell recovery or persistence, and development of resistance. Additionally, the study considered DnaN foci as a proxy for DNA replication sites, but it is known that these foci do not always colocalise with the replication fork (Mäkelä et al., 2021). This suggests that the foci may not report active DNA replication sites and would require further investigations to characterise active replication in TMP-treated cells.

It is worth noting that the study primarily investigated the effects of the antibacterial agents in a minimal medium. Hence, the findings may not fully represent the complexity of interactions in natural environments or host-associated conditions. Particularly, thymidine may be present in the body, and could dampen the effects of TMP. Free thymidine has been described as present in traces

only in the human body, with a concentration around 0.01 μg/ml in blood, and below that in urine (Nottebrock & Then, 1977). However, the precise concentration of exogenous and available thymidine in healthy or UTIs patients, often treated with TMP, would be important to assess in order to evaluate the true impact of the antibiotic in patients. Exploring the dynamics of thymidine availability during TMP treatment could be very relevant physiologically. This would include examining how variations in thymidine levels impact bacterial responses.

The T6SS study has several limitations that should be considered. For that study, artificial plasmid expression of the effector was used to isolate its effect from that of puncture and delivery by the T6SS. However, the use of a plasmid to express the effector and immunity proteins could introduce a fitness cost to the cells, potentially influencing the observed effects. The study only considered one of the many effectors encoded by the attacker cells and could be extended to consider other nucleases from the T6SS or found in nature, such as bacteriophages' endonucleases (Hampton et al., 2020). The T6SS effectors could also be characterized further with biochemical assays to validate their predicted functions. In the experiments, I used *E. coli* as a model prey organism for T6SS, however, the responses could be studied in a natural prey of the attacker *Neisseria cinerea*, to get relevant information in an *in vivo* context.

Finally, in both cases and after an optimisation step, the antibacterial agents were used at a single concentration, and for TMP, this was a sub-inhibitory concentration. Although this was chosen to ensure a sufficient level of cell survival to observe effects of the antibiotic, more concentrations, including inhibitory ones, could be tested for comparison. Particularly, the lethal effects associated with the agents tested could be greater with increasing concentration and could help discriminate between bacteriostatic and bactericidal conditions for TMP even in population-based assays.

Additionally, the strength of the bacterial stress responses could be altered, which could suggest that the damage in the cells fluctuates with the antibacterial agents' concentration. In the case of T6SS, the precise concentration of effector delivered by an attacker cell could be determined in prey cells and used to closer mimic a natural attack. Different periods of plasmid induction for the T6SS effectors could also be tested to assess the effects of a short exposure in prey cells.

3. OUTLOOK

Many studies have been conducted about the antibiotic TMP. However, the studies tend to present with important caveats that prevent getting a full picture of its action. Most studies were carried out only at a population level using genomic or transcriptomic studies and flow cytometry for instance (Giroux et al., 2017; T. V. P. Rao & Kuzminov, 2022; Sangurdekar et al., 2011). Together with others exploring the single cell level (Mitosch et al., 2019), the findings in these studies have raised additional questions and have provided crucial information and hypothesis. Thus, in order to understand what its mechanism of action could reveal, this study approached TMP as an agent that can disrupt more than one pathway and cause large variations between cells. This research suggests that the literature, with conflicting conclusions for a single pathway explaining the mechanism of action of TMP, is correct. Indeed, the underlying mechanism of action for the antibiotic appears to encompass many pathways, that each become disrupted to varying degrees and force the cells into a state of disorder.

This thesis has drawn from the conclusion of a study on ageing dynamics and antibiotic persistence (Kaplan et al., 2021) to suggest a unifying model which could be applicable for a wider range of

antibacterial agents. According to this model, TMP-treated cells experience defects in multiple pathways in parallel, causing a state of disorder leading to growth arrest in cells. For the bacteriostatic medium, removal of treatment after a short period allowed the cells to eventually resume growth. Stress responses facilitated the transition from disorder to an ordered state of cell growth. By contrast, TMP treatment in bactericidal medium threw the cells into an irreversible state of disorder. Further study on the dynamics of recovery and regrowth including different treatment durations could be used to test the model's predictions further. For example, the duration of the growth arrest should scale with the distribution of cell recovery time. This would also help understand the efficacy of treatment and combat antibiotic failure due to cell persistence rather than resistance.

Another aspect revealed in this study is the stark contrast between bacteriostatic and bactericidal outcomes of an antibiotic. This distinction could have broader implications for antibiotics and should be carefully considered in understanding their mechanism of action. This study could also translate into strategies to combine TMP treatment with metabolites to potentiate its effects, or agents to cause further disorder in the cells. Particularly, one conclusion suggesting that short treatment with sub-inhibitory concentration of TMP appeared more lethal for the cells in bactericidal conditions, and was not mutagenic in bacteriostatic medium, could be exploited in the fight against antibacterial resistance.

For the T6SS nuclease effector, this study gave some insight into the disruptions caused in prey cells when the effector is acting intracellularly. Specifically, this study revealed that the SOS response can play a protective role in prey cells against T6SS effectors. A better understanding of the interactions between the effector and its target, in this case DNA, could help gain understanding of

the mode of action of the nuclease. Additionally, it would be interesting to test whether the delivery of the effectors is always lethal to the prey cells, or if stress responses can sometimes help them survive the attack. Specifically, can the induction of the SOS response contribute to DNA damage repair and help cells survive or is it solely a side effect of a lethal dose of DNA damage in prey cells. Monitoring and corelating responses involved in DNA repair with cell states using single cell measurement could help investigate this phenomenon. The insights from this study could be applied to understand the ecological role of T6SS effectors in microbial communities, particularly their influence on interspecies competition. This could also be applied in the context of infections.

Finally, this study, by comparing with similar methods a simple perturbation with the T6SS effector and a more complex one with TMP suggested vastly different routes for killing. For the T6SS, a defined route appeared, with DNA likely becoming fragmented at the first sign of attack by the nuclease, rendering the cells defenceless and undergoing immediate and permanent growth arrest. The cells became overwhelmed and unable to induce stress responses or counter defences, resulting in failure to survive. By contract, in the case of TMP, it seemed that the cells were able to induce stress responses, in fact, all of the responses studied could be induced. This resulted in a state of profound disorder for the cells, overwhelming them to the point of being unable to exit growth arrest. Overall, this study suggests a disorder-based model to explain the mechanism of action of a complex antibacterial agent, as opposed to more streamlined effects for targeted DNA damaging agents. The method developed and used in this study could generally be applicable to study other DNA damaging antibacterial agents and determinants of heterogeneous cell fates during stress.

REFERENCES

Abdizadeh, H., Tamer, Y. T., Acar, O., Toprak, E., Atilgan, A. R., & Atilgan, C. (2017). Increased substrate affinity in the Escherichia coli L28R dihydrofolate reductase mutant causes trimethoprim resistance. *Physical Chemistry Chemical Physics*, *19*(18), 11416–11428. https://doi.org/10.1039/c7cp01458a

Acharya, S., Foster, P. L., Brooks, P., & Fishel, R. (2003). The Coordinated Functions of the E. coli MutS and MutL Proteins in Mismatch Repair of hereditary nonpolyposis colorectal cancer (HNPCC) families (for review see Muller and Fishel, 2002, and references therein). *Molecular Cell*, *12*, 233–246.

Ahmad, S. I., Kirk, S. H., & Eisenstark, A. (1998). Thymine metabolism and thymineless death in prokaryotes and eukaryotes. *Annual Review of Microbiology*, *52*, 591–625. https://doi.org/10.1146/annurev.micro.52.1.591

Alcoforado Diniz, J., Liu, Y. C., & Coulthurst, S. J. (2015). Molecular weaponry: Diverse effectors delivered by the Type VI secretion system. In *Cellular Microbiology* (Vol. 17, Issue 12, pp. 1742–1751). Blackwell Publishing Ltd. https://doi.org/10.1111/cmi.12532

Alqarni, A. M., & Zeidler, M. P. (2020). How does methotrexate work? *Biochemical Society Transactions*, *48*(2), 559–567. https://doi.org/10.1042/BST20190803

AlRabiah, H., Allwood, J. W., Correa, E., Xu, Y., & Goodacre, R. (2018). pH plays a role in the mode of action of trimethoprim on Escherichia coli. *PLoS ONE*, *13*(7), 1–20. https://doi.org/10.1371/journal.pone.0200272

Amyes, S. G., & Smith, J. T. (1974). Trimethoprim action and its analogy with thymine starvation. *Antimicrobial Agents and Chemotherapy*, *5*(2), 169–178. https://doi.org/10.1128/AAC.5.2.169

Angermayr, S. A., Pang, T. Y., Chevereau, G., Mitosch, K., Lercher, M. J., & Bollenbach, T. (2022). Growth-mediated negative feedback shapes quantitative antibiotic response. *Molecular Systems Biology*, *18*(9), 1–19. https://doi.org/10.15252/msb.202110490

Baba, T., Ara, T., Hasegawa, M., Takai, Y., Okumura, Y., Baba, M., Datsenko, K. A., Tomita, M., Wanner, B. L., & Mori, H. (2006). Construction of Escherichia coli K-12 in-frame, single-gene knockout mutants: The Keio collection. *Molecular Systems Biology*, *2*. https://doi.org/10.1038/msb4100050

Baharoglu, Z., Bikard, D., & Mazel, D. (2010). Conjugative DNA transfer induces the bacterial SOS response and promotes antibiotic resistance development through integron activation. *PLoS Genetics*, *6*(10), 1–10. https://doi.org/10.1371/journal.pgen.1001165

Baharoglu, Z., Krin, E., & Mazel, D. (2012). Connecting environment and genome plasticity in the characterization of transformation-induced SOS regulation and carbon catabolite control of the Vibrio cholerae integron integrase. *Journal of Bacteriology*, *194*(7), 1659–1667. https://doi.org/10.1128/JB.05982-11

Baharoglu, Z., & Mazel, D. (2011). Vibrio cholerae Triggers SOS and Mutagenesis in Response to a Wide Range of Antibiotics : a Route towards multiresistance. *ANTIMICROBIAL AGENTS AND CHEMOTHERAPY*, *55*(5), 2438–2441. https://doi.org/10.1128/AAC.01549-10

Baharoglu, Z., & Mazel, D. (2014). SOS, the formidable strategy of bacteria against aggressions. *FEMS Microbiology Reviews*, *38*(6), 1126–1145. https://doi.org/10.1111/1574-6976.12077

Balasubramanian, B., Pogozelski, W. K., & Tullius, T. D. (1998). DNA strand breaking by the hydroxyl radical is governed by the accessible surface areas of the hydrogen atoms of the DNA backbone. *Proceedings of the National Academy of Sciences of the United States of America*, *95*(17), 9738–9743. https://doi.org/10.1073/pnas.95.17.9738

Balleza, E., Kim, J. M., & Cluzel, P. (2018). Systematic characterization of maturation time of fluorescent proteins in living cells. *Nature Methods*, *15*(1), 47–51. https://doi.org/10.1038/nmeth.4509

Banaz, N., Mäkelä, J., & Uphoff, S. (2019). Choosing the right label for single-molecule tracking in live bacteria: Side-by-side comparison of photoactivatable fluorescent protein and Halo tag dyes. *Journal of Physics D: Applied Physics*, *52*(6). https://doi.org/10.1088/1361-6463/aaf255

Baquero, F., & Levin, B. R. (2021). Proximate and ultimate causes of the bactericidal action of antibiotics. *Nature Reviews Microbiology*, *19*(2), 123–132. https://doi.org/10.1038/s41579-020-00443-1

Barner, H. D., & Cohen, S. S. (1954). The induction of thymine synthesis by T2 infection of a thymine requiring mutant of Escherichia coli. *Journal of Bacteriology*, *68*(1), 80–88. https://doi.org/10.1128/jb.68.1.80-88.1954

Battesti, A., Majdalani, N., & Gottesman, S. (2011). The RpoS-Mediated General Stress Response in Escherichia coli. *Annual Review of Microbiology*, *65*(1), 189–213. https://doi.org/10.1146/annurev-micro-090110-102946

Baute, J., & Depicker, A. (2008). Base excision repair and its role in maintaining genome stability. *Critical Reviews in Biochemistry and Molecular Biology*, *43*(4), 239–276. https://doi.org/10.1080/10409230802309905

Baym, M., Lieberman, T. D., Kelsic, E. D., Chait, R., Gross, R., Yelin, I., & Kishony, R. (2016). Spatiotemporal microbial evolution on antibiotic landscapes. *Science*, *353*(6304), 1147–1152. https://doi.org/10.1126/science.aag0822

Beaber, J. W., Hochhut, B., & Waldor, M. K. (2004). SOS response promotes horizontal dissemination of antibiotic resistance genes. *Nature*, *427*(6969), 72–74. https://doi.org/10.1038/nature02241

Beattie, T. R., & Reyes-Lamothe, R. (2015). A replisome's journey through the bacterial chromosome. *Frontiers in Microbiology*, *6*(JUN), 1–12. https://doi.org/10.3389/fmicb.2015.00562

Belenky, P., Ye, J. D., Porter, C. B. M., Cohen, N. R., Lobritz, M. A., Ferrante, T., Jain, S., Korry, B. J., Schwarz, E. G., Walker, G. C., & Collins, J. J. (2015). Bactericidal Antibiotics Induce Toxic Metabolic Perturbations that Lead to Cellular Damage. *Cell Reports*, *13*(5), 968–980. https://doi.org/10.1016/j.celrep.2015.09.059

Bennett, R. J., Dunderdale, H. J., & West, S. C. (1993). Resolution of holliday junctions by RuvC resolvase: Cleavage specificity and DNA distortion. *Cell*, *74*(6), 1021–1031. https://doi.org/10.1016/0092-8674(93)90724-5

Benz, J., & Meinhart, A. (2014). Antibacterial effector/immunity systems: It's just the tip of the iceberg. *Current Opinion in Microbiology*, *17*(1), 1–10. https://doi.org/10.1016/j.mib.2013.11.002

Bergkessel, M., Basta, D. W., & Newman, D. K. (2016). The physiology of growth arrest: Uniting molecular and environmental microbiology. In *Nature Reviews Microbiology* (Vol. 14, Issue 9, pp. 549–562). Nature Publishing Group. https://doi.org/10.1038/nrmicro.2016.107

Bermingham, A., & Derrick, J. P. (2002). The folic acid biosynthesis pathway in bacteria: Evaluation of potential for antibacterial drug discovery. *BioEssays*, *24*(7), 637–648. https://doi.org/10.1002/bies.10114

Bernard, R., Marquis, K. A., & Rudner, D. Z. (2010). Nucleoid occlusion prevents cell division during replication fork arrest in Bacillus subtilis. *Molecular Microbiology*, *78*(4), 866–882. https://doi.org/10.1111/j.1365-2958.2010.07369.x

Bi, E., & Lutkenhaus, J. (1991). FtsZ ring structure associated with division in Escherichia coli. *Nature*, *354*(6349), 161–164. https://doi.org/10.1038/354161a0

Bianco, P. R. (2020). Dna helicase-ssb interactions critical to the regression and restart of stalled dna replication forks in Escherichia coli. *Genes*, *11*(5), 19–23. https://doi.org/10.3390/genes11050471

Bingle, L. E., Bailey, C. M., & Pallen, M. J. (2008). Type VI secretion: a beginner's guide. *Current Opinion in Microbiology*, *11*(1), 3–8. https://doi.org/10.1016/j.mib.2008.01.006

Boubakri, H., De Septenville, A. L., Viguera, E., & Michel, B. (2010). The helicases DinG, Rep and UvrD cooperate to promote replication across transcription units in vivo. *EMBO Journal*, *29*(1), 145–157. https://doi.org/10.1038/emboj.2009.308

Boyer, F., Fichant, G., Berthod, J., Vandenbrouck, Y., & Attree, I. (2009). Dissecting the bacterial type VI secretion system by a genome wide in silico analysis: What can be learned from available microbial genomic resources? *BMC Genomics*, *10*. https://doi.org/10.1186/1471-2164-10-104

Brown, A., Fernández, I. S., Gordiyenko, Y., & Ramakrishnan, V. (2016). Ribosome-dependent activation of stringent control. *Nature*, *534*(7606), 277–280. https://doi.org/10.1038/nature17675

Burchall, J. (1973). Mechanism of action of Trimethoprim-Sulfamethoxazole-II. *Journal of Infectious Diseases*, *128*, 437–441.

Busby, J. N., Panjikar, S., Landsberg, M. J., Hurst, M. R. H., & Lott, J. S. (2013). The BC component of ABC toxins is an RHS-repeat-containing protein encapsulation device. *Nature*, *501*(7468), 547–550. https://doi.org/10.1038/nature12465

Bushby, S. R., & Hitchings, G. H. (1968). Trimethoprim, a sulphonamide potentiator. *British Journal of Pharmacology and Chemotherapy*, *33*(1), 72–90. https://doi.org/10.1111/j.1476-5381.1968.tb00475.x

Cambray, G., Sanchez-Alberola, N., Campoy, S., Guerin, É., Da Re, S., González-Zorn, B., Ploy, M. C., Barbé, J., Mazel, D., & Erill, I. (2011). Prevalence of SOS-mediated control of integron integrase expression as an adaptive trait of chromosomal and mobile integrons. *Mobile DNA*, *2*(1), 6. https://doi.org/10.1186/1759-8753-2-6

Camerini-Otero, R. D., & Hsieh, P. (1995). Homologous recombination proteins in prokaryotes and eukaryotes. *Annual Review of Genetics*, *29*(1), 509–552. https://doi.org/10.1146/annurev.ge.29.120195.002453

Carter, C., Hutchison, A., Rudder, S., Trotter, E., Waters, E. V., Elumogo, N., & Langridge, G. C. (2023). Uropathogenic Escherichia coli population structure and antimicrobial susceptibility in Norfolk, UK. *Journal of Antimicrobial Chemotherapy*, *78*(8), 2028–2036. https://doi.org/10.1093/jac/dkad201

Castanie-Cornet, M.-P., Penfound, T. A., Smith, D., Elliott, J. F., & Foster, J. W. (1999). Control of Acid Resistance in Escherichia coli. *Journal of Bacteriology*, *181*(11), 3525–3535. https://doi.org/10.1128/JB.181.11.3525-3535.1999

Chatterjee, N., & Walker, G. C. (2017). Mechanisms of DNA damage, repair, and mutagenesis. *Environmental and Molecular Mutagenesis*, *58*(5), 235–263. https://doi.org/10.1002/em.22087

Chaurasiya, K. R., Ruslie, C., Silva, M. C., Voortman, L., Nevin, P., Lone, S., Beuning, P. J., & Williams, M. C. (2013). Polymerase manager protein UmuD directly regulates Escherichia coli DNA polymerase III α binding to ssDNA. *Nucleic Acids Research*, *41*(19), 8959–8968. https://doi.org/10.1093/nar/gkt648

Cheng, K., Wilkinson, M., Chaban, Y., & Wigley, D. B. (2020). A conformational switch in response to Chi converts RecBCD from phage destruction to DNA repair. *Nature Structural and Molecular Biology*, *27*(1), 71–77. https://doi.org/10.1038/s41594-019-0355-2

Chodavarapu, S., & Kaguni, J. M. (2016). Replication Initiation in Bacteria. *Enzymes*, *39*, 1–30. https://doi.org/10.1016/bs.enz.2016.03.001

Choudhary, D., Lagage, V., Foster, K. R., & Uphoff, S. (2023). Phenotypic heterogeneity in the bacterial oxidative stress response is driven by cell-cell interactions. *Cell Reports*, *42*(3), 112168. https://doi.org/10.1016/j.celrep.2023.112168

Christian, T. D., Romano, L. J., & Rueda, D. (2009). Single-molecule measurements of synthesis by DNA polymerase with base-pair resolution. *Proceedings of the National Academy of Sciences of the United States of America*, *106*(50), 21109–21114. https://doi.org/10.1073/pnas.0908640106

Cirz, R. T., Chin, J. K., Andes, D. R., De Crécy-Lagard, V., Craig, W. A., & Romesberg, F. E. (2005). Inhibition of mutation and combating the evolution of antibiotic resistance. *PLoS Biology*, *3*(6), 1024–1033. https://doi.org/10.1371/journal.pbio.0030176

Cohen, S. S., & Barner, H. D. (1954). Studies on Unbalanced Growth in Escherichia Coli. *Proceedings of the National Academy of Sciences*, *40*(10), 885–893. https://doi.org/10.1073/pnas.40.10.885

Cole, S. T. (1983). Characterisation of the promoter for the LexA regulated sulA gene of Escherichia coli. *MGG Molecular & General Genetics*, *189*(3), 400–404. https://doi.org/10.1007/BF00325901

Cooper, S., & Helmstetter, C. E. (1968). Chromosome replication and the division cycle of Escherichia coli. *Journal of Molecular Biology*, *31*(3), 519–540. https://doi.org/10.1016/0022-2836(68)90425-7

Costa, T. R. D., Felisberto-rodrigues, C., Meir, A., Prevost, M. S., Redzej, A., Trokter, M., & Waksman, G. (2015). Secretion systems in Gram-negative insights. *Nature Publishing Group*, *13*(6), 343–359. https://doi.org/10.1038/nrmicro3456

Coughlin, C. A., & Adelberg, E. A. (1956). Studies in Mutagenesis: Bacterial Mutation induced by Thymine Starvation. *Nature*, *178*(4532), 531–532. https://doi.org/10.1038/178531a0

Courcelle, J., Khodursky, A., Peter, B., Brown, P. O., & Hanawalt, P. C. (2001). Comparative Gene Expression Profiles Following UV Exposure in Wild-Type and SOS-Deficient *Escherichia coli*. *Genetics*, *158*(1), 41–64. https://doi.org/10.1093/genetics/158.1.41

Couvé, S., Ishchenko, A. A., Fedorova, O. S., Ramanculov, E. M., Laval, J., & Saparbaev, M. (2013). Direct DNA Lesion Reversal and Excision Repair in Escherichia coli . *EcoSal Plus*, *5*(2). https://doi.org/10.1128/ecosalplus.7.2.4

Crane, J. K., Alvarado, C. L., & Sutton, M. D. (2021). Role of the SOS Response in the Generation of Antibiotic Resistance In Vivo. In *Antimicrobial Agents and Chemotherapy* (Issue April). https://doi.org/10.1128/aac.00013-21

Custodio, R., Ford, R. M., Ellison, C. J., Liu, G., Mickute, G., Tang, C. M., & Exley, R. M. (2021). Type VI secretion system killing by commensal Neisseria is influenced by expression of type four pili. *ELife*, *10*, 1–31. https://doi.org/10.7554/eLife.63755

Da Re, S., Garnier, F., Guérin, E., Campoy, S., Denis, F., & Ploy, M. C. (2009). The SOS response promotes qnrB quinolone-resistance determinant expression. *EMBO Reports*, *10*(8), 929–933. https://doi.org/10.1038/embor.2009.99

Dalebroux, Z. D., & Swanson, M. S. (2012). PpGpp: Magic beyond RNA polymerase. *Nature Reviews Microbiology*, *10*(3), 203–212. https://doi.org/10.1038/nrmicro2720

Dao, V., & Modrich, P. (1998). Mismatch-, MutS-, MutL-, and helicase II-dependent unwinding from the single-strand break of an incised heteroduplex. *Journal of Biological Chemistry*, *273*(15), 9202–9207. https://doi.org/10.1074/jbc.273.15.9202

Dapa, T., Fleurier, S., Bredeche, M.-F., & Matic, I. (2017). *The SOS and RpoS Regulons Contribute to Bacterial*. *206*(July), 1349–1360.

Davies, B. W., Kohanski, M. A., Simmons, L. A., Winkler, J. A., Collins, J. J., & Walker, G. C. (2009). Hydroxyurea Induces Hydroxyl Radical-Mediated Cell Death in Escherichia coli. *Molecular Cell*, *36*(5), 845–860. https://doi.org/10.1016/j.molcel.2009.11.024

Dawes, J., & Foster, M. A. (1971). Vitamin B12 and methionine synthesis in Escherichia coli. *BBA - General Subjects*, *237*(3), 455–464. https://doi.org/10.1016/0304-4165(71)90263-7

Del Val, E., Nasser, W., Abaibou, H., & Reverchon, S. (2019). RecA and DNA recombination: A review of molecular mechanisms. *Biochemical Society Transactions*, *47*(5), 1511–1531. https://doi.org/10.1042/BST20190558

DellaVecchia, M. J., Croteau, D. L., Skorvaga, M., Dezhurov, S. V., Lavrik, O. I., & Van Houten, B. (2004). Analyzing the handoff of DNA from UvrA to UvrB utilizing DNA-protein photoaffinity

labeling. *Journal of Biological Chemistry*, *279*(43), 45245–45256. https://doi.org/10.1074/jbc.M408659200

Denamur, E., Tenaillon, O., Deschamps, C., Skurnik, D., Ronco, E., Gaillard, J. L., Picard, B., Branger, C., & Matic, I. (2005). Intermediate mutation frequencies favor evolution of multidrug resistance in Escherichia coli. *Genetics*, *171*(2), 825–827. https://doi.org/10.1534/genetics.105.045526

Dewachter, L., Fauvart, M., & Michiels, J. (2019a). Bacterial Heterogeneity and Antibiotic Survival: Understanding and Combatting Persistence and Heteroresistance. *Molecular Cell*, *76*(2), 255–267. https://doi.org/10.1016/j.molcel.2019.09.028

Dewachter, L., Fauvart, M., & Michiels, J. (2019b). Bacterial Heterogeneity and Antibiotic Survival: Understanding and Combatting Persistence and Heteroresistance. In *Molecular Cell* (Vol. 76, Issue 2, pp. 255–267). Cell Press. https://doi.org/10.1016/j.molcel.2019.09.028

DeWitt, S. K., & Adelberg, E. A. (1962). the Occurrence of a Genetic Transposition in a Strain of Escherichia Coli. *Genetics*, *47*(5), 577–585. https://doi.org/10.1093/genetics/47.5.577

Didier, J. P., Villet, R., Huggler, E., Lew, D. P., Hooper, D. C., Kelley, W. L., & Vaudaux, P. (2011). Impact of ciprofloxacin exposure on Staphylococcus aureus genomic alterations linked with emergence of rifampin resistance. *Antimicrobial Agents and Chemotherapy*, *55*(5), 1946–1952. https://doi.org/10.1128/AAC.01407-10

Dizdaroglu, M. (2012). Oxidatively induced DNA damage: Mechanisms, repair and disease. *Cancer Letters*, *327*(1–2), 26–47. https://doi.org/10.1016/j.canlet.2012.01.016

Do Thi, T., López, E., Rodríguez-Rojas, A., Rodríguez-Beltrán, J., Couce, A., Guelfo, J. R., Castañeda-García, A., & Blázquez, J. (2011). Effect of recA inactivation on mutagenesis of Escherichia coli

exposed to sublethal concentrations of antimicrobials. *Journal of Antimicrobial Chemotherapy*, *66*(3), 531–538. https://doi.org/10.1093/jac/dkq496

Dong, T. G., Dong, S., Catalano, C., Moore, R., Liang, X., & Mekalanos, J. J. (2015). Generation of reactive oxygen species by lethal attacks from competing microbes. *Proceedings of the National Academy of Sciences of the United States of America*, *112*(7), 2181–2186. https://doi.org/10.1073/pnas.1425007112

Dörr, T., Vulić, M., & Lewis, K. (2010). Ciprofloxacin causes persister formation by inducing the TisB toxin in Escherichia coli. *PLoS Biology*, *8*(2), 29–35. https://doi.org/10.1371/journal.pbio.1000317

Ducker, G. S., & Rabinowitz, J. D. (2017). One-Carbon Metabolism in Health and Disease. *Cell Metabolism*, *25*(1), 27–42. https://doi.org/10.1016/j.cmet.2016.08.009

Elez, M., Murray, A. W., Bi, L. J., Zhang, X. E., Matic, I., & Radman, M. (2010). Seeing mutations in living cells. *Current Biology*, *20*(16), 1432–1437. https://doi.org/10.1016/j.cub.2010.06.071

Estrada, A., Wright, D. L., & Anderson, A. C. (2016). Antibacterial antifolates: From development through resistance to the next generation. *Cold Spring Harbor Perspectives in Medicine*, *6*(8), 1–9. https://doi.org/10.1101/cshperspect.a028324

Fang, F. C. (2013). Antibiotic and ROS linkage questioned. *Nature Biotechnology*, *31*(5), 415–416. https://doi.org/10.1038/nbt.2574

Flores-Mireles, A. L., Walker, J. N., Caparon, M., & Hultgren, S. J. (2015). Urinary tract infections: Epidemiology, mechanisms of infection and treatment options. In *Nature Reviews Microbiology* (Vol. 13, Issue 5, pp. 269–284). Nature Publishing Group. https://doi.org/10.1038/nrmicro3432

Fonville, N. C., Bates, D., Hastings, P. J., Hanawalt, P. C., & Rosenberg, S. M. (2010). Role of RecA and the SOS response in thymineless death in Escherichia coli. *PLoS Genetics*, *6*(3). https://doi.org/10.1371/journal.pgen.1000865

Fonville, N. C., Vaksman, Z., Denapoli, J., Hastings, P. J., & Rosenberg, S. M. (2011). Pathways of resistance to thymineless death in Escherichia coli and the function of UvrD. *Genetics*, *189*(1), 23–36. https://doi.org/10.1534/genetics.111.130161

Foster, J. W. (2004). Escherichia coli acid resistance: Tales of an amateur acidophile. *Nature Reviews Microbiology*, *2*(11), 898–907. https://doi.org/10.1038/nrmicro1021

Foti, J. J., Devadoss, B., Winkler, J. A., Collins, J. J., & Walker, G. C. (2012). Oxidation of the guanine nucleotide pool underlies cell death by bactericidal antibiotics. *Science*, *336*(6079), 315–319. https://doi.org/10.1126/science.1219192

Fowler, R. G., White, S. J., Koyama, C., Moore, S. C., Dunn, R. L., & Schaaper, R. M. (2003). Interactions among the Escherichia coli mutT, mutM, and mutY damage prevention pathways. *DNA Repair*, *2*(2), 159–173. https://doi.org/10.1016/S1568-7864(02)00193-3

Frick, D. N., & Richardson, C. C. (2001). DNA Primases. *Annual Review of Biochemistry*, *70*(1), 39–80. https://doi.org/10.1146/annurev.biochem.70.1.39

Fritz, G., Walker, N., & Gerland, U. (2019). Heterogeneous Timing of Gene Induction as a Regulation Strategy. *Journal of Molecular Biology*, *431*(23), 4760–4774. https://doi.org/10.1016/j.jmb.2019.05.020

Fromme, J. C., & Verdine, G. L. (2002). Structural insights into lesion recognition and repair by the bacterial 8-oxoguanine dna glycosylase mutm. *Nature Structural Biology*, *9*(7), 544–552. https://doi.org/10.1038/nsb809

Giroux, X., Su, W. L., Bredeche, M. F., & Matic, I. (2017). Maladaptive DNA repair is the ultimate contributor to the death of trimethoprim-treated cells under aerobic and anaerobic conditions. *Proceedings of the National Academy of Sciences of the United States of America*, *114*(43), 11512–11517. https://doi.org/10.1073/pnas.1706236114

Goodman, M. F., McDonald, J. P., Jaszczur, M. M., & Woodgate, R. (2016). Insights into the complex levels of regulation imposed on Escherichia coli DNA polymerase V. *DNA Repair*, *44*(5), 42–50. https://doi.org/10.1016/j.dnarep.2016.05.005

Goodman, M. F., & Woodgate, R. (2013). Translesion DNA polymerases. *Cold Spring Harbor Perspectives in Biology*, *5*(10), 1–20. https://doi.org/10.1101/cshperspect.a010363

Granato, E. T., Smith, W. P. J., & Foster, K. R. (2023). Collective protection against the type VI secretion system in bacteria. *The ISME Journal*, *17*(7), 1052–1062. https://doi.org/10.1038/s41396-023-01401-4

Gratzner, H. G. (1982). Monoclonal Antibody to 5-Bromo- and 5-Iododeoxyuridine : A New Reagent for Detection of DNA Replication Placental Mononuclear Phagocytes as a Source of Interleukin-1. *Science*, *218*(October), 474–475.

Guarné, A., Ramon-Maiques, S., Wolff, E. M., Ghirlando, R., Hu, X., Miller, J. H., & Yang, W. (2004). Structure of the MutL C-terminal domain: A model of intact MutL and its roles in mismatch repair. *EMBO Journal*, *23*(21), 4134–4145. https://doi.org/10.1038/sj.emboj.7600412

Gullberg, E., Cao, S., Berg, O. G., Ilbäck, C., Sandegren, L., Hughes, D., & Andersson, D. I. (2011). Selection of resistant bacteria at very low antibiotic concentrations. *PLoS Pathogens*, *7*(7), 1–9. https://doi.org/10.1371/journal.ppat.1002158

Guzman, L.-M., Belin, D., Carson, M. J., & Beckwith, J. (1995). Tight Regulation, Modulation, and High-Level Expression by Vectors Containing the Arabinose P BAD Promoter. In *JOURNAL OF BACTERIOLOGY* (Vol. 177, Issue 14). https://journals.asm.org/journal/jb

Hampton, H. G., Watson, B. N. J., & Fineran, P. C. (2020). The arms race between bacteria and their phage foes. In *Nature* (Vol. 577, Issue 7790, pp. 327–336). Nature Research. https://doi.org/10.1038/s41586-019-1894-8

Hanawalt, P. C. (1963). Involvement of Synthesis of RNA in Thymineless Death. *Nature*, *198*(286), 1963.

Henrikus, S. S., van Oijen, A. M., & Robinson, A. (2018). Specialised DNA polymerases in Escherichia coli: roles within multiple pathways. *Current Genetics*, *64*(6), 1189–1196. https://doi.org/10.1007/s00294-018-0840-x

Hersch, S. J., Lam, L., & Dong, T. G. (2021). Engineered Type Six Secretion Systems Deliver Active Exogenous Effectors and Cre Recombinase. *MBio*, *12*(4), 1–14. https://doi.org/10.1128/mBio.01115-21

Hersch, S. J., Watanabe, N., Stietz, M. S., Manera, K., Kamal, F., Burkinshaw, B., Lam, L., Pun, A., Li, M., Savchenko, A., & Dong, T. G. (2020). Envelope stress responses defend against type six secretion system attacks independently of immunity proteins. *Nature Microbiology*, *5*(5), 706–714. https://doi.org/10.1038/s41564-020-0672-6

Hibbing, M. E., Fuqua, C., Parsek, M. R., & Peterson, S. B. (2010). Bacterial competition: Surviving and thriving in the microbial jungle. In *Nature Reviews Microbiology* (Vol. 8, Issue 1, pp. 15–25). https://doi.org/10.1038/nrmicro2259

Ho, B. T., Dong, T. G., & Mekalanos, J. J. (2014). A view to a kill: The bacterial type VI secretion system. *Cell Host and Microbe*, *15*(1), 9–21. https://doi.org/10.1016/j.chom.2013.11.008

Hocquet, D., & Bertrand, X. (2014). Metronidazole increases the emergence of ciprofloxacin- and amikacin-resistant pseudomonas aeruginosa by inducing the SOS response. *Journal of Antimicrobial Chemotherapy*, *69*(3), 852–854. https://doi.org/10.1093/jac/dkt435

Hocquet, D., Llanes, C., Thouverez, M., Kulasekara, H. D., Bertrand, X., Plésiat, P., Mazel, D., & Miller, S. I. (2012). Evidence for induction of integron-based antibiotic resistance by the SOS response in a clinical setting. *PLoS Pathogens*, *8*(6). https://doi.org/10.1371/journal.ppat.1002778

Hong, Y., Li, L., Luan, G., Drlica, K., & Zhao, X. (2017). Contribution of reactive oxygen species to thymineless death in Escherichia coli. *Nature Microbiology*, *2*(12), 1667–1675. https://doi.org/10.1038/s41564-017-0037-y

Hong, Y., Zeng, J., Wang, X., Drlica, K., & Zhao, X. (2019). Post-stress bacterial cell death mediated by reactive oxygen species. *Proceedings of the National Academy of Sciences of the United States of America*, *116*(20), 10064–10071. https://doi.org/10.1073/pnas.1901730116

Hughes, C. D., Simons, M., Mackenzie, C. E., Van Houten, B., & Kad, N. M. (2014). Single molecule techniques in DNA repair: A primer. *DNA Repair*, *20*, 2–13. https://doi.org/10.1016/j.dnarep.2014.02.003

Huovinen, P., Sundstrom, L., Swedberg, G., & Skold, O. (1995). Trimethoprim and sulfonamide resistance. *Antimicrobial Agents and Chemotherapy*, *39*(2), 279–289. https://doi.org/10.1128/aac.39.2.279

Hutchings, M., Truman, A., & Wilkinson, B. (2019). Antibiotics: past, present and future. *Current Opinion in Microbiology*, *51*(Figure 1), 72–80. https://doi.org/10.1016/j.mib.2019.10.008

Imlay, J. A. (2003). Pathways of Oxidative Damage. In *Annual Review of Microbiology* (Vol. 57, pp. 395–418). https://doi.org/10.1146/annurev.micro.57.030502.090938

Imlay, J. A. (2008). Cellular Defenses against Superoxide and Hydrogen Peroxide. *Annual Review of Biochemistry*, *77*(1), 755–776. https://doi.org/10.1146/annurev.biochem.77.061606.161055

Imlay, J. A. (2013a). The molecular mechanisms and physiological consequences of oxidative stress: Lessons from a model bacterium. *Nature Reviews Microbiology*, *11*(7), 443–454. https://doi.org/10.1038/nrmicro3032

Imlay, J. A. (2013b). The oxidative stress : lessons from a model bacterium. In *Nature Reviews Microbiology* (Vol. 11, Issue 7). https://doi.org/10.1038/nrmicro3032.The

Imlay, J. A. (2019). Where in the world do bacteria experience oxidative stress? *Environmental Microbiology*, *21*(2), 521–530. https://doi.org/10.1111/1462-2920.14445

Imlay, J. A., & Fridovich, I. (1991). Assay of metabolic superoxide production in Escherichia coli. *Journal of Biological Chemistry*, *266*(11), 6957–6965. https://doi.org/10.1016/s0021-9258(20)89596-9

Indiani, C., Patel, M., Goodman, M. F., & O'Donnell, M. E. (2013). RecA acts as a switch to regulate polymerase occupancy in a moving replication fork. *Proceedings of the National Academy of Sciences of the United States of America*, *110*(14), 5410–5415. https://doi.org/10.1073/pnas.1303301110

Irving, S. E., Choudhury, N. R., & Corrigan, R. M. (2021). The stringent response and physiological roles of (pp)pGpp in bacteria. *Nature Reviews Microbiology*, *19*(4), 256–271. https://doi.org/10.1038/s41579-020-00470-y

Jana, B., Fridman, C. M., Bosis, E., & Salomon, D. (2019). A modular effector with a DNase domain and a marker for T6SS substrates. *Nature Communications*, *10*(1). https://doi.org/10.1038/s41467-019-11546-6

Jana, B., & Salomon, D. (2019). Type VI secretion system: a modular toolkit for bacterial dominance. *Future Microbiology*, *14*, 1451–1463. https://doi.org/10.2217/fmb-2019-0194

Johansson, E., & Dixon, N. (2013). Replicative DNA polymerases. *Cold Spring Harbor Perspectives in Biology*, *5*(6). https://doi.org/10.1101/cshperspect.a012799

Jones, E. C., & Uphoff, S. (2021). Single-molecule imaging of LexA degradation in Escherichia coli elucidates regulatory mechanisms and heterogeneity of the SOS response. *Nature Microbiology*, *6*(8), 981–990. https://doi.org/10.1038/s41564-021-00930-y

Junop, M. S., Obmolova, G., Rausch, K., Hsieh, P., & Yang, W. (2001). Composite active site of an ABC ATPase: MutS uses ATP to verify mismatch recognition and authorize DNA repair. *Molecular Cell*, *7*(1), 1–12. https://doi.org/10.1016/S1097-2765(01)00149-6

Kaguni, J. M. (2011). Replication initiation at the Escherichia coli chromosomal origin. *Current Opinion in Chemical Biology*, *15*(5), 606–613. https://doi.org/10.1016/j.cbpa.2011.07.016

Kamal, F., Liang, X., Manera, K., Pei, T. T., Kim, H., Lam, L. G., Pun, A., Hersch, S. J., & Dong, T. G. (2020). Differential Cellular Response to Translocated Toxic Effectors and Physical Penetration by the Type VI Secretion System. *Cell Reports*, *31*(11). https://doi.org/10.1016/j.celrep.2020.107766

Kaplan, Y., Reich, S., Oster, E., Maoz, S., Levin-Reisman, I., Ronin, I., Gefen, O., Agam, O., & Balaban, N. Q. (2021). Observation of universal ageing dynamics in antibiotic persistence. *Nature*, *600*(7888), 290–294. https://doi.org/10.1038/s41586-021-04114-w

Kasai, H., & Nishimura, S. (1984). Hydroxylation of deoxyguanosine at the C-8 position by ascorbic acid and other reducing agents. *Nucleic Acids Research*, *12*(4), 2137–2145. https://doi.org/10.1093/nar/12.4.2137

Kath, J. E., Jergic, S., Heltzel, J. M. H., Jacob, D. T., Dixon, N. E., Sutton, M. D., Walker, G. C., & Loparo, J. J. (2014). Polymerase exchange on single DNA molecules reveals processivity clamp control of translesion synthesis. *Proceedings of the National Academy of Sciences of the United States of America*, *111*(21), 7647–7652. https://doi.org/10.1073/pnas.1321076111

Kavakli, I. H., Baris, I., Tardu, M., Gül, Ş., Öner, H., Çal, S., Bulut, S., Yarparvar, D., Berkel, Ç., Ustaoğlu, P., & Aydın, C. (2017). The Photolyase/Cryptochrome Family of Proteins as DNA Repair Enzymes and Transcriptional Repressors. In *Photochemistry and Photobiology* (Vol. 93, Issue 1, pp. 93–103). Blackwell Publishing Inc. https://doi.org/10.1111/php.12669

Kennedy, N. W., & Comstock, L. E. (2024). Mechanisms of bacterial immunity, protection, and survival during interbacterial warfare. In *Cell Host and Microbe* (Vol. 32, Issue 6, pp. 794–803). Cell Press. https://doi.org/10.1016/j.chom.2024.05.006

Ketcham, A., Freddolino, P. L., & Tavazoie, S. (2022). Intracellular acidification is a hallmark of thymineless death in E. coli. In *PLoS Genetics* (Vol. 18, Issue 10). https://doi.org/10.1371/journal.pgen.1010456

Khademian, M., & Imlay, J. A. (2021). How Microbes Evolved to Tolerate Oxygen. *Trends in Microbiology*, *29*(5), 428–440. https://doi.org/10.1016/j.tim.2020.10.001

Khan, S. R., & Kuzminov, A. (2022). Thymine-starvation-induced chromosomal fragmentation is not required for thymineless death in Escherichia coli. *Molecular Microbiology*, *117*(5), 1138–1155. https://doi.org/10.1111/mmi.14897

Khan, S. R., & Kuzminova, A. (2019). Thymineless death in Escherichia coli is unaffected by chromosomal replication complexity. *Journal of Bacteriology*, *201*(9). https://doi.org/10.1128/JB.00797-18

Khodursky, A., Guzmán, E. C., & Hanawalt, P. C. (2015). Thymineless Death Lives On: New Insights into a Classic Phenomenon. *Annual Review of Microbiology*, *69*(1), 247–263. https://doi.org/10.1146/annurev-micro-092412-155749

Kim, S. R., Maenhaut-Michel, G., Yamada, M., Yamamoto, Y., Matsui, K., Sofuni, T., Nohmi, T., & Ohmori, H. (1997). Multiple pathways for SOS-induced mutagenesis in Escherichia coli: An overexpression of dinB/dinP results in strongly enhancing mutagenesis in the absence of any exogenous treatment to damage DNA. *Proceedings of the National Academy of Sciences of the United States of America*, *94*(25), 13792–13797. https://doi.org/10.1073/pnas.94.25.13792

Klug, D., Rabani, J., & Fridovich, I. (1972). A direct demonstration of the catalytic action of superoxide dismutase through the use of pulse radiolysis. *Journal of Biological Chemistry*, *247*(15), 4839–4842. https://doi.org/10.1016/s0021-9258(19)44987-9

Kohanski, M. A., DePristo, M. A., & Collins, J. J. (2010). Sublethal Antibiotic Treatment Leads to Multidrug Resistance via Radical-Induced Mutagenesis. *Molecular Cell*, *37*(3), 311–320. https://doi.org/10.1016/j.molcel.2010.01.003

Kohanski, M. A., Dwyer, D. J., Hayete, B., Lawrence, C. A., & Collins, J. J. (2007). A Common Mechanism of Cellular Death Induced by Bactericidal Antibiotics. *Cell*, *130*(5), 797–810. https://doi.org/10.1016/j.cell.2007.06.049

Kordus, S. L., & Baughn, A. D. (2019). Revitalizing antifolates through understanding mechanisms that govern susceptibility and resistance. *MedChemComm*, *10*(6), 880–895. https://doi.org/10.1039/c9md00078j

Korshunov, S., & Imlay, J. (2011). Two sources of endogenous H2O2 in Escherichia coli. *Mol Microbiol.*, *75*(6), 1389–1401. https://doi.org/10.1111/j.1365-2958.2010.07059.x.Two

Koskiniemi, S., Lamoureux, J. G., Nikolakakis, K. C., De Roodenbeke, C. T. K., Kaplan, M. D., Low, D. A., & Hayes, C. S. (2013). Rhs proteins from diverse bacteria mediate intercellular competition. *Proceedings of the National Academy of Sciences of the United States of America*, *110*(17), 7032–7037. https://doi.org/10.1073/pnas.1300627110

Kowalczykowski, S. C., & Krupp, R. A. (1987). Effects of Escherichia coli SSB protein on the single-stranded DNA-dependent ATPase activity of Escherichia coli RecA protein. Evidence that SSB protein facilitates the binding of RecA protein to regions of secondary structure within single-stranded DNA. *Journal of Molecular Biology*, *193*(1), 97–113. https://doi.org/10.1016/0022-2836(87)90630-9

Kraithong, T., Hartley, S., Jeruzalmi, D., & Pakotiprapha, D. (2021). A peek inside the machines of bacterial nucleotide excision repair. *International Journal of Molecular Sciences*, *22*(2), 1–20. https://doi.org/10.3390/ijms22020952

Kuhn, H. (1988). ECA, the enterobacterial common antigen. *FEMS Microbiology Letters*, *54*(3), 195–222. https://doi.org/10.1016/0378-1097(88)90002-X

Kuong, K. J., & Kuzminov, A. (2010). Stalled replication fork repair and misrepair during thymineless death in Escherichia coli. *Genes to Cells*, *15*(6), 619–634. https://doi.org/10.1111/j.1365-2443.2010.01405.x

Kuong, K. J., & Kuzminov, A. (2012). Disintegration of nascent replication bubbles during thymine starvation triggers RecA- and RecBCD-dependent replication origin destruction. *Journal of Biological Chemistry*, *287*(28), 23958–23970. https://doi.org/10.1074/jbc.M112.359687

Kuypers, M. M. M., Marchant, H. K., & Kartal, B. (2018). The microbial nitrogen-cycling network. *Nature Reviews Microbiology*, *16*(5), 263–276. https://doi.org/10.1038/nrmicro.2018.9

Kwon, Y. K., Higgins, M. B., & Rabinowitz, J. D. (2010). Antifolate-induced depletion of intracellular glycine and purines inhibits thymineless death in E. coli. *ACS Chemical Biology*, *5*(8), 787–795. https://doi.org/10.1021/cb100096f

Lagage, V., Chen, V., & Uphoff, S. (2023). Adaptation delay causes a burst of mutations in bacteria responding to oxidative stress. *EMBO Reports*, *24*(1), 2022.05.25.493234. https://doi.org/10.15252/embr.202255640

Landgraf, D., Okumus, B., Chien, P., Baker, T. A., & Paulsson, J. (2012). Segregation of molecules at cell division reveals native protein localization. *Nature Methods*, *9*(5), 480–482. https://doi.org/10.1038/nmeth.1955

Lange, R., & Hengge-Aronis, R. (1994). The cellular concentration of the σ(S) subunit of RNA polymerase in Escherichia coli is controlled at the levels of transcription, translation, and protein stability. *Genes and Development*, *8*(13), 1600–1612. https://doi.org/10.1101/gad.8.13.1600

Lavery, P. E., & Kowalczykowski, S. C. (1992). A postsynaptic role for single-stranded DNA-binding protein in recA protein-promoted DNA strand exchange. *Journal of Biological Chemistry*, *267*(13), 9315–9320. https://doi.org/10.1016/s0021-9258(19)50425-2

Lee, H., Popodi, E., Tang, H., & Foster, P. L. (2012). Rate and molecular spectrum of spontaneous mutations in the bacterium Escherichia coli as determined by whole-genome sequencing. *Proceedings of the National Academy of Sciences of the United States of America*, *109*(41). https://doi.org/10.1073/pnas.1210309109

Lenhart, J. S., Sharma, A., Hingorani, M. M., & Simmons, L. A. (2013). DnaN clamp zones provide a platform for spatiotemporal coupling of mismatch detection to DNA replication. *Molecular Microbiology*, *87*(3), 553–568. https://doi.org/10.1111/mmi.12115

Lewin, C. S., & Amyes, B. (1991). *The role of the SOS response in bacteria exposed to zidovudine or trimethoprim*. *34*(June 1990), 329–332.

Lewis, J. S., Spenkelink, L. M., Jergic, S., Wood, E. A., Monachino, E., Horan, N. P., Duderstadt, K. E., Cox, M. M., Robinson, A., Dixon, N. E., & van Oijen, A. M. (2017). Single-molecule visualization of fast polymerase turnover in the bacterial replisome. *ELife*, *6*. https://doi.org/10.7554/eLife.23932

Lewis, K. (2010). Persister cells. *Annual Review of Microbiology*, *64*, 357–372. https://doi.org/10.1146/annurev.micro.112408.134306

Li, F., Liu, Q., Chen, Y. Y., Yu, Z. N., Zhang, Z. P., Zhou, Y. F., Deng, J. Y., Bi, L. J., & Zhang, X. E. (2008). Escherichia coli mismatch repair protein MutL interacts with the clamp loader subunits of DNA polymerase III. *Mutation Research - Fundamental and Molecular Mechanisms of Mutagenesis*, *637*(1–2), 101–110. https://doi.org/10.1016/j.mrfmmm.2007.07.008

Li, G. M. (2008). Mechanisms and functions of DNA mismatch repair. *Cell Research*, *18*(1), 85–98. https://doi.org/10.1038/cr.2007.115

Li, X., & Heyer, W. D. (2008). Homologous recombination in DNA repair and DNA damage tolerance. In *Cell Research* (Vol. 18, Issue 1, pp. 99–113). https://doi.org/10.1038/cr.2008.1

Li, X. Z., Plésiat, P., & Nikaido, H. (2015). The challenge of efflux-mediated antibiotic resistance in Gram-negative bacteria. *Clinical Microbiology Reviews*, *28*(2), 337–418. https://doi.org/10.1128/CMR.00117-14

Liang, S.-T., Bipatnath, M., Xu, Y.-C., Chen, S.-L., Dennis, P., Ehrenberg, M., & Bremer, H. (1999). Activities of constitutive promoters in Escherichia coli 1 1Edited by D. E. Draper. *Journal of Molecular Biology*, *292*(1), 19–37. https://doi.org/10.1006/jmbi.1999.3056

Lien, Y. W., & Lai, E. M. (2017). Type VI secretion effectors: Methodologies and biology. *Frontiers in Cellular and Infection Microbiology*, *7*(JUN), 1–11. https://doi.org/10.3389/fcimb.2017.00254

Lin, J., In Soo Lee, Frey, J., Slonczewski, J. L., & Foster, J. W. (1995). Comparative analysis of extreme acid survival in Salmonella typhimurium, Shigella flexneri, and Escherichia coli. *Journal of Bacteriology*, *177*(14), 4097–4104. https://doi.org/10.1128/jb.177.14.4097-4104.1995

Liochev, S. I., Hausladen, A., & Fridovich, I. (1999). Nitroreductase A is regulated as a member of the soxRS regulon of Escherichia coli. *Proceedings of the National Academy of Sciences of the United States of America*, *96*(7), 3537–3539. https://doi.org/10.1073/pnas.96.7.3537

Liu, Y., & Imlay, J. A. (2013). Cell death from antibiotics without the involvement of reactive oxygen species. *Science*, *339*(6124), 1210–1213. https://doi.org/10.1126/science.1232751

Longley, D. B., Harkin, D. P., & Johnston, P. G. (2003). 5-Fluorouracil: Mechanisms of action and clinical strategies. *Nature Reviews Cancer*, *3*(5), 330–338. https://doi.org/10.1038/nrc1074

Lovett, S. T., & Kolodner, R. D. (1989). Identification and purification of a single-stranded-DNA-specific exonuclease encoded by the recJ gene of Escherichia coli. *Proceedings of the National Academy of Sciences of the United States of America*, *86*(8), 2627–2631. https://doi.org/10.1073/pnas.86.8.2627

Lu, T. K., & Collins, J. J. (2009). Engineered bacteriophage targeting gene networks as adjuvants for antibiotic therapy. *Proceedings of the National Academy of Sciences of the United States of America*, *106*(12), 4629–4634. https://doi.org/10.1073/pnas.0800442106

Maciag, M., Kochanowska, M., Łyzeń, R., Wegrzyn, G., & Szalewska-Pałasz, A. (2010). ppGpp inhibits the activity of Escherichia coli DnaG primase. *Plasmid*, *63*(1), 61–67. https://doi.org/10.1016/j.plasmid.2009.11.002

MacLean, R. C., Torres-Barceló, C., & Moxon, R. (2013). Evaluating evolutionary models of stress-induced mutagenesis in bacteria. *Nature Reviews Genetics*, *14*(3), 221–227. https://doi.org/10.1038/nrg3415

Mäkelä, J., Uphoff, S., & Sherratt, D. J. (2021). Nonrandom segregation of sister chromosomes by Escherichia coli MukBEF. *Proceedings of the National Academy of Sciences of the United States of America*, *118*(33). https://doi.org/10.1073/pnas.2022078118

Maki, H., & Sekiguchi, M. (1992). MutT protein specifically hydrolyses a potent mutagenic substrate for DNA synthesis. *Nature*, *355*(6357), 273–275. https://doi.org/10.1038/355273a0

Mallik, S., Popodi, E. M., Hanson, A. J., & Foster, P. L. (2015). Interactions and localization of Escherichia coli error-prone DNA polymerase IV after DNA damage. *Journal of Bacteriology*, *197*(17), 2792–2809. https://doi.org/10.1128/JB.00101-15

Manna, M. S., Tamer, Y. T., Gaszek, I., Poulides, N., Ahmed, A., Wang, X., Toprak, F. C. R., Woodard, D. N. R., Koh, A. Y., Williams, N. S., Borek, D., Atilgan, A. R., Hulleman, J. D., Atilgan, C., Tambar, U., & Toprak, E. (2021). A trimethoprim derivative impedes antibiotic resistance evolution. *Nature Communications*, *12*(1). https://doi.org/10.1038/s41467-021-23191-z

Martín, C. M., & Guzmán, E. C. (2011). DNA replication initiation as a key element in thymineless death. *DNA Repair*, *10*(1), 94–101. https://doi.org/10.1016/j.dnarep.2010.10.005

Martín, C. M., Viguera, E., & Guzmán, E. C. (2014). Rifampicin suppresses thymineless death by blocking the transcription-dependent step of chromosome initiation. *DNA Repair*, *18*(1), 10–17. https://doi.org/10.1016/j.dnarep.2014.03.004

Maslowska, K. H., Makiela-Dzbenska, K., & Fijalkowska, I. J. (2019). The SOS system: A complex and tightly regulated response to DNA damage. *Environmental and Molecular Mutagenesis*, *60*(4), 368–384. https://doi.org/10.1002/em.22267

Maso, L., Vascon, F., Chinellato, M., Goormaghtigh, F., Bellio, P., Van Melderen, L., Ruzzene, M., Pardon, E., Angelini, A., Celenza, G., Steyaert, J., Tondi, D., & Cendron, L. (2022). Nanobodies targeting LexA autocleavage disclose novel suppression strategy of SOS-response pathway. *Under Revision*, 1–15. https://doi.org/10.1016/j.str.2022.09.004

McKeown, M., Kahn, M., & Hanawalt, P. (1976). Thymidine uptake and utilization in Escherichia coli: a new gene controlling nucleoside transport. *Journal of Bacteriology*, *126*(2), 814–822. https://doi.org/10.1128/jb.126.2.814-822.1976

Medina, M., & Castillo-Pino, E. (2019). An introduction to the epidemiology and burden of urinary tract infections. *Therapeutic Advances in Urology*, *11*(6), 175628721983217. https://doi.org/10.1177/1756287219832172

Meier, U., & Mayer, H. (1985). Genetic location of genes encoding enterobacterial common antigen. *Journal of Bacteriology*, *163*(2), 756–762. https://doi.org/10.1128/jb.163.2.756-762.1985

Meier-Dieter, U., Barr, K., Starman, R., Hatch, L., & Rick, P. D. (1992). Nucleotide sequence of the Escherichia coli rfe gene involved in the synthesis of enterobacterial common antigen: Molecular cloning of the rfe-rff gene cluster. *Journal of Biological Chemistry*, *267*(2), 746–753. https://doi.org/10.1016/s0021-9258(18)48347-0

Meier-Dieter, U., Starman, R., Barr, K., Mayer, H., & Rick, P. D. (1990). Biosynthesis of enterobacterial common antigen in Escherichia coli. Biochemical characterization of Tn10 insertion mutants defective in enterobacterial common antigen synthesis. *Journal of Biological Chemistry*, *265*(23), 13490–13497. https://doi.org/10.1016/s0021-9258(18)77373-0

Merrikh, H., Zhang, Y., Grossman, A. D., & Wang, J. D. (2012). Replication-transcription conflicts in bacteria. *Nature Reviews Microbiology*, *10*(7), 449–458. https://doi.org/10.1038/nrmicro2800

Meyer, R. R., Glassberg, J., Scott, J. V., & Kornberg, A. (1980). A temperature-sensitive single-stranded DNA-binding protein from Escherichia coli. *Journal of Biological Chemistry*, *255*(7), 2897–2901. https://doi.org/10.1016/s0021-9258(19)85824-6

Michel, B., Boubakri, H., Baharoglu, Z., LeMasson, M., & Lestini, R. (2007). Recombination proteins and rescue of arrested replication forks. *DNA Repair*, *6*(7), 967–980. https://doi.org/10.1016/j.dnarep.2007.02.016

Mitosch, K., Rieckh, G., & Bollenbach, T. (2017). Noisy Response to Antibiotic Stress Predicts Subsequent Single-Cell Survival in an Acidic Environment. *Cell Systems*, *4*(4), 393-403.e5. https://doi.org/10.1016/j.cels.2017.03.001

Mitosch, K., Rieckh, G., & Bollenbach, T. (2019). Temporal order and precision of complex stress responses in individual bacteria. *Molecular Systems Biology*, *15*(2), 1–15. https://doi.org/10.15252/msb.20188470

Modrich, P. (1989). Methyl-directed DNA mismatch correction. *Journal of Biological Chemistry*, *264*(12), 6597–6600. https://doi.org/10.1016/s0021-9258(18)83467-6

Modrich, P. (1991). Mechanisms and biological effects of mismatch repair. *Annual Review of Genetics*, *25*, 229–253. https://doi.org/10.1146/annurev.ge.25.120191.001305

Modrich, P., & Lahue, R. (1996). Mismatch repair in replication fidelity, genetic recombination, and cancer biology. *Annual Review of Biochemistry*, *65*, 101–133. https://doi.org/10.1146/annurev.bi.65.070196.000533

Moffitt, J. R., Lee, J. B., & Cluzel, P. (2012). The single-cell chemostat: An agarose-based, microfluidic device for high-throughput, single-cell studies of bacteria and bacterial communities. *Lab on a Chip*, *12*(8), 1487–1494. https://doi.org/10.1039/c2lc00009a

Moolman, M. C., Krishnan, S. T. iruvadi, Kerssemakers, J. W. J., van den Berg, A., Tulinski, P., Depken, M., Reyes-Lamothe, R., Sherratt, D. J., & Dekker, N. H. (2014). Slow unloading leads to DNA-bound β2-sliding clamp accumulation in live Escherichia coli cells. *Nature Communications*, *5*, 5820. https://doi.org/10.1038/ncomms6820

Morimatsu, K., & Kowalczykowski, S. C. (2003). RecFOR proteins load RecA protein onto gapped DNA to accelerate DNA strand exchange: A universal step of recombinational repair. *Molecular Cell*, *11*(5), 1337–1347. https://doi.org/10.1016/S1097-2765(03)00188-6

Mukherjee, A., Cao, C., & Lutkenhaus, J. (1998). Inhibition of FtsZ polymerization by SulA, an inhibitor of septation in Escherichia coli. *Proceedings of the National Academy of Sciences of the United States of America*, *95*(6), 2885–2890. https://doi.org/10.1073/pnas.95.6.2885

Murray, C. J., Ikuta, K. S., Sharara, F., Swetschinski, L., Robles Aguilar, G., Gray, A., Han, C., Bisignano, C., Rao, P., Wool, E., Johnson, S. C., Browne, A. J., Chipeta, M. G., Fell, F., Hackett, S., Haines-Woodhouse, G., Kashef Hamadani, B. H., Kumaran, E. A. P., McManigal, B., … Naghavi, M. (2022). Global burden of bacterial antimicrobial resistance in 2019: a systematic analysis. *The Lancet*, *399*(10325), 629–655. https://doi.org/10.1016/S0140-6736(21)02724-0

Navarro-Garcia, F., Ruiz-Perez, F., Cataldi, Á., & Larzábal, M. (2019). Type VI secretion system in pathogenic escherichia coli: Structure, role in virulence, and acquisition. *Frontiers in Microbiology*, *10*(AUG), 1–17. https://doi.org/10.3389/fmicb.2019.01965

Nicolaidis, A. A., & Holland, I. B. (1978). Evidence for the specific association of the chromosomal origin with outer membrane fractions isolated from Escherichia coli. *Journal of Bacteriology*, *135*(1), 178–189. https://doi.org/10.1128/jb.135.1.178-189.1978

Nottebrock, H., & Then, R. (1977). Thymidine concentrations in serum and urine of different animal species and man. *Biochemical Pharmacology*, *26*(22), 2175–2179. https://doi.org/10.1016/0006-2952(77)90271-4

Oakley, A. J. (2019). A structural view of bacterial DNA replication. *Protein Science*, *28*(6), 990–1004. https://doi.org/10.1002/pro.3615

O'Donnell, M., Langston, L., & Stillman, B. (2013). Principles and concepts of DNA replication in bacteria, archaea, and eukarya. *Cold Spring Harbor Perspectives in Biology*, *5*(7), 1–13. https://doi.org/10.1101/cshperspect.a010108

Okagaki, H., Tsubota, Y., & Sibatani, A. (1960). Unbalanced growth and bacterial death in thymine-deficient and ultraviolet irradiated Escherichia coli. *Journal of Bacteriology*, *80*, 762–771. https://doi.org/10.1128/jb.80.6.762-771.1960

Okazaki, R., Okazaki, T., & Kuriki, Y. (1959). Incorporation of [3H]thymidine in a deoxyriboside-requiring bacterium. *Biochimica et Biophysica Acta*, *33*(1), 289–291. https://doi.org/10.1016/0006-3002(59)90543-8

Opperman, T., Murli, S., Smith, B. T., & Walker, G. C. (1999). A model for a umuDC-dependent prokaryotic DNA damage checkpoint. *Proceedings of the National Academy of Sciences of the United States of America*, *96*(16), 9218–9223. https://doi.org/10.1073/pnas.96.16.9218

Parsons, C. A., Stasiak, A., & West, S. C. (1995). The E. coli RuvAB proteins branch migrate Holliday junctions through heterologous DNA sequences in a reaction facilitated by SSB. *EMBO Journal*, *14*(22), 5736–5744. https://doi.org/10.1002/j.1460-2075.1995.tb00260.x

Pillon, M. C., Babu, V. M. P., Randall, J. R., Cai, J., Simmons, L. A., Sutton, M. D., & Guarné, A. (2015). The sliding clamp tethers the endonuclease domain of MutL to DNA. *Nucleic Acids Research*, *43*(22), 10746–10759. https://doi.org/10.1093/nar/gkv918

Pinney, R. J., & Smith, J. T. (1972). R factor elimination during thymine starvation: effects of inhibition of protein synthesis and readdition of thymine. *Journal of Bacteriology*, *111*(2), 361–367. https://doi.org/10.1128/jb.111.2.361-367.1972

Pissaridou, P., Allsopp, L. P., Wettstadt, S., Howard, S. A., Mavridou, D. A. I., & Filloux, A. (2018). The Pseudomonas aeruginosa T6SS-VgrG1b spike is topped by a PAAR protein eliciting DNA damage to bacterial competitors. *Proceedings of the National Academy of Sciences of the United States of America*, *115*(49), 12519–12524. https://doi.org/10.1073/pnas.1814181115

Poole, K. (2012). Bacterial stress responses as determinants of antimicrobial resistance. *Journal of Antimicrobial Chemotherapy*, *67*(9), 2069–2089. https://doi.org/10.1093/jac/dks196

Potvin-Trottier, L., Luro, S., & Paulsson, J. (2018). Microfluidics and single-cell microscopy to study stochastic processes in bacteria. *Current Opinion in Microbiology*, *43*, 186–192. https://doi.org/10.1016/j.mib.2017.12.004

Pribis, J. P., García-Villada, L., Zhai, Y., Lewin-Epstein, O., Wang, A. Z., Liu, J., Xia, J., Mei, Q., Fitzgerald, D. M., Bos, J., Austin, R. H., Herman, C., Bates, D., Hadany, L., Hastings, P. J., & Rosenberg, S. M. (2019). Gamblers: An Antibiotic-Induced Evolvable Cell Subpopulation Differentiated by Reactive-Oxygen-Induced General Stress Response. *Molecular Cell*, *74*(4), 785-800.e7. https://doi.org/10.1016/j.molcel.2019.02.037

Pritha Rao, T. V., & Kuzminov, A. (2020). Exopolysaccharide defects cause hyper-thymineless death in Escherichia coli via massive loss of chromosomal DNA and cell lysis. *Proceedings of the National Academy of Sciences of the United States of America*, *117*(52), 33549–33560. https://doi.org/10.1073/PNAS.2012254117

Rao, P., & Kuzminov, A. (2019). Sources of thymidine and analogs fueling futile damage-repair cycles and ss-gap accumulation during thymine starvation in Escherichia coli. *DNA Repair*, *75*(5), 1–17. https://doi.org/10.1016/j.dnarep.2019.01.002

Rao, T. V. P., & Kuzminov, A. (2020). Exopolysaccharide defects cause hyper-thymineless death in Escherichia coli via massive loss of chromosomal DNA and cell lysis. *Proceedings of the National Academy of Sciences*, *117*(52), 33549–33560. https://doi.org/10.1073/pnas.2012254117

Rao, T. V. P., & Kuzminov, A. (2021). Electron microscopy reveals unexpected cytoplasm and envelope changes during thymineless death in escherichia coli. *Journal of Bacteriology*, *203*(17), 1–13. https://doi.org/10.1128/JB.00150-21

Rao, T. V. P., & Kuzminov, A. (2022). Oxidative Damage Blocks Thymineless Death and Trimethoprim Poisoning in Escherichia coli. *Journal of Bacteriology*, *204*(1). https://doi.org/10.1128/JB.00370-21

Raser, J. M., & O'Shea, E. K. (2005). Noise in Gene Expression: Origins, Consequences, and Control. *Science*, *309*(5743), 2010–2013. https://doi.org/10.1126/science.1105891

Recacha, E., Machuca, J., Díaz de Alba, P., Ramos-Güelfo, M., Docobo-Pérez, F., Rodriguez-Beltrán, J., Blázquez, J., Pascual, A., & Rodríguez-Martínez, J. M. (2017). Quinolone resistance reversion by targeting the SOS response. *MBio*, *8*(5), 1–12. https://doi.org/10.1128/mBio.00971-17

Reyes-Lamothe, R., Sherratt, D. J., & Leake, M. C. (2010). Stoichiometry and Architecture of Active DNA Replication Machinery in Escherichia coli. *Science*, *328*(5977), 498–501. https://doi.org/10.1126/science.1185757

Reyes-Lamothe, R., Tran, T., Meas, D., Lee, L., Li, A. M., Sherratt, D. J., & Tolmasky, M. E. (2014). High-copy bacterial plasmids diffuse in the nucleoid-free space, replicate stochastically and are randomly partitioned at cell division. *Nucleic Acids Research*, *42*(2), 1042–1051. https://doi.org/10.1093/nar/gkt918

Rios, A. C., & Tor, Y. (2013). On the origin of the canonical nucleobases: An assessment of selection pressures across chemical and early biological evolution. In *Israel Journal of Chemistry* (Vol. 53, Issues 6–7, pp. 469–483). https://doi.org/10.1002/ijch.201300009

Rösch, T. C., Altenburger, S., Oviedo-Bocanegra, L., Pediaditakis, M., Najjar, N. El, Fritz, G., & Graumann, P. L. (2018). Single molecule tracking reveals spatio-temporal dynamics of bacterial DNA repair centres. *Scientific Reports*, *8*(1), 1–14. https://doi.org/10.1038/s41598-018-34572-8

Rosenberg, S. M., Shee, C., Frisch, R. L., & Hastings, P. J. (2012). Stress-induced mutation via DNA breaks in Escherichia coli: A molecular mechanism with implications for evolution and medicine. *BioEssays*, *34*(10), 885–892. https://doi.org/10.1002/bies.201200050

Rowland, I., Gibson, G., Heinken, A., Scott, K., Swann, J., Thiele, I., & Tuohy, K. (2018). Gut microbiota functions: metabolism of nutrients and other food components. *European Journal of Nutrition*, *57*(1), 1–24. https://doi.org/10.1007/s00394-017-1445-8

Russell, A. B., Peterson, S. B., & Mougous, J. D. (2014). Type VI secretion system effectors: Poisons with a purpose. *Nature Reviews Microbiology*, *12*(2), 137–148. https://doi.org/10.1038/nrmicro3185

Samuel, G., & Reeves, P. (2003). Biosynthesis of O-antigens: Genes and pathways involved in nucleotide sugar precursor synthesis and O-antigen assembly. *Carbohydrate Research*, *338*(23), 2503–2519. https://doi.org/10.1016/j.carres.2003.07.009

Sanchez-Vazquez, P., Dewey, C. N., Kitten, N., Ross, W., & Gourse, R. L. (2019). Genome-wide effects on Escherichia coli transcription from ppGpp binding to its two sites on RNA polymerase. *Proceedings of the National Academy of Sciences of the United States of America*, *116*(17), 8310–8319. https://doi.org/10.1073/pnas.1819682116

Sands, R. H. (1960). The role of “free radicals” in radiation. *Cancer*, *13*(6 S), 27–30. https://doi.org/10.1002/1097-0142(196011/12)13:6+<27::AID-CNCR2820130707>3.0.CO;2-5

Sangurdekar, D. P., Hamann, B. L., Smirnov, D., Srienc, F., Hanawalt, P. C., & Khodursky, A. B. (2010). Thymineless death is associated with loss of essential genetic information from the replication origin. *Molecular Microbiology*, *75*(6), 1455–1467. https://doi.org/10.1111/j.1365-2958.2010.07072.x

Sangurdekar, D. P., Zhang, Z., & Khodursky, A. B. (2011). The association of DNA damage response and nucleotide level modulation with the antibacterial mechanism of the anti-folate drug Trimethoprim. *BMC Genomics*, *12*(1), 583. https://doi.org/10.1186/1471-2164-12-583

Schaaper, R. M., & Mathews, C. K. (2013). Mutational consequences of dNTP pool imbalances in E. coli. *DNA Repair*, *12*(1), 73–79. https://doi.org/10.1016/j.dnarep.2012.10.011

Schroeder, J. W., Hirst, W. G., Szewczyk, G. A., & Simmons, L. A. (2016). The Effect of Local Sequence Context on Mutational Bias of Genes Encoded on the Leading and Lagging Strands. *Current Biology*, *26*(5), 692–697. https://doi.org/10.1016/j.cub.2016.01.016

Seaver, L. C., & Imlay, J. A. (2001). Alkyl hydroperoxide reductase is the primary scavenger of endogenous hydrogen peroxide in Escherichia coli. *Journal of Bacteriology*, *183*(24), 7173–7181. https://doi.org/10.1128/JB.183.24.7173-7181.2001

Sedgwick, B., & Lindahl, T. (2002). Recent progress on the Ada response for inducible repair of DNA alkylation damage. *Oncogene*, *21*(58 REV. ISS. 8), 8886–8894. https://doi.org/10.1038/sj.onc.1205998

Seipke, R. F., Kaltenpoth, M., & Hutchings, M. I. (2012). Streptomyces as symbionts: An emerging and widespread theme? *FEMS Microbiology Reviews*, *36*(4), 862–876. https://doi.org/10.1111/j.1574-6976.2011.00313.x

Sen, A., & Imlay, J. A. (2021). How Microbes Defend Themselves From Incoming Hydrogen Peroxide. *Frontiers in Immunology*, *12*(April), 1–19. https://doi.org/10.3389/fimmu.2021.667343

Seo, S. W., Kim, D., Szubin, R., & Palsson, B. O. (2015). Genome-wide Reconstruction of OxyR and SoxRS Transcriptional Regulatory Networks under Oxidative Stress in Escherichia coli K-12 MG1655. *Cell Reports*, *12*(8), 1289–1299. https://doi.org/10.1016/j.celrep.2015.07.043

Shapiro, R. S. (2015). Antimicrobial-Induced DNA Damage and Genomic Instability in Microbial Pathogens. In *PLoS Pathogens* (Vol. 11, Issue 3, pp. 1–8). Public Library of Science. https://doi.org/10.1371/journal.ppat.1004678

Shee, C., Gibson, J. L., Darrow, M. C., Gonzalez, C., & Rosenberg, S. M. (2011). Impact of a stress-inducible switch to mutagenic repair of DNA breaks on mutation in Escherichia coli. *Proceedings of the National Academy of Sciences of the United States of America*, *108*(33), 13659–13664. https://doi.org/10.1073/pnas.1104681108

Shneider, M. M., Buth, S. A., Ho, B. T., Basler, M., Mekalanos, J. J., & Leiman, P. G. (2013). PAAR-repeat proteins sharpen and diversify the type VI secretion system spike. *Nature*, *500*(7462), 350–353. https://doi.org/10.1038/nature12453

Siede, W. (2020). DNA Interstrand Crosslink Repair. In *Encyclopedia of Life Sciences* (pp. 683–694). Wiley. https://doi.org/10.1002/9780470015902.a0029226

Sinha, A. K., Løbner-Olesen, A., & Riber, L. (2020). Bacterial Chromosome Replication and DNA Repair During the Stringent Response. *Frontiers in Microbiology*, *11*(August), 1–9. https://doi.org/10.3389/fmicb.2020.582113

Sobol, R. W. (2012). For MutY, It's all about the OG. *Chemistry and Biology*, *19*(3), 313–314. https://doi.org/10.1016/j.chembiol.2012.03.002

Spies, M., & Stephen C. Kowalczykowski. (2005). RecBCD and RecF Pathways. *The Bacterial Chromosome*, 389–403.

Spinks, R. R., Spenkelink, L. M., Stratmann, S. A., Xu, Z. Q., Stamford, N. P. J., Brown, S. E., Dixon, N. E., Jergic, S., & Van Oijen, A. M. (2021). DnaB helicase dynamics in bacterial DNA replication resolved by single-molecule studies. *Nucleic Acids Research*, *49*(12), 6804–6816. https://doi.org/10.1093/nar/gkab493

Spivak, G. (2016). Transcription-coupled repair: an update. In *Archives of Toxicology* (Vol. 90, Issue 11, pp. 2583–2594). Springer Verlag. https://doi.org/10.1007/s00204-016-1820-x

Stracy, M., Jaciuk, M., Uphoff, S., Kapanidis, A. N., Nowotny, M., Sherratt, D. J., & Zawadzki, P. (2016). Single-molecule imaging of UvrA and UvrB recruitment to DNA lesions in living Escherichia coli. *Nature Communications*, *7*. https://doi.org/10.1038/ncomms12568

Stracy, M., Schweizer, J., Sherratt, D. J., Kapanidis, A. N., Uphoff, S., & Lesterlin, C. (2021). Transient non-specific DNA binding dominates the target search of bacterial DNA-binding proteins. *Molecular Cell*, *81*(7), 1499-1514.e6. https://doi.org/10.1016/j.molcel.2021.01.039

Tan, K. W., Pham, T. M., Furukohri, A., Maki, H., & Akiyama, M. T. (2015). Recombinase and translesion DNA polymerase decrease the speed of replication fork progression during the DNA damage response in Escherichia coli cells. *Nucleic Acids Research*, *43*(3), 1714–1725. https://doi.org/10.1093/nar/gkv044

Taylor, A. F., & Smith, G. R. (2003). RecBCD enzyme is a DNA helicase with fast and slow motors of opposite polarity. *Nature*, *423*(6942), 889–893. https://doi.org/10.1038/nature01674

Tham, K. C., Hermans, N., Winterwerp, H. H. K., Cox, M. M., Wyman, C., Kanaar, R., & Lebbink, J. H. G. (2013). Mismatch repair inhibits homeologous recombination via coordinated directional unwinding of trapped DNA structures. *Molecular Cell*, *51*(3), 326–337. https://doi.org/10.1016/j.molcel.2013.07.008

Tolkoff-Rubin, N. E., Weber, D., Fang, L. S. T., Kelly, M., Wilkinson, R., & Rubin, R. H. (1982). Single-dose therapy with trimethoprim-sulfamethoxazole for urinary tract infection in women. *Reviews of Infectious Diseases*, *4*(2), 444–448. https://doi.org/10.1093/clinids/4.2.444

Toprak, E., Veres, A., Michel, J. B., Chait, R., Hartl, D. L., & Kishony, R. (2012). Evolutionary paths to antibiotic resistance under dynamically sustained drug selection. *Nature Genetics*, *44*(1), 101–105. https://doi.org/10.1038/ng.1034

Trewick, S. C., Henshaw, T. F., Hausinger, R. P., Lindahl, T., & Sedgwick, B. (2002). Oxidative demethylation by Escherichia coli AlkB directly reverts DNA base damage. *Nature*, *419*(6903), 174–178. https://doi.org/10.1038/nature00908

Trusca, D., Scott, S., Thompson, C., & Bramhill, D. (1998). Bacterial SOS checkpoint protein SulA inhibits polymerization of purified FtsZ cell division protein. *Journal of Bacteriology*, *180*(15), 3946–3953. https://doi.org/10.1128/jb.180.15.3946-3953.1998

Tsai-Wu, J. J., Liu, H. F., & Lu, A. L. (1992). Escherichia coli MutY protein has both N-glycosylase and apurinic/apyrimidinic endonuclease activities on A°C and A°G mispairs. *Proceedings of the National Academy of Sciences of the United States of America*, *89*(18), 8779–8783. https://doi.org/10.1073/pnas.89.18.8779

Umezu, K., Nakayama, K., & Nakayama, H. (1990). Escherichia coli RecQ protein is a DNA helicase. *Proceedings of the National Academy of Sciences of the United States of America*, *87*(14), 5363–5367. https://doi.org/10.1073/pnas.87.14.5363

Uphoff, S. (2018). Real-time dynamics of mutagenesis reveal the chronology of DNA repair and damage tolerance responses in single cells. *Proceedings of the National Academy of Sciences of the United States of America*, *115*(28), E6516–E6525. https://doi.org/10.1073/pnas.1801101115

Uphoff, S., Lord, N. D., Okumus, B., Potvin-Trottier, L., Sherratt, D. J., & Paulsson, J. (2016). Stochastic activation of a DNA damage response causes cell-to-cell mutation rate variation. *Science*, *351*(6277), 1094–1097. https://doi.org/10.1126/science.aac9786

Uphoff, S., Reyes-Lamothe, R., De Leon, F. G., Sherratt, D. J., & Kapanidis, A. N. (2013). Single-molecule DNA repair in live bacteria. *Proceedings of the National Academy of Sciences of the United States of America*, *110*(20), 8063–8068. https://doi.org/10.1073/pnas.1301804110

Uphoff, S., & Sherratt, D. J. (2017). Single-Molecule Analysis of Bacterial DNA Repair and Mutagenesis. *Annual Review of Biophysics*, *46*(1), 411–432. https://doi.org/10.1146/annurev-biophys-070816-034106

Vedyaykin, A., Rumyantseva, N., Khodorkovskii, M., & Vishnyakov, I. (2020). SulA is able to block cell division in Escherichia coli by a mechanism different from sequestration. *Biochemical and Biophysical Research Communications*, *525*(4), 948–953. https://doi.org/10.1016/j.bbrc.2020.03.012

Verhoeven, E. E. A., Van Kesteren, M., Moolenaar, G. F., Visse, R., & Goosen, N. (2000). Catalytic sites for 3’ and 5’ incision of Escherichia coli nucleotide excision repair are both located in UvrC. *Journal of Biological Chemistry*, *275*(7), 5120–5123. https://doi.org/10.1074/jbc.275.7.5120

Vincent, M. S., & Uphoff, S. (2020). Bacterial phenotypic heterogeneity in DNA repair and mutagenesis. *Biochemical Society Transactions*, *48*(2), 451–462. https://doi.org/10.1042/BST20190364

Vincent, M. S., & Uphoff, S. (2021). Cellular heterogeneity in DNA alkylation repair increases population genetic plasticity. *Nucleic Acids Research*, *49*(21), 12320–12331. https://doi.org/10.1093/nar/gkab1143

Wang, B., Dai, P., Ding, D., Del Rosario, A., Grant, R. A., Pentelute, B. L., & Laub, M. T. (2019). Affinity-based capture and identification of protein effectors of the growth regulator ppGpp. *Nature Chemical Biology*, *15*(2), 141–150. https://doi.org/10.1038/s41589-018-0183-4

Wang, D., Zhu, L., Zhen, X., Yang, D., Li, C., Chen, Y., Wang, H., Qu, Y., Liu, X., Yin, Y., Gu, H., Xu, L., Wan, C., Wang, Y., Ouyang, S., & Shen, X. (2022). A secreted effector with a dual role as a toxin and as a transcriptional factor. *Nature Communications*, *13*(1). https://doi.org/10.1038/s41467-022-35522-9

Weber, H., Polen, T., Heuveling, J., Wendisch, V. F., & Hengge, R. (2005). Genome-Wide Analysis of the General Stress Response Network in Escherichia coli : σ S -Dependent Genes, Promoters, and Sigma Factor Selectivity. *Journal of Bacteriology*, *187*(5), 1591–1603. https://doi.org/10.1128/JB.187.5.1591-1603.2005

Whittaker, V. K., & Blakley, R. L. (1961). The Biosynthesis of Thymidylic Acid. *Journal of Biological Chemistry*, *236*(3), 838–841. https://doi.org/10.1016/s0021-9258(18)64317-0

Wigley, D. B. (2013). Bacterial DNA repair: Recent insights into the mechanism of RecBCD, AddAB and AdnAB. *Nature Reviews Microbiology*, *11*(1), 9–13. https://doi.org/10.1038/nrmicro2917

Wiktor, J., Gynnå, A. H., Leroy, P., Larsson, J., Coceano, G., Testa, I., & Elf, J. (2021). RecA finds homologous DNA by reduced dimensionality search. *Nature*, *597*(February). https://doi.org/10.1038/s41586-021-03877-6

Wong, G. T., Bonocora, R. P., Schep, A. N., Beeler, S. M., Lee Fong, A. J., Shull, L. M., Batachari, L. E., Dillon, M., Evans, C., Becker, C. J., Bush, E. C., Hardin, J., Wade, J. T., & Stoebel, D. M. (2017).

Genome-Wide Transcriptional Response to Varying RpoS Levels in Escherichia coli K-12. *Journal of Bacteriology*, *199*(7), 1–17. https://doi.org/10.1128/JB.00755-16

Wozniak, K. J., & Simmons, L. A. (2022). Bacterial DNA excision repair pathways. *Nature Reviews Microbiology*, *20*(8), 465–477. https://doi.org/10.1038/s41579-022-00694-0

Wu, C. C., Lin, J. L. J., & Yuan, H. S. (2020). Structures, Mechanisms, and Functions of His-Me Finger Nucleases. In *Trends in Biochemical Sciences* (Vol. 45, Issue 11, pp. 935–946). Elsevier Ltd. https://doi.org/10.1016/j.tibs.2020.07.002

Wu, L. J., & Errington, J. (2012). Nucleoid occlusion and bacterial cell division. *Nature Reviews Microbiology*, *10*(1), 8–12. https://doi.org/10.1038/nrmicro2671

Xu, Y., Zhao, Z., Tong, W., Ding, Y., Liu, B., Shi, Y., Wang, J., Sun, S., Liu, M., Wang, Y., Qi, Q., Xian, M., & Zhao, G. (2020). An acid-tolerance response system protecting exponentially growing Escherichia coli. *Nature Communications*, *11*(1), 1–13. https://doi.org/10.1038/s41467-020-15350-5

Yakimov, A., Bakhlanova, I., & Baitin, D. (2021). Targeting evolution of antibiotic resistance by SOS response inhibition. *Computational and Structural Biotechnology Journal*, *19*, 777–783. https://doi.org/10.1016/j.csbj.2021.01.003

Yang, H., Wolff, E., Kim, M., Diep, A., & Miller, J. H. (2004). Identification of mutator genes and mutational pathways in Escherichia coli using a multicopy cloning approach. *Molecular Microbiology*, *53*(1), 283–295. https://doi.org/10.1111/j.1365-2958.2004.04125.x

Yeeles, J. T. P., & Marians, K. J. (2013). Dynamics of leading-strand lesion skipping by the replisome. *Molecular Cell*, *52*(6), 855–865. https://doi.org/10.1016/j.molcel.2013.10.020

Zaslaver, A., Bren, A., Ronen, M., Itzkovitz, S., Kikoin, I., Shavit, S., Liebermeister, W., Surette, M. G., & Alon, U. (2006). A comprehensive library of fluorescent transcriptional reporters for Escherichia coli. *Nature Methods*, *3*(8), 623–628. https://doi.org/10.1038/nmeth895

Zhang, A. P. P., Pigli, Y. Z., & Rice, P. A. (2010). Structure of the LexA-DNA complex and implications for SOS box measurement. *Nature*, *466*(7308), 883–886. https://doi.org/10.1038/nature09200

Zhang, D., de Souza, R. F., Anantharaman, V., Iyer, L. M., & Aravind, L. (2012). Polymorphic toxin systems: Comprehensive characterization of trafficking modes, processing, mechanisms of action, immunity and ecology using comparative genomics. *Biology Direct*, *7*(1), 18. https://doi.org/10.1186/1745-6150-7-18

Zhang, D., Iyer, L. M., & Aravind, L. (2011). A novel immunity system for bacterial nucleic acid degrading toxins and its recruitment in various eukaryotic and DNA viral systems. *Nucleic Acids Research*, *39*(11), 4532–4552. https://doi.org/10.1093/nar/gkr036

Zhang, X., Yin, M., & Hu, J. (2022). Nucleotide excision repair: a versatile and smart toolkit. *Acta Biochimica et Biophysica Sinica*, *54*(6), 807–819. https://doi.org/10.3724/abbs.2022054

Zhang, Y., Morar, M., & Ealick, S. E. (2008). Structural biology of the purine biosynthetic pathway. *Cellular and Molecular Life Sciences*, *65*(23), 3699–3724. https://doi.org/10.1007/s00018-008-8295-8

Zheng, D., Liwinski, T., & Elinav, E. (2020). Interaction between microbiota and immunity in health and disease. *Cell Research*, *30*(6), 492–506. https://doi.org/10.1038/s41422-020-0332-7

APPENDIX

1. TABLE S1 : LIST OF STRAINS USED IN THE STUDY

Species	Genotype	Plasmids	Antibiotic Resistance	Reference
E. coli AB1157	*flhD*-, P_{RNAI}-mKate2, MutL-mYPet	pUA-*PgrxA*-CFP	Kanamycin	Lagage *et al.*, 2023
E. coli AB1157	*flhD*-, P_{RNAI}-mKate2, MutL-mYPet	pUA-*PrecA*-CFP	Kanamycin	Lagage *et al.*, 2023
E. coli AB1157	*flhD*-, CFP, DnaN-Ypet		Kanamycin	This study (P1 Transduction and Tn7 Transduction of a construct from Reyes-Lamothe *et al.*, 2014)
E. coli AB1157	*flhD*-, P_{RNAI}-mKate2, MutL-mYPet, Δ*muts*		Kanamycin	Lagage *et al.*, 2023
E. coli AB1157	*flhD*-, P_{RNAI}-mKate2, MutL-mYPet	pUA-*PsodA*-CFP	Kanamycin	This study (Transformation), using Zaslaver Library strain (PEC3876-98156246)
E. coli AB1157	*flhD*-, P_{RNAI}-mKate2, *recA*mwg-SYFP2	pUA-*PsodA*-CFP	Kanamycin	Made using a construct from Wiktor et al., 2021
E. coli AB1157	*flhD*-, P_{RNAI}-mKate2, MutL-mYPet	pUA-*PahpC*-CFP	Kanamycin	Choudhary *et al.*, 2023
E. coli AB1157	LexA-27aaHelix-Halo			Jones & Uphoff, 2021
E. coli AB1157	*flhD*-, P_{RNAI}-mKate2	pUA-*PgadB*-GFP	Kanamycin	This study (Transformation), using Zaslaver Library strain (PEC3876-98144867)
E. coli AB1157	*flhD*-, P_{RNAI}-mKate2, MutL-mYPet	pUA-*PfolA*-CFP	Kanamycin	This study (Transformation), using Zaslaver Library strain (PEC3876-98155011)
E. coli AB1157	*flhD*-, P_{RNAI}-mKate2, MutL-mYPet, *lexA3ind*$^{-}$	pUA-*PrecA*-CFP	Tetracycline, Kanamycin	This study (Transformation), using a strain from Uphoff, 2018
E. coli AB1157	*flhD*-, P_{RNAI}-mKate2, MutL-mYPet, *ΔrecA*	pUA-*PsodA*-CFP	Tetracycline, Kanamycin	This study (Transformation), using a strain from Jones & Uphoff, 2021

E. coli AB1157	*flhD*-, P_{RNAI}-mKate2, MutL-mYPet, *ΔsulA*	pUA-*PrecA*-CFP	Kanamycin	This study (P1 Transduction), using a strain from Jones & Uphoff, 2021
E. coli AB1157	*flhD*-, P_{RNAI}-mKate2, MutL-mYPet, *ΔdinB*, *ΔumuC*	pUA-*PrecA*-CFP	Kanamycin	This study (Transformation), using a strain from Uphoff, 2018
E. coli AB1157	*flhD*-, P_{RNAI}-mKate2, MutL-mYPet, *ΔmutM*, *ΔmutY*	pUA-*PrecA*-CFP	Kanamycin	This study (Transformation)
E. coli AB1157	*flhD*-, P_{RNAI}-mKate2, MutL-mYPet	pUA-*PrecA*-CFP, pTcr-*folA* L28R	Kanamycin, Ampicilin	This study (Transformation), using a GeneArt custom-built plasmid
E. coli AB1157	*flhD*-, P_{RNAI}-mKate2, MutL-mYPet, *ΔrffC*	pUA-*PrecA*-CFP	Kanamycin	This study (P1 Transduction), using Keio strain OEC4987-200829683
E. coli AB1157	*flhD*-, P_{RNAI}-mKate2, MutL-mYPet	pUA-*PrecA*-CFP, pBAD33-Nte3	Kanamycin, Chloramphenicol	This study (Transformation of a plasmid from Custodio *et al.*, 2021)
E. coli AB1157	*flhD*-, P_{RNAI}-mKate2, MutL-mYPet	pUA-*PrecA*-CFP, pBAD33-Nte3/Nti3	Kanamycin, Chloramphenicol	This study (Transformation of a plasmid from Custodio *et al.*, 2021)
E. coli AB1157	*flhD*-, P_{RNAI}-mKate2, MutL-mYPet, *lexA3ind*$^{-}$	pUA-*PrecA*-CFP, pBAD33-Nte3	Tetracycline, Kanamycin, Chloramphenicol	This study (Transformation of a plasmid from Custodio *et al.*, 2021)
E. coli AB1157	*flhD*-, P_{RNAI}-mKate2, MutL-mYPet, *lexA3ind*$^{-}$	pUA-*PrecA*-CFP, pBAD33-Nte3/Nti3	Tetracycline, Kanamycin, Chloramphenicol	This study (Transformation of a plasmid from Custodio *et al.*, 2021)
E. coli AB1157	*flhD*-, P_{RNAI}-mKate2, MutL-mYPet	pUA-*PsodA*-CFP, pBAD33-Nte3	Kanamycin, Chloramphenicol	This study (Transformation of a plasmid from Custodio *et al.*, 2021)
E. coli AB1157	*flhD*-, P_{RNAI}-mKate2, MutL-mYPet	pUA-*PsodA*-CFP, pBAD33-Nte3/Nti3	Kanamycin, Chloramphenicol	This study (Transformation of a plasmid from Custodio *et al.*, 2021)
E. coli AB1157	*flhD*-, P_{RNAI}-mKate2, MutL-mYPet	pUA-*PsodA*-CFP, pBAD33-Nte3 FL H1306A	Kanamycin, Chloramphenicol	This study (Transformation), plasmid engineered by Veronika Bakulova (Unpublished, Tang Lab)
E. coli AB1157	*flhD*-, P_{RNAI}-mKate2, MutL-mYPet	pBAD33-CFP	Chloramphenicol	This study (Transformation), using a GeneArt custom-built plasmid

2. TABLE S2 : LIST OF REAGENTS USED IN THIS STUDY

Reagent	Product Code	Brand
M9 minimal salts 5X	M9956-500mL	Sigma-Aldrich
MEM amino acids	11130-036	Gibco
L-Arginine	A5006-100G	Sigma-Aldrich
L-Histidine	H8000-100G	Sigma-Aldrich
L-Leucine	L8000-100G	Sigma-Aldrich
L-Threonine	T825-100G	Sigma-Aldrich
L-Proline	A3453,0100	BioChemica
Thiamine	A0955,0050	BioChemica
Pluronic F-127	P2443-250G	Sigma
Coverslips No 1.5 184kit	631-0147	VWR
Dow Corning Sylgard 184 kit	1667370	Farnell Electronic
Tygon Microbore silicon tubing	ND 100-80	VWR
TMR dye	G8251	Promega
Agarose	1613100	BioRad
L-Methionine	M9625-5G	Sigma-Aldrich
Adenine	A8626-5G	Sigma-Aldrich
Glycine	G7126-100G	Sigma-Aldrich
Thymidine	T1895-1G	Sigma-Aldrich
L-Arabinose	A3556-250G	Sigma-Aldrich
Ampicilin Sodium Salt	A0839,0010	BioChemica
Tetracycline Hydrochloride	A2228,0025	BioChemica
Kanamycin Sulfate	A1496,0050	BioChemica
Chloramphenicol	A1806,0025	BioChemica
Carbanecilin Disodium Salt	A1491,0010	BioChemica
Ethanol	32221-2.5L-M	Sigma-Aldrich
Acetone	24201-2.5L-M	Sigma-Aldrich
Isopropanol	J30Q727	Alta Aesar

3. TABLE S3 : LIST OF PRIMERS USED IN THIS STUDY

Sequence	Description
ATGTATATCTCCTTCTTAAATCTAGAGG	pUA backbone - Replace GFP by CFP (Fwd)
ATGTCCAGACCTGCAGGC	pUA backbone - Replace GFP by CFP (Rev)
TTTAAGAAGGAGATATACATATGAGTAAAGGAGAAGAAC	CFP - Replace GFP by CFP (Fwd)
ATGCCTGCAGGTCTGGACATTTATTTGTATAGTTCATCCATGC	CFP - Replace GFP by CFP (Rev)